# ULTRASONOGRAPHIC AND COMPUTATIONAL INSIGHT INTO THE THYROID DISORDERS


A THESIS SUBMITTED TO THE

**CENTRAL DEPARTMENT OF PHYSICS**

**INSTITUTE OF SCIENCE AND TECHNOLOGY**

**TRIBHUVAN UNIVERSITY**

**NEPAL**

**FOR THE AWARD OF**

**DOCTOR OF PHILOSOPHY**

**IN PHYSICS**

BY

**TIKA RAM LAMICHHANE**

**JANUARY 2021**

# ULTRASONOGRAPHIC AND COMPUTATIONAL INSIGHT INTO THE THYROID DISORDERS


A THESIS SUBMITTED TO THE

**CENTRAL DEPARTMENT OF PHYSICS**

**INSTITUTE OF SCIENCE AND TECHNOLOGY**

**TRIBHUVAN UNIVERSITY**

**NEPAL**

**FOR THE AWARD OF**

**DOCTOR OF PHILOSOPHY**

**IN PHYSICS**

BY

**TIKA RAM LAMICHHANE**

**JANUARY 2021**

# DECLARATION

Thesis entitled **"ULTRASONOGRAPHIC AND COMPUTATIONAL INSIGHT INTO THE THYROID DISORDERS"** which is being submitted to the Central Department of Physics, Institute of Science and Technology (IOST), Tribhuvan University, Nepal for the award of the degree of Doctor of Philosophy (PhD), is a research work carried out by me under the supervision of Assoc. Prof. Dr. Hari Prasad Lamichhane, Central Department of Physics, Tribhuvan University (TU), Kirtipur, Kathmandu, Nepal and under the co-supervision of Assoc. Prof. Dr. Sharma Paudel, Department of Radiology, Institute of Medicine, TU Teaching Hospital, Maharajgunj, Kathmandu, Nepal.

This research is original and has not been submitted earlier in part or full in this or any other form to any university or institute, here or elsewhere, for the award of any degree.

. . . . . .

Tika Ram Lamichhane

# RECOMMENDATION

This is to recommend that **Mr. Tika Ram Lamichhane** has carried out research entitled **"ULTRASONOGRAPHIC AND COMPUTATIONAL INSIGHT INTO THE THYROID DISORDERS"** for the award of Doctor of Philosophy (PhD) in **Physics** under our supervision. To our knowledge, this work has not been submitted for any other degree.

He has fulfilled all the requirements laid down by the Institute of Science and Technology (IOST), Tribhuvan University, Kirtipur for the submission of the thesis for the award of PhD degree.

. . . . . .

**Dr. Hari Prasad Lamichhane**

**Supervisor**

**Associate Professor**

Central Department of Physics

Tribhuvan University (TU)

Kirtipur, Kathmandu, Nepal

. . . . . .

**Dr. Sharma Paudel**

**Co-supervisor**

**Associate Professor**

Department of Radiology

Institute of Medicine, TU Teaching Hospital

Marajgunj, Kathmandu, Nepal

**January 2021**

# LETTER OF APPROVAL

[Date: 10 January 2021]

On the recommendation of **Dr. Hari Prasad Lamichhane** and **Dr. Sharma Paudel**, this PhD thesis submitted by **Tika Ram Lamichhane**, entitled **"ULTRASONOGRAPHIC AND COMPUTATIONAL INSIGHT INTO THE THYROID DISORDERS"** is forwarded by Central Department Research Committee (CDRC) to the Dean, Institute of Science and Technology (IOST), Tribhuvan University.

. . . . . .

**Dr. Om Prakash Niraula**
Professor,
Head,
Central Department of Physics
Tribhuvan University
Kirtipur, Kathmandu, Nepal

# ACKNOWLEDGMENTS

At first, I am very pleased to extend my gratefulness to all respected persons, friends and family members who provided me motivation, support, guidance and inspiration for the completion of this research work.

I would like to express my sincere gratitude to my supervisor and co-supervisor for their valuable supervision, suggestions, time and effort in completing this research work. Their guidance, constant support, monitoring and encouragement throughout the research period leads to the successful finalization of this work.

I am grateful to Prof. Dr. Binil Aryal, Dean, Institute of Science and Technology (IoST), TU and Prof. Dr. Om Prakash Niraula, Head of Central Department of Physics (CDP), TU, Kirtipur for his suggestions, encouragement and support by providing homely environment to perform this research work at this department.

I would like to acknowledge Assoc. Prof. Dr. Binod Kumar Yadav, Head of Department of Biochemistry, Institute of Medicine, TU Teaching Hospital, Maharajgunj, Kathmandu, Nepal for providing data of thyroid function tests and for helping in clinical data analysis related to this research work.

My special thanks go to Prof. Dr. Raju Khanal for providing computing facility as a support to this research work at CDP, TU, Kirtipur.

I am thankful to Prof. Dr. Shesh Kanta Aryal, Prof. Dr. Lok Naryan Jha, Prof. Dr. Naryan Prasad Adhikari, Prof. Dr. Ishwar Koirala, Prof Dr. Ram Prasad Regmi, Dr. Balram Ghimire, Dr. Ajay Kumar Jha, Dr. Gopi Chandra Kafle, Dr. Madhab Prasad Ghimire, Dr. Nurapati Panta, Dr. Niraj Dhital, Dr. Sanju Shrestha, Mr. Rajendra Prasad Koirala, Mr. Hari Shankar Mallik, Mr. Pramod Thakur, Mrs. Sangita Maharjan and all teaching and non-teaching staffs at CDP, TU for their support and encouragement during the research work.

I acknowledge Mr. Sandeep Prashad Pant, Mr. Binod Lamichhane and Mr. Chhabindra Gautam for helping in clinical data collection related to this research work.

I would like to thank the head and team members of Department of Radiology, team

members of Department of Biochemistry, the head of Institutional Review Board, and endocrinologists, Institute of Medicine, TU Teaching Hospital, Maharajgunj, Kathmandu, Neapl for their technical support related to this research work.

I would like to thank AAPPS and Institut Fizik Malaysia; Engineering Information Institute, China; Central Department of Physics, TU and Amrit Science Campus, TU for giving me the opportunity of presenting this research work in the related international conferences.

I am thankful to Central Department of Physics, Institute of Science and Technology, TU for providing me study leave to perform this research work. I also thank to Nepal Academy of Science and Technology for providing me the PhD fellowship and to University Grants Commission, Nepal for providing me the travel and the publication support grants related to this research work.

Finally, I would like to thank my parents and family members for their encouragement, patience and regular support.

Tika Ram Lamichhane

January 2021

# ABSTRACT

Objective of this research is to evaluate thyroid dysfunction states (euthyroidism, hypothyroidism, hyperthyroidism and resistance to thyroid hormones) by using thyroid function tests (TFTs) of the hospital based subjects in central Nepal followed by thyroid ultrasonographic (USG) examinations and to explore the related impacts on the molecular levels by means of nanoscale molecular dynamics (NAMD) simulations of thyroid hormone receptors (THRs). To develop the complex correlations among thyroid variables and to find the conformational changes, energy distributions and thermal properties such as heat capacity, diffusion and conduction of THRs in the cases of overt thyroid disorders are the major physics questions which have been solved in this research. Euthyroidism, hypothyroidism and resistance to thyroid hormones (RTH) are associated with the structural and physical properties of liganded, unliganded and mutated THRs, respectively. In a total of 3425 thyroid patients, there were 70.45% euthyroid, 18.95% subclinical hypothyroid, 3.30% overt hypothyroid, 5.11% subclinical hyperthyroid and 2.19% overt hyperthyroid subjects. An isolated group of 48 patients fell in the category of RTH who have elevated serum free triiodothyronine (FT3) and thyroxin (FT4) but not suppressed thyroid stimulating hormone (TSH) affected by point mutation on THR-$\beta$ gene. Thyroid USG and TFTs of euthyroid subjects recommend age- and gender-specific reference levels of thyroid lobe volume, FT3, FT4 and TSH. Normal thyroid size first increases and then decreases whereas FT4 first decreases and then slightly increases with aging. Right thyroid lobe of males has greater size than that of females in all age-groups except in menarche and menopause. There is a linear relation between FT3 and FT4 and their correlation increases from euthyroidism ($r$ = 0.1) to overt thyroid dysfunctions ($r$ = 0.91, $p$ <0.001). The four parameter logistic (4PL) model has been better fitted ($R^2$ = 0.97, $p$ <0.001) supporting non-linear relation between ln(TSH) and FT4 in both hypothyroidism and hyperthyroidism on the basis of euthyroidism. The fitted non-linear curves are response trajectories of pituitary TSH by the deviation in serum FT4. The negative correlations and slopes of the linear fits in ln(TSH) *vs* FT4 or FT3 are indicators of negative feedback mechanism in the thyroid cycle. Hypothyroid patients suffer from goitre, thyroiditis, benign type of nodular and/or cystic lesions, diffused echogenicity

and vascularity. Some patients with normal TFTs also have cystic and/or hypoechoic and even malignant lesions in the thyroid gland. The patients with THR-$\beta$ mutations suffer from RTH and goitre. Thyroid dysfunction is a consequence of THR-malfunctions due to its unliganded and/or mutated forms. In both constrained and unconstrained dynamics, temperature auto-correlations and echo-curves show distinct characteristics of T3 liganded and unliganded THRs. Under the effect of anharmonicity on the phase coherent state of normal modes, the dephasing time lies in a range of 0.6-0.8 ps when the THR-systems are perturbed suddenly. T3 makes some increase in heat capacity upon binding to THR-$\beta$ ligand binding domain (LBD) in both anhydrous and hydrous states that signifies the effect of receptor-ligand interactions, and hydrophobic, vibrational and conformational changes. The specific heat of the THR isoforms in solution ranges from 2000 to 2200 $Jkg^{-1}K^{-1}$ at 310 K which is about 20% higher than that in anhydrous state in agreement with the experimental results. Providing temperature relaxation from 310 K to 200 K across protein-water interface in nanodroplets, the thermal diffusivity of THRs ranges from $1.28 \times 10^{-7}$ to $1.57 \times 10^{-7}$ $m^2/s$ which is around $1.46 \times 10^{-7}$ $m^2/s$ for water. The thermal conductivity of THRs lies in the range of 0.26–0.30 $Wm^{-1}K^{-1}$ which is about half the value, 0.64 $Wm^{-1}K^{-1}$ for water at 310 K. In euthyroidism, the THRT3 isoforms with lower thermal conductivity are responsible for the regulation of body scale temperature through thermogenesis and metabolism. The hypothyroid patients with lower hormone-receptor interactions suffer from cold intolerance. The point mutations like L330S on THR-$\beta$ LBD make changes on Ramachandran plots, solvent accessible surface area, radial distribution functions, root mean square deviations and fluctuations, and interaction and internal energies in comparison with its wild type. These physical parameters reflect that L330S-mutant causes steric hindrance while binding T3 into THR-$\beta$ LBD resulting RTH in the thyroid patients. Thus, prevalence of thyroid disorders, correlations among thyroid variables and physical properties of THRs responsible for thyroid dysfunction states are explored clinically and computationally.

# LIST OF ACRONYMS AND ABBREVIATIONS

| | |
|---|---|
| ANOVA | Analysis of Variance |
| BPTI | Bovine Pancreatic Trypsin Inhibitor |
| CHARMM | Chemistry at Harvard Macromolecular Mechanics |
| $C_{T,T}$ | Temperature Auto-correlation |
| CVH2 | Constrained Vibrations with Rigid H-atoms at 2 fs/step |
| DNA | Deoxyribonucleic Acid |
| ECI | Enhanced Chemiluminescence Immunoessay |
| FNAC | Fine Needle Aspiration Cytology |
| FT3 | Free Triiodothyronine |
| FT4 | Free Tetraiiodothyronine or Thyroxine |
| FVA1 | Free Vibrations of all Atoms at 1 fs/step |
| GFP | Green Fluorescent Protein |
| GLY | Glycine |
| GUI | Graphical User Interface |
| HPT | Hypothalamus Pituitary Thyroid |
| ILE | Isoleucine |
| IQR | Inter Quartile Range |
| IR | Infrared |
| IRB | Institutional Review Board |
| IU | International Unit |
| LBD | Ligand Binding Domain |
| LEU | Leucine |
| LLV | Left Lobe Volume |
| MD | Molecular Dynamics |
| mRNA | Messenger Ribonucleic Acid |
| NAMD | Nanoscale Molecular Dynamics |
| NVE | Number of Atoms, Volume and Energy |
| NVT | Number of Atoms, Volume and Temperature |
| RG | Radius of Gyration |
| RLV | Right Lobe Volume |

| | |
|---|---|
| RMSD | Root Mean Square Deviation |
| RMSF | Root Mean Square Fluctuation |
| RNA | Ribonucleic Acid |
| RTH | Resistance to Thyroid Hormones |
| rT3 | Reverse Triiodothyronine |
| SA | Solvent Accessibility |
| SASA | Solvent Accessible Surface Area |
| SE | Standard Error |
| SER | Serine |
| SD | Standard Deviation |
| TCL | Tool Command Language |
| T3 | Triiodothyronine |
| T4 | Tetraiiodothyronine or Thyroxine |
| TFT | Thyroid Function Test |
| TGV | Thyroid Gland Volume |
| TH | Thyroid Hormones |
| THR | Thyroid Hormone Receptor |
| THR-MT | Mutated Thyroid Hormone Receptor |
| THRT3 | T3 Liganded Thyroid Hormone Receptor |
| THRT3T4 | T3 and T4 Liganded Thyroid Hormone Receptor |
| THR-WT | Wlid Type Thyroid Hormone Receptor |
| TIP3P | Three-Site Transferrable Intermolecular Potential |
| TRE | Thyroid Response Elements |
| TRH | Thyrotropin Releasing Hormone |
| TSH | Thyroid Stimulating Hormone or Thyrotropin |
| TUTH | Tribhuvann University Teaching Hospital |
| USG | Ultrasonography |
| VAL | Valine |
| vdW | van der Waals |
| VMD | Visual Molecular Dynamics |
| 4PL | Four Parameter Logistic |

# LIST OF TABLES

**Page No.**

# LIST OF FIGURES

**Page No.**

# TABLE OF CONTENTS

# CHAPTER 1

## INTRODUCTION

Thyroid is an endocrine gland which is located at the front of the neck, below the Adam's apple. It consists of two lobes connected by isthmus. The thyroid hormones (TH) are triiodothyronine (T3) and thyroxine or tetraiodothyronine (T4) which influence metabolic rate, protein synthesis, body functions and development. Since thyroid gland produces T3 and T4 hormones under the controlled mechanism of thyroid stimulating hormone (TSH) secreted by pituitary gland, the thyroid function is interconnected with pituitary, the master endocrine gland. Along with the pituitary functions, the pituitary dimensions change slightly with gender and aging as reported in Lamichhane *et al.* (2015) by evaluating the pituitary MRI of healthy Nepalese people. Hypothalamus produces thyrotropin releasing hormone (TRH) that further controls the secretion of TSH. Conversely, T3 and T4 are feeded back to hypothalamus and pituitary through the bloodstream that control the production of TRH and TSH. In normal thyroid functions, the higher concentrations of T3 and T4 result the lower TSH level and vice versa. These phenomena complete through a cycle which is called thyroid cycle (Figure 1). Moreover, T3 and T4 hormones are transprted to the peripheral cells by the carrier proteins and these hormones pass through the channel proteins present on the cell membrane. T4 is converted into T3 and reverse T3 (rT3) under the active role of TH deiodinases (D1, D2 and D3) in the cytoplasm. D2 and D3 are useful to regulate homeostatis through the maintainance of T3 concentration in the plasma and cellular levels. As the members of a large family of nuclear receptors, thyroid hormone receptors (THRs) are coactivated by T3 for the DNA transcription to produce messenger RNA (mRNA).

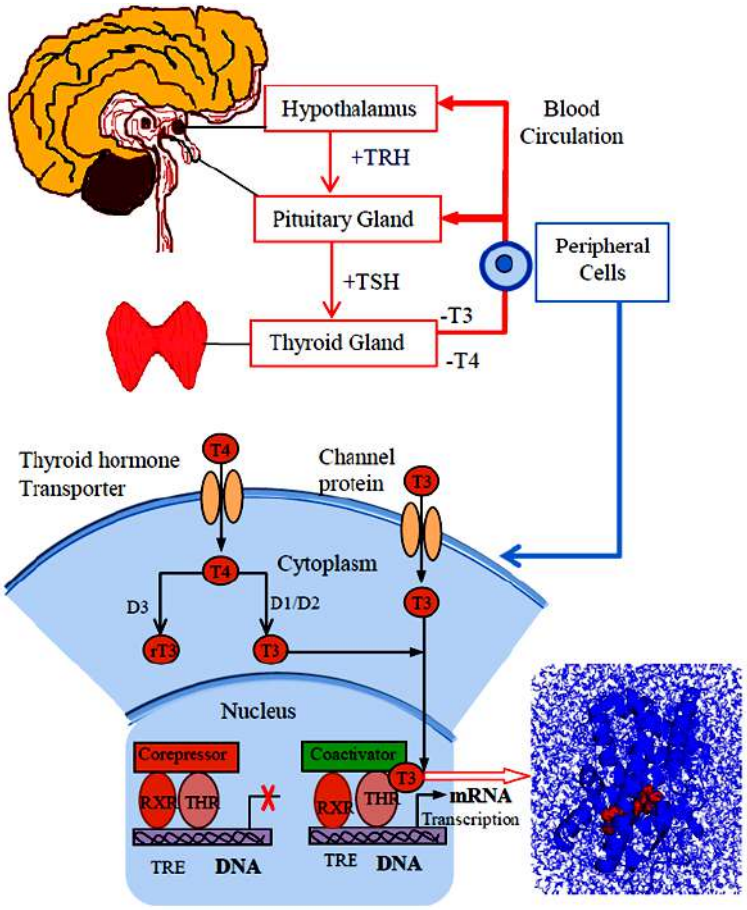


**Figure 1:** Thyroid cycle showing the negative feedback of thyroid hormones to hypothalamus and pituitary through the peripheral cells. Thyroid hormone receptor (THR) in presence of T3 regulates gene expressions as a part of endocrine functions

## 1.1 Thyroid Disorders

Thyroid related health problems are found to be increasing due to the various causes like stressful life style, environmental pollutants and contaminants, thinking and feeding habits of the individuals, lack of health awareness to the general public, lack of dietary iodine, smoking, alcoholism, and drug abuse. Some kinds of the thyroid diseases come from genetics. Most of the autoimmune diseases can not be prevented. However, the timely medication can reduce the defective features of the thyroid dysfunctions coming even from genetics. The thyroid clinical features are generally classified into euthyroidism, hypothyroidism and hyperthyroidism resulting normal, suppressive and excessive TH levels in the bloodstream of the patients, respectively (Monaco, 2003). The thyroid dysfunction states categorized on the basis of increase or decrease in TSH and TH levels from the normal reference ranges are shown in Figure 2. Here, hypo- and hyperthyroidism

are subdivided into subclinical and overt thyroid disorders. In the state of resistance to thyroid hormone (RTH), the TH-levels rise without fall in TSH. The euthyroid subjects have normal levels of TH and TSH concentrations. The possible thyroid disorders are also distinctly shown by the different regions of a block diagram (Figure 3) where TSH is correlated with TH concentrations (serum free thyroid hormones: FT3 and FT4) under the regulations of hypothalamus-pituitary-thyroid (HPT) axis in thyroid cycle.

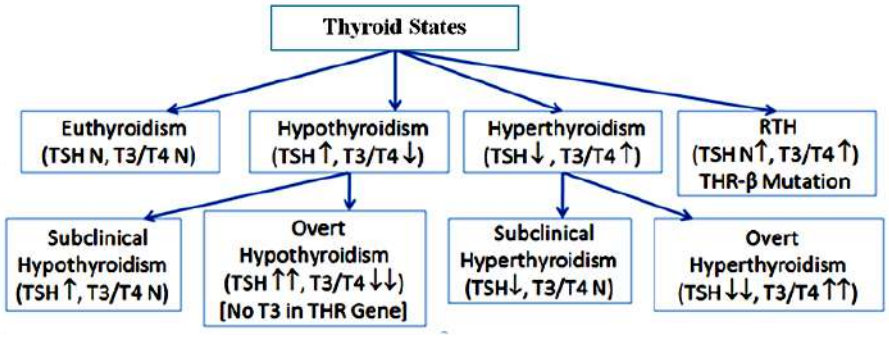


**Figure 2:** Major classes of thyroid clinical states evaluated from TFT measurements where N refers to normal and arrow indicates increased or decreased hormone concentrations from their reference levels in the blood serum

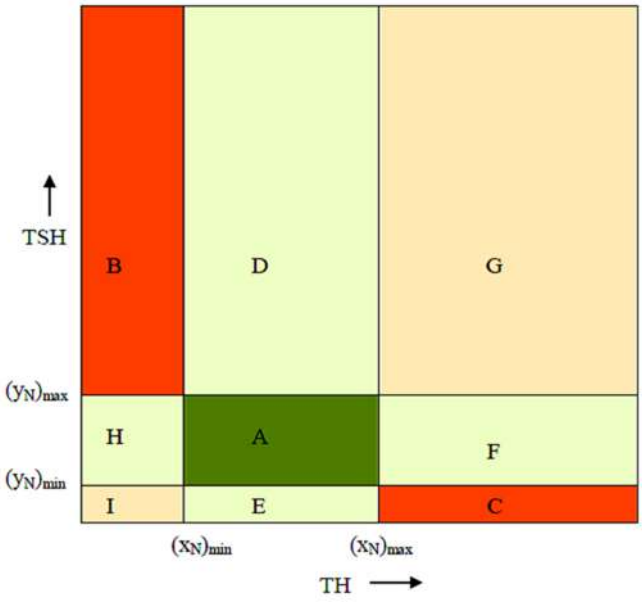


**Figure 3:** Possible regions of thyroid dysfunctions in the plots of TSH *vs* FT3 or FT4 (A: normal thyroid/euthyroid with liganded THR, B: overt hypothyroid with unliganded THR, C: overt hyperthyroid, D: subclinical hypothyroid, E: subclinical hyperthyroid, F/G: RTH by THR-$\beta$ mutation and H/I: central hypothyroid probably by pituitary adenoma). Here, normal range of TSH is $(y_N)_{min}$ to $(y_N)_{max}$ and that of TH is $(x_N)_{min}$ to $(x_N)_{max}$

Any disorder in the feedback loop or thyroid cycle is primarily evaluated by thyroid function tests (TFTs) whereas thyroid gland abnormalities are observed by thyroid

ultrasonography (USG). In association with the regulatory role of HPT axis, T3-mediated thyroid hormone receptors (THR-$\alpha$ and THR-$\beta$) regulate gene expressions (Ortiga-Carvalho, *et al.*, 2014) in response to the normal thyroid functioning. The dysregulations of TH levels throughout the body parts of hypo- or hyperthyroid patients are associated with thyroid gland abnormalities such as goitre, thyroiditis, diffused echogenicity, vascularіy, nodules, cysts, malignancy, etc.

Thyroid status can be evaluated by two ways: TFT analyses followed by thyroid USG examinations of the hospital based subjects and MD simulations of normal and diseased state THRs. The unliganded and mutational states of THRs repress gene expressions which further inhibit the regulatory role of HPT axis by abnormal production of T3, T4 and TSH (Hashimoto, *et al.*, 2001; Brent, 2012 ). So, comparing the structural and thermophysical properties of liganded, unliganded and mutated THRs is important to better understand the thyroid functions in molecular levels. The biochemical analyses of TFTs are used for the clinical diagnosis of the related thyroid abnormality. The biophysical properties of liganded and unligaded THRs are concerned with euthyroidism and hypothyroidism, respectively (Hashimoto, *et al.*, 2001). The RTH resulting with excessive TH levels but not suppressed TSH is caused by a point mutation in the THR-$\beta$ gene and such type of thyroid disorder is basically associated with the genetic defects or family history of the thyroid patients (Shuto, *et al.*, 1992).

## 1.2 Thyroid Ultrasonography

The USG of thyroid lesions is performed by using a linear-array transducer which produces high frequency ultrasound ranging from 7-15 MHz. A patient is placed in supine position with hyperextended neck and gray-scale or color Doppler techniques are used to examine the imaging characteristics providing size, shape, location, vascularity, contents, margins, and echogenicity (Chaudhary, *et al*., 2013). The ultrasound is produced by the transducer probe by piezoelectric method and the probe also records the pulse of echo coming back from the tissue interface. The sound is reflected from the tissue boundary due to the acoustic impedance (Hendee, *et al*., 2003) which is defined by

$$z = \frac{\Delta p}{u} = \rho v \tag{1.1}$$

where $\Delta p$ is the excess pressure, u is particle velocity, v is wave velocity and $\rho$ is the density of the tissue medium through which sound wave travels. If $Z_1$ and $Z_2$ are the acoustic impedances in both sides of the tissue interface, the reflection and transmission coefficients of the ultrasound wave are given by

$$R = \frac{(Z_2 - Z_1)^2}{(Z_2 + Z_1)^2} \tag{1.2}$$

$$T = \frac{4Z_1Z_2}{(Z_1 + Z_2)^2} \tag{1.3}$$

The Doppler ultrasound depends on the Doppler shift (Hendee, *et al.*, 2002) defined by

$$\Delta f = \frac{2fv'cos\theta}{v} \tag{1.4}$$

where f is frequency of sound used, *v'* is the source or blood flow speed, $\theta$ is angle of incidence and *v* is the sound speed. The total thyroid volume is the sum of volume of left lobe and right lobe. The volume of a lobe having length ($l$), breadth ($b$) and thickness ($t$) is measured by using the ellipsoid formula (Kayastha, *et al.*, 2010):

$$V = \frac{\pi}{6} \times l \times b \times t \tag{1.5}$$

Clinical ultrasound physics (Abu-Zidan, *et al.*, 2011) explains that brightness mode (B-mode) is basically used to examine the ultrasonographic images of body parts. The good quality image is produced by using actual frequency of ultrasound, emission time, sonation angle, size and curvature of the transducer and by minimizing the effects of reverberation, enhancement, edge and mirror artifacts.

Thyroid USG is a very useful tool for guidance of diagnostic and therapeutic interventional procedures related to different types of thyroid diseases (Chaudhary, *et al.*, 2013). The thyroid USG guides fine needle aspiration (FNA) biopsy of thyroid nodules, cysts, and/or focal masses. The USG technique can not determine thyroid function whether the gland is normal or underactive or overactive in molecular level so that biochemical or radioactive iodine uptake test is usually required. TFT assists the biochemical analysis of thyroid status. Ultrasound scanning confirms the presence of various kinds of goitres, nodules, cystic lesions, echogenicity for differentiating benign and malignant thyroid masses,

vascularity, lymphadenopathy and heterogenous thyroid echotextures.

In addition to the conventional USG, shear wave elastography and power Doppler examinations are used to diagnose thyroid disorders by measuring size and echogenicity, tissue stiffness or elasticity and vascularity, respectively. Thyroid cancers are less elastic than benign lesions. The presence of calcification increases the nodule stiffness so that cysts are less elastic than solid nodules. The lesions found in thyroid isthmus are less elastic than the nodules present in thyroid lobes (Szczepanek-Parulska, *et al.*, 2014).

### 1.3 Thyroid Function Tests

The TFTs are related to the measurements of concentration levels of T3, T4 and TSH present on the blood serum of the patients. These tests are performed by the technique of enhanced chemiluminescence immunoassay (ECI). In a chemiluminescent reaction, a substrate (chemiluminescent precursor) and an oxidant react to form a product in presence of cofactors and a catalytic enzyme (Weeks, *et al.*, 1986; Fereja, *et al.*, 2013). Some fraction of the product in the electronically excited state subsequently returns to the ground state with the emission of photons. The metal ions or the catalytic enzymes provide the adequate environment for the production of efficient chemiluminescence by reducing the activation energy. The electronic excitation occurs in case of exothermic reactions where the free energy used is written as

$$\Delta G = \Delta H - T\Delta S \tag{1.6}$$

where $\Delta H$ is the change in enthalpy, T is absolute temperature and $\Delta S$ is the small change in entropy. The difference between activation energy and reaction energy should be greater than or equal to excitation energy for the chemiluminescene to occur, i. e.

$$\Delta E_{ex} \leq \Delta H_A - T\Delta S_r \tag{1.7}$$

In this case, the free energy is

$$\Delta G \geq \frac{hc}{\lambda_{ex}} \tag{1.8}$$

where $\lambda_{ex}$ is the wavelength (400-750 nm) of the photons emitted in the exothermic reaction. In the ECI technique, the reaction in the presence of base catalyst is of the type:

$$\text{luminol} + \text{hydrogen peroxide} \rightarrow 3 - \text{aminophthalene} + hc/\lambda_{ex} \tag{1.9}$$

The light emission stabilizes in less than two minutes and it lasts for the several minutes. The chemical energy may be transferred to the heat and then to the vibrational and rotational energy which disturb the reaction pathway to channel out the excitation energy reducing fluorescence efficiency. The intensity $I_C$ of the emitted photons depends on quantum yield $\phi_C$ and reaction rate $-dC/dt$ for the consumption of chemiluminescent precursor C (Fereja, *et al.*, 2013) which is given by

$$I_C = \phi_C(-dC/dt) \tag{1.10}$$

The intensity $I_C$ is detected by the luminescent signal instrument such as phosphoimager or charged-coupled device (CCD)-based digital imager.

## 1.4 Thyroid Hormones and Nuclear Receptors

Basically, thyroid gland produces two major hormones: 3,5,3'-triiodo-L-thyronine (T3) and 3,5,3',5'-tetraiodo-L-thyronine (T4) which consist of 3 and 4 iodine atoms in their alpha and beta aromatic rings, respectively. T3 is formed from T4 by releasing an iodine atom during the local deiodination process. The chemical structures of T3 and T4 are shown in Figure 4 and 5, respectively. T3 has higher affinity of binding to THR ligand binding domain (LBD) than T4 though the serum T4 is found in higher concentration than the serum T3.

The thyroid disorders are interconnected with the physicochemical role of THRs towards ligand binding and dissociation, gene expressions, neural functions and metabolic activities (Brent, 2012). The nuclear receptor proteins such as THR-$\alpha$ and THR-$\beta$ subtypes actively bind to the DNA domain in order to assist gene transcription. Their LBDs differ by single amino acid residue: Asn331 in beta subtype instead of Ser277, and their full structural chemistry slightly differs by the amino acid sequencing (Souza, *et al.*, 2014). THR-$\alpha$ is found in muscle parts, heart and brain whereas THR-$\beta$ subtypes:

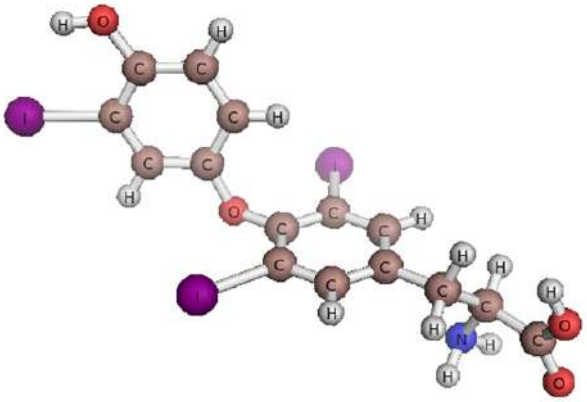

**Figure 4:** Structure of T3: $C_{15}H_{12}I_3NO_4$ with molar mass = 650.98 g/mol prepared with PyMOL molecular graphics system

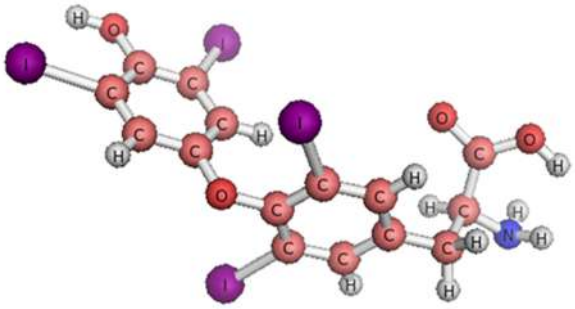

**Figure 5:** Structure of T4: $C_{15}H_{11}I_4NO_4$ with molar mass = 776.87 g/mol prepared with PyMOL molecular graphics system

THR-$\beta$1 is found widely in body tissues, THR-$\beta$2 is in eye and brain area, and THR-$\beta$3 is present in liver, kidney and lung (Brent, 2012). The biophysical role of each isoform towards the body functions depends on the amount of thyroid hormones (THs) produced, circulation of THs by the carrier proteins and their binding affinity to the respective genes. The most stable globular forms of T3-liganded THR-$\beta$ obtained from 3GwS.pdb and T3/T4-liganded THR-$\alpha$ obtained from 4LNX.pdb are respectively shown in Figures 6-a and 6-b (Lamichhane, *et al.*, 2019). Here, in the original x-ray crystallographic structures, 4LNX.pdb consists of total weight 32205.79 amu, atoms counts 2236 and residue counts 267 (Souza, *et al.*, 2014), and 3GwS.pdb consists of total weight 30258.83 amu, atoms counts 1957 and residue counts 259 (Nascimento, *et al.*, 2006).

Some point mutations on the nuclear receptors resist the actual binding and dissociation of thyroid hormones. Such type of thyroid disorder is basically found in THR-$\beta$ gene which is called RTH (Brent, 2012; Bochukova, *et al.*, 2012). Most of the THR LBD is made by alpha helices in which helix 12 dynamics is responsible for the interaction with

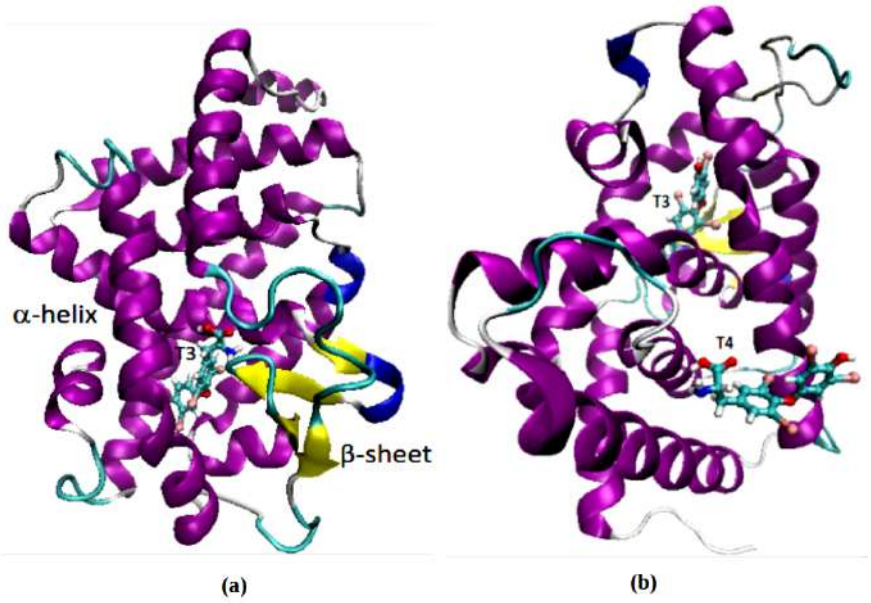


**Figure 6:** Cartoon structures of THRs prepared with VMD showing (a) T3 -liganded THR-$\beta$ obtained from the code: 3GwS.pdb and (b) T3/T4 -liganded THR-$\alpha$ obtained from the code: 4LNX.pdb

the active ligands and the DNA binding domains. T3 activated nuclear receptors regulate gene expressions. The underactive thyroid or overt hypothyoid condition is related to the T3 deficient THR systems. The unliganded THR represses DNA transcription called as transcriptional silencing. It further dysregulates the production of TRH and TSH, and hence THs by means of the negative feedback mechanism in the thyroid cycle (Figure 1). The underactive and overactive thyroid dysfunctions are associated with the conformational changes and biophysical misguiding of unliganded THRs resulting genetic repressions (Brent, *et al.*, 1994).

### 1.5 NAMD Simulations

Nanoscale molecular dynamics (NAMD) is a computer software which is used to study the biophysical properties of a molecular system by classical MD simulations. The algorithms of NAMD simulations are based on Newtonian equations of motion (Allen, 2004; Phillips, *et al.*, 2005):

$$m_i \ddot{r}_i = -\frac{\partial U(r_i)}{\partial r_i}, \qquad i = 1, 2, 3, ...., N \tag{1.11}$$

where $m_i$ is the mass of $i^{th}$ atom and $U(r_i)$ is the total potential energy depending on atomic positions $r_i$. The potential energy represents the atomic interactions through the MD force field. The net potential function is the sum of bonded and non-bonded potentials. The NAMD simulations of the protein-hormone systems use CHARMM force field and CHARMM potential function (Mackerell, *et al.*, 1998; Phillips, *et al.*, 2005) which is given by

$$U = U_{\text{bonded}} + U_{\text{non-bonded}} = [U_{\text{bond}} + U_{\text{angle}} + U_{\text{dihed}}] + [U_{\text{vdW}} + U_{\text{Coulomb}}] \quad (1.12)$$

where $U_{\text{bond}}$ is energy due to oscillations about the equilibrium bond length $r_0$, $U_{\text{angle}}$ is energy due to oscillations of 3 atoms about an equilibrium bond angle $\theta_0$, $U_{\text{dihed}}$ is dihedral energy due to torsional rotation of 4 atoms about a central bond subject to the tortion angle $\phi$, and $U_{\text{non-bonded}}$ is the sum of energy terms given by Lennard-Jones or van der Waal's and electrostatic interactions.

$$U_{\text{bonded}} = \sum_i k_i^{\text{bond}}(r_i - r_0)^2 + \sum_i k_i^{\text{angle}}(\theta_i - \theta_0)^2 + \sum_i k_i^{\text{dihed}}\,[1 + cos(n_i\phi_i - \gamma_i)] \quad (1.13)$$

$$U_{\text{non-bonded}} = \sum_i \sum_{j \neq i} 4\epsilon_{ij}\left[\left(\frac{\sigma_{ij}}{r_{ij}}\right)^{12} - \left(\frac{\sigma_{ij}}{r_{ij}}\right)^{6}\right] + \sum_i \sum_{j \neq i} \frac{q_i q_j}{\epsilon r_{ij}} \quad (1.14)$$

As the energy $U$ is a function of the atomic positions of all the atoms in the system which is usually expressed in term of Cartesian coordinates, its value is calculated from the sum of internal or bonded terms which describe the bonds, angles and bond rotations in a molecule, and a sum of external or non-bonded terms that account for interactions between non-bonded atoms or atoms separated by 3 or more covalent bonds. According to Mackerell *et al.* (1998), the additional energy terms are required to complete the net potential function which are improper and Urey-Bradley terms. These terms are defined by the Equations 1.15 and 1.16.

$$U_{\text{improper}} = \sum_i k_i^{\text{imp}}(\psi - \psi_0)^2 \quad (1.15)$$

$$U_{\text{Urey-Bradley}} = \sum_i k_i^{\text{UB}}(s - s_0)^2 \quad (1.16)$$

where $\psi$ is the improper torsion angle and $s$ is the Urey-Bradley 1,3-distance.

The CHARMM force field (e.g. the current versions: CHARMM27 and/or CHARMM36) uses topology files defining the type, mass and charge of every atom of the system to generate the protein structure file (psf), and parameter files defining all of the numerical constants needed to evaluate forces and energies. To run the MD simulations of the biomolecular system provided with the cellular environment, we make a configuartion file which includes structure (psf), coordinates (pdb), ensemble type (constant temperature or pressure defined for Langevin dynamics), force field parameters specified by CHARMM, integrator parameters (e.g. time step, rigid bonds, non-bonded frequency and full electrostatic frequency), output and restart frequencies, cell basis vectors and cell origin for periodic or non-periodic boundary conditions, and NAMD run-steps for energy minimization and equilibration.

NAMD uses the velocity Verlet algorithm (Verlet, 1996) to calculate the trajectory of atomic particles by integrating Newton's equations of motion. In MD simulations, Langevin dynamics means the controlling of kinetic energy, i.e. the temperature and/or pressure of the system. The Langevin equation for a single particle is the modified form of Newtonian force $F_i$ in classical mechanics which is written as Equation 1.17 (Berendsen, *et al.*, 1984).

$$m_i \ddot{x}_i(t) = F_i(x_i(t)) - \gamma_i \dot{x}_i(t) m_i + R_i(t) \tag{1.17}$$

where $F_i$ is the systematic force and the two additional terms in the right side represent the ordinary forces experienced by the particle, i.e. the frictional damping term with damping constant $\gamma_i$ and solvent interaction term $R_i(t)$(Gaussian stochastic variable with zero mean).

As per analysis of the structural trajectory, root mean square deviation (RMSD) *vs* time graph explains the conformational stability of the molecular system during the MD simulations. The RMSD is a numerical measure of the difference between the protein structures defined by Equation 1.18 (Walser, *et al.*, 2002; Riniker, *et al.*, 2012).

$$\text{RMSD} = \sqrt{\frac{\sum_{i=1}^{N} \left(r_i - r_{i,ref}\right)^2}{N}} \tag{1.18}$$

where $N$ is the number of atoms whose positions are to be compared, $r_i$ is the position of atom $i$ and $r_{i,ref}$ is the position of atom $i$ in the reference configuration defined by X-ray structure of the protein system.

In addition to RMSD, the equilibrations of the system can be analyzed with root mean square fluctuations (RMSF) and radius of gyration (RG) throughout the simulations. The RMSD from the average over time can be referred to as the RMSF. The RMSF of residue $i$ is given by Equation 1.19 (Riniker, *et al.*, 2012).

$$\text{RMSF} = \sqrt{\frac{\sum_{i=1}^{N_t} (r_i(t) - \langle r_i \rangle)^2}{N_t}} \tag{1.19}$$

where $N_t$ is the number of time steps giving new configurations in the simulations, $r_i(t)$ is the position of residue $i$, $\langle r_i \rangle = \frac{1}{N_t} \sum_{t_j=1}^{N_t} r_i(t_j)$ is the average position of residue $i$ at time $t_j$.

The RG is a measure of compactness describing the extent of collapse or extension of the protein backbone (Hu, *et al.*, 2010; Riniker, *et al.*, 2012). It represents the deviation of atoms in a molecule from its centre of mass defined by the Equation 1.20.

$$\text{RG} = \sqrt{\frac{\sum_{i=1}^{N}(r_i - r_{cm})^2}{N}} \tag{1.20}$$

where N is the total number of protein atoms, $r_i$ is the position of atom $i$, $r_{cm} = \frac{1}{M} \sum_{i=1}^{N} m_i r_i$ is the centre of mass, $m_i$ is the mass of atom $i$ and $M$ is the total mass of the protein atoms.

Solvent accessible surface area (SASA) is the area described by the locus of the center of the water molecule when it rolls along the protein complex by making the maximum permitted van der Waals contacts without penetrating any other atom. The SASA is calculated by using the Equation 1.21 (Lee, *et al.*, 1971; Ausaf Ali, *et al.*, 2014).

$$\text{SASA} = \sum_i (R/\sqrt{R^2 - Z_i^2}).D.L_i \tag{1.21}$$

where $D = \Delta Z/2 + \Delta' Z$, $R = r + r_s$ = sum of van der Waals radius of the atom and chosen radius of the solvent molecule, $L_i$ = length of arc drawn on a given section $i$, $Z_i$ =

the perpendicular distance from the center of the sphere to the section $i$, $\Delta Z$ = the spacing between the sections, and $\Delta' Z = \Delta Z/2$ or $R - Z_i$, whichever is smaller. The summation ranges over all of the arcs drawn for the given atom. Here, the solvent accessibility is defined by $SA = 100.SASA/4\pi R^2$.

In this way, NAMD calculates the spherical atomic radial distribution function (RDF/$g(r)$) between the atom coordinates in two selections over a given trajectory using GUI Plugin (Version 1.3) in VMD as explained by Levine *et al.* (2011). The normalized distance-dependent RDF for the atom pairs with types $i$ and $j$ is defined by the Equation 1.22 (Gohlke, *et al.*, 2000).

$$g_{i,j}(r) = \frac{N_{i,j}(r)/4\pi r^2}{\sum_r (N_{i,j}(r)/4\pi r^2)} \tag{1.22}$$

where scaling to $4\pi r^2$ accounts for the volume of the spherical shell of radius $r$ and thickness $dr$. The number $N_{i,j}(r)$ of atom pairs $i, j$ at a distance between $r$ and $r + dr$ is found by counting the occurrences $N_{i,j}(r) = \sum_i \sum_j \delta(|r_i - r_j|, r)$ where the delta function is $\delta = 1$ if $r \leq |r_i - r_j| \leq r + dr$ and otherwise it is zero. Here, the bin size $dr$ is chosen with high resolution between $r_{\min}$ and $r_{\max}$ including the atom pairs.

NAMD computes spectral densities from trajectories using time series data created with the *measure dipole* command in VMD-GUI, i.e. IR Spectral Density Calculator Plugin (Version 1.3). The details of theory and methods of NAMD simulations to calculate vibrational spectra of proteins were explained by Malolepsza *et al.* (2014). The classical IR spectral density, $I_{cl}(\omega)$ is given by Fourier transform of the auto-correlation function $G_{cl}(t)$ of the dipole moment operator (Rekik, *et al.*, 2018).

$$I_{cl}(\omega) = Re\left[\int_0^\infty G_{cl}(t) e^{-i\omega t} dt\right] \tag{1.23}$$

where $G_{cl}(t) = tr\left\{\rho(\beta)\mu(0)\mu(t)^\dagger\right\}$. Here, $\mu(0)$ is the dipole moment operator at the initial time and $\mu(t)$ is the same operator at the time $t$ and $\rho(\beta)$ is Boltzmann density operator with the statistical parameter $\beta = 1/K_B T$.

For a non-relativistic classical system of $N$ atoms, the equipartition theorem of statistical mechanics for the kinetic energy yields Equation 1.24 as mentioned by Xu *et al.* (1995),

Plastino *et al.* (1999) and Eastwood *et al.* (2010).

$$\left\langle \sum_{i=1}^{N_i} \frac{1}{2} m_i v_i^2 \right\rangle = \frac{3}{2} N K_B T \tag{1.24}$$

The Maxwell-Boltzmann (MB) distribution function for the kinetic energy ($\epsilon_k$) is given by

$$f(\epsilon_k) = \frac{1}{\sqrt{\pi}} \frac{1}{(K_B T)^{3/2}} \sqrt{\epsilon_k} exp\left(-\frac{\epsilon_k}{K_B T}\right) \tag{1.25}$$

The distribution function for the temperature fluctuations $\Delta T = T - T_0$ with $T = 2\epsilon_k / 3K_B$ is approximately Gaussian according to the central limit theorem which is defined by

$$P(\Delta T) = C.exp\left(\frac{-(\Delta T)^2}{2\sigma^2}\right) \tag{1.26}$$

where $C$ is a normalization constant and $\sigma^2 = 2T^2/3N$. For a finite $N$, the distribution is broad but for infinite $N$, it is very sharp.

The physical principles that are used specifically in analysis of the results obtained after MD simulations of normal and diseased state THRs are explained in the Section 3.2, Methods of MD Simulations.

### 1.6 Rationale of the Study

Thyroid dysfunction is a major public health problem. As our study focuses on the clinical data analysis and computational findings in the thyroid dysfunction states, it will be important for researchers, clinicians and people with thyroid disease to understand the disease, the goals of treatment modalities, and the drug designing models by complex interactions between thyroid hormones and their nuclear receptors. It has been noted that there is variation in the information regarding the localized reference levels of thyroid variables which influence understanding, diagnosis and use of medication. Nepal does not have its own reference interval for the thyroid function test panel so that the cutoffs which are used are still recommended by the manufacturer of the kit and by other studies. From the big data analysis of the hospital-based subjects, we have explored the age and gender specific changes of FT3, FT4, TSH and thyroid size by USG and TFT cross-sectional analysis that recommend for the new reference levels. The non-linear

complex relationships between thyroid hormones and thyrotropin in different thyroid states address the pathways of thyroid disorders and recovery modes. The USG results of gland abnormalities in association with TFT reports and patient's family status, habit and environmental conditions suggest for the essential treatment modality. This research will also provide guidance on the type of information and support to clinician as well as thyroid patient for making decisions about the disease management.

The information regarding the role of T3 hormone toward body temperature regulation, metabolism, HPT-axis regulation and THR activity for gene transcription suggests the patients to maintain its actual concentration in the blood serum even by medication. Because T3 liganded, unliganded and mutated THRs are the byproducts of euthyroid, hypothyroid and RTH states of the patients, the structural, vibrational and heat conduction properties of such normal and diseased state THRs will be important in drug discovery. The study of T3 stimulated biophysical phenomena helps to understand the momentum and energy transfer mechanism of THRs towards gene expressions. A patient with RTH suffers from single gene mutation or monogenic disorder and such type of mutational impact in the molecular level can be studied by NAMD simulations. Along with USG and TFT cross-sectional analysis, study in the molecular levels is also necessary for the actual evaluation of the thyroid status in the patients. To develop the complex correlations among thyroid variables and to explore the conformational changes, energy distributions and thermal properties such as heat capacity, diffusion and conduction of THRs in the cases of overt thyroid disorders are the major physics questions which have been solved in this research.

## 1.7 Research Objectives

In this research, we aim to focus on evaluating thyroid status by analyzing TFTs of the patients in central Nepal followed by thyroid USG examinations in euthyroid and hypothyroid subjects, and exploring physical properties of liganded, unliganded and mutated THRs related to euthyroidism, hypothyroidism and resistance to thyroid hormones by means of nanoscale molecular dynamics (NAMD) simulations of THRs. The specific objectives are as follows.

(a) To study thyroid disorder patterns by analyzing the prevalence, complex correlations

among thyroid variables (serum free TH, i.e. FT3 and FT4, thyroid stimulating hormone-TSH and thyroid size)in hypo and hyperthyroidism, age/gender specific changes and gland abnormalities from the USG and TFT clinical data of the thyroid patients.

(b) To explore the structural properties and thermophysical properties such as echo features, heat capacity, thermal diffusivity and thermal conductivity of liganded, unliganded and mutated THRs by using MD simulations.

## 1.8 Chapter Organization

The chapters of this thesis have been organized as follows:

**Chapter-1:** This chapter presents introduction to thyroid disorders, thyroid ultrasonography, thyroid function tests, thyroid hormones and nuclear receptors and NAMD simulations. Additionally, it includes rationale of the study and research objectives.

**Chapter-2:** This chapter named as Literature Review includes the review of ultrasonographic and biochemical status of thyroid dysfunction states, and thyroid hormone-receptor interactions including temperature echoes, heat conduction properties and mutational impacts on the protein systems. It aims to identify the research problems and justify the objectives of the current work.

**Chapter-3:** In Materials and Methods section, the methods of data collection by thyroid function tests and ultrasonographic examinations and the methods of data analysis and MD simulations of normal and diseased state protein-hormone systems have been presented.

**Chapter-4:** In Results and Discussion section, the obtained results and their interpretations have been discussed.

**Chapter-5:** This chapter named as Conclusions and Recommendations presents the conclusions of the present work and its possible extension.

**Chapter-6:** In the Summary section, a brief overview of the whole study has been presented.

Finally, the references are listed before closing this document.

# CHAPTER 2

## LITERATURE REVIEW

Many diagnostic and medicinal practices have been performed by researchers and doctors for the treatment of thyroid abnormalities since the prehistoric times to the present era of modern technology. In a well documented history of thyroid, the first partial thyroidectomy was performed by P. S. Dessault in 1789 and full thyroidectomy of a tumor was successfully carried out by Guillance Dupuytren in 1808 (Leoutsakos, 2004). The importance of iodine for thyroid function was explained by David Marine in 1907; thyroxin (T4) being isolated in 1914, it was synthesized in 1927 and T3 in 1952; TSH was invented in early to mid 20th century, and TRH was discovered by Andrew V. Schally in 1970 who was awarded by Nobel Prize in part in 1977 (https://www.thyroid.org/thyroid-history-timeline/; https://www.nobelprize.org/prizes/medicine/1977/summary/accessed: March 10, 2019). For the work on the physiology, pathology and surgery of the thyroid gland, Theodor Kocher was provided the Nobel Prize in physiology and medicine in 1909 (https://www.nobelprize.org/prizes/medicine/ 1909/summary/accessed: March 12, 2019). Many researchers described about thyroid disorders such as cretinism and myxeodema in 19th century, and hypothyroidism, hyperthyroidism and resistance to thyroid hormones (RTH) in late 19th to mid 20th century. The modern treatments and investigative modalities including radioactive iodine, thiouracil and fine needle aspiration (FNA) have been evolving since mid 20th century. The literature reviews of ultrasonographic, biochemical and computational analyses concerning respectively with thyroid gland dimensions and related abnormalities, TFT analysis of thyroid clinical status and thyroid hormone-receptor interactions have been performed as mentioned in the following Sections 2.1 and 2.2.

## 2.1 Ultrasonographic and Biochemical Status of Thyroid Disorders

### 2.1.1 Euthyroidism

The clinical diagnostic tests are specified from the reference levels taken. The published reference ranges of normal thyroid size and TFT levels are slightly different for the subjects under study as reported in the different literatures. The TFT reports and the thyroid USG findings change with age, gender, demography, ethnicity, pregnancy, medication, genetics, environmental factors, and non-thyroid illness. As the thyroid functions are influenced by the regulations of TSH, T3 and T4, we have reviewed and analyzed the correlations between thyroid size and TFT reports of euthyroid subjects varying along with gender and aging.

In a study performed by Hegedus *et al.* (1983), the mean thyroid volume in vivo of 271 healthy subjects aged 13-91 years was 18.6±4.5 mL with 19.6±4.7 mL for males and 17.5±4.2 mL for females where the thyroid volume (V) is related with body weight (W) and age (A) by the relation: $V = 1.97 + 0.21W + 0.06A$. According to Berghout *et al.* (1987), the USG findings of the thyroid volume of 50 healthy subjects (25M + 25F) was 12.7±4.4 mL for males and 8.7±3.9 mL for females with no correlation between thyroid volume and serum T3 or T4 or TSH concentrations. In the USG measurements of thyroid volume of 256 euthyroid subjects of age group 0-20 years in Brussels (Chanoine, *et al.*, 1991), mean thyroid volume was 2.7±0.8 mL in prepubertal aged 8-11 years and 11.6±4.4 mL in late pubertal aged >17 years. According to Ivanac *et al.* (2004), 51 randomly selected females of mean age 22 years (range: 20-38 years) in Croatia had the normal TFT results (TSH: 2.14±1.03 mIU/L; FT3: 5.65±0.54 pmol/L; FT4: 14.23±3.12 pmol/L) and the normal USG reports finding the mean thyroid volume 10.68±2.83 mL ranging from 5.71 to 17.01 mL. As reported by Kayastha *et al.* (2010), the mean thyroid volume of the hospital based Nepalese euthyroid subjects(264F + 221M) aged 1-83 years was 6.63±2.50 mL. These studies show the significantly different thyroid volume which should be due to demographic variations, age, gender, body mass index and body surface area.

The seasonal, daytime and nighttime variations of TH-levels were also reported even in normal thyroid conditions (Leppaluoto, *et al.*, 1998; Raj, *et al.*, 2014). In a study

performed by Leppaluoto, the polar T3 syndrome appears in a person with decreasing FT3 in the winter season. Without any change observed in thyroid status, about 20% variation in TSH levels was found (Raj, *et al.*, 2014). The normal levels of FT3, FT4 and TSH published in some literature (Roy, *et al.*, 2006; Shivaraj, *et al.*, 2009; Biondi, *et al.*, 2013) were 0.25-0.65 ng/dL, 1.0-3.0 ng/dL and 0.5-4.5 mIU/L, respectively. Mahato *et al.* (2015) reported that 71% of 5230 patients in the central Nepal were diagnosed to be clinically euthyroid who had the TFTs: TSH = 2.3±1.1 mIU/L, FT3 = 2.3±0.6 pg/mL and FT4 = 11.5±2.0 pg/mL. In the hilly region of Nepal, 76.7% of 3136 patients had euthyroid conditions (Dangol, *et al.*, 2017). Even in normal thyroid conditions, FT4 trends to decrease slightly with aging and its concentration in blood serum is lower in adult males than in adult females (Lipson, *et al.*, 1979; Kratzsch, *et al.*, 2005; Fontes, *et al.*, 2013; Chaurasia, *et al.*, 2017). In the study performed by Kratzsch, the reference levels of serum TSH, FT3 and FT4 were 0.40-3.77 mIU/L, 4.02-6.79 pmol/L and 12.8-20.4 pmol/L, respectively that were established from a constraint group of 453 healthy blood donors.

Basically, euthyroidism is the state of normal thyroid functioning with definite structural and biophysical role of T3-liganded THRs towards the gene expressions for the DNA transcription, thermogenesis and metabolic regulations. However, autonomous and solitary thyroid nodules were diagnosed in some euthyroid subjects by the USG scanning (Evered, *et al.*, 1974; Gupta, *et al*., 2010). The USG guided FNAC and biopsy declared thyroid malignancy in euthyroid asymptotic patients as reported by Corrias *et al.* (2010) and Hwang *et al.* (2016). The thermophysical properties of T3 mediated THRs interactions and the related impacts on the thyroid gland still remain unsolved which is important to understand the molecular mechanism of thyroid functions.

The previous researches show that the reference levels of TSH, T3 and T4 are found to be slightly changing with aging and demogaphy of the people under study. As a part of our research, the USG and TFT cross-sectional analysis has been performed which is necessary to understand normal thyroid functions and to recommend the age and gender based reference levels of thyroid variables such as thyroid size, FT3, FT4 and TSH. Furthermore, by the correlative changes of T3 concentrations, the structural and physical properties of THRs are also changed. These things are addressed in our rsearch through the hormone-receptor interactions.

### 2.1.2 Hypothyroidism

Subclinical hypothyroidism is a case of elevated TSH from the reference limit with normal FT3 and FT4 and normal HPT-axis without severe illness whereas in overt hypothyroidism, FT3 and FT4 fall below the reference rage with elevated TSH (Biondi, *et al.*, 2007; Garber, *et al.*, 2012). Iodine deficiency is a common cause of hypothyroidism. Hashimoto's thyroiditis, autoimmune thyroid disease, radioiodine and surgical treatment, thyroid benign nodule and cancer, and chronic non-thyroid diseases are other causes of hypothyroidism (Pearce, *et al.*, 2003; Garber, *et al.*, 2012). Central hypothyroidism arises from insufficient thyrotropin stimulation or with mildly elevated serum TSH and usually low FT4 by means of pituitary-hypothalamic defects.

The etiology of hypothyroidism is the reduced peripheral action of thyroid hormones, altered handling of intracellular calcium and impaired left ventricular diastolic filling with slow myocardial reflection (Biondi, *et al.*, 2007). T3 promotes vascular-muscle relaxation. The reducing T3 causes muscle pain or fatigue, hypertension and metabolic dysfunction (Almandoz, *et al.*, 2012). Hypothyroidism is more prevalent in women, elderly and certain ethnic groups. The chronic autoimmune (Hashimoto's) thyroiditis is characterized by diffused lymphocytic infiltration with increased level of antithyroid peroxidase (TPO) antibody leading to subsequent destruction of thyroid gland. The different causes and effects of thyroid disorder encompass the complex correlations among FT3, FT4 and TSH. Underactive thyroid being concerned with unliganded THR functions (Hashimoto, *et al.*, 2001), there is a research problem of finding the structural and physical properties of THRs and thyroid gland abnormalities in clinically hypothyroid patients.

In the cases of thyroidectomy and inadequate substitution of levothyroxin, hypothyroidism may be diagnosed in the patients. The USG examination is important in the patients after thyroidectomy to observe the possible presence of residual tissues and lymphadenopathy. The self-limiting inflametory disease, subacute thyroiditis (SAT) is painful in thyroid which arised in about 5% whereas permanent hypothyroidism arised in about 6% of thyroid abnormalities (Fatourechi, *et al.*, 2003; Nishihara, *et al.*, 2009). The patients with SAT commonly suffer from early transient hypothyroidism. The thyroid status after SAT depends on extent of hypoechogenicity and on treatment modality. The

initial evaluation of hypoechogenicity is significantly important for the subjects at the risk of hypothyroidism. Some cases of bilateral thyroid agenesis with adenomatous isthmus and hypothyroidism also appeared in the USG examinations (Kumar, *et al.*, 2010). The patients with thyroid USG reports of normoechogenic irregular background showing autoimmune thyroiditis (AIT) and nodular variants are in high risk of papillary thyroid carcinoma (Januś, *et al.*, 2018). Higher thyroid stimulating hormone (TSH) concentration or even in the normal range are associated with the development of thyroid malignancy in preclinical phase of chronic thyroid disorders. Moreover, there are lower T3 levels in the patients with thyroid cancer than patients with benign disease (Jonklaas, *et al.*, 2008). In primary autoimmune hypothyroidism, thyroid atrophy and goitre do not represent separate disorders and they are extremes within normal distribution of thyroid size (Carlé, *et al.*, 2009). Children may also suffer from transient hypothyroidism and thyroid agenesis. If no thyroid tissue is observed in USG examination, agenesis is diagnosed and if one lobe is absent, hemiagenesis is diagnosed (Nair, *et al.*, 2010). The thyroid USG findings of the clinically euthyroid and hypothyroid patients in association with the computational analysis of liganded and unliganded THRs are discussed in our research.

### 2.1.3 Hyperthyroidism

Subclinical hyperthyroidism arises due to the reduced serum TSH and normal FT3 and FT4 whereas thyrotoxicosis or overt hyperthyroidism is clinically diagnosed with suppressed TSH and elevated FT3 and FT4 from the respective reference ranges (Biondi, *et al.*, 2007; Bahn, *et al.*, 2011). Thyrotoxicosis consists of increased heart rate, systolic blood pressure, muscle weakness, tremor, lid-lag, irritation, exercise intolerance, emotional liability, and depression (Trzepacz, *et al.*, 1989; Bahn, *et al.*, 2011). The majority of the hyperthyroid patients have Grave's disease, multinodular goitre and solitary toxic adenoma influenced by the endemic iodine exposure (Abraham-Nordling, *et al.*, 2008). All of these symptoms and diseases are associated with the biochemically active relationship among FT3, FT4 and TSH.

The reference ranges for FT3, FT4 and TSH are different at different clinical laboratories which result significant changes in judging thyroid status. The graphical analysis by fitting

the observed data points yielded the deviating results in defining the correlations among these variables. Developing from simple linear fits among the TFT values, log-linear relationships between TSH and FT4 of both normal and abnormal thyroid were reported in the previous studies (Hoermann, *et al.*, 2014; Larsen, *et al.*, 1981; Benhadi, *et al.*, 2010). In addition to the log-linear transformations, the data sets of serum TSH and FT4 were also tried to fit with some mathematical models showing the non-linear relationships based on sigmoidal functions, error function and fourth-order polynomial as analyzed by Hoermann *et al.* (2010), Hadlow *et al.* (2013), Leow *et al.* (2007) and Clark *et al.* (2012). However, developing the actual relationships among TFT values under the prevalence of different dysfunction states has been yet remained unsolved. In our study, we have used four-parameter (4-P) logistic model to explain the complex correlations between TSH and FT4 when thyroid disorder develops from euthyroidism to subclinical and overt thyroid disorders.

## 2.2 Thyroid Hormone-Receptor Interactions

The TH-levels in the blood serum is controlled by the production of pituitary TSH. The deviation of these hormone levels from their reference ranges causes hypo or hyperthyroid disorders (Obregon, *et al.*, 2005) and such dysfunction states misconduct the working principle of THRs. T3-liganded THR-$\beta$ LBD regulates gene expressions and metabolism which further controls the hormone secretory mechanism of HPT-axis (Chiamolera, *et al.*, 2009). The THR-$\beta$ mutations result into the thyroid hormone resistance or RTH by the ligand-receptor interactions. The RTH has a wide range of symptoms including goitre formation, refractory depression, irregular heartbeat and pituitary dysfunction (Forrest, *et al.*, 1996). The unliganded THR-$\beta$ has the conformational changes which represses the basal trancription by altering helix-12 dynamics and AF1/AF2 transactivation domains (Souza, *et al.*, 2014; Sandler, *et al.*, 2004). Any point mutation on the helix-12 of THR LBD also inhibits T3 activated gene expressions by blocking the cofactors of AF2 domain (Ortiga-Carvalho, *et al.*, 2004). The T3 dissociation pathways are influenced by THR heterodimers (Zhuang, *et al.*, 2013). All of these evidences are the examples of THR-T3 interactions. According to Lu *et al.* (2018), the bisphenol S (BPS) is also able to interact with THR-$\beta$ LBD that result into the conformational changes of its globular

forms. The cartoon structure of T3-bound THR-$\beta$ LBD has been shown in the Figure 7 (Lamichhane, *et al.*, 2019). The previously reported biophysical principles as mentioned in the Subsections 2.2.1-2.2.3 have been implemented to study thyroid hormone-receptor interactions in normal and diseased states of thyroid functions by using MD simulations .

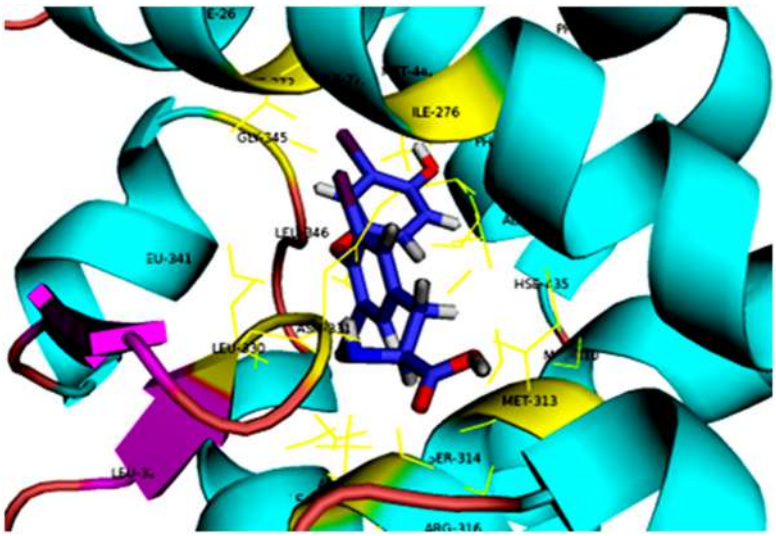


**Figure 7:** T3-liganded THR-$\beta$ LBD shown with yellow region around T3 by 4 Å distance which is prepared with PyMOL and the structure is obtained from the x-ray crystallography of 3GwS.pdb

### 2.2.1 Temperature Echoes in Proteins

MD simulations are performed by employing constrained or unconstrained dynamics of the atomic clusters. Even for a supercomputing system, it is difficult to proceed the long-run simulations of a complex biomolecule. The rapid vibrations of H-like atoms can be constrained so that the system's backbone is not distorted. The constrained MD simulations save the computer time by reducing the vibrational modes or the degrees of freedom (König, *et al.*, 2015; Van Gunsteren, *et al.*, 1977; Ryckaert, *et al.*, 1977; Van Gunsteren, *et al.*, 1982). However, for the exact quantum as well as classical calculations, we should implement free vibrations of all atoms keeping the internal degrees of freedom unchanged.

When the harmonic motion of the molecular system is suddenly perturbed with a suitable signal, the phase coherence of normal modes is observed in terms of echo beats or resonances. The vibrational dephasing or the decaying of such echo beats is due to anharmonicity of the atomic cluster dynamics (Fayer, *et al.*, 2001; Rector, *et al.*, 1997; Rella, *et al.*, 1996). According to Noid *et al.* (2004); the vibrational dephasing, rephasing

and stability of classical trajectories are studied by using nonlinear response functions describing the nuclear dynamics of the molecular systems.

By using MD simulations, the phase coherent state of a protein system is probed by temperature quenching or velocity reassignment to observe the echoes in temperature and energy profiles (Xu, *et al.*, 1995; Schulten, *et al.*, 1997). As demonstrated by these literatures, short-run simulations also result the exact phase coherent states or resonances in the protein systems. The time dependent echo depth is measured by finding the temperature autocorrelation function under harmonic approximations. The impact of anharmonic oscillations make the echo depth of these coherent states decay with time which is measured in terms of dephasing time. The dephasing time is 884 fs for bovine pancreatic trypsin inhibitor (BPTI) protein (Xu, *et al.*, 1995) and its value is 700 fs for bacteriorhodopsin protein (Schulten, *et al.*, 1997).

With some modifications, we have used the theory of temperature quenching and echo formation described by Xu *et al.* (1995) to calculate partial heat capacity, echo dephasing time, and diffusion and mobility constants of anharmonicity for liganded and unliganded THR-$\beta$ by using the protocols of NAMD simulations employed with constrained and unconstrained dynamics of the systems. The theoretical details are given in the Section 3.2, Methods of MD Simulations.

### 2.2.2 Heat Transfer Properties of Proteins

The biomolecules gain heat energy from the natural processes such as chemical kinetics, catalysis and radiation exposure. The higher temperature decays exponentially with time to the body scale temperature by the anisotropic flow of heat energy through the thermally agitating lattices of the constituent atoms. This phenomenon is implemented by MD simulations to understand the heat transfer properties of the protein-ligand complexes (Leitner, *et al.*, 2008). The physical parameters such as specific heat, heat diffusion coefficient and thermal conductivity are functions of temperature whose values differ in anhydrated and hydrated forms, energy transport channels, hydrophobic and hydrophillic LBDs, solvent accessible surfaces, interactive zones and polar and non-polar regions of the protein systems (Prabhu, *et al.*, 2005). In this regard, the ligand entry and dissociation make change in heat capacity of THR isoforms in nuclear receptor

superfamily. The specific heat of a native protein widely varies from 1200-2300 $Jkg^{-1}K^{-1}$ at room temperature. This range is also applicable to the specific heat of an indiviadual amino acid (Privalov, *et al.*, 1986; Privalov, *et al.*, 1989). The anharmonic vibrational modes present in the molecular system increase the rate of heat conduction (Yu, *et al.*, 2005). The interactive sites including hormone binding domains of the receptors are easier pathways for the propagation of the heat wave signal. The temperature rate of change in mean energy or the internal energy fluctuations in the canonical ensemble of a thermodynmic system evaluates its specific heat capacity at constant volume. Basically, enthalpy or mean energy of the complex system is determined from the total sum of averaged energy terms of the potential function (Prabhu, *et al.*, 2005). By using the temperature-relaxation procedures of transient non-equilibrium thermodynamics across the protein-water boundary, we can determine the thermal diffusion coefficient $D_p$ and thermal conductivity $k_p$ of a protein (Lervik, *et al.*, 2010; Helbing, *et al.*, 2011). Yu *et al.* (2005) and Lervik *et al.* (2010) obtained the value of $D_p$ near to that of water, i.e. 1.46 $\times 10^{-7}$ $m^2/s$ and the value of $k_p$ ranging from 0.13 to 0.28 W $m^{-1}K^{-1}$ for the different proteins at room temperature. This process has been implemented to explore the heat conduction properties of liganded and unliganded THR isoforms in our research. The related theories are explained in the Section 3.2, Methods of MD Simulations.

### 2.2.3 Mutations in THR-Beta and Resistance to Thyroid Hormones

Several point mutations were previously identified on the THR-$\beta$ isoforms that cause generalized resistance to thyroid hormones called RTH. The genetic disorder, RTH has the clinical features of elevating TH-levels without suppressing TSH in the blood serum. The RTH patients suffer from inadequate secretions by HPT-axis. RTH reduces T3 binding affinity to THR-$\beta$ LBD and it further resists the binding affinity to DNA binding domain resulting in gene repressions. The wild type THR-$\beta$ (THR-WT) is able to select the coactivators for the basal transcription whereas mutated THR-$\beta$ (THR-MT) recruits corepressors inhibiting the transcription factors. Thus, being linked with genetic defects, THR-MT results neoplasia and several endocrine disorders. Goitre formation, dizziness, speech disorder and tachycardia are common causes of RTH. All of these clinical facts are associated with the previously identified THR-$\beta$ mutations such as homozygous

mutant (Thrb-/-) in mice (Forrest, *et al.*, 1996); R383H in a 54-year-old woman (Safer, *et al.*, 1999); R429Q in mice (Machado, *et al.*, 2009); T327I in a girl aged 9 years (Lee, *et al.*, 2014); A268G in a girl aged 15 years (EI Shafie, *et al.*, 2014) and G344R in a 10-month-old female (Yang, *et al.*, 2016). For example, in the point mutation T327I, threonine(T) in $327^{th}$ codon of THR-WT is replaced by isoleucine (I) forming a type of THR-MT. Some of the active mutational sites identified in THR-$\beta$ gene are shown in Figure 8 (Lamichhane, *et al.*, 2019). In THR-$\beta$ LBD, helix 12 dynamics is responsible for the corepressor recognition as a selective gatekeeper and such work is not performed well by THR-MT (Rosen, *et al.*, 2011; Rosen, *et al.*, 2009). As a result, THR-MTs dysregulate the physiological and neurological functions giving rise to a thyroid disease, RTH.

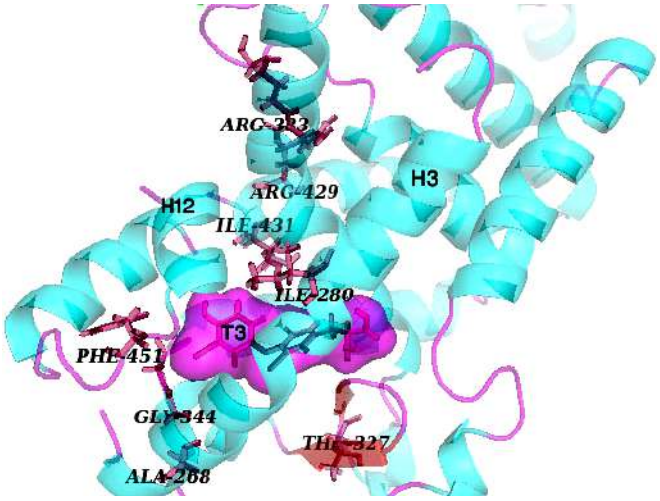


**Figure 8:** Some previously identified sites of point mutations on THR-$\beta$ gene prepared with PyMOL from the structure of 3GwS.pdb

According to Ferreira Azevedo *et al.* (2008), I431V mutation was identified on THR-$\beta$ gene of a Brazilian girl aged 14 years who had the symptoms of RTH and goiter. THR-MT with I431V impairs T3 binding and dissociation, and it recruits corepressors which repress DNA transcription. In this case, T3 binding affinity of THR-MT is 2.6 times lower than THR-WT. In this way, L330S was identified in an 11-year-old boy with RTH showing the symptoms of both hypo- and hyperthyroidism, goitre and speech disorder (Pohlenz, *et al.*, 1997). The L330S mutation was also detected in a 19-year Thai woman with RTH and goitre (Ditudompo, *et al.*, 1999).

To explore the mutational impacts on THR-$\beta$ gene of the patients with RTH, it is necessary to compare the structural and physical properties of THR-MT with that of liganded/unliganded THR-WT. For this purpose, we can perform MD simulations of

each system and analyze root mean square deviation (RMSD), radius of gyration (RG), root mean square fluctuation (RMSF), classical as well as quantum IR spectral density (IRSD), radial distribution function (RDF), solvent accessible surface area (SASA), Ramachandran plots for the dihedral-angle distributions and interaction or internal energies. These types of analysis were performed by Khan *et al.* (2016) to explore the mutational effects in Ras-related protein and by Rajendran *et al.* (2012) to investigate the molecular mechanism of laminopathy due to a point mutation R482W in lamin A/C protein. The SASA calculations of the residues in protein folding and unfolding states ranging from 0-300 $Å^2$ were reviewed by Ausaf Ali *et al.* (2014). The protein stability influenced by buried and surface point mutations are due to physicochemical, energetic, and conformational properties of amino acid residues as reflected by the mutant positions on Ramachandran plots (Gromiha, *et al.*, 1999; Gromiha, *et al.*, 2002; Zou, *et al.*, 2016).

# CHAPTER 3

## MATERIALS AND METHODS

Thyroid disorder patterns with respect to normal thyroid conditions of the patients have been explored from the experimental data analysis. The thyroid status changes in accordance with thyroid hormone levels in blood serum. Euthyroid subjects have normal (T3-bound) THRs, hypothyroid subjects have diseased state THRs due to deficiency of T3/T4 ligands and the subjects with RTH have point mutation(s) in THR-$\beta$ gene. The thyroid functions in the molecular levels are reflected from the structural and thermophysical properties of normal and abnormal THRs which have been studied by MD simulatins.

### 3.1 Thyroid Function Tests and Ultrasonographic Examinations

TFT reports, i.e. FT3, FT4 and TSH in the blood serum of the outpatients were obtained from Department of Biochemistry and thyroid USG examinations of the subjects recommended by TFT evaluations were performed at Department of Radiology, Institute of Medicine, Tribhuvan University Teaching Hospital (TUTH), Maharajgunj, Kathmandu, Nepal during January 2017 to December 2018. The TFT values were measured by the enhanced chemiluminescence immunoassay (ECI) technique using Vitros 3600 machine. About 2-3 mL blood sample was taken from antecubital vein in a plain vial. The sample was allowed to clot and then it was centrifuged at 4000 rpm for 10 minutes to separate serum to be used for TFT measurements. The thyroid USG scan was examined with SAMSUNG UGEO H60 having 7.5 MHz linear transducer. The USG machine was used in the brightness mode to obtain quality scan of the thyroid gland by adjusting frequency, sonation angle and transducer curvature. The patient was placed at supine

position with hyperextended neck and both transverse and longitudinal sections of thyroid lobes were scanned to observe the lobe size, echogenicity, vascularity, cystic lesions, goitrous and nodular masses, and thyroiditis. The lobe dimensions were measured to find its volume using the Equation 1.5. The results obtained from the USG scans were evaluated by the highly experienced radiologists at TUTH and the possibly malignant masses of the thyroid gland were suggested for a biopsy test called as USG guided FNA biopsy. This research was carried out under the ethical consent and approval mentioned in the Subsection 3.1.2.

The data records of the patients having analytical interference with TFTs, impacts of medication, factors confounding the HPT axis response and lack of information, i.e. unknown about entry date or age or sex or one of the TFT values were excluded from this study. A total of 3473 outpatients aged <1 to 93 years enrolled for their TFT measurements during the observation period. The TFTs of these patients were categorized into euthyroid, hypothyroid, hyperthyroid and RTH groups, and the related data were analyzed in order to explore the insights into the thyroid disorders. From physical and/or biochemical evaluations, the endocrinologists suggested for the USG scan of thyroid lobes of some patients. As per the research objectives, the data from thyroid USG examinations of 270 euthyroid and 38 hypothyroid patients were analyzed being associated with liganded and unliganded THR functions. The USG reports were used to determine the prevalence of normal thyroid conditions, goitres, nodules, cysts, echogenicity, vascularity, malignancy and enlarged isthmus. The additional information of the patients such as age, gender, pregnancy, family history, demography, psychology, smoking, alcoholism, feeding and sleeping habits were also noted down during the USG examinations in order to study their impacts on thyroid functions. The laboratory reference ranges for the normal TFTs were 4.26-8.10 pmol/L for FT3, 10.20-28.20 pmol/L for FT4 and 0.46-4.68 mIU/L for TSH. Subclinical hypothyroidism was defined as TSH >4.68 mIU/L with normal FT3 and normal FT4, and overt hypothyroidism as TSH >4.68 mIU/L, FT3 <4.26 pmol/L and FT4 <10.20 pmol/L. Conversely, subclinical hyperthyroidism was defined as TSH <0.46 mIU/L with normal FT3 and normal FT4, and overt hyperthyroidism as TSH <0.46 mIU/L, FT3 >8.10 pmol/L and FT4 >28.20 pmol/L. The patients with TSH ≥4.68 mIU/L, FT3 >4.26 pmol/L and FT4 >10.20 pmol/L were categorized as RTH group. Due to the lack of sufficient information that come only from the genetic tests, a group of 48

patients having possibly RTH has been isolated from the statistical and graphical analysis. However, the impacts of point mutations on the THR-$\beta$ gene reated to the previously identified patients with RTH and goitre were studied by molecular dynamics approach.

### 3.1.1 Data Analysis

The TFT data sets related to the dysfunction states: euthyroidism, hypothyroidism and hyperthyroidism were statistically analyzed along with linear fits between FT3 and FT4, and log-linear fits between ln(TSH) and FT3 or FT4. Also, the non-linear fits and the complex correlations between ln(TSH) and FT4 were analyzed by using four-parameter logistic (4PL) model in hypothyroid and hyperthyroid states on the basis of euthyroidism. The equation of 4PL model suggested by Bortolotto *et al.* (2015) and Azadeh *et al.* (2018) for the ligand binding assay is given by

$$y = A + \frac{B - A}{1 + (x/x_0)^m} \tag{3.1}$$

where $y$ is ln(TSH), $x$ is FT4, $A$ is minimum asymptotic $y$-value or response value for the maximum standard FT4, $B$ is maximum asymptotic $y$-value or response value for the minimum FT4, $x_0$ is inflection point or $x$-value corresponding to half-way between $A$ and $B$, and $m$ is Hill's slope or steepness of the curve. The 4PL curve is sigmoid symmetric in nature.

The euthyroid group having normal USG scans was taken as a control or reference group in order to evaluate the thyroid USG reports and TFTs of the patients. Here, age and gender based mean values, standard deviations and standard errors in the measurements of thyroid size, i.e. left lobe volume (LLV), right lobe volume (RLV) and total gland volume (TGV), and TFT values (FT3, FT4 and TSH) were calculated and they were presented graphically. Statistical and graphical analyses of the related data were carried out using the software packages: Origin-2017 and MS Excel-2007. Along with descriptive statistics and linear regression analysis, t-tests and ANOVA-tests of the related data were performed for finding Pearson's correlation ($r$), coefficient of determination ($R^2$) and calculated probability ($p$-value) in the relevant cases to check the significance of the obtained results. The test results with $p$-value <5% are statistically significant.

### 3.1.2 Ethical Consent and Approval

This research work was performed by the informed consent to each patient under the ethical guidelines provided by and taking authority from Institutional Review Board (IRB), Institute of Medicine (IOM), Tribhuvan University Teaching Hospital (TUTH), Maharajgunj, Kathmandu, Nepal.

## 3.2 Methods of MD Simulations

The initial structures of T3 and/or T4 liganded THR isoforms, i.e. THRT3-$\beta$, THRT3-$\beta$1 and THRT3T4-$\alpha$ were obtained from the x-ray crystallographic protein data bank (PDB) codes: 3GWS.pdb (Nascimento, *et al.*, 2006), 1XZX.pdb (Sandler, *et al.*, 2004) and 4LNX.pdb (Souza, *et al.*, 2014), respectively. Topologies and parameters required to prepare the complete simulated systems were used from the CHARMM force field (MacKerell, *et al.*, 2004; MacKerell, *et al.*, 1998; Zoete, *et al.*, 2011). The ligands (T3 and T4) being the hetero-molecules, they were suitably parameterized to define numerical constants, atomic masses and charges required to evaluate forces and energies (Zoete, *et al.*, 2011). Starting from generation of protein structure files (psf), all the simulations for energy minimization, equilibration and production runs were performed with nanoscale molecular dynamics (NAMD-2.12) (Phillips, *et al.*, 2004). The simulated systems were analyzed with visual molecular dynamics (VMD-1.9.3) (Humphrey, *et al.*, 1996). The softwares used for data analysis and plotting were Xmgrace, Origin-2017 and MS Excel-2007. The details of simulation technique and data analysis for finding the thermophysical properties of normal and diseased state (unliganded or mutated) THRs are explained in the following Subsections 3.2.1-3.2.3 as reported by Lamichhane *et al.* (2018), Lamichhane *et al.* (2019) and Lamichhane *et al.* (2020).

### 3.2.1 Temperature Echoes and Dephasing by THR Dynamics

After generating protein structure files of unliganded thyroid hormone receptor-beta (THR) and T3-liganded thyroid hormone receptor-beta (THRT3), each of these systems was simulated with the same procedures in water-ion environment and then in vacuo by using NAMD to study the physical role of T3 in its receptor proteins by the temperature

echo method. The complete simulation procedures and the related theory are discussed below.

THR and THRT3 were separately solvated forming a droplet having radius 37.48 Å each and it was neutralized with 0.15 mol/L concentration of $Na^+$ and $Cl^-$ ions. The THR and THRT3 droplets consist of 21157 and 21192 atoms, respectively. The system's energy was minimized up to 3000 conjugate gradient (CG) steps. Keeping the temperature fixed at 310 K, the systems were separately equilibrated up to 7 ns under the spherical boundary conditions. The vibrational echoes of protein dynamics are more distinctly observed in anhydrous states than in solution so that the final coordinates of THR and THRT3 were extracted from their equilibrated droplets. The THR and THRT3 structures thus formed were equilibrated in vacuo up to 1 ns at 310 K. The simulation paprameters were configured by adjusting scaling factor for 1-4 coulombic interactions 1.0, electrostatic and van der Waals cut-off distance 12.0 Å, switching distance 10.0 Å and pair list distance 14.0 Å. The simulations were performed by using both constrained vibrations with rigid bonds of H-atoms at 2 fs/step (CVH2) and unconstarined or free vibrations of all atoms at 1 fs/step (FVA1), and the obtained results were compared to know the impact of constrained dynamics in biomolecular simulations. The Langevin piston's temperature was 310 K and the damping coefficient was 1.0/ps. In NAMD simulations,the atomic trajectories are calculated by integating Newton's equations of motion using Verlet algorithm (Verlet, 1996). The nature of RMSD and/or RG curves plotted over the course of MD simulations were analysed to check the degree of conformational stability of THR and THRT3 systems.

Each of the finally prepared THR and THRT3 systems equilibrated in vacuo was then subjected to NVE simulations up to 5 ps by removing the thermostat at 310 K. The temperature autocorrelation function was determined for each system by using Equation 3.6 and it was plotted with respect to the simulation time. The single exponential function best fitted with the autocorrelation function was used to approximate the decay time for both normal and diseased state THRs.

The two methods of echo formation, i.e. temperature quenching and constant velocity replacement were implemented to the equilibrated THR and THRT3 systems under the cases of both CVH2 and FVA1 dynamics in NVE ensemble for the different values of

delay time $\tau$ ranging from 0.1 to 2 ps. From the data sets of 15-20 different simulations, we compared the physical properties such as decay time $\tau_d$, echo depth $\Delta T$, partial heat capacity $C_V$, anharmonicity diffusion coefficient $D_0$ and dephasing time $\tau_0$ between THR and THRT3 in their anhydrous states. The nature of echo feature curves in temperature and energy were also compared under the harmonic approximation (Equation 3.7). The graph of echo depth *vs* delay time was used to obtain the dephasing time. The dephsaing of normal modes of vibration in the liganded and unliganded receptors was observed under CVH2 and FVA1 cases.

In the echo-time zone, the internal energy terms, i.e. bonding and non-bonding potentials were plotted and analysed for THR and THRT3 in both CVH2 and FVA1 cases. Since these are the temperature changing phenomena, the variation of RG w.r.t. $N_H$ (number of H-bonds) was also plotted to know the conformational changes in the T3 dependent nuclear receptors. During the echo formation, the molecular system suffers from the large range of temperature variation. The rate of change of internal potential energy with temperature yields partial heat capacity $C_V$. The simulations were repeated three times using NAMD protocols and the correctness of the results were tested in all cases of THR and THRT3 systems.

The mathematical formulations associated with MD simulations and data analysis for evaluating echo features, vibrational dephasing and heat capacity change under the constrained and unconstrained dynamics of normal and diseased state THRs have been discussed below.

During MD simulations of the complex biomolecular systems, each atom acts as a harmonic oscillator and the coherence of normal mode vibrations can be probed with a second signal such as temperature quenching leading to the resonance called echo. The magnitude of echo depth depends on the delay time, the time interval between synchronization signal and probing signal. Asssociated with $i^{th}$ normal mode under harmonic approximation of atomic particle having mass $m$, angular frequency $\omega_i = 2\pi f_i$, amplitude $a_i$ and phase constant $\delta_i$; the displacement equation is given by

$$y_i(t) = a_i cos(\omega_i t + \delta_i) \tag{3.2}$$

The rate of change of atomic displacement gives its linear momentum, i.e.

$$p_i(t) = m_i \frac{dy_i(t)}{dt} = -m_i a_i \omega_i sin(\omega_i t + \delta_i) \tag{3.3}$$

Hamiltonian of the particle in its $i^{th}$ normal mode is the sum of kinetic and potential energies, i.e.

$$H_i = \frac{p_i^2}{2m_i} + \frac{1}{2} m_i \omega_i^2 y_i^2 \tag{3.4}$$

Here, the time evolution of kinetic energy of the whole system having $N$ atoms at absolute temperature $T(t)$ is written as

$$E_k(t) = \frac{(3N-6)K_B T(t)}{2} = \sum_i \frac{p_i^2}{2m_i} = \sum_i \frac{1}{2} m_i a_i^2 \omega_i^2 sin^2(\omega_i t + \delta_i) \tag{3.5}$$

where $K_B$ is Boltzmann constant. In NVE simulations, the normalized autocorrelation function in terms of kinetic energy or temperature (Schulten, *et al.*, 1997) is defined by

$$C_{T,T}(t) = \frac{\langle E_k(t) E_k(0) \rangle - \langle E_k(0) \rangle^2}{\langle [E_k(t)]^2 \rangle - \langle E_k(0) \rangle^2} = \frac{\langle T(t) T(0) \rangle - \langle T(0) \rangle^2}{\langle [T(t)]^2 \rangle - \langle T(0) \rangle^2} \tag{3.6}$$

After substituting the values of $E_k(t)$ and $E_k(0)$ from Equation 3.5 in Equation 3.6 and using the averaging technique as performed by Xu *et al.* (1995), we get

$$C_{T,T}(t) = \frac{\sum_i m_i^2 a_i^4 \omega_i^4 cos(2\omega_i t)}{\sum_i m_i^2 a_i^4 \omega_i^4} = \langle cos(2\omega_i t) \rangle_i \tag{3.7}$$

where the $\langle .... \rangle_i$ refers to the averaging over all the normal modes or the degrees of freedom $(3N-6)$ in unconstrained dynamics of the protein-hormone systems. The oscillatory function $C_{T,T}(t)$, having initial value $C_{T,T}(0) = 1$, can be approximated with a single exponential function: $C_{T,T}(t) \approx e^{-t/\tau_d}$ to obtain its decay time $\tau_d$. The function $C_{T,T}(t) \approx 0$ for $t >> \tau_d$.

The atomic velocities are reassigned twice for the echo formation. At the synchronizing signal, the first reassigned velocity related to $i^{th}$ normal mode is $v_i(0) = \lambda_1 u_i$. At the probing signal applied after some delay time $(\tau)$, the second reassigned velocity is $v_i(\tau) = \lambda_2 u_i$ which probes the phase coherent state and then resonance or echo is observed. Here, $\lambda_1$ and $\lambda_2$ are the velocity multipliers that depend on temperature. For the given equilibrium temperature $T_0$, the temperatures of the system during the first and second

velocity reasssignments are: $T_1 = \lambda_1^2 T_0$ and $T_2 = \lambda_2^2 T_0$. We can define three cases of echo formation: (a) temperature quench echo for $\lambda_1 = \lambda_2 = 0$ or $T_1 = T_2 = 0$, (b) constant velocity replacement echo for $\lambda_1 = \lambda_2 = 1$ or $T_1 = T_2 = T_0$ and (c) velocity replacement echo for $\lambda_1 \neq \lambda_2 \neq 1$. Depending on this theory of velocity reassignment, Xu *et al.* (1995) and Schulten *et al.* (1997) derived an expression for the temperature response function (Equation 3.8) of the biomolecular system under harmonic approximation at $t \geq \tau >> \tau_d$.

$$T(t) \approx T_0 \left[ \frac{1 + \lambda_1^2 + 2\lambda_2^2}{4} - \frac{1 + \lambda_1^2 - 2\lambda_2^2}{4} C_{T,T}(T - \tau) - \frac{\lambda_1 \lambda_2}{2} C_{T,T}(|t - 3\tau/2|) - \frac{1 - \lambda_1^2}{8} C_{T,T}(|t - 2\tau|) \right] \tag{3.8}$$

In the right side of Equation 3.8, first term refers to new average temperature and second term refers to recovery temperature after the second velocity reassignment at t = $\tau$, third term refers to $\frac{3\tau}{2}$-pulse related to case-b or c, and fourth term refers to $2\tau$-pulse related to case-a. The related echo depths are: $\Delta T(3\tau/2) = \frac{T_0}{2}\lambda_1\lambda_2$ and $\Delta T(2\tau) = \frac{T_0}{8}(1 - \lambda_1^2)$.

The temperature quench echo occurs for $\lambda_1 = \lambda_2 = 0$ so that the echo temperature in terms of the correlation function (Equation 3.8) becomes

$$T(t) \approx \frac{T_0}{4} \left[ 1 - C_{T,T}(t - \tau) - \frac{1}{2} C_{T,T}(|t - 2\tau|) \right] \tag{3.9}$$

These harmonic approximations result in estimating the depth of temperature quench echo $\Delta T(2\tau) = T_0/8$ and the depth of constant velocity replacement echo $\Delta T(3\tau/2) = T_0/2$ which are independent of delay time $\tau$. However, in real practice, the anharmonic interactions effect on $\Delta T$ so that it is a function of $\tau$. The anharmonicity arises due to coulombic, torsional and van der Waals interactions among the atomic particles during MD simulations of the complex systems. According to Xu *et al.* (1995), $\Delta T(\tau)$ decays exponentially with delay time $\tau$ as given in Equation 3.10 where $\Delta T_0$ is the initial maximum value and $\tau_0$ is the dephasing time.

$$\Delta T(t) = \Delta T_0 e^{-\tau/\tau_0} \tag{3.10}$$

In NVE simulations, the total energy remains constant throughout the time evolution of kinetic temperature, i.e. $E_k(t) + U(t) = E_{\text{tot}} \approx$ constant. Thus, the echo depth in temperature results the echo depth in kinetic energy and hence in potential energy, i.e.

$\Delta E_k(t) \approx -\Delta U(t)$. Furthermore, a partial heat capacity of a thermodynamic system is defined by two ways in NVE ensemble, i.e. $C_{V1}$ from the temperature rate of change of kinetic energy and $C_{V2}$ from the temperature rate of change of potential energy as given in Equation 3.11.

$$C_{V1} = \left(\frac{\partial E_k}{\partial T}\right)_{N,V,E} \approx -\left(\frac{\partial U}{\partial T}\right)_{N,V,E} = C_{V2} \tag{3.11}$$

For the CVH2 simulations, the constrained degrees of freedom for the rigid H-atoms is $N_C$ (say) under which the kinetic energy is expressed as

$$E_k(t) = \left(\frac{3N - N_C - 6}{2}\right) K_B T(t) \tag{3.12}$$

In the case of FVA1 simulations, $N_C = 0$. From Equations 3.11 and 3.12, the echo depths in kinetic energy and temperature are related as

$$\Delta E_k(t) = \left(\frac{3N - N_C - 6}{2}\right) K_B \Delta T(t) = C_{V1} \Delta T(t) \tag{3.13}$$

Here, the heat capacity defined from kinetic energy in terms of internal degrees of freedom is $C_{V1} = \left(\frac{3N-N_C-6}{2}\right) K_B$. The heat capacity $C_{V2}$ defined from internal potential energy slightly changes in the temperature echo zone where the large temperature difference can be observed. It is an evidence for the temperature dependance of the heat capacity. In protein complexes, U(t) comprises the energy terms such as electrostatic, van der Waals, bond, angle, dihedral and improper energies. The heat capacity components can be separated in terms of different physical contributions such as bonding and non-bonding potentials, folding and unfolding states, solvent interactions and protein-ligand interactions (Prabhu, *et al.*, 2005; Gomez, *et al.*, 1995). Here, $C_{V2}$ calculation is responsible for the temperature dependance of internal energy of THR or THRT3 in its native globular form. From the Equations 3.10 and 3.13, we find that

$$\Delta E_k(t) = C_{V1} \Delta T(t) = C_{V1} \Delta T_0 e^{-\tau/\tau_0} = \Delta E_{k0} e^{-b_0 \tau} \tag{3.14}$$

where $b_0$ is a damping coefficient of vibrational echoes which arises due to the anharmonicity in MD simulations. The fluctuating frictional forces make the phase coherent states dephase with delay time. This principle is used to study the energy transfer mechanism in MD simulations of the complex biomolecular systems (Fujisaki, *et al.*,

2006). The anharmonicity diffusion $D_i$ and mobility $\mu_i$ in the $i^{th}$ normal mode of vibration are related by Einstein's diffusion equation: $D_i = \mu_i K_B T$. As derived by Xu *et al.* (1995), the echo depth at $t = 2\tau$ is written as

$$\Delta T(\tau) \approx \frac{T_0}{8}\langle e^{-3\mu_i K_B T_0 \tau}\rangle_i = \frac{T_0}{8}\langle e^{-3D_i\tau}\rangle_i = \Delta T_0 \langle e^{-3D_i\tau}\rangle_i \tag{3.15}$$

If the constant $D_i$ is the same value $D_0$ for each normal mode, the echo depth is expressed as

$$\Delta E_k(\tau) = C_{V1}\Delta T(\tau) \approx C_{V1}\Delta T_0 e^{-3\mu_0 K_B T_0 \tau} = \Delta E_{k0} e^{-3D_0\tau} \tag{3.16}$$

Finally, dephasing time $\tau_0$, anharmonic diffusion constant $D_0$ and mobility constant $\mu_0$ are related as

$$D_0 = \frac{1}{3\tau_0} = \frac{b_0}{3} = \mu_0 K_B T_0 \tag{3.17}$$

The Equation 3.16 can be written as a straight line equation, i.e.

$$ln(\Delta E_k) = A - b_0\tau \tag{3.18}$$

By fitting the straight line (Equation 3.18) with the $ln(\Delta E_k)$ *vs* $\tau$ graph plotted from the results of MD simulations, the heat capacity $C_{V1}$ is determined from the intercept: $A = ln(C_{V1}\Delta T_0)$, and the constants $b_0$, $D_0$ and $\tau_0$ are obtained from the slope.

### 3.2.2 Heat Conduction by THR Isoforms

First of all, each of the unliganded and the T3 and/or T4 liganded nuclear receptors, i.e. THR-$\beta$, THRT3-$\beta$, THRT3-$\beta$1 and THRT3T4-$\alpha$ was solvated explicitly with TIP3P-water and neutrallized with $Na^+$ and $Cl^-$ ions in 0.15 mol/L concentrations under the spherical boundary conditions. Thus formed nanodroplets had radii of 37.48, 36.99 and 31.29 Å for THR-$\beta$ or THRT3-$\beta$, THRT3-$\beta$1 and THRT3T4-$\alpha$, respectively. Here, a part of the free strand including residues 145-156 of THRT3T4-$\alpha$ was omitted to make its simulations more stable and faster. Using the NAMD protocols and the parametric conditions as stated in the Subsection 3.2.1, each of these nanodroplets was subjected to energy minimization up to 5000 CG steps and equilibration up to 20 ns at 310 K under CVH2 conditions. The production runs were performed up to 2 ns for each nanodroplet

in the canonical ensemble at 310 K. The RMSD and RG plots were used to test their conformational stability over the course of simulations. The slightly fluctuating internal energy of the system was used to obtain its ensemble averaged values $\langle U \rangle$, $\langle U \rangle^2$ and $\langle U^2 \rangle$. Then, the heat capcity $C_V$ of each droplet was determined by using the principle of energy fluctuations (Equation 3.20).

Again, each of unliganded THR-$\beta$ and T3 liganded THRT3-$\beta$ was solvated fully with TIP3P-water and neutrallized with $Na^+$ and $Cl^-$ ions in 0.15 mol/L concentration under the periodic boundary conditions forming a water-box of cell basis vectors 50.36, 60.92 and 74.78 Å. Thus prepared systems were geometrically optimized up to 3000 CG steps and then equilibrated up to 2 ns each at five different constant temperatures 300, 305, 310, 315 and 320 K under CVH2 conditions. Here, the parametric conditions implemented for MD simulations, i.e. force field and integrator parameters, Langevin temperature and pressure were configured as stated in the Subsection 3.2.1. From the equilibrated structures of THR-$\beta$ and THRT3-$\beta$ in the last 0.5 ns simulation, the mean internal energy $\langle U \rangle$ of each system was observed at the five different temperatures. The partial heat capacity $C_V$ of a mixture of THR-$\beta$ or THRT3-$\beta$, water and ions was determined at 310 K from the slope of $\langle U \rangle$ *vs* $T$ straight line. Thus found $C_V$ was compared with that obtained by energy fluctuations of the related syatem under spherical boundary conditions. By the same procedure, the partial heat capacity $C_V^W$ of a neutral water-ion box was determined at 310 K. The neutral water-ion box had the cell basis vectors 30, 45 and 60 Å. For the CVH2 case, $C_V^W$ is contributed only by the non-bonding (electrostatic and van der Waals) energy terms. Finally, the partial specific heats $c_V^p$ of the unliganded and liganded THR isoforms were obtained by using the method of mixture or the principle of mole fraction (Equation 3.21) and the results were compared to understand the heat conduction role of thyroid hormones in their nuclear receptors.

In order to determine the heat diffusivity and hence thermal conductivity of the THR isoforms, the final coordinates of the nanodroplets were extracted from their equilibrated structures at 310 K. Since heat flows from higher to lower temperature region, we set the temperature of the outer shell of thickness $\Delta r$ at $T_f$ = 200 K and that of the inner sphere having radius $R$ at $T_i$ = 310 K. In THR-$\beta$ or THRT3-$\beta$, THRT3-$\beta$1 and THRT3T4-$\alpha$; the sets of $(R, \Delta r)$ are (33, 4.48), (33, 3.99) and (27, 4.29) in Å scale, respectively. Then, MD simulations were performed with free vibrations of all atoms to observe the temperature

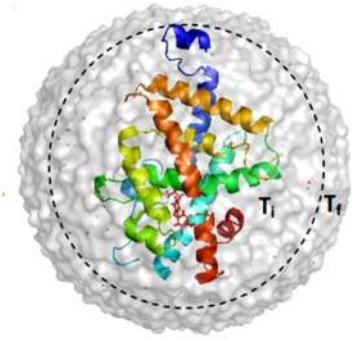


**Figure 9:** THRT3-$\beta$ nanodroplet modelled with inner sphere having temperature $T_i$ and outer shell having temperature $T_f$ where $T_i > T_f$ for thermal diffusion during MD simulations

relaxation in each system. The cooling process was completed in 20 ps. The simulated temperature *vs* time graph was fitted with the theoretical expression of cooling curve (Equation 3.23) to obtain thermal diffusivity $D$ of the related system. Finally, thermal conductivity $k$ was determined using Equation 3.24 and the results of $c_V^p$, $D$ and $k$ were compared for each of the given THR isoforms. The theories, on which the calculations of heat conduction paramaters depend, have been discussed below.

The internal energy $U$ of the biomolecular system comprises the energy terms $U_i$ such as angle, bond, dihedral, van der Waals, electrostatic, improper and cross-terms related to the CHARMM potential function. The terms $U_i$ depend on temperature, any perturbation, mutation and liganded or unliganded forms of THRs. The mean energy $E$ is defined by the ensemble averaged value of $U$ (Prabhu, *et al.*, 2005), i.e.

$$E = \langle U \rangle = \sum_{i=1}^{N} \langle U_i \rangle = \sum_{i=1}^{N} E_i \tag{3.19}$$

Here, each of the terms $\langle U_i \rangle$ contributes partial heat capacity. The internal energy of the equilibrated system slightly fluctuates during its simualtion in NVT ensemble. The principle of energy fluctuations can be used to obtain the partial heat capacity in canonical ensemble as given by Equation 3.20 (Nosé, 1984; Prabhu, *et al.*,2005).

$$C_V = \frac{dE}{dT} = \frac{d\langle U \rangle}{dT} = \frac{\langle \delta U^2 \rangle}{K_B T^2} = \frac{\langle U^2 \rangle - \langle U \rangle^2}{K_B T^2} = m c_V \tag{3.20}$$

where $\langle U \rangle$ is the mean energy, $m$ is the mass and $c_V$ is the partial specific heat capacity of the system, and $\mathrm{K_B} = 0.00198657\ \mathrm{kcal\ mol^{-1} K^{-1}}$ is Boltzmann constant. The heat capacity of a complex biomolecule is influenced by the additional terms such as protein-folding

and unfolding states, polar and apolar hydration, protein-ligand interactions, H-bonding and conformational entropy. The THR-nanodroplet is a mixture of protein-hormone system, water and ions so that the specific heats of these constituents are related by a mole-fraction fromula (Suurkuusk, 1974; Yang, *et al.*, 1979). Under thermal equilibrium of the mixture in NVT ensemble, $Mc_V = M_p c_V^p + M_w c_V^w$ where M is mass, 'p' stands for protein+ligands and 'w' stands for water+ions. Then, the partial specific heat capacity $c_V^p$ of a THR-isoform in solution is obtained from Equation 3.21.

$$c_V^p = \frac{Mc_V - M_w c_V^w}{M_p} \tag{3.21}$$

According to the linear response theory, thermal gradient is developed into a complex biomolecule by some perturbation and heat transport occurs until its equilibrium state arises from the non-equilibrium phase. In case of the THR-nanodroplets, temperature relaxation occurs from the internal sphere to the outer shell so that the local temperature $T$ is a functon of both position $r$ and time $t$. The heat diffusion equation governing the temperature relaxation across the modelled sphere-shell boundary (Figure 9) is given by

$$\frac{\partial T(r,t)}{\partial t} = D\nabla^2 T(r,t) \tag{3.22}$$

where $D$ is thermal diffusion constant. The boundary conditions that can be implemented to solve the Equation 3.22 are: $T(r,0) = T_i$ for $r < R$, and $T(r,t) = T_f$ for $r > R$ provided that $T_i > T_f$. Then, using the approach of average temperature over the droplet volume by removing the spatial dependence, a solution to the heat diffusion equation 3.22 (Lervik, *et al.*, 2009) can be expressed as

$$\langle T(r,t)\rangle_V = T(t) = T_f + 6\frac{T_i - T_f}{\pi^2}\sum_{n=1}^{\infty}\frac{1}{n^2}exp\left[-\left(\frac{n\pi}{R}\right)^2 Dt\right] \tag{3.23}$$

The best fitted $T(t)$ *vs* $t$ curve with the simulated data results thermal diffusivity $D$ while cooling the system (Figure 9) within the temperature range $T_i$ to $T_f$. Thermal conductivity $k$ is equal to the multiplication of density $\rho$, specific heat capacity $c_V$ and heat diffucion coefficient $D$ at the known temperature $T$ of the biomolecular system, i.e.

$$k = \rho c_V D \tag{3.24}$$

### 3.2.3 Point Mutations in THR-Beta and Structural Analysis

From the wild type (WT) native structure of T3-liganded thyroid hormone receptor-beta (THRT3-WT), the mutated (MT) nuclear receptor (THRT3-MT) was prepared after the point mutation L330S on 330-codon replacing LEU by SER with the help of PyMOL-Mutagenesis. Each of the systems, i.e. unliganded THR-WT, THRT3-WT and L330S-mutant THRT3-MT was solvated with 17220 water molecules (TIP3P) forming a water-sphere which was neutralized with $Na^+$ and $Cl^-$ ions in the concentration of 0.15 mol/L as explained in the Subsections 3.2.1 and 3.2.2. Each water-sphere had the boundary conditions of radius 37.48 Å, centre coordinates (4.14, 25.05, 20.60 Å), and force constant 10 kcal $mol^{-1}Å^{-2}$ and exponent 2 for the first potential to be applied. The tool command language (TCL) script file called configuration file was prepared to provide the simulation details. As stated earlier, the Langevin piston temperature is 310 K and damping coefficient is 1 $ps^{-1}$. The Langevin dynamics (Feller, *et al.*, 1995; Bussi, *et al.*, 2007) was implemented for the CVH2 case of NAMD simulations. Multilevel summation method (MSM) was active with the grid spacing of 2.5 Å for the electrostatic force evaluation (Hardy, *et al.*, 2015). In order to evaluate the electrostatic and van der Waals interactions, the force field related terms such as 1-4 scaling, cut-off, switching and pair-list distances were set as 1.0, 12 Å, 10 Å and 14 Å, respectively. Then, the energy of each system was minimized up to 3000 CG steps and its equilibration run was performed up to 20 ns at the body scale temperature 310 K. The new trajectories of the constituent atoms were calculated by using the velocity Verlet algorithm (Verlet, 1967).

The conformational changes in the unliganded, the T3-liganded and the mutated THR-$\beta$ were analyzed from the nature of RMSD, RG, RMSF and SASA plots related to their protein-backbone, T3-hormone and residues of interest, i.e. L330 and L330S. Ramachandran plots were used to observe the distributions of dihedral angles and the possible steric hindrances among $\alpha$-helices, $\beta$-sheets, side chains and residues during the MD simulations. With the help of NAMD Energy Plugin (Version 1.4), the interaction energies (coulombic and van der Waals) between the native or mutated residues on the 330 codon and T3-hormone were observed in the related system. Furthermore, $N_H$

distribution, RDF, IRSD and internal energy of T3 and L330 codons were analyzed in both wild type and mutated systems (Lamichhane, *et al.*, 2020). By the same procedure, the results of I431V mutational impacts on THR-$\beta$ LBD were also compared with its wild type. The results of I431V mutation on THR-$\beta$ by using NAMD simulations under the periodic boundary conditions have been reported by Lamichhane *et al.* (2019).

# CHAPTER 4

## RESULTS AND DISCUSSION

Thyroid functions are very complex biological phenomena regulated by the endocrine systems. Thyroid disorders are basically diagnosed by TFT evaluations and the nature of thyroid gland abnormalities are identified by USG examinations. The results obtained from the normal thyroid analysis are important for evaluating thyroid dysfunction states in the patients. Euthyroidism, hypothyroidism and RTH are thyroid disorders associated with T3 sufficient, deficient and obstructed states in peripheral cells as the results of liganded, unliganded and mutated THRs, respectively. Based on these facts, the results drawn from the clinical analysis of normal and abnormal thyroid conditions are discussed in the Sections 4.1-4.3. As the molecular insights into the thyroid disorders, structural and thermophysical properties of liganded, unliganded and mutated THRs by using MD simulations are discussed in the Sections 4.4-4.6

### 4.1 Prevalence of Thyroid Disorders and Thyroid Hormones-Thyrotropin Inter-relationships in Thyroid Dysfunction States

In a total of 3425 subjects involved in TFT analysis of thyroid disorders, there is a prevalence of 70.45% (665M + 1748F) euthyroid with normal TFTs, 18.95% (164M + 485F) subclinical hypothyroid, 3.30% (29M + 84F) overt hypothyroid, 5.11% (46M + 129F) subclinical hyperthyroid and 2.19% (17M + 58F) overt hyperthyroid patients. As reflected by Figure 10, females (F) are found to be more vulnerable of thyroid disorders than males (M) which was also concluded in the previous studies (Sawin, *et al.*, 1979; Manji, *et al.*, 2006; Fade, *et al.*, 1991). Here, the patients are suffering more from hypothyroidism than from hyperthyroidism as reported by Aoki *et al.* (2007) and Canaris

*et al.* (2000). The descriptive statistics, i.e. mean, standard deviation (SD), minimum and maximum values of age, TSH, FT4 and FT3 for all data sets are depicted in Table 1.

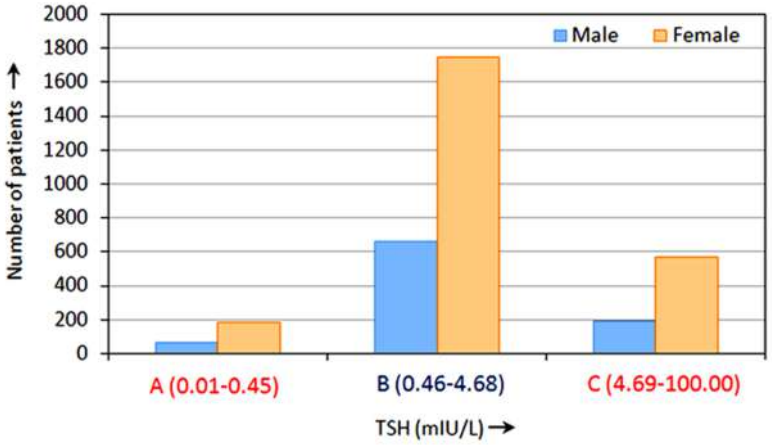


**Figure 10:** Prevalence of A: hyperthyroidism, B: euthyroidism and C: hypothyroidism in males and females evaluated from TSH levels

By the normal thyroid analysis of euthyroid subjects aged 35.94 ± 16.47 years, the mean ± SD of TSH, FT4 and FT3 are 2.30 ± 0.98 mIU/L, 14.17 ± 2.82 pmol/L and 5.47 ± 0.83 pmol/L, respectively which act as the new reference levels of TFTs used for the clinical evaluations of thyroid disorders. The subclinical hypothyroidism appears with the average values of TSH, FT4 and FT3 as 7.62± 3.74 mIU/L, 13.53 ± 3.03 pmol/L and 5.38 ± 0.88 pmol/L, respectively in the mean age of 38.49 ± 17.37 years. The overt hypothyroidism appears mainly in the higher age, i.e. 43.32 ± 18.33 years with the elevated TSH of 56.23 ± 37.42 mIU/L along with the suppressed FT4 of 5.02 ± 3.17 pmol/L and FT3 of 3.10 ± 34.20 pmol/L. The subclinical hyperthyroid patients have the suppressed TSH of 0.15 ± 0.14 mIU/L including normal FT4 of 17.15 ± 3.97 pmol/L and FT3 of 6.04 ± 1.14 pmol/L in the mean age of 43.03 ± 19.17 years. The overt hyperthyroidism appears in the mean age of 37.04 ± 12.37 years with the highly suppressed TSH of 0.02 ± 0.03 mIU/L along with the elevated FT4 as 53.37 ± 21.03 pmol/L and FT3 as 20.22 ± 9.52 pmol/L. Each of the TFTs has $p$ <0.001 over the different groups(Table 1). Our observations show that the chances of being overt or extreme thyroid disorder is lower in the infant age than in the higher age as explained in the earlier studies (Prisant, *et al.*, 2006; Mariotti, *et al.*, 1997; Van Boxtel, *et al.*, 2004). Most of the children suffer from congenital thyroid dysfunction and the adults suffer from autoimmune thyroiditis, cardiac failure by thyrotoxicosis with hypertension, thyroid nodules, cysts, vascularity, hypo-and

hyperechoic leisons and diffused or toxic goitre as reported by Rabbiosi *et al.* (2013). The details of USG and TFT analysis of underactive thyroid are in Section 4.3.

**Table 1:** Descriptive statistics of age(year), TSH(mIU/L), FT4(pmol/L) and FT3(pmol/L) in normal and abnormal thyroid conditions of 3425 patients where ANOVA single factor of each TFT is $p$ <0.001 over the different groups

| Thyroid status | Values | Age | TSH | FT4 | FT3 | N |
|---|---|---|---|---|---|---|
| Euthyroidism | Mean | 35.94 | 2.30 | 14.17 | 5.47 | 2413(70.45%) (665M+1748F) |
| | SD | 16.47 | 0.98 | 2.82 | 0.83 | |
| | Min | 0.50 | 0.47 | 10.10 | 4.20 | |
| | Max | 93.00 | 4.68 | 28.20 | 8.10 | |
| Subclinical-hypothyroidism | Mean | 38.49 | 7.62 | 13.53 | 5.38 | 649(16.80%) (164M+485F) |
| | SD | 17.37 | 3.74 | 3.03 | 0.88 | |
| | Min | 0.01 | 4.70 | 10.10 | 4.10 | |
| | Max | 92.00 | 35.30 | 28.00 | 8.20 | |
| Overt-hypothyroidism | Mean | 43.32 | 56.23 | 5.02 | 3.10 | 113(2.92%) (29M+84F) |
| | SD | 18.33 | 37.42 | 3.17 | 0.89 | |
| | Min | 2.00 | 4.72 | 0.88 | 1.20 | |
| | Max | 84.00 | 100.00 | 10.10 | 4.20 | |
| Subclinical-hyperthyroidism | Mean | 43.03 | 0.15 | 17.15 | 6.05 | 175(4.53%) (46M+129F ) |
| | SD | 19.17 | 0.14 | 3.97 | 1.14 | |
| | Min | 0.16 | 0.01 | 10.10 | 4.10 | |
| | Max | 92.00 | 0.45 | 27.70 | 8.10 | |
| Overt-hyperthyroidism | Mean | 37.04 | 0.02 | 53.37 | 20.22 | 75(1.94%) (17M+58F) |
| | SD | 12.37 | 0.03 | 21.03 | 9.52 | |
| | Min | 14.00 | 0.01 | 28.50 | 8.65 | |
| | Max | 73.00 | 0.26 | 90.00 | 35.00 | |

FT3 and FT4 have stronger linear relationship (positive correlation) in overt hypothyroidism ($r$ = 0.66, $p$ <0.001) and in overt hyperthyroidism ($r$ = 0.91, $p$ <0.001) than in subclinical hypothyroidism ($r$ = 0.21), subclinical hyperthyroidism ($r$ = 0.10) and euthyroidism ($r$ = 0.11). The positive slope of linear fit in FT3 *vs* FT4 also increases from euthyroidism to overt hypothyroidism and to overt hyperthyroidism as depicted in Table 2. The larger slope in the overt hyperthyroidism means that the lesser amount of FT4 is converted into FT3 during the local deiodination. In the overt thyroid dysfunction, the extreme values of TSH are taken to be 0.01 and 100 mIU/L. While studying the log-linear relationship between TSH and FT4 or FT3, the coefficients of the best linear fit in ln(TSH) *vs* FT4 (or FT3) are analyzed. We find the significantly negative correlation ($r$ = -0.75, $p$ <0.001 in ln(TSH) *vs* FT4 and $r$ = -0.52, $p$ <0.06 in ln(TSH) *vs* FT3) in case of overt hypothyroidism, but no significant correlations with $p$-value ranging from <0.001 to 0.72 in other cases as presented in Table 2. This result emphasizes the non-linear

relationship between TSH and FT4 (or FT3). The underlying factors controlling the expression of body function develop the non-linear relationship between TSH and FT4. The related contributing factors are age, sex, body-mass index, HPT-axis, thyroid and non-thyroid illness, genetics, environmental factors, depression, anxiety and medications (Hoermann, *et al.*, 2014; Bacci, *et al.*, 1982; Engum, *et al.*, 2002; Bunevicius, *et al.*, 2010). The TSH-centered TFT reflects thyroid status in different pathophysiological and physiological conditions.

**Table 2:** Coefficients of linear fit: $y = ax + b$ among the variables $log_e$ of TSH (mIU/L), FT3 (pmol/L) and FT4 (pmol/L) in euthyroidism, hypothyroidism and hyperthyroidism included with standard errors in slope and intercept, and $p$-value from F-test

| Thyroid status | Values | ln(TSH) *vs* FT4 | ln(TSH) *vs* FT3 | FT3 *vs* FT4 |
|---|---|---|---|---|
| Euthyroidism (N = 2413) | Slope(a) | -0.02±0.003 | -0.02±0.01 | 0.03±0.006 |
| | Intercept(b) | 0.99±0.05 | 0.84±0.06 | 5.00±0.08 |
| | Pearson's *r* | -0.11 | -0.03 | 0.11 |
| | *p*-value | <0.001 | 0.06 | <0.001 |
| Subclinical-hypothyroidism (N = 649) | Slope(a) | -0.005±0.004 | -0.04±0.02 | 0.06±0.01 |
| | Intercept(b) | 2.02±0.06 | 2.16±0.08 | 4.56±0.15 |
| | Pearson's *r* | -0.04 | -0.10 | 0.21 |
| | *p*-value | 0.26 | 0.013 | <0.001 |
| Overt-hypothyroidism (N = 113) | Slope(a) | -0.23±0.02 | -0.56±0.09 | 0.18±0.02 |
| | Intercept(b) | 4.84±0.11 | 5.40±0.29 | 2.17±0.12 |
| | Pearson's *r* | -0.75 | -0.51 | 0.66 |
| | *p*-value | <0.001 | 0.06 | <0.001 |
| Subclinical-hyperthyroidism (N = 175) | Slope(a) | -0.05±0.02 | -0.46±0.08 | 0.03±0.02 |
| | Intercept(b) | -1.79±0.46 | 0.21±0.52 | 5.53±0.38 |
| | Pearson's *r* | -0.13 | -0.38 | 0.10 |
| | *p*-value | 0.07 | <0.001 | 0.17 |
| Overt-hyperthyroidism (N = 75) | Slope(a) | 0.002±0.003 | 0.003±0.007 | 0.41±0.02 |
| | Intercept(b) | -4.44±0.19 | -4.40±0.16 | -1.79±1.25 |
| | Pearson's *r* | 0.07 | 0.04 | 0.91 |
| | *p*-value | 0.56 | 0.72 | <0.001 |

The non-linear equation of 4PL model representing ln(TSH) *vs* FT4 curve including all the data sets of euthyroidism, subclinical hypothyroidism and overt hypothyroidism is given by

$$\ln(\text{TSH}) = 0.81 + \frac{4.20 - 0.81}{1 + (\text{FT4}/8.73)^{5.96}} = 0.81 + \frac{3.39}{1 + (\text{FT4}/8.73)^{5.96}} \qquad (4.1)$$

Comparing with Equation 3.1 and including standard errors in the coefficients, we write the minimum asymptote $A = 0.81 \pm 0.08$ responding maximum FT4 = 28.20 pmol/L, the maximum asymptote $B = 4.20 \pm 0.12$ responding minimum FT4 = 0.88 pmol/L,

inflection point $x_0$ = 8.73 ± 0.30 pmol/L, and Hill's slope $m$ = 5.96 ± 1.07. This non-linear fit is symmetric with the nature of sigmoid curve fitting (Hoermann, *et al.*, 2010; Abraham-Nordling, *et al.*, 2008) and it has stronger correlation ($R^2$ = 0.97 and $p$ <0.001) than the log-linear fit ($r$ = - 0.41 and $p$ <0.001). The second term in the right side of Equation 4.1 appears from the effect of hypothyroidism. The log-linear fit related to Figure 11 has the negative slope -0.10 ± 0.004 and y-intercept 2.51 ± 0.06 with $r$ = -0.41 that indicates the negative feedback mechanism of thyroid hormones into hypothalamus and pituitary, and controlled production of TSH.

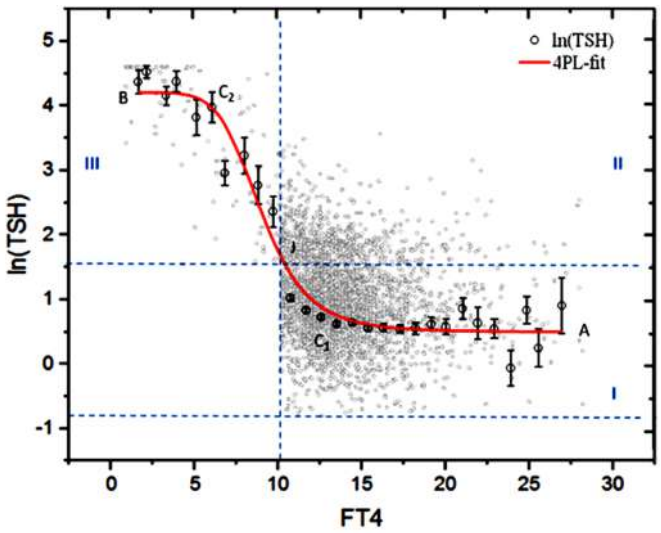


**Figure 11:** Non-linear relations between TSH (mIU/L) and FT4 (pmol/L) when patients (885M + 2317F) suffer from euthyroidism (I) to subclinical(II) and overt (III) hypothyroidism. The 4PL curve has $R^2$ = 0.97 fitted along the mean data points of FT4 bins (1 pmol/L) shown with error bars (SE) in TSH

The interesting thing is that the non-linear curve (Figure 11) passes through the junction point J of euthyroid region, subclinical hypothyroid region and overt hypothyroid region. The point J can be taken as the turning point of normal to abnormal thyroid function and vice-versa. The patients suffering from overt hypothyroidism should have the history of changing TSH and FT4 through the curve $C_1JC_2$. Almost constant TSH along $AC_1$ represents clinically euthyroidism, the curvature $C_1J$ arises due to subclinical hypothyroidism, $JC_2$ demonstrates the biochemically degrading thyroid towards overt hypothyroidism and $C_2B$ shows FT4 falling to zero at almost constant but the highest TSH above 100.00 mIU/L.

In Figure 12, the best fitted 4PL curve in $\log_e$(TSH) *vs* FT4 gets steepness from euthyroid to subclinical hyperthyroid and to overt hyperthyroid regions of the data points. The

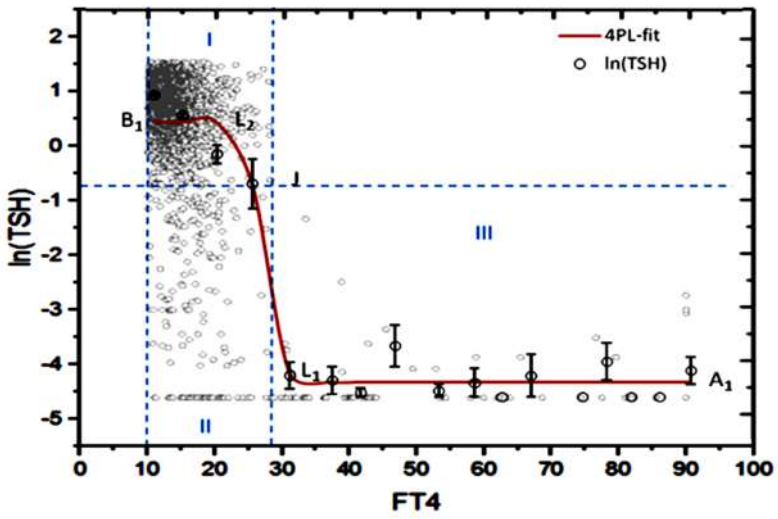


**Figure 12:** Non-linear relations between TSH (mIU/L) and FT4 (pmol/L) in the patients (728M + 1935F) suffering from euthyroidism(I) to subclinical(II) and overt (III) hyperthyroidism. The 4PL curve has $R^2$ = 0.97 fitted along the mean data points of FT4 bins (5 pmol/L) shown with error bars (SE) in TSH

enhanced correlation ($R^2$ = 0.97 for the logistic model) from the linear fit ($r$ = - 0.58) with $p$ <0.001 emphasizes the non-linear relationship between TSH and FT4 in the patients suffering from euthyroidism to hyperthyroidism. In this logistic curve (Equation 4.2), we find the minimum asymptote $A_1$ = - 4.35 ± 0.09 responding maximum FT4 = 90.00 pmol/L the maximum asymptote $B_1$ = 0.20 ± 0.19 responding minimum FT4 = 10.10 pmol/L and, inflection point $x_0$ = 28.15 ± 0.76 pmol/L, and Hill's slope ($m$) = 24.55 ± 12.60.

$$\ln(\text{TSH}) = -4.35 + \frac{0.20 + 4.35}{1 + (\text{FT4}/28.15)^{24.55}} = -4.35 + \frac{4.55}{1 + (\text{FT4}/28.15)^{24.55}} \qquad (4.2)$$

The best fitted linear equation for ln(TSH) *vs* FT4 related to the hyperthyroidism on the basis of euthyroidism (Figure 12) has the negative slope -0.09 ± 0.004 and y-intercept 1.83 ± 0.04 with $r$ = -0.58 which is the indicator of negative feedback mechanism in the thyroid cycle.

Referring to Figure 12, the hyperthyroidism develops in the patients from euthyroidism through the logistic curve $B_1L_2L_1A_1$. Here, the linear fit passes through the junction J of euthyroidism, subclinical- and overt hyperthyroidism whereas the non-linear fit passes through the subclinical hyperthyroid region. The steepness or Hill's slope arises due to the negative correlations between TSH and FT4. The curvatures at points $L_1$ and $L_2$

come from the influence of overt hyperthyroidism and subclinical hyperthyroidism in the patients, respectively. The nearly straight line $L_1A_1$ signifies the continuous increment of FT4 up to 90.00 pmol/L at the lowest level of TSH below 0.01 mIU/L in the region of overt hyperthyroidism.

From the above discussions, one can predict that the patients under proper medication of overt hypothyroidism slowly return back to the normal condition through the curve $BC_2C_1$ (Figure 11). In this way, the patients under proper medication of overt hyperthyroidism slowly return back to the normal condition through the curve $A_1L_1L_2$ (Figure 12). Finally, the gap: $B - A = 3.30$ in hypothyroidism (Equation 4.1) totally vanishes when such thyroid disorder is completely cured. The non-zero second term in the right side of Equation 3.1 refers to the hypothyroid dysfunction depending on the parameters: $A$, $B$, FT4, $x_0$ and $m$. Obviously, $A$ equals to $B$ when Hill's slope is $m = 0$. The minimum asymptote $A$ refers to the normal TSH so that the maximum asymptote $B$ should be corrected to $A$ by reducing TSH for the subjects suffering from hypothyroidism. Similarly, the maximum asymptote $B_1$ refers to the normal TSH so that the minimum asymptote $A_1$ should be corrected to $B_1$ by adding TSH for the subjects suffering from hyperthyroidism.

The 4PL model showing the non-linear relationship between TSH and FT4 is better fitted separately in hypothyroidism and hyperthyroidism on the basis of euthyroidism. In this model, the biological interpretation of TSH response by FT4 deviation is significantly important than other models such as linear (Larsen, *et al.*, 1981), log-linear (Jonklaas, *et al.*, 2009), non-linear sigmoid (Leow, *et al.*, 2007), error function (Hoermann, *et al.*, 2010) and fourth-order polynomial (Clark, *et al.*, 2012).

According to Reichlin *et al.* (1967), TSH secretion is finely regulated for a wide range of FT4 concentrations and there is a curvilinear relationship between TSH and FT4 supporting the negative feedback system of HPT axis. Midgley *et al.* (2013) suggested for analyzing separately euthyroid, hypothyroid and hyperthyroid panels to understand the correlation between TSH and FT4 because the functional segments appear differently regulated as the trends between these states change. Hypothyroidism and hyperthyroidism make the patients adaptive challenge to regulate the homeostatic system and to restore euthyroidism or ameliorate thyroid dysfunction.The effect of different functional states of the feedback system and the physiological variables such as ethnicity, age, iodine supply,

T3 responsive features of nuclear receptors and many others add complexity to understand the functional relation between TSH and FT4. Here, ln(TSH) *vs* FT4 trend line differs in its nature as it passes from euthyroid to hypothyroid or to hyperthyroid set points. On the other hand, hysteresis in the HPT axis represents adaptive endocrine response by the evolutionarily conserved survival advantages (Leow, 2016). The temporarily persistent elevation of TSH despite the normalized FT4 levels indicates the transient hysteresis. Thyrotoxicosis is a state that leads to a lag time in recovery of TSH and a delayed recovery of T3 regulated genes. During the transition from thyrotoxicosis to euthyroidism, about 10% genes show incomplete recovery. During the recovery period of extreme hypo- and hyperthyroidism, the nature of ln(TSH) *vs* FT4 curves change showing the existence of hysteresis of HPT-axis. These facts are further associated with the different values of inflection point $x_0$ and Hill's slope $m$ resulting logistic curves governed by the Equations 4.1 and 4.2 which are fitted graphically in Figures 11 and 12 for hypothyroidism and hyperthyroidism on the basis of euthyroidism. Berberich *et al.* (2018) performed a sensitivity analysis of a derived model revealing the dependency of TSH and thyroid hormones on the different system parameters by incorporating TSH-FT3-shunt inside the thyroid. Berberich's study claims the understanding of thyroid hormone homeostasis developing a mathematical model of the HPT-loop. In our actual data analysis, the deviations in ln(TSH ) *vs* FT4 trend lines at the set points between euthyroidism and hypo- or hyperthyroidism reflect the actual insight into the negative feedback mechanism of the thyroid cycle.

The biochemical analysis of TFT values measured in a data-slot of 47 subjects has been performed by means of a dropline diagram shown in Figure 13. Here, the concentration levels between two red (or blue) horizontal lines represent the normal reference levels for FT4 (or TSH). The extreme points lying out of reference range, i.e. A, B, C and D are related to overt hypothyroidism, and a, b, c, d, e and f are related to overt hyperthyroidism. The unusual TFT values are seen in the subjects 29 and 37 who have pregnancy period and a case of subclinical hypothyroidism, respectively. The subjects having normal TFT values lie in the category of euthyroidism. Figure 13 demonstartes the stronger negative correlation between TSH and FT4 (or FT3) in the disorderd stages than in the normal stages supporting the principle of negative feedback mechanism in the thyroid cycle. The results obtained in this section are also reported by Lamichhane *et al.* (2020).

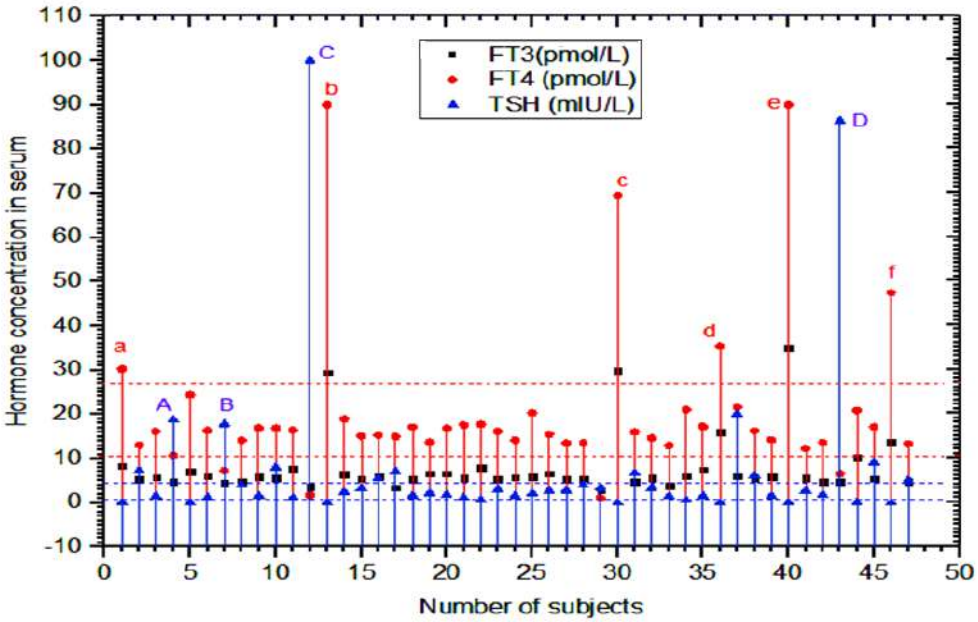


**Figure 13:** Biochemical analysis of thyroid disorders in a data slot of 47 patients supporting the principle of negative feedback mechanism in thyroid cycle (A, B, C and D are related to overt hypothyroidism; a, b, c, d, e and f are related to overt hyperthyroidism, and the unusual nature seen in the subjects 29 and 37 are related to period of pregnancy and subclinical hypothyroidism, respectively)

## 4.2 Variations of Thyroid Hormone Levels and Thyroid Size with Age and Gender

As reported in the Section 4.1, the TFT evaluations suggest that 2413 subjects are clinically euthyroid. The thyoid USG examinations performed in 270 euthyroid subjects result normal thyroid gland in 221 and abnormal thyroid gland in 49 subjects. The thyroid gland abnormalities are discussed in the Section 4.3. Based on the TFT and USG data of euthyroid subjects, age- and gender specific changes of normal thyroid size, TSH, FT4 and FT3 have been analyzed as discussed in the following Subsections 4.2.1-4.2.3.

### 4.2.1 TFT Analysis

The euthyroid sujects (665M + 1748F) of mean age 35.94 ± 16.47 years have the average TSH = 2.30 ± 0.98 mIU/L, FT4 = 14.17 ± 2.82 pmol/L and FT3 = 5.47 ± 0.83 pmol/L provided with the standard deviation (SD) as given in Table 1. Here, this value of FT3 is higher than 3.5 pmol/L, i.e. FT3 of euthyroid subjects observed by Mahato *et al.* (2015). We found slightly lower FT4 than that mentioned in Rohil *et al.* (2010). In normal thyroid

conditions, the log-linear plots of TSH *vs* FT3 or FT4 show weak negative correlations ($r$ = -0.11) between pituitary and thyroid hormones. In this way, the linear plot of FT3 *vs* FT4 shows weak positive correlation ($r$ = 0.11) between thyroid hormones. The best fitted equations of the form: $y = Ax + B$ with the coefficients A and B for ln(TSH) *vs* FT4, ln(TSH) *vs* FT3 and FT3 *vs* FT4 are given by the Table 2.

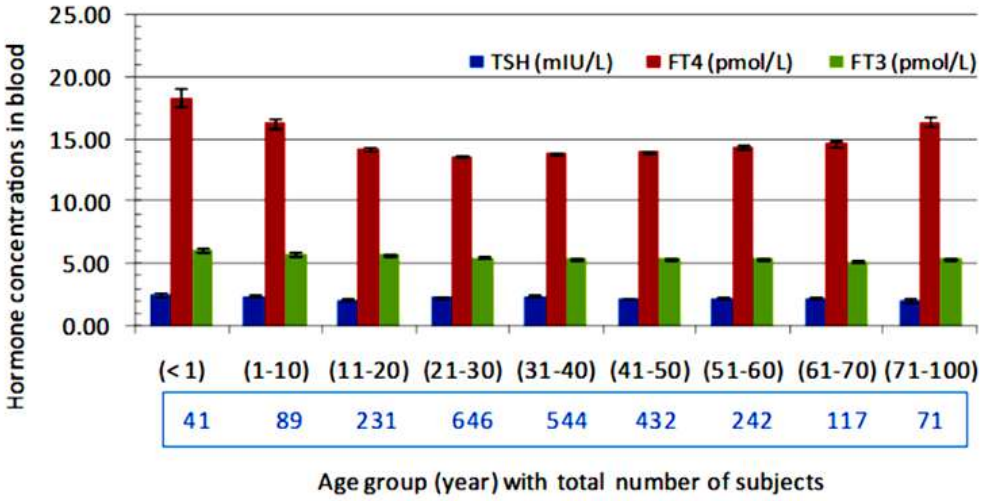


**Figure 14:** Age-specific changes in the normal TFTs given with the standard error bars and $p$ <0.001 over the age groups

It has been observed that the TFT values are higher in the infants than in the adults. The FT4 concentration slightly decreases from childhood to adulthood and then slightly increases in elderly for both genders as shown in the Figure 14. The largest TSH recorded is 2.58 ± 0.89 pmol/L in the infants' age group and the lowest TSH is 2.05 ± 0.93 pmol/L in the elderly (71-100 years). We can see the negative correlations between TSH and FT3 or FT4 (Tables 3 and 4) which is associated with the negative feedback cycle of the HPT-axis. Most of the results of our study lie in the close agrrements as reported by the previous studies performed at the different places all over the world. According to Fontes *et al.* (2013), FT4 decreases with aging as a result of increasing TSH. In this way, Chaurasia *et al.* (2011) studied the age dependent variations of TFTs in the hospital based subjects at Gujarat, India in which T4 concentration is the lowest in the adults (20-40 years). As reported by Lipson *et al.* (1979), TSH significantly increases in response to the slightly decreasing T3 with aging of the euthyroid adults. The patients' backround and their biochemical reports suggest that the change in TFTs with aging is related to endocrine developments, brain functions, cell growth rate, metabolic activity, nutritions

and environmental effects.

**Table 3:** TFT values averaged in the different age groups of 1748 female euthyroid subjects where the ANOVA single factor-test for each TFT gives $p$ <0.05 over such age groups

| Variables | Age(yrs) | <1 | 1-10 | 11-20 | 21-30 | 31-40 |
|---|---|---|---|---|---|---|
| TSH(mIU/L) | Mean | 2.58 | 2.30 | 2.11 | 2.34 | 2.50 |
| | SD | 0.91 | 0.89 | 1.00 | 0.94 | 0.92 |
| FT4(pmol/L) | Mean | 19.87 | 16.73 | 13.99 | 13.49 | 13.76 |
| | SD | 5.63 | 2.82 | 2.74 | 2.13 | 2.49 |
| | Mean | 5.59 | 5.65* | 5.62 | 5.46 | 5.32 |
| FT3(pmol/L) | SD | 1.13 | 0.95 | 0.80 | 0.81 | 0.80 |
| | N | 11 | 39 | 162 | 511 | 408 |
| Variables | Age(yrs) | 41-50 | 51-60 | 61-70 | 71-80 | 81-100 |
| TSH(mIU/L) | Mean | 2.29 | 2.35 | 2.31 | 2.12 | 2.55 |
| | SD | 0.95 | 1.07 | 1.21 | 0.88 | 1.32 |
| FT4(pmol/L) | Mean | 13.98 | 14.50 | 14.58 | 16.75 | 17.90 |
| | SD | 2.42 | 2.65 | 2.49 | 3.84 | 4.15 |
| | Mean | 5.33 | 5.40 | 5.04 | 5.19 | 5.64 |
| FT3(pmol/L) | SD | 0.76 | 0.81 | 0.68 | 0.83 | 0.94 |
| | N | 332 | 175 | 72 | 31 | 7 |

**Table 4:** TFT values averaged in the different age groups of 665 male euthyroid subjects where the ANOVA single factor-test for each TFT gives $p$ <0.05 over such age groups

| Variables | Age(yrs) | <1 | 1-10 | 11-20 | 21-30 | 31-40 |
|---|---|---|---|---|---|---|
| TSH(mIU/L) | Mean | 2.56 | 2.56 | 2.11 | 2.22 | 2.28 |
| | SD | 0.88 | 1.17 | 0.91 | 0.97 | 0.91 |
| FT4(pmol/L) | Mean | 17.78 | 15.91 | 14.81 | 13.90 | 14.02 |
| | SD | 4.03 | 3.84 | 3.47 | 2.58 | 2.88 |
| | Mean | 6.20 | 5.88* | 5.96 | 5.69 | 5.54 |
| FT3(pmol/L) | SD | 1.13 | 0.95 | 0.80 | 0.81 | 0.80 |
| | N | 30 | 50 | 69 | 135 | 136 |
| Variables | Age(yrs) | 41-50 | 51-60 | 61-70 | 71-80 | 81-100 |
| TSH(mIU/L) | Mean | 2.03 | 2.12 | 2.15 | 1.88 | 1.88 |
| | SD | 0.90 | 1.05 | 1.30 | 0.92 | 0.74 |
| FT4(pmol/L) | Mean | 14.10 | 14.19 | 14.69 | 15.14 | 17.46 |
| | SD | 2.70 | 3.12 | 3.86 | 2.93 | 3.71 |
| | Mean | 5.64 | 5.45 | 5.41 | 5.36 | 6.07 |
| FT3(pmol/L) | SD | 0.82 | 0.84 | 0.77 | 0.77 | 0.92 |
| | N | 100 | 67 | 45 | 26 | 7 |

The age- and gender-specific changes of TSH, FT4 and FT3 are well reflected from the Tables 3 and 4 . Here, the TH-levels are not changing much from 11 to 60 years in both genders. The graphs potted for the TFT values *vs* age groups as shown in Figure 14 reflect almost same nature in both males and females. The TSH is distinctly changed in the elderly (>71 years) which is 2.34 ± 1.1 mIU/L for males and 1.88 ± 0.81 mIU/L for

females. The TFTs are higher in the age group <1 years than in the other age groups of both genders. Franklyn *et al.* (1985) suggested that the TFTs are not evidently changed with aging but FT3 is lower in adult females than in adult males (16-29 years). In this way, Sujuky *et al.* (2012) concluded that FT3 or FT4 is negatively correlated with aging of males, but not correlated in females and however, TSH increases with aging in both genders. In our study, FT4 is observed to be distinctly changed with aging rather than TSH and FT3 in both genders. Conclusively, FT4 firstly decreases to the minimum level in the adulthood (21-50 years) and then slightly increases with aging.

### 4.2.2 Thyroid USG Analysis

From the USG reports of the euthyroid subjects (90M + 131F) having mean age 32 ± 17.18 years, the average left lobe volume (LLV) = 2.12 ± 1.07 mL, right lobe volume (RLV) = 2.61 ± 1.40 mL and thyroid gland volume (TGV) = 4.74 ± 2.30 mL.The normal thyroid gland has RLV > LLV. The reference ranges of normal thyroid size observed in euthyroid subjects with normal USG reports are given in the Table 5. The variales such as age $x$ and TGV $y$ are related by the polynomial fit in $y$ *vs* $x$ graph (Figure 15). The trendline equation of the second order polynomial fit with the coefficient of determination $R^2$ = 0.87 and $p$ <0.001 is given by

$$y = (-0.002 \pm 0.0005)x^2 + (0.21 \pm 0.04)x + (1.10 \pm 0.67) \tag{4.3}$$

Here, the coefficients of Equation 4.3 are provided with the standard errors.

**Table 5:** Normal thyroid size of the euthyroid subjects (90M+131F)where the t-test for LLV *vs* RLV gives $p$ <0.001

| Variables | Age(yr) | LLV(mL) | RLV(mL) | TGV(mL) |
|---|---|---|---|---|
| Mean | 32.02 | 2.12 | 2.62 | 4.74 |
| SE | 1.16 | 0.07 | 0.09 | 0.15 |
| SD | 17.18 | 1.07 | 1.40 | 2.30 |
| Min. | 1.50 | 0.16 | 0.24 | 0.40 |
| Max. | 86.00 | 7.01 | 7.76 | 13.87 |

The euthyroid adults have the greater thyroid size than the early pubertal and the elderly as reflected from the Figure 15. It agrees with the results from the different literatures (Chanoine, *et al.*, 1991; Hegedus, *et al.*, 1983 ; Seker, *et al.*, 2010). However, the thyroid

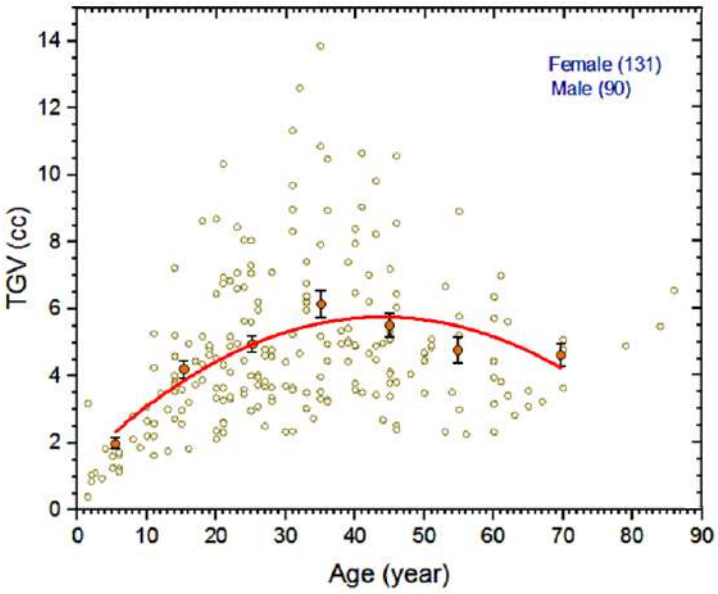


**Figure 15:** Variation of normal thyroid size or thyroid gland volume (TGV) with aging where the error bars indicate SE in the mean values from the age-groups given in the Table 6

size of both genders that we observed in central Nepal is smaller than that reported in these literatures. The total volume of thyroid gland observed by Seker *et al.* (2010) was 13.00 ± 6.27 mL for the subjects aged 15-78 years. Our result for the total size of the normal thyroid lobes is a bit smaller than 6.63 ± 2.50 mL that was reported by Kayastha *et al.* (2010) from the euuthyroid subjects aged 1-83 years in TUTH, Kathmandu, Nepal.

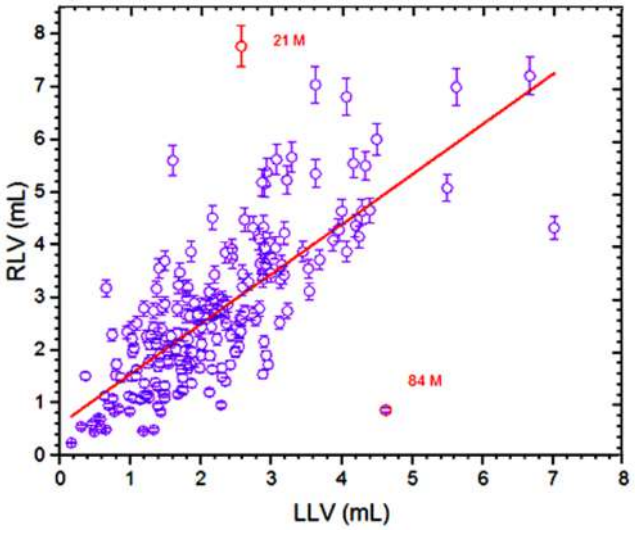


**Figure 16:** Correlation between right lobe volume (RLV) and left lobe volume (LLV) of normal thyroid gland where the error-bars indicate 5% of the measured value. The marginal red datapoints are related to 21-year-old and 84-year-old males

Here, LLV and RLV are positively correlated (Figure 16) provided with Pearson's $r = 0.73$

and $p$ <0.001. Let the variables, RLV and LLV be represented by $x$ and $y$, respectively. The equation of the best fitted straight line in $y$ *vs* $x$ plot is given by

$$y = (0.95 \pm 0.06)x + (0.60 \pm 0.14) \tag{4.4}$$

The physical significance of the Equation 4.4 is that RLV can be estimated when LLV is observed.

As averaged from the both genders (Table 6), the maximum TGV is 6.09 ± 2.78 mL observed in the adults aged 31-40 years and the minimum TGV is 1.73 ± 0.17 mL observed in the children aged 1-10 years. The male adults aged 31-40 years have the largest thyroid size, i.e. 7.84 ± 3.18 mL. However, the females have the maximum TGV, i.e. 5.62 ± 2.49 mL in the age group 41-50 years including menopause phase and such value exceeds the TGV of males in this age group. The females in the age group 11-20 years including menarche phase also have the higher TGV than that of males in the same group. The age and gender based variations of the thyroid size can be analyzed from the Table 6 and from the Figures 17 and 18. The additional factors that influence thyroid size of the patients are body mass index, body surface area, medication, family history or genetics, smoking, alcoholism, drug abuse, iodine deficiency and overdose, sleeping and feeding habit, hypertension, demographic changes and environmental pollutants. From this hospital based study, we find that the Nepalese euthyroid subjects have smaller thyroid lobes than the other euthyroid subjects as mentioned in the previous literatures. In a study performed by Seker *et al.* (2010) in Turkey, the normal thyroid size in males is 15.87 ± 7.18 mL and that in females is 10.94 ± 4.53 mL. In another study performed by Oberhofer *et al.* (1989) in 500 healthy adults living in an area of endemic goitre, the thyroid size in males is 14.94 mL and that in females is 12.09 mL.

The continuous physical exercise may also influence on the thyroid size. It was stated by Ying *et al.* (2009) that the right handed subjects have RLV > LLV. According to Lewinisky *et al.* (1982) and Gerendai *et al.*(2001), the HPT-axis functions unilaterally so that the right labe has the greater size. In our study, the males of mean age 29.92 ± 19.72 years have LLV = 2.13 ± 1.20 mL and RLV = 2.73 ± 1.55 mL provided with SD and $p$ = 0.004 for LLV *vs* RLV. The females of mean age 33.46 ± 15.10 years have LLV = 2.12 ± 0.98 mL and RLV = 2.54 ± 1.29 mL with $p$ = 0.003 (Table 7). As demonstrated by

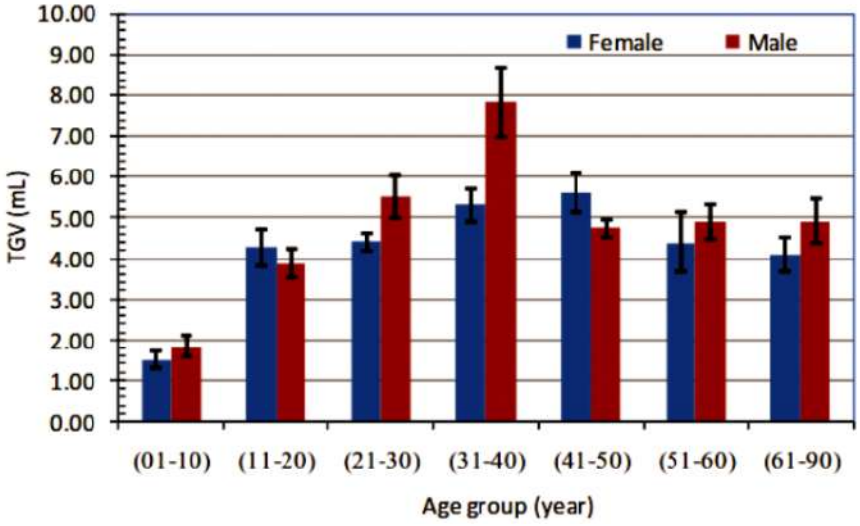


**Figure 17:** Column plots for the normal thyroid size given with standard error bars related to the gender based age groups (Table 6)

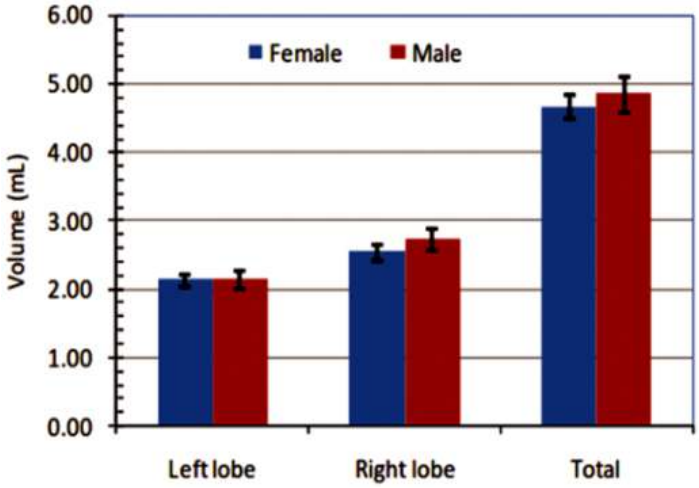


**Figure 18:** Gender-specific changes in normal thyroid size with standard error bars from the data sets of 90 males and 131 females

**Table 6:** Normal thyroid size averaged over different age groups where SE referers to standard error and N refers to number of subjects including 90 males and 131 females where the ANOVA single factor-test for TGV in such age groups gives $p$ <0.001

| Group | Female | | | Male | | |
|---|---|---|---|---|---|---|
| Age(yrs) | TGV (mL) | SE | N | TGV (mL) | SE | N |
| 01-10 | 1.53 | 0.22 | 8 | 1.86 | 0.25 | 12 |
| 11-20 | 4.27 | 0.43 | 17 | 3.88 | 0.35 | 21 |
| 21-30 | 4.41 | 0.23 | 32 | 5.54 | 0.52 | 20 |
| 31-40 | 5.31 | 0.40 | 31 | 7.84 | 0.85 | 14 |
| 41-50 | 5.62 | 0.48 | 27 | 4.74 | 0.19 | 7 |
| 51-60 | 4.40 | 0.73 | 9 | 4.91 | 0.41 | 9 |
| 61-90 | 4.09 | 0.42 | 7 | 4.93 | 0.56 | 7 |

**Table 7:** Normal values of thyroid lobe volumes in 90 males and 131 females where the t-test for LLV *vs* RLV gives $p = 0.003$

| Gender | Values | Age(yrs) | LLV(mL) | RLV(mL) | TGV(mL) |
|---|---|---|---|---|---|
| Female | Mean | 33.46 | 2.12 | 2.54 | 4.66 |
| | SE | 1.32 | 0.09 | 0.11 | 0.19 |
| | SD | 15.10 | 0.98 | 1.29 | 2.12 |
| | Min. | 1.50 | 0.16 | 0.24 | 0.40 |
| | Max. | 79.00 | 5.62 | 7.03 | 12.61 |
| Male | Mean | 29.92 | 2.13 | 2.73 | 4.85 |
| | SE | 2.08 | 0.13 | 0.16 | 0.27 |
| | SD | 19.72 | 1.20 | 1.55 | 2.56 |
| | Min. | 1.50 | 0.30 | 0.49 | 0.85 |
| | Max. | 86.00 | 7.01 | 7.76 | 13.87 |

the column plots in the Figure 18, the LLV is same in both genders whereas the RLV is higher in males. In general, RLV is greater than LLV giving rise to the larger thyroid size in males.

### 4.2.3 Normal USG and TFT Cross-Sectional Analysis

It is important to perform both thyroid scanning and biochemical tests for the better diagnosis of thyroid disorders in a patient. A group of healthy adults can be taken as a control group and the thyroid variables measured from such group are the reference ranges used for the thyroid clinical evaluations. From the normal USG and TFT cross-sectional study in 34 euthyroid adults (4M + 30F) aged 33.56 ± 11.13 years (18-50 years), the average TGV = 5.05 ± 2.06 mL, FT3 = 5.62 ± 0.80 pmol/L, FT4 = 14.89 ± 3.38 pmol/L and TSH = 2.31 ± 0.89 mIU/L provided with SD.

The TFTs are correlated as suggested by the negative feedback mechanism of HPT-axis forming the thyroid cycle for the endocrine regulations. The dropline diagram (Figure 19) plotted for the individual subjects shows the negative correlation between TSH and FT3 or FT4 whereas positive correlation between FT3 and FT4. In most of the subjects, the observed datapoint of FT3 or FT4 lying above its average reference line corresponds to the datapoint of TSH lying below its reference line, and vice versa. However, the $16^{th}$ subject whose FT4 lies in the upper boundary of the given reference range doesnot follow this rule due to the unknown cause. During pregnancy, mensturation period, medication and non-thyroid illness; the thyroid hormone regulation may be disturbed even if the thyroid gland functions normally.

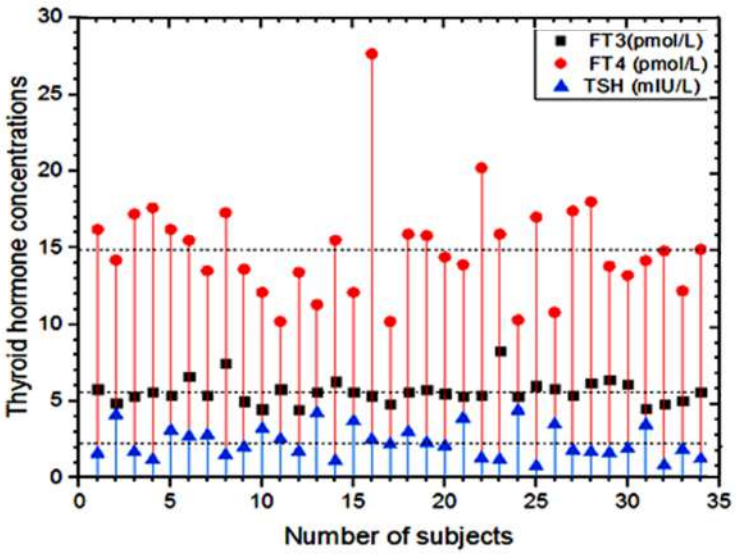


**Figure 19:** Fluctuations in normal TFT values in 34 adults having normal thyroid scans where the horizontal dotted lines represent the observed mean values

From the TFTs of 2413 and the normal USG scans of 221 euthyroid subjects, the average values of TGV, FT3, FT4 and TSH are plotted with respect to the age groups as shown in the Figure 20. This shows that FT4 primarily decreases to the minimum level in adulthood (21-50 years) and then slightly increases in elderly followed by the minimal changes in FT3 and TSH levels. Conversely, the normal thyroid size increases up to the middle age group (31-40 years) and then decreases in elderly.

Thyroid size, FT3, FT4 and TSH vary along with age and gender so that these are said to be covariates of the endcrine system. The interrelationships among such variables of the euthyroid subjects, as explained in the Section 4.2, are also also published in the paper by Lamichhane *et al.* (2019). Referring to these facts; Dix, 2019 pointed out that the risk of thyroid cancer begins to increase in females during menarche whose thyroid size is greater than that in males. There are so many factors that influence thyroid functions. The controlled life style with mental, biochemical and physical fitness has beneficial effect on endocrine regulations. Exercise, health awareness, nutritional foods and healthy environment are supporting factors for the healthy thyroid and metabolism. One should not take alcohol, smoking and drugs to make his/her thyroid fucnction well. Meng *et al.* (2015) reported that females have higher incidence of thyroid disorders than males characterized by the changing lipid profile, hyperinsulinemia, android obesity and hypertension. Thyroid disorders and metabolic syndrome increase with aging. Females

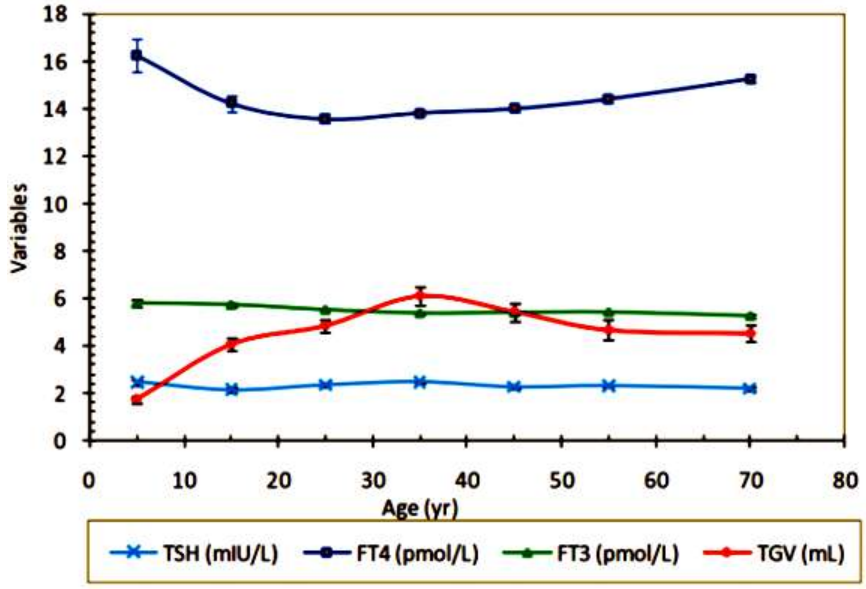


**Figure 20:** Healthy thyroid status with aging where the markers indicate the mean values in the age groups of 10 years interval from the data sets of 2413 TFTs and 221 USG scans

suffer from the estrogen's protective efects on metabolic syndrome so that adverse changes in their TFTs are observed in menarche and menopause.

The insight of normal thyroid functioning is the role of T3 activated gene expressions regulated by THRs upon binding to hormone response elements. The physical properties of THRs in presence and absence of T3-hormone under normal and abnormal thyroid conditions are discussed in the Sections 4.4-4.6.

### 4.3 Thyroid Ultrasonographic Findings in Euthyroid and Hypothyroid Patients

As explained earlier in the Subsection 4.2.3, the control group of 34 adults have normal thyroid USG and normal TFTs along with normal conditions of psychology, sleeping and feeding habits, and without family history of thyroid diseases. The mean values of TGV, FT3, FT4 and TSH related to such control group (Table 8) are very close to the values averaged from the normal USG reports of 221 subjects and the normal TFT reports of 2413 subjects included in this study. So, these values can be taken as the reference values for the evaluation of thyroid status in the patients. In addition to the normal thyroid analysis, the biophysical parameters related to 49 euthyroid patients (6M + 43F) having abnormal USG scans and 38 hypothyroid patients (5M + 33F) having normal as well as abnormal USG scans are depicted in Table 8. Furthermore; mean, median, range in

1.5 interquartile range (IQR) and outliers taking logarithm of the measured parameters related to the different groups are shown in the box plots (Figures 21, 22 and 23).

**Table 8:** Mean, SD and range of normal and abnormal thyroid size along with related TFT values where age is in year; LLV, RTV and TGV are in mL; FT3 and FT4 are in pmol/L, and TSH is in mIU/L (the ANOVA single factor analysis gives $p$ <0.001)

| Thyroid status | Statistics | Age | LLV | RLV | TGV | FT3 | FT4 | TSH |
|---|---|---|---|---|---|---|---|---|
| Normal-USG | Mean | 33.56 | 2.36 | 2.71 | 5.07 | 5.62 | 14.89 | 2.31 |
| + normal-TFT | SD | 11.13 | 0.89 | 1.39 | 2.06 | 0.80 | 3.38 | 1.03 |
| (4M + 30F) | Min. | 18 | 1.23 | 0.21 | 2.54 | 4.47 | 10.20 | 0.78 |
| | Max. | 50 | 5.40 | 7.65 | 11.46 | 8.30 | 27.65 | 4.40 |
| Thyroid-USG | Mean | 37.92 | 5.43 | 5.94 | 11.50 | 5.04 | 9.62 | 23.60 |
| + hypo-TFT | SD | 13.56 | 5.34 | 4.81 | 9.75 | 1.46 | 4.93 | 30.77 |
| (5M + 33F) | Min. | 15.00 | 0.94 | 1.03 | 2.73 | 1.90 | 0.68 | 4.80 |
| | Max. | 70.00 | 32.21 | 25.52 | 57.73 | 9.80 | 17.70 | 100.00 |
| Abnormal-USG | Mean | 43.02 | 7.65 | 8.41 | 16.06 | 5.59 | 15.21 | 1.93 |
| + normal-TFT | SD | 13.84 | 13.08 | 13.85 | 21.75 | 0.81 | 2.57 | 1.07 |
| (6M + 43F) | Min. | 16.00 | 0.93 | 0.70 | 2.42 | 4.00 | 11.00 | 0.47 |
| | Max. | 72.00 | 76.06 | 89.70 | 119.11 | 8.00 | 21.40 | 4.60 |

The hypothyroid patients aged 37.92 ± 13.56 years have mean thyroid size, FT3, FT4 and TSH as 11.50 ± 9.75 mL, 5.04 ± 1.46 pmol/L, 9.62 ± 4.93 pmol/L and 23.60± 30.77 mIU/L, respectively given with SD. This group includes 21 subclinical hypothyroid and 17 overt hypothyroid patients. FT4 has four outliers below the lower quartile of the box plot (Figure 22) with more deviated values of mean and median. TSH ranges from 4.80 to 100.00 mIU/L resulting the variety of clinically hypothyroid patients.

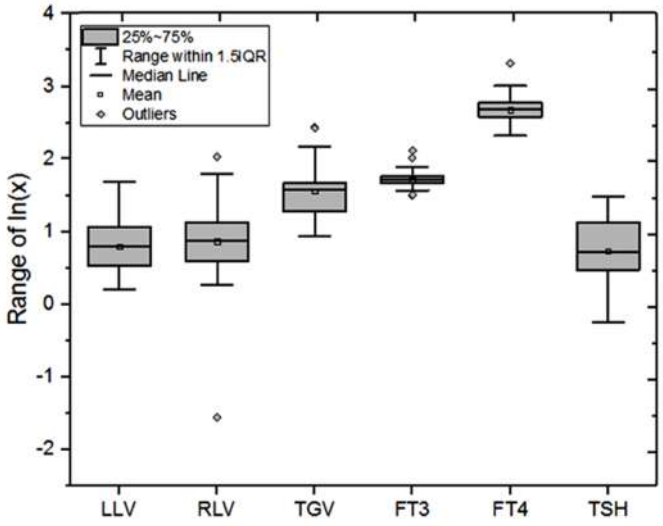


**Figure 21:** Box plots for $\log_e$ of LLV(mL), RLV(mL), TGV(mL), FT3(pmol/L), FT4(pmol/L) and TSH(mIU/L) in 34 euthyroid subjects having normal USG and normal TFTs

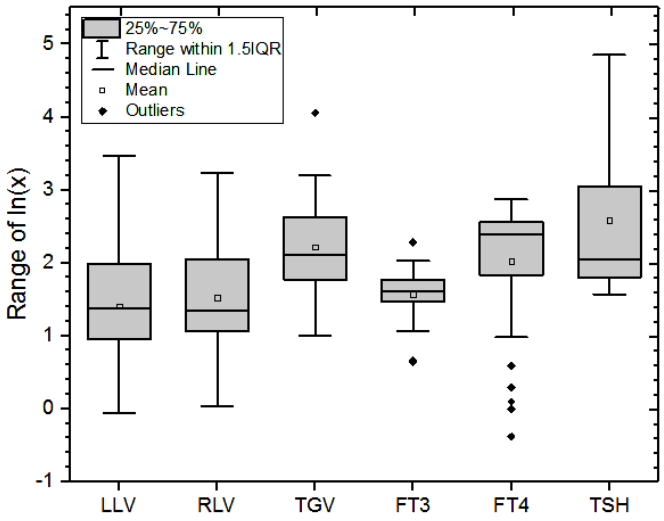


**Figure 22:** Box plots for $\log_e$ of LLV(mL), RLV(mL), TGV(mL), FT3(pmol/L), FT4(pmol/L) and TSH(mIU/L) in 38 hypothyroid subjects having abnormal USG and abnormal TFTs

The additional findings related to the group of 21 subclinical hypothyroid patients are as follows:

1. Seven patients have normal thyroid-USG reports with insomnia in two subjects, family history of thyroid abnormality in one subject and one losing pregnancy.
2. Single patient has benign type of diffuse goitre with normal conditions of psychology, habit and family history.
3. Five patients suffer from benign type of thyroid nodules with hypo- and/or hyperechogenicity (hypoechoic lesion is shown in Figure 25), one of them from iodine deficient area, stressful lifestyle in two subjects and one having insomnia.
4. Five patients have thyroiditis with insomnia in one of them, enlarged isthmus found in one subject suffering from stressful lifestyle and smoking habit, and family history of thyroid disease in one subject.
5. A patient has hypoechogenic lesions with smoking habit.
6. A patient is suffering from papillary thyroid cancer with pregnancy loss.
7. A patient has cystic lesions in thyroid gland with normal conditions of psychology, habit and family history.

In this way, there are following additional findings in 17 patients suffering from overt hypothyroidism:

1. Two patients have normal thyroid-USG reports with thyroid disease in family of one

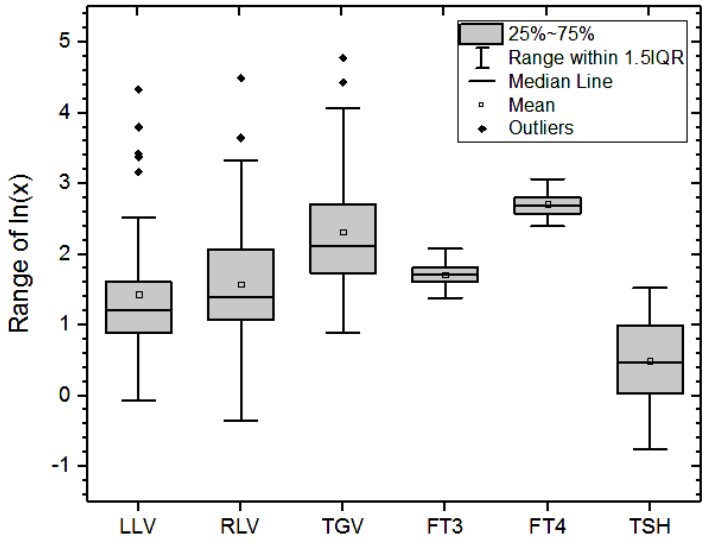


**Figure 23:** Box plots for $\log_e$ of LLV(mL), RLV(mL), TGV(mL), FT3(pmol/L), FT4(pmol/L) and TSH(mIU/L) in 49 euthyroid subjects having abnormal USG and normal TFTs

subject.

2. Five patients suffer from benign, nodular and/or diffuse goitres with vascularity (as in Figure 26) and/or enlarged isthmus in two of them, lymphadenopathy in two subjects, history of thyroid disease in family of one subject, insomnia in two subjects and pregnancy loss in one subject.

3. Four patients have benign thyroid nodules (0.5-1.0 cm in size as shown in Figure 27) with smoking and alcoholism in two subjects, family history of thyroid disorder in one subject and stressful lifestyle in one subject.

4. Six patients suffer from thyroiditis with insomnia in two subjects, smoking habit in one subject, stressful lifestyle in two of them, family history of thyroid disease in one subject.

Almost all of the overt hypothyroid patients suffer from the common symptom, cold intolerance that is linked with the heat conduction properties of the protein-hormone systems in the Sections 4.4 and 4.5. The imaging features of thyroid disorders (goitre, nodule, echogenicity, vascularity and thyroiditis) in overt hypothyroidism are more associated with family history of thyroid disease or genetics, insomnia, stressful lifestyle, smoking, alcoholism and pregnancy loss than in subclinical hypothyroidism. These features of thyroid disorders can also be seen in some patients even if they have normal TFT reports. As depicted in Table 8, the group of 49 euthyroid patients with abnormal USG and normal TFTs has mean age of 43.02 ± 13.84 years and thyroid size of 16.06 ±

21.75 mL. The thyroid size is compared with TFT logarithmic values in the box plots (Figure 23) where LLV has four outliers above its upper quartile range. In this group, 12 subjects have goitrogenicity, 24 patients suffer from nodularity with mixed vascularity in some of them, 5 subjects have thyroiditis including Hashimoto's disease, 3 subjects have hypo- and/or hyperechoic lesions, 3 of them have cystic lesions and 2 subjects of this category are confirmed with thyroid malignancy after FNA biopsy test.

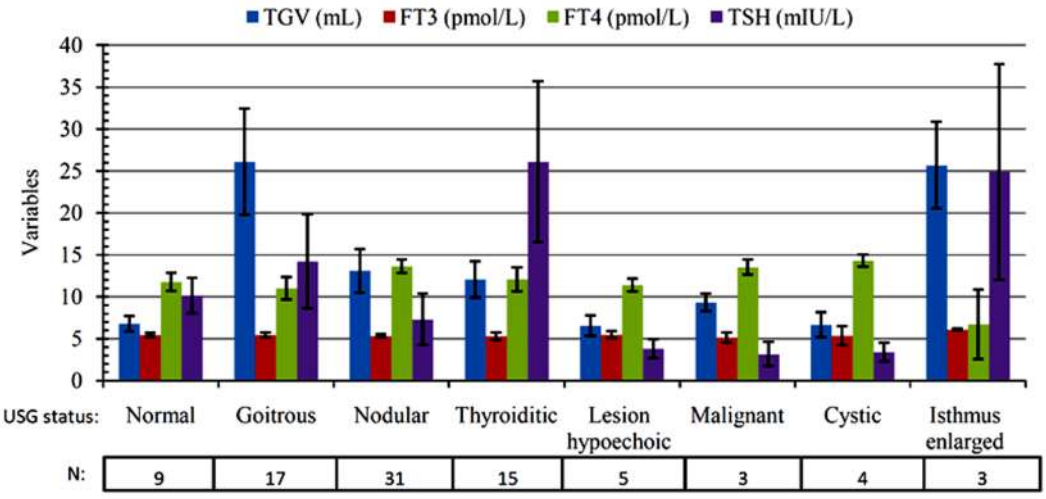


**Figure 24:** Status of hypothyroid disorders evaluated from the USG scans and TFTs of 87 patients (11M + 76F). Lesion hypoechoic, malignant and cystic groups have normal TFTs and others are clinically hypothyroid in average. The error bar indicates the standard error in the corresponding group

The USG examination can differentiate simple cysts from mixed cystic and solid nodules. Simple cysts have low risk of being malignant. However, nodules have 5% chance of being cancerous (Hegedüs, 2004). The initial evaluation of nodules includes the measurement of serum TSH, echogenicity test and USG guided FNA. The patients having family history of multiple endocrine neoplasia or medullar thyroid carcinoma are suggested to check serum calcitonin as well. The likelihood of thyroid carcinoma is higher for a solitary nodule than for a non-solitory nodule (Frates, *et al.*, 2006).

The degree of echogenicity is related to the circulating levels of thyroid autoantibodies and thyrotropin. The spatial echogenic pattern indicates the autoimmune involvement of the gland predicting hypothyroidism. Diffuse thyroid hypoechogenicity usually correlates with autoimmune (Hashimoto's) thyroiditis (Marcocci, *et al.*, 1991; Pedersen, *et al.*, 2000). The decreased echogenicity is associated with the increased TSH of the patients

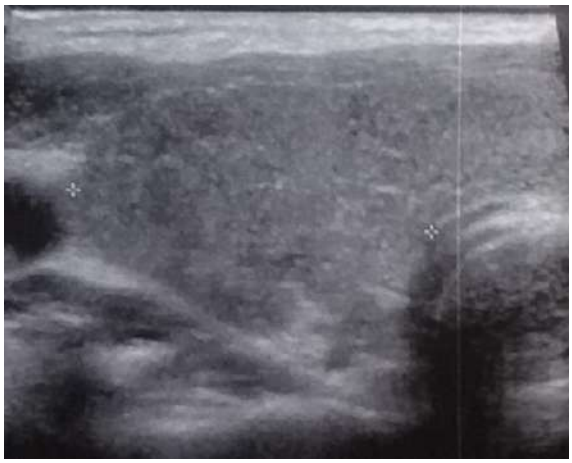

**Figure 25:** USG scan of right thyroid lobe of 55 year old male with heterogenous echogenicity or multiple poorly marginated hypoechoic areas who has diffusely enlarged thyroid gland having features of diffuse thyroiditis whose LLV and RLV are 11.06 mL and 11.82 mL, respectively. His TFT reports for FT3, FT4 and TSH are 4.20 pmol/L, 4.90 pmol/L and 34.30 mIU/L, respectively indicating overt hypothyroidism

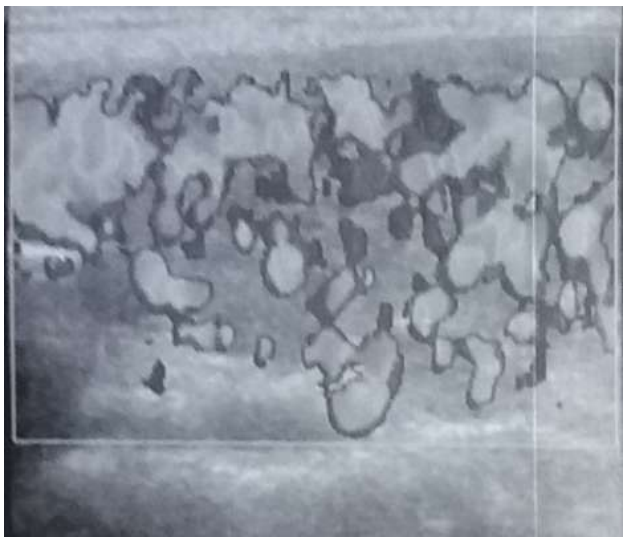

**Figure 26:** Increased vascularity in case of Figure 25

having tendency of thyroid dysfunction from euthyroidism to subclinical hypothyroidism to overt hypothyroidism (Vejbjerg, *et al.*, 2006).

Stress affects autoimmunity through direct and indirect activation of neural as well as endocrine system. The impact of stress on autoimmune thyroid disease is well reflected as Grave's disease in hyperthyroidism and Hashimoto's thyroiditis in hypothyroidism (Mizokami, *et al.*, 2004). Subtle thyroid dysfunction is a negative prognostic factor for depression with an activation of autoimmune process and it needs some therapeutic intervention. There is a triangular relationship among thyroid dysfunction, atypicality and refractory depression (Fountoulakis, *et al.*, 2004).

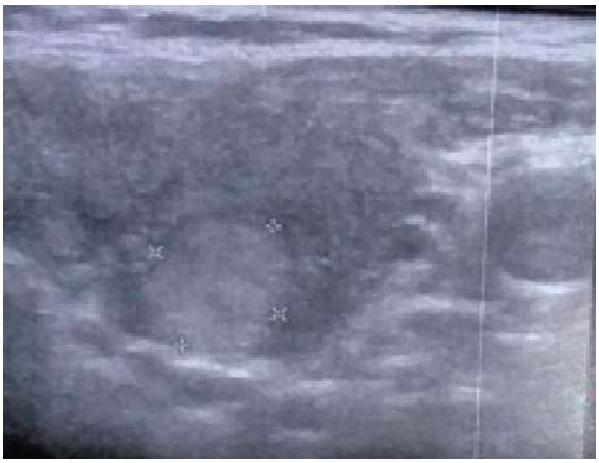

**Figure 27:** USG scan of left thyroid lobe of 70 year old female showing well defined hyperechoic nodule of nearly 0.8 cm in size with surrounding hypoechoic or sonolucent halo-rim. LLV and RLV are 9.42 mL and 11.60 mL, respectively noted as diffusely enlarged thyroid lobes (likely colloid goitre without vascularity) with multiple hypoechoic nodules (benign). Here TFT values for FT4 is 1.10 pmol/L and for TSH is 20.20 mIU/L indicating a case of overt hypothyroidism. Isthmus size is 10.10 mm

Hypothyroid disorder is related to pregnancy loss as early embryo loss and lower gestational age at abortion (De Vivo, *et al.*, 2010; Casey, *et al.*, 2005). There is increased pregnancy loss in euthyroid women having positive thyroid-antibody and TSH between 2.5-5.0 mIU/L in the first trimester (Negro, *et al.*, 2010). It is a strong evidence for redefining the upper limit of TSH for the women in the first trimester. Adequate treatment of hypothyroidism reduces pregnancy complications (Abalovich, *et al.*, 2002).

The USG diagnostic features of thyroid dysfunctions are also explained in disease based category within 87 (49 euthyroid + 38 hypothyroid) patients as depicted in Table 9 and shown in Figure 24. The USG scans of these patients are classified as normal, goitrous, nodular, thyroidytic, lesion hypoechoic, malignant, cystic and isthmus enlarged thyroid glands. Based on these categories of underactive thyroid, 9 hypothyroid patients (10.34%) aged 38.22 ± 11.53 years have normal thyroid gland with TGV of 6.77 ± 2.71 mL, TSH of 10.14 ± 6.32 mIU/L and normal FT4 or FT3 in average. 17 patients (19.54%) aged 41.65 ± 17.48 years have goitrous mass with TGV of 26.09 ± 28.20 mL ranging from 5.39 to 119.11 mL, TSH of 14.22 ± 25.00 pmol/L ranging from 0.47 to 100.00 mIU/L and FT4 of 11.00 ± 5.99 pmol/L ranging from 1.00 to 17.00 pmol/L.

31 patients (35.63%) aged 42.06 ± 12.67 years have thyroid nodules whose thyroid size is 13.09± 14.71 mL ranging from 4.31 to 84.29 mL, TSH is 7.28 ± 17.68 mIU/L ranging from 0.60 to 100.00 mIU/L and FT4 is 13.63 ± 4.51 pmol/L ranging from 0.68 to 20.54

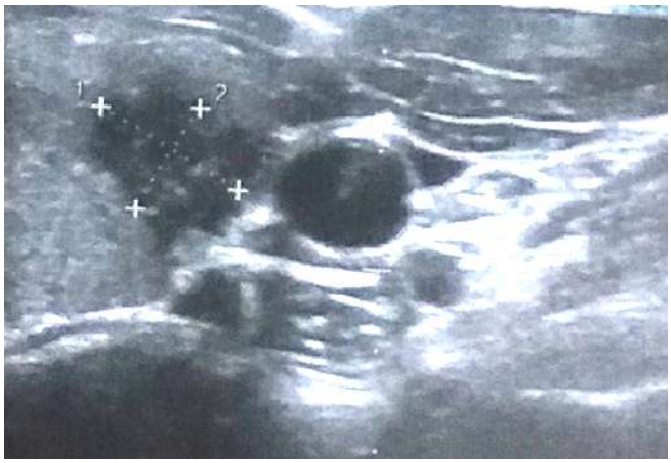

**Figure 28:** USG scan of left thyroid lobe of 21 year old female showing predominantly hypoechoic lesion of nearly 0.5 cm in size with minimal vascularity and lobulated outline. LLV and RLV are 8.99 mL and 2.25 mL, respectively having bilateral hypoechoic lesions for which FNA biopsy is suggested. Her TFT values for FT3, FT4 and TSH are 5.32 pmol/L, 11.10 pmol/L and 5.15 mIU/L indicating subclinical hypothyroidism

**Table 9:** Mean ± SD of age(year), TGV(mL), FT3(pmol/L), FT4(pmol/L) and TSH(mIU/L) in 87 patients (11M + 76F) where lesion hypoechoic, malignat and cystic groups have normal TFT values and others are clinically hypothyroid in average

| USG status | Normal | Goitrous | Nodular | Thyroiditic |
|---|---|---|---|---|
| N(%) | 9(10.34%) | 17(19.54%) | 31(35.63%) | 15(17.24%) |
| Age | 38.22± 11.53 | 41.65± 17.48 | 42.06± 12.67 | 39.35± 13.39 |
| TGV | 6.77± 2.71 | 26.09± 28.20 | 13.09± 14.71 | 12.05± 8.85 |
| FT3 | 5.43± 0.70 | 5.45± 1.22 | 5.32± 0.92 | 5.29± 1.80 |
| FT4 | 11.74± 3.22 | 11.00± 5.99 | 13.63± 4.51 | 12.07± 5.85 |
| TSH | 10.14± 6.32 | 14.22± 25.00 | 7.28± 17.68 | 26.08± 39.54 |
| USG status | Lesion hypoechoic | Malignant | Cystic | Isthmus enlarged |
| N(%) | 5(5.74%) | 3(3.45%) | 4(4.60%) | 3(3.45%) |
| Age | 45.20± 21.65 | 42.66± 7.02 | 34.75± 15.48 | 42.00± 25.53 |
| TGV | 6.55± 2.74 | 9.33± 1.82 | 6.64± 2.96 | 25.66± 8.96 |
| FT3 | 5.47± 0.85 | 5.13± 1.06 | 5.35± 1.62 | 6.1± 0.14 |
| FT4 | 11.38± 1.52 | 13.53± 1.57 | 14.3± 1.42 | 6.70± 7.18 |
| TSH | 3.79± 2.56 | 3.15± 2.51 | 3.41± 2.25 | 24.87± 22.27 |

pmol/L. In this category, two patients have larger thyroid size (84.29 mL and 32.19 mL) with multinodular goitre whereas others have the nodular thyroid ranging from 4.31 to 24.42 mL in size.

15 patients (17.24%) aged 39.35 ± 13.39 years whose thyroid volume is 12.05 ± 8.85 mL, TSH is 26.08 ± 39.54 mIU/L ranging from 0.60 to 100.00 mIU/L and FT4 is 12.07 ± 5.85 pmol/L ranging from 1.34 to 21.40 pmol/L with $p$ <0.001. Three patients have enlarged isthmus up to 10 mm in size with no nodular mass found by USG examination along with goitrous thyroid gland of size 25.66 ± 8.96 mL and TSH of 24.87 ± 22.27 pmol/L. The

remaining patients have cystic, hypoechoic and malignant lesions with normal thyroid size and normal TFT values in average as depicted in Table 9 and shown in Figure 24.

Hong *et al.* (2015) reviewed the pictorial essay of USG examinations related to echogenicity, diffuse thyroiditis, nodules, cysts and heterogenicity of thyroid disorder in children and adolescents. Our study presents both USG findings and biochemical status of hypothyroid patients on the basis of euthyroid subjects along with their conditions of psychology, habit, family history and pregnancy. A male patient aged 55 years has overt hypothyroidism and thyroid USG scan with poorly marginated hypoechoic areas and increased vascularity showing diffuse thyroiditis in the enlarged lobes (Figures 25 and 26). A female aged 70 years with overtly hypothyroid gland has a nodule of 0.8 cm in size surrounded by the hypoechoic or sonolucent rim in right thyroid lobe as shown in Figure 27.

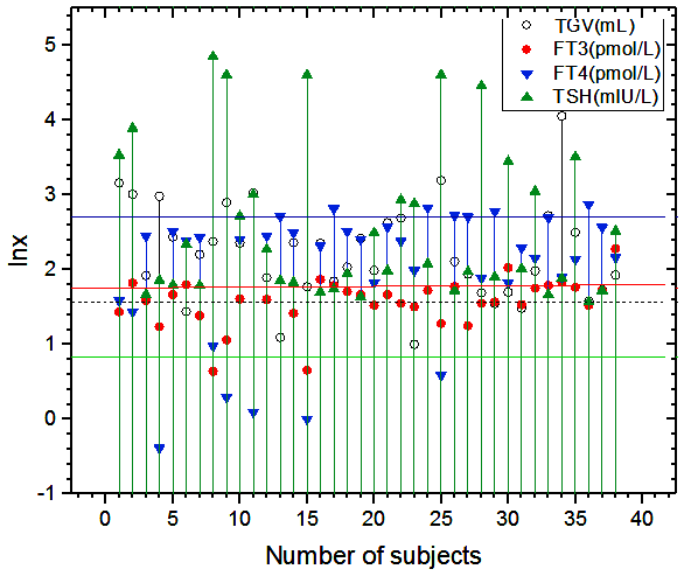


**Figure 29:** Distributions of TGV, FT3, FT4 and TSH taking logarithm of such variables in hypothyroid patients where horizontal lines represent corresponding reference levels taking average from eutthyroid or control group having normal thyroid USG and TFTs

A female aged 21 years has been suffering from subclinical hypothyroidism reflecting bilateral hypoechoic lesions in thyroid USG scan (Figure 28) whose FNAC suggested for the biopsy test. Peccin *et al.* (2002) reported USG analysis of thyroid nodules associated with malignancy characterized by absent halo, microcalcifications and hypoechogenicity. Caterugli *et al.* (2015) reviewed clinical and diagnostic features of Hashimoto's thyroiditis that relies on the circulating thyroid hormones, thyrotropin, thyroglobulin

and thyroperoxidase, and the reduced echogenicity on thyroid USG scan. Polyzos *et al.* (2008) reported that the patients presenting with thyroid nodules have increasing risk of malignancy with TSH concentration within the normal range. Thyroid USG results in association with biochemical reports and patients' family status, habits and environmental conditions are important for guiding treatment of thyroid dysfunctions.

The thyroid status of the hypothyroid patients (5M + 33F) aged 37.92 ± 13.56 years ranging from 15 to 70 years has been demonstrated by Figure 29. Among the distribution of logarithm of TGV, FT3, FT4 and TSH in the individuals, most of TGV and TSH lie above whereas FT3 and FT4 lie below the average reference line. The reference line is obtained from the control group having normal thyroid conditions. The linear regression analysis suggests that TGV and TSH have weak positive correlation ($r$ = 0.10, p = 0.57), TGV and FT4 are negatively correlated ($r$ = - 0.35, $p$ = 0.04), FT3 and FT4 are positively correlated ($r$ = 0.34, $p$ = 0.04), TSH and FT4 are negatively correlated ($r$ = -0.71, $p$ <0.001), FT3 and TSH have negative correlation ($r$ = -0.52, $p$ = 0.001) whereas no correlation between TGV and FT3. The strong negative correlations between TSH and FT3 or FT4 indicate the negative feedback mechanism of thyroid cycle in HPT-axis (Reichlin, *et al.*, 1967; Surks, *et al.*, 1990; Vagenakis, *et al.*, 1974). The circulating levels of FT3, FT4 and TSH are strongly correlated in hypothyroidism. The thyroid gland gets stressed by the increased TSH secretion and the gland abnormalities arise as a consequence of genetic misguiding by unliganded THRs.

## 4.4 Temperature Echoes and Dephasing by THR-Beta Dynamics in Euthyroid and Hypothyroid States

The euthyroid state has the normal TFT levels in the blood serum so that it is also said to be the T3 liganded state of THRs. The hypothyroid patients suffer from the disorders linked with thyroid gland as well as biochemical changes as explained in the Section 4.3. It is also necessary to explore the biophysical properties in molecular levels of such disordered states. The underactive thyroid has the T3 deficient phase of THRs so that the T3 activated and deactivated states of these nuclear receptors are to be analyzed from the echo feature curves. In the vibrational echo methods, the phase coherent states of normal modes are observed finely even from the short-run simulations of an anhydrous protein

complex. Many physical parameters associated with the protein dynamics can be explored from this technique by saving the computer time. The most important nuclear receptor, THR-$\beta$ liganded with T3 hormone plays a key regulatory role in basal transcription, metabolism and thyroid functioning. The THR-$\beta$ complex (3GWS.pdb) is built from a sequence of 259 amino acids. The T3 liganded THR-$\beta$ (THRT3) comprises 3930 atoms, mass of 28291 amu and 1964 bonds of H-atoms. The T3 hormone contributes additional mass, interacting atoms and H-bonds to the THR-$\beta$ LBD. The unliganded THR-$\beta$ (THR) constitutes 3895 atoms, mass of 27640 amu and 1952 bonds of H-atoms. Due to these facts, the results of THR and THRT3 systems also differ in the cases of FVA1 and CVH2 simulations.

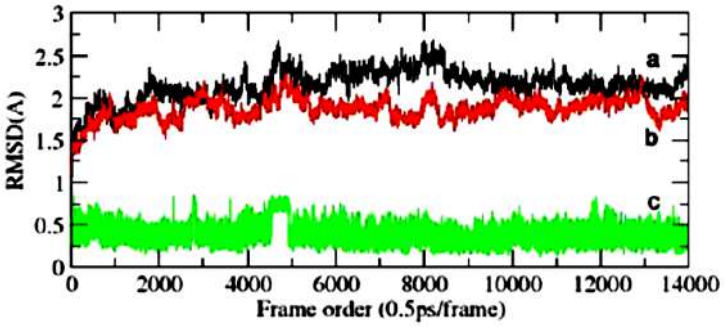


**Figure 30:** RMSD plots of (a) THR-protein, (b) THRT3-protein and (c) T3-hormone during equilibrations in water-ion solution under CVH2 condition at 310 K

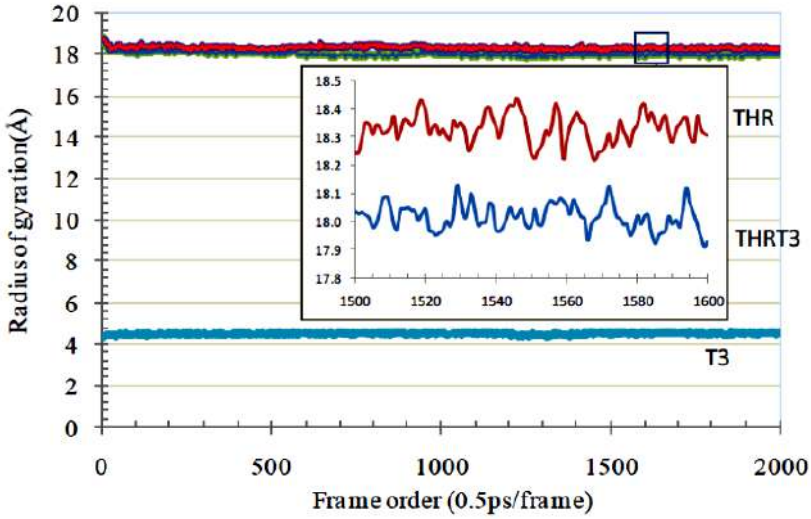


**Figure 31:** RG plots of THR and THRT3 during equilibrations in vacuo under CVH2 condition at 310 K

As shown by the Figure 30, the RMSD of the protein backbone in THR or THRT3 system lies quite below 2.5 Å during the equilibration and production runs in water-ion

solution as well as vacuo. It reflects the conformational stability of the molecules. The small fluctuations seen in RMSD and RG plots are due to the continuous breaking and reforming of some H-bonds between free residues and stable strands of the receptor protein during MD simulations (Rahat, *et al.*, 2009).

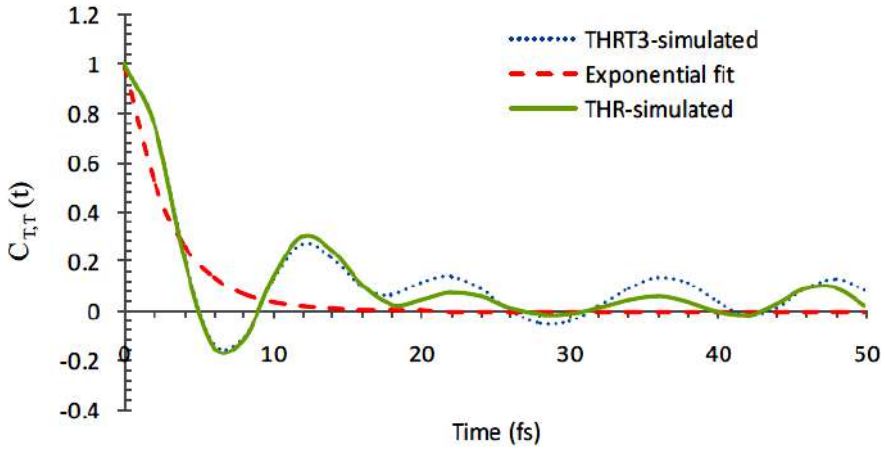


**Figure 32:** Temperature autocorrelation functions of THR and THRT3 during NVE simulations under CVH2 conditions

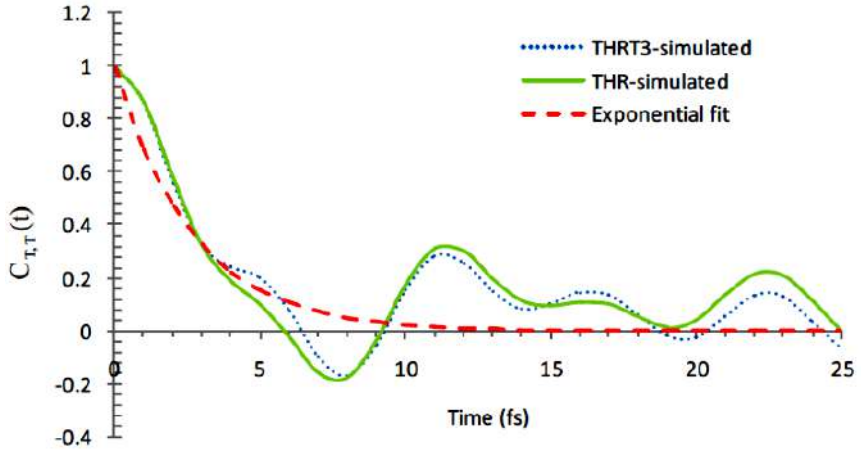


**Figure 33:** Temperature autocorrelation functions of THR and THRT3 during NVE simulations under FVA1 conditions

While performing equilibrating simulations of the nanodroplets, the THR or THRT3 molecule has the average RG of 18.33 ± 0.40 Å. The molecules are stable in vaucuum simulations also. Their stability is explained by the almost constant values of RG plotted in Figure 31 where the mean RGs of THR, THRT3 and T3 are 18.35 ± 0.08 Å, 18.04 ± 0.09 Å and 4.50 ± 0.05 Å, respectively. The value of RG indicates the protein structure compactness (Lobanov, *et al.*, 2008). In NVT simulations, the fluctutating temperature around 310 K shows the dynamic nature of atomic particles. There is a higher impact

of anharmonic interactions in hydrous state than in anhydrous state of proteins so that the phase coherent states or echo features are more distinctly observed in vacuo than in solution.

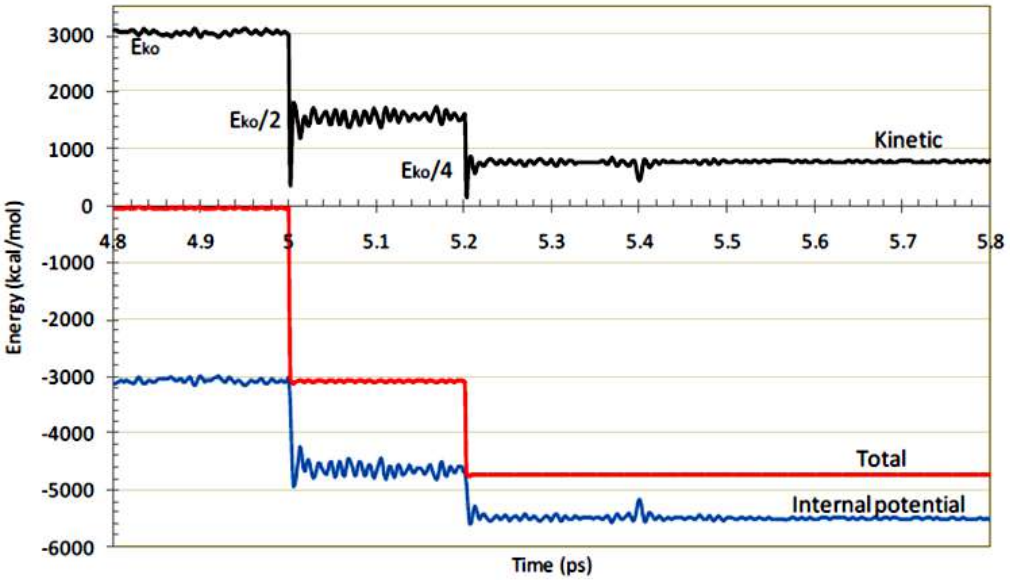


**Figure 34:** Perturbed kinetic, internal potential and total energy distributions parallel to the temperature distribution in THRT3 by the CVH2 simulations in NVE ensemble for the delay time $\tau$ = 0.2 ps

During the NVE simulations in vacuo, the temperature autocorrelation function $C_{T,T}(t)$ varies distinctly for THR and THRT3 in both CVH2 and FVA1 conditions as shown in Figures 32 and 33. The effect of anharmonicity is higher in free vibrations than in constrained vibrations of the protein atoms. So, the function $C_{T,T}(t)$ is smoother in the CVH2 case than in the FVA1 case. The impact of T3 is reflected by the distinctly changing $C_{T,T}(t)$ in THR w.r.t. THRT3. The function $C_{T,T}(t)$ is decaying exponentially with time and its decay time $\tau_d$ is calculated by fiiting with the single exponential function $e^{-t/\tau_d}$. The value of $\tau_d$ for THR or THRT3 lies within some error limit which is 3.00 ± 0.03 fs in the CVH2 and 2.80 ± 0.15 fs in the FVA1 simulations. These values are in close agreement with the decay time, 2.67 fs for the bacteriorhodopsin protein as calculated by Schulten, *et al*., 1997. The effect of anharmonic interactions is such that the function $C_{T,T}(t)$ decays faster in the FVA1 than in the CVH2 simulations.

The temperature quenching at the particular delay time $\tau$ makes the system perturb and its response is observed at $2\tau$ in the form of echo in both cases CVH2 and FVA1. The depth of echo and its nature differ in THRT3 from that of THR due to the presence of

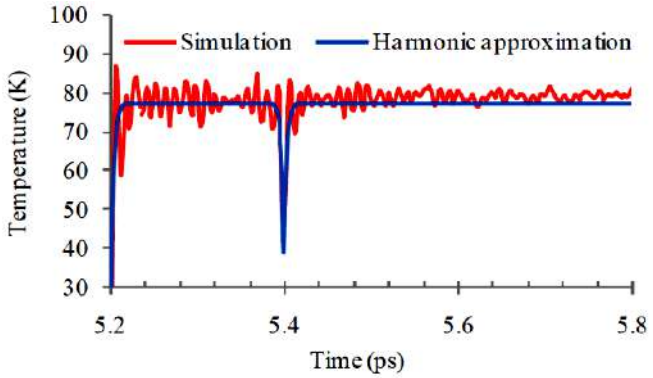


**Figure 35:** Temperature quench echo in THRT3 under harmonic approximation by CVH2 simulations in NVE ensemble for $\tau$ = 0.2 ps

T3 hormone. These are the inherent properties of the hormone-receptor interactions applicable for the euthyroid or T3 liganded state and the overt hypothyroid or unliganded state of thyroid disorders. The status of kinetic, internal potential and total energy distributions during temperature quenching and echo formation are demonatrated in the Figure 34 by reassigning the atomic velocities at $t_0$ = 5 ps and at $t_1$ = 5.2 ps, i.e. for the delay time $\tau = t_1 - t_0$ = 0.2 ps. Then, the echo appears at $t = t_0 + 2\tau$ = 5.4 ps. For the smaller $\tau$, the temperture echo obtained by the MD simualtions is approximately matching with the theoretical plot of harmonic approximation (Equation 3.9) as shown in the Figure 35. The effect of anharmonicity increases with increase in $\tau$ resulting with the decreasing echo depth. Such impact is more intensive in FVA1 than in CVH2 simulations. For $\tau$ = 0.2 ps, the depths of temperature quench echo are $\Delta T$ = 31.86 K and $\Delta E_K$ = 311.05 kcal/mol in THRT3 whereas $\Delta T$ = 33.92 K and $\Delta E_K$ = 327.96 kcal/mol in THR molecule during the CVH2 simulations.

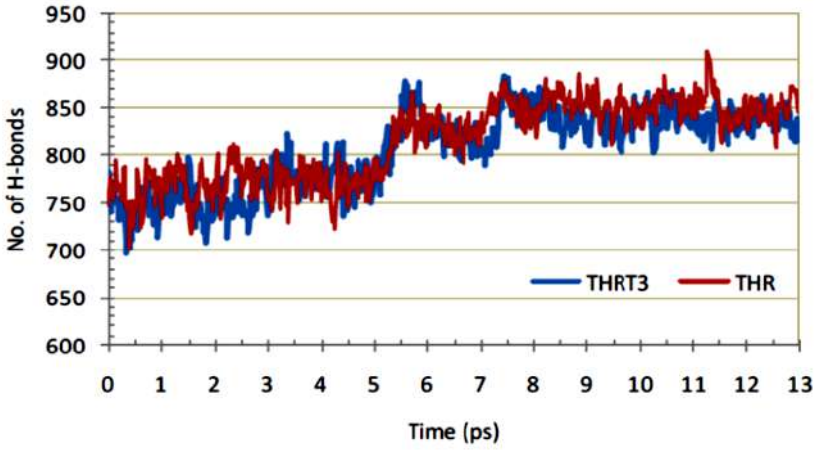


**Figure 36:** Changing H-bonds during the temperature quenching in NVE ensembles of THR and THRT3 for the case of CVH2 and $\tau$ = 2 ps

We analyze the conformations of THR and THRT3 when they are perturbed by quenching the temperature twice to zero and released. At such quenching points, the protein becomes more globular by decreasing RG and increasing H-bonds $N_H$. As shown in Figure 36, $N_H$ gets step-up jump at the temperature quenching points, i.e. at $t_1$ = 5 ps and $t_2$ = 7 ps. Here, donor-acceptor distance = 4 Å and cut-off angle = $40^o$ while counting $N_H$. The molecules are conformationally changed by the formation of new H-bonds (Rahat, *et al.*, 2009). The molecule THRT3, while implementing second quenching, gets jiggled slightly to return to its normal mode as shown by the kink in RG plot (Figure 37). It may be due to the presence of the heavy ligand T3 in THR-$\beta$ LBD. $N_H$ is negatively correlated with RG and T as demonstrated by their observed values in the Table 10. Also, the Figure 38 shows that the Pearson's correlation between $N_H$ and RG is $r$ = -0.86 taking the case of CVH2 simulations in NVE ensembles of THRT3.

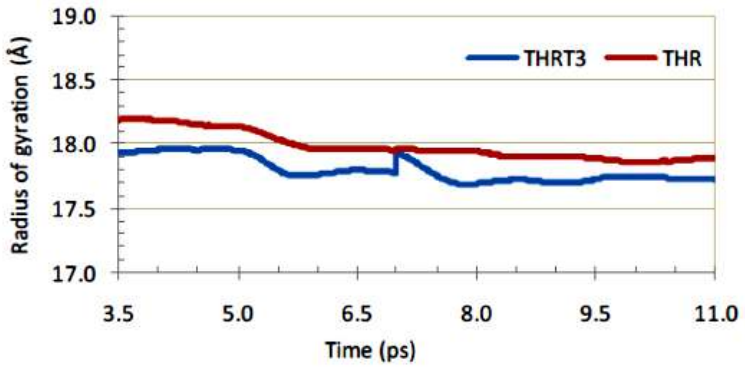


**Figure 37:** RG plots of THR and THRT3 during the temperature quenching where the RG of THRT3 gets jiggled at the second quenching point $t_2$ = 7ps

**Table 10:** Mean values of physical parameters observed by the CVH2 simulations during the temperature quenching in NVE ensembles of THR and THRT3 for the delay time $\tau$ = 2 ps

| Time frame | Molecule | $T$(K) | $E_{\text{tot}}$(kcal/mol) | $N_H$ | RG(Å) |
|---|---|---|---|---|---|
| $0 \leq t \leq 5$ ps | THR | 312.52 | -150.44 | 770 | 18.14 |
| | THRT3 | 311.12 | -43.17 | 761 | 17.95 |
| $5 \leq t \leq 7$ ps | THR | 153.55 | -3331.33 | 821 | 18.00 |
| | THRT3 | 160.43 | -3095.94 | 824 | 17.81 |
| $7 \leq t \leq 13$ ps | THR | 77.29 | -4854.71 | 852 | 17.91 |
| | THRT3 | 78.77 | -4743.17 | 840 | 17.73 |

At the temperature quenching points, the total energy also gets step jump along with the kinetic and potential energies (Figure 34). In spite of the largely changing kinetic temperature, the total energy remains almost constant in the vicinity of echo where the downward echo pulse in kinetic energy is compensated by the upward echo pulse in total

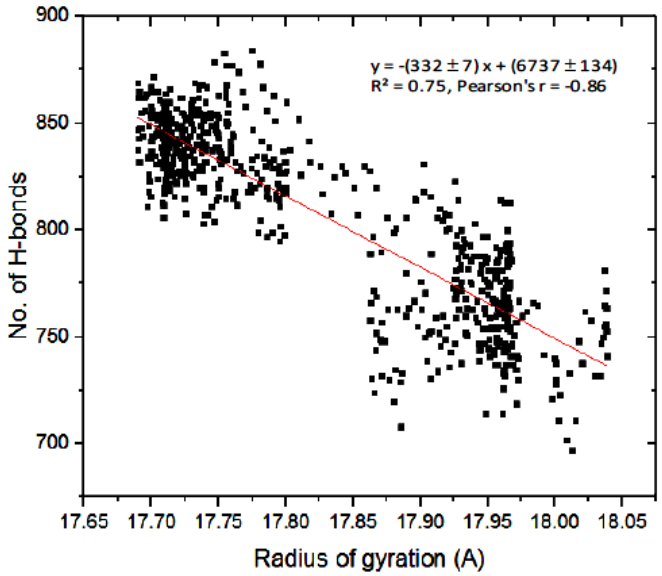


**Figure 38:** $N_H$ *vs* RG plot during the temperature quenching in NVE ensemble of THRT3 for the case of CVH2 and $\tau$ = 2 ps

internal potential (Figure 39 and 40). This principle is applicable for each and every cases of CVH2 and FVA1 simulations of THR and THRT3 and also for the different delay time $\tau$ ranging from 0.1 to 2 ps. Referring to the energy terms, the largest echo is observed in the bond angle potential (BP) due to the skeletal motion of the normal modes in the constituent atoms.

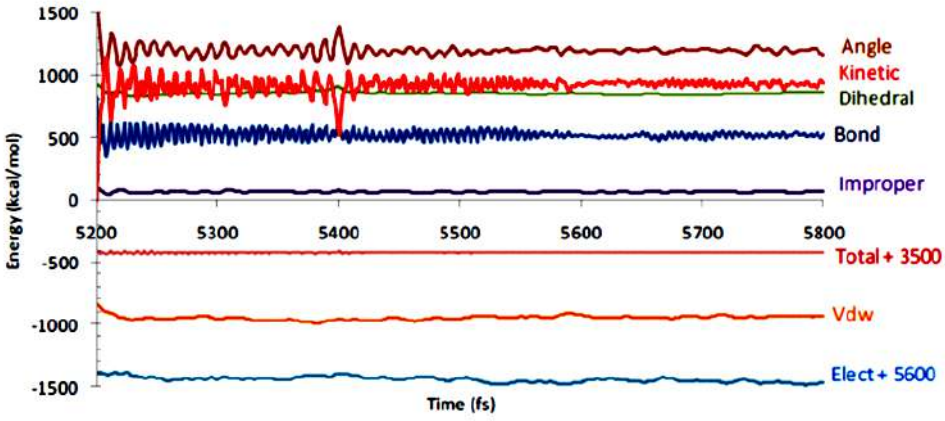


**Figure 39:** Temperature quench echoes in the kinetic and internal potential energies by the FVA1 simulations of THRT3 in NVE ensemble for $\tau$ = 0.2 ps

In the case of constant velocity (at T = 310 K) replacement echo for the condition of CVH2 and $\tau$ = 0.2 ps, the maximum energy difference at the echo-time zone (t = 5.400 ± 0.008ps) are $\Delta E_K$ = 1415.68 kcal/mol and $\Delta E_{BP}$ = 987.73 kcal/mol in THR whereas

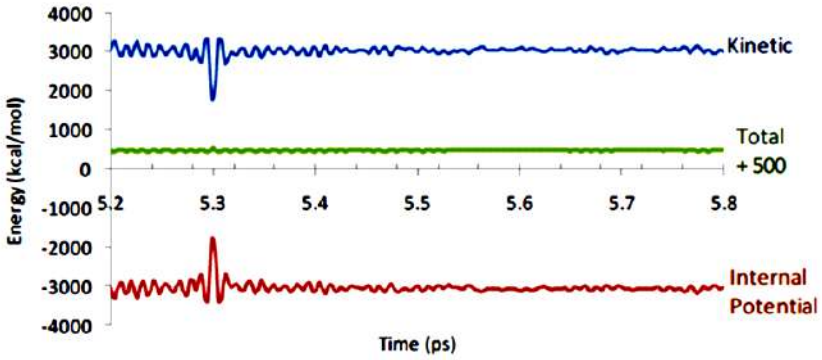


**Figure 40:** Vicinity of constant velocity (at T = 310 K) replacement echoes in the kinetic and internal potential energies by the CVH2 simulations of THRT3 in NVE ensemble for $\tau$ = 0.2 ps

$\Delta E_K$ = 1552.84 kcal/mol and $\Delta E_{\mathrm{BP}}$ = 1025.85 kcal/mol in THRT3. The higher $\Delta E_{\mathrm{BP}}$ in THRT3 is due to the additional skeletal motion provided by the T3 hormone to its THR-$\beta$ LBD. It suggests that the momentum transfer mechanism is resisted in overt hypothyroidism. The T3 deficient or the unliganded THR-$\beta$ acts as a repressor of gene transcription.

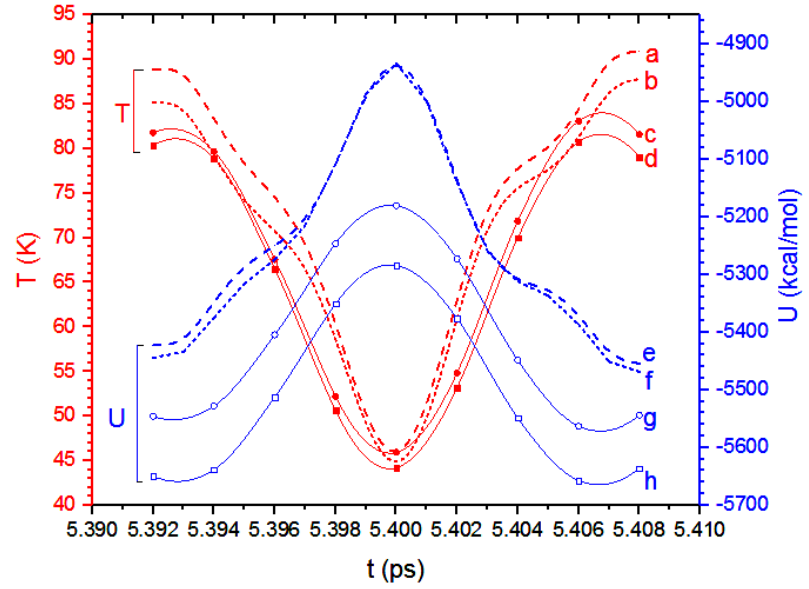


**Figure 41:** The nature of echo pulses in THR (curves: a,d,f,h) and THRT3 (curves: b,c,e,g) shown with the changing temperature $T$ (red) and internal potential $U$ (blue) at the echo-time zone, i.e. t = 5.400 ± 0.008 ps where the dotted curves (a,b,e,f) represent FVA1 and the smooth curves (c,d,g,h) represent CVH2 simulations for $\tau$ = 0.2 ps

The diseased state THR is signficantly different from the normal THRT3 regarding the nature of echo pulses observed in temperature $T$ and internal potential $U$ as shown in the Figure 41. Such echo pulses appear by quenching the temperature twice to zero for the

delay time $\tau$ = 0.2 ps. The echo curves consist of shoulder like features in FVA1 and these are smoother in CVH2 simulations. The FVA1 simulations include the anharmonic interactions of all atoms so that the distinct features are seen in the phase coherent state or resonance. The largely changing $U$ w.r.t. $T$ in the echo-time zone (t = 5.400 ± 0.008 ps) results the heat capacity $C_{V2}$ of the related system. The effect of anharmonicity increases with the delay time $\tau$ so that the height $\Delta U(t)$ or the depth $\Delta T(t)$ of echo pulse decreases with $\tau$ (Figure 42). However, $\Delta U(t)$ as well as $\Delta T(t)$ increases with the increase in temperature of quenching from 0 K to the higher scale (Figure 35 and 40).

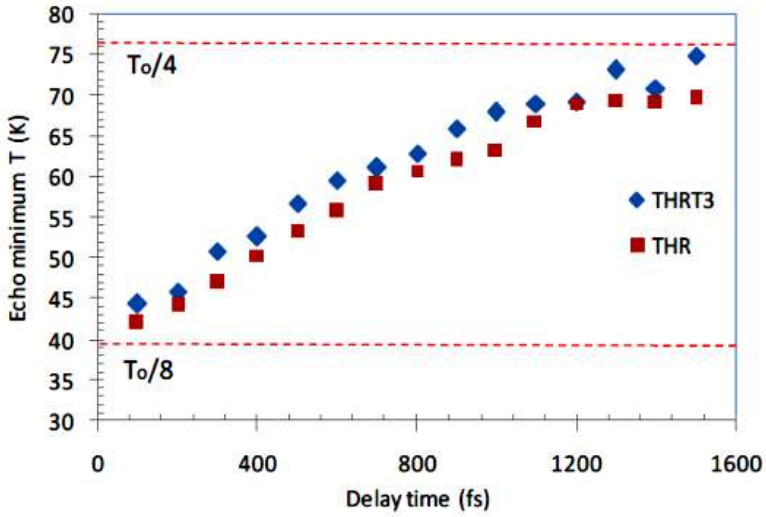


**Figure 42:** Variation of echo-minimum temperature with the delay time $\tau$ while dephasing THR and THRT3 by temperature quenching under CVH2 condition

The echo-minimum temperature $T_{min}(t)$ changes exponentially with the dealy time $\tau$ as shown in the Figure 42. It shows that the dephasing of phase coherent state in THRT3 differs from THR due to the change in degrees of freedom and anharmonic interactions. In both CVH2 and FVA1 conditions, the data of $E_K(t)$, $U(t)$ and $E_{tot}(t)$ are plotted w.r.t. $T_{min}(t)$ related to the values of $\tau$ ranging from 0.1 to 2 ps for both THR and THRT3 (Figure 43). A perfect straight line ($R^2$ = 1) is obtained for the kinetic energy with a positive slope equivalent to the partial heat capacity $C_{V1}$. Also, the straight line ($R^2$ = 0.98 ± 0.1) with negative slope is obtained for the internal potential energy in which the slope represents the partial heat capacity $C_{V2}$ of normal or diseased state THR-$\beta$. The constancy of total energy slightly fluctuates due to the temperature dependancy of changing $U(t)$ in NVE ensemble. Also, it supports the fact behind temperature dependent nature of $C_{V2}$.

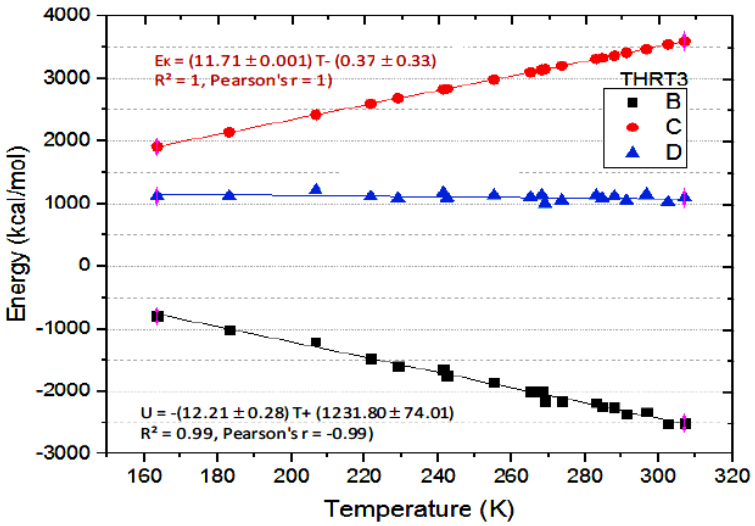


**Figure 43:** Change in potential energy (B), kinetic energy (C) and total energy (D) with echo-minimum temperature during the vibrational dephasing of THRT3 by the constant velocity (at T = 310 K) reassignments under FVA1 condition in NVE ensemble

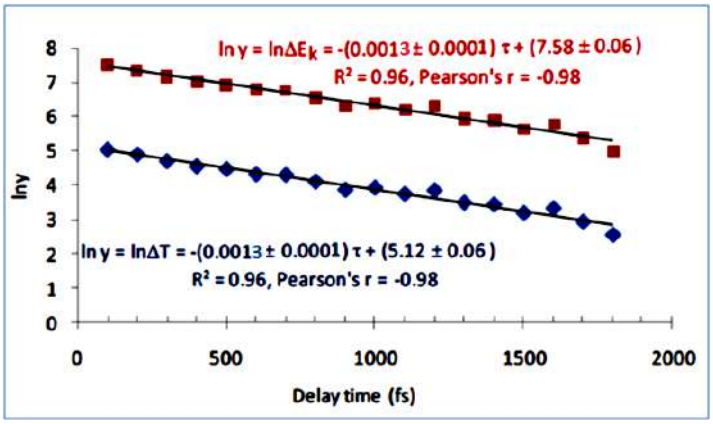


**Figure 44:** Linear fit in logarithm of echo depth $\Delta E_K(t)$ or $\Delta T(t)$ with the delay time $\tau$ during the vibrational dephasing of THRT3 by the constant velocity (at T = 310 K) reassignments under FVA1 condition

In the CVH2 simulations of THR and THRT3, the constarined degrees of freedom $N_C$ are 1952 and 1964 so that the values of $C_{V1}$ (using the Equation 3.13) are 9.66 and 9.75 kcal mol$^{-1}$K$^{-1}$, respectively. In the FVA1 case, $N_C = 0$ so that the Equation 3.13 yields $C_{V1}$ as 11.60 and 11.70 kcal mol$^{-1}$K$^{-1}$ for THR and THRT3, respectively. These values of $C_{V1}$ are matching with the results obtained from the simulations within the error limit ± 0.01 kcal mol$^{-1}$K$^{-1}$ (see the slope of $E_K$ vs $T$ straight line in the Figure 43). In the echo-temperature range $\Delta T = 40 \leq T_{min} \leq 80$ K, the values of $C_{V2}$ are 11.24 ± 0.65 and 11.62 ± 0.66 kcal mol$^{-1}$K$^{-1}$ for the FVA1 case of THR and THRT3, respectively. The related values are slightly higher in the higher range $\Delta T = 160 \leq T_{min} \leq 310$ K as depicted in the Table 11. The temperature range $\Delta T$ in the quench echoes differs from

the constant velocity replacement echoes.

**Table 11:** Physical parameters given with standard error (SE) resulting from vibrational dephsing of THR and THRT3 under CVH2 and FVA1 simulations where $C_{V2}$ is calculated in the echo-temperature range $\Delta T$ and others are at 310 K (the results are compared with the experimental values** shown at the bottom)

| **Parameters** | **Constrained H-atoms with 2 fs/step (CVH2)** | | | |
|---|---|---|---|---|
| Molecule | THR | | THRT3 | |
| $\tau_0$ (ps) | 0.83 ± 0.034 | | 0.62 ± 0.04 | |
| $b_0$ (ps$^{-1}$) | 1.21 ± 0.05 | | 1.60 ± 0.10 | |
| $D_0$ (rad ps$^{-1}$) | 0.40 ± 0.02 | | 0.53 ± 0.03 | |
| $\mu_0$ (mol/kcal/ps) | 0.65 ± 0.03 | | 0.86 ± 0.05 | |
| $\Delta T$(K) | 40-80 | 160-310 | 40-80 | 160-310 |
| $C_{V2}$(kcal/mol/K) | 8.89±0.79 | 10.18±0.46 | 9.09± 0.72 | 10.78±0.60 |
| $C_{V2}$(J/kg/K) | 1347.97±119.69 | 1542.42± 69.69 | 1345.58±106.58 | 1595.75± 88.81 |
| **Parameters** | **Free vibrations with 1 fs/step (FVA1)** | | | |
| Molecule | THR | | THRT3 | |
| $\tau_0$ (ps) | 0.81 ± 0.02 | | 0.79 ± 0.03 | |
| $b_0$ (ps$^{-1}$) | 1.23 ± 0.03 | | 1.27 ± 0.05 | |
| $D_0$ (rad ps$^{-1}$) | 0.41 ± 0.01 | | 0.42 ± 0.02 | |
| $\mu_0$ (mol/kcal/ps) | 0.66 ± 0.02 | | 0.68 ± 0.03 | |
| $\Delta T$(K) | 40-80 | 160-310 | 40-80 | 160-310 |
| $C_{V2}$(kcal/mol/K) | 11.24±0.65 | 11.64±0.49 | 11.62±0.66 | 12.21±0.28 |
| $c_{V2}$(J/kg/K) | 1703.03±98.48 | 1763.63±74.24 | 1720.09±97.69 | 1807.43±41.44 |

**

1. $c_{V2}$ of native proteins varies from 1200 to 2300 Jkg$^{-1}$K$^{-1}$ at 298 K (Privalov, *et al.*, 1986).
2. $\tau_0$ = 884 fs for BPTI protein (Xu, *et al.*, 1995).
3. $\tau_0$ = 700 fs and $b_0$ = 1.43 ps$^{-1}$ for bacteriorhodopsin protein (Schulten, *et al.*, 1997).

The key thyroid hormone T3 contributes the partial heat capacity $C_{V2}$ = 0.57 kcal mol$^{-1}$K$^{-1}$ to its receptor protein THR-$\beta$ in the euthyroid state (at about 310 K). The unliganded THR has lower specific heat so that the patients have the symptom of cold intolerence in the overt hypothyroid state. In our study under the free atomic vibrations FVA1, the partial specific heat capacities ($c_{V2}$) of THR and THRT3 are 1763.63 ± 74.24 and 1807.43 ± 41.44 Jkg$^{-1}$K$^{-1}$, respectively. All the values of $c_{V2}$ mentioned in the Table 11 lie within the experimental ange: 1200-2300 Jkg$^{-1}$K$^{-1}$ as determined by Privalov *et al.* (1986) for the native proteins at about 300 K. Under CVH2 conditions, $c_{V2}$ of THR and THRT3 at about 300 K are 1542.42 ± 69.69 and 1595.75 ± 88.81 Jkg$^{-1}$K$^{-1}$, respectively which are slightly greater than 1250 ± 13 Jkg$^{-1}$K$^{-1}$ as observed by Gomez *et al.* (1995) for the anhydrous proteins at 298 K.

The linearly fitted plots of $ln(\Delta E_K)$ *vs* $\tau$ (Equation 3.18 fitted with the simulated data as in Figure 44) give the values of anharmonic constants, i.e. dephasing time $\tau_0$, damping

constant $b_0$, diffusion constant $D_0$ and mobility $\mu_0$ from the slope and the partial heat capacity $C_{V1}$ from the intercept. All these values related to THR and THRT3 under CVH2 and FVA1 simulations are depicted in the Table 11. $\tau_0$ of THR and THRT3 under FVA1 condition are 813 ± 20 fs and 787 ± 31 fs, respectively. In both FVA1 and CVH2 cases, $\tau_0$ of normal and diseased state THR-$\beta$ lies in a range 0.6-0.8 ps. It is also in agreement with $\tau_0$ = 884 fs of BPTI protein (Xu, *et al.*, 1995) and 700 fs of bacteriorhodopsin protein (Schulten, *et al.*, 1997). The cause behind the faster dephasing of hormone binding nuclear receptors is the higher effect of anharmonicity on the normal modes of vibrations when the systems are perturbed suddenly and released. These inherent properties, differently observed in euthyroid and hypothyroid states, are significantly important to understand the energy transfer mechanism from THRT3 to T3 response elements (TREs) of DNA sequences probing gene expressions. The results associated with echo dephasing of T3-liganded and unliganded THR-$\beta$ genes are also published in the paper by Lamichhane *et al.* (2019).

### 4.5 Heat Conduction by THR Isoforms in Euthyroid and Hypothyroid States

The heat transfer properties of unliganded THR-$\beta$ related to hypothyroidism and that of T3/T4 liganded THR isoforms (THRT3-$\beta$, THRT3-$\beta$1 and THRT3T4-$\alpha$) related to euthyroidism are discussed in this Section 4.5. The results are obtained by means of NAMD simulations under the periodic as well as spherical bounadry conditions. The detailed method has been written in the Section 3.2.2. During the equilibrating simulations up to 20 ns, each of the systems is conformationally stable as verified by the RG or RMSD plots (Figure 45 and 46). The mean RMSDs of THR-$\beta$, THRT3-$\beta$, THRT3-$\beta$1 and THRT3T4-$\alpha$ proteins are 2.61 ± 0.50, 2.13 ± 0.38, 1.98 ± 0.21 and 2.24 ± 0.31 Å, respectively; and the related RGs are 18.70 ± 0.09, 18.74 ± 0.07, 18.84 ± 0.11, and 18.41 ± 0.06 Å given with standard deviation (SD). The H-bond breaking and reformation among free residues and stable strands make the RG or RMSD plots fluctuate minutely during the MD simulations. The THR-nanodroplets are subjected to production runs to obtain their partial heat capacity in canonical ensemble. During the production runs, the RMSDs are mcuh lower values, i.e. 1.23 ± 0.11, 1.41 ± 0.18 and 1.13 ± 0.11 Å for THRT3-$\beta$, THRT3-$\beta$1 and THRT3T4-$\alpha$ proteins, respectively.

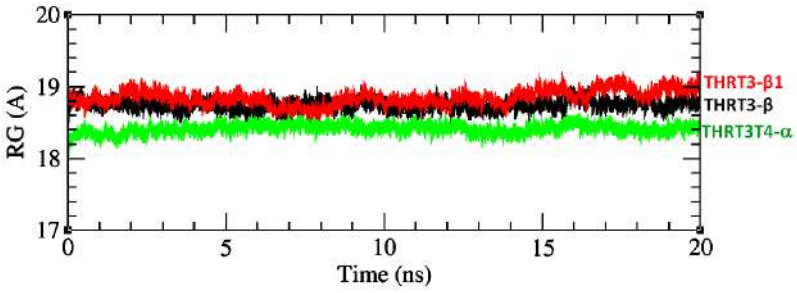


**Figure 45:** RG plots of the protein backbone during equilibrations of THR-nanodroplets at 310K

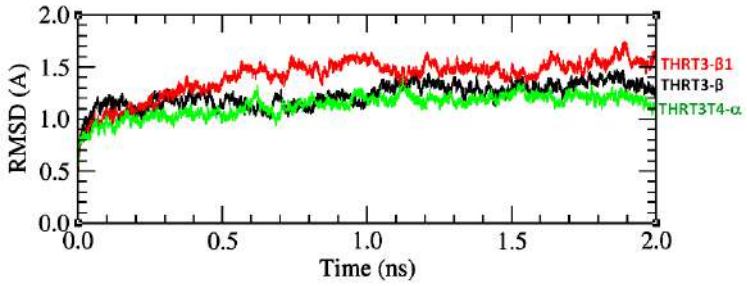


**Figure 46:** RMSD plots of the protein backbone during NVT production runs of of THR-nanodroplets at 310K

The molecules THR-$\beta$ and THRT3-$\beta$ are subjectued to NVT simulations at the temperature differences of 5 K across 310 K under the periodic boundary conditions. The mean energy $< U >$ of both systems is recorded for each $T$. The slope of linear fit in $< U >$ *vs* $T$ datapoints ($R^2$ = 0.99 in Figure 47) results the partial heat capacity $C_V$ = 85.59 ± 1.12 kcal mol$^{-1}$K$^{-1}$ for THR-$\beta$ water-box (mass = 131186 amu) and 84.59 ± 0.74 kcal mol$^{-1}$K$^{-1}$ for THRT3-$\beta$ water-box (mass = 131765 amu). The related specific heats are 2732.31 ± 35.75 and 2688.52 ± 23.52 Jkg$^{-1}$K$^{-1}$ at about 310 K. In this way, the NVT simulations of a modelled water-ion box (mass = 45357 amu) are performed under the same CVH2 conditions in order to plot for $< U >$ *vs* $T$ sraight line. The slope of the best linear fit ($R^2$ = 0.99 in Figure 48) results the partial heat capcaity $C_V^w$ = 31.72 ± 0.43 kcal mol$^{-1}$K$^{-1}$, i.e. the partial specific heat $c_V^w$ = 2928.75 ± 39.70 Jkg$^{-1}$K$^{-1}$ which is contributed only by electrostatic and van der Waal energy of the neutral water-ion box for the CVH2 case. The masses of anhydrous THR-$\beta$ and THRT3-$\beta$ are 27640 amu and THRT3-$\beta$ is 28291 amu, respectively. By using the Equation 3.21, the partial specific heat of THR-$\beta$ in solution is $c_V^p$ = 1996.25 ± 20.95 Jkg$^{-1}$K$^{-1}$ and that of THRT3-$\beta$ is 1809.88 ± 35.66 Jkg$^{-1}$K$^{-1}$. The T3 hormone-receptor interactions include hydrophobic, vibrational and conformational contributions to change the heat capcity of the system in solution (Eftink, *et al.*, 1983 and Sturtevant, *et al.*, 1977).

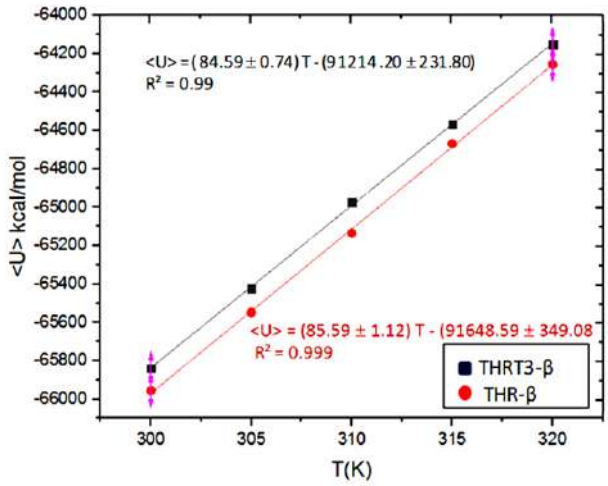


**Figure 47:** Variations of mean energy $< U >$ with temperature $T$ of THR-$\beta$ and THRT3-$\beta$ water-box where the slope of the best fitted straight line gives their partial heat capacity

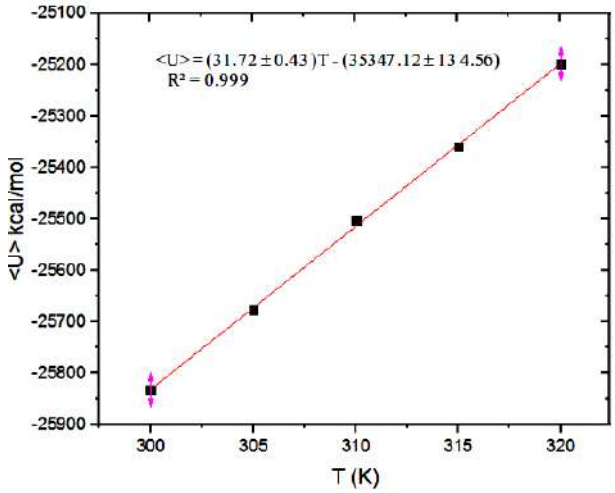


**Figure 48:** Variations of mean energy $< U >$ with temperature $T$ of a neutral water-ion box where the slope of the best fitted straight line gives its partial heat capacity

The heat capacities of THR and THRT3 determined from the linear best fit in $< U >$ *vs* $T$ as discussed above are matching with their values obtained from the method of energy fluctuations in NVT ensemble (using Equation 3.20). The partial heat capacities $C_V$ along with the related parameters such as number of atoms $N$, total mass $M$, mean square energy $< U^2 >$ and $< U >^2$ of the diseased state and normal THR-nanodroplets are presented in the Table 12. The fluctuating internal energy $U$ of THR-$\beta$ as well as THRT3-$\beta$ nanodroplet at 310 K is shown in Figure 49 where $< U >$ = -66286.35 ± 128.43 and -66218.22 ± 128.76 kcal/mol, respectively. The fluctuating energy levels for obtaining $< \delta U^2 >$ of T3/T4 liganded THR-nanodroplets are plotted in Figure 50 from the data of NVT production runs perfomed after the 20 ns equilibrations. The

partial specific heat capacities $c_V^p$ of the THR-isoforms are depicted in Table 13 which are obtained by putting the related values of protein mass $M_P$, solution or water-ion mass $M_W$, total mass $M$, specific heat $c_V$ of the mixture droplet and specific heat $c_V^w$ of water-ion in the Equation 3.21. Here, $c_V^p$ (THRT3) = 2030.62 ± 105.32 $Jkg^{-1}K^{-1}$ and $c_V^p$ (THR) = 2008.75 ± 107.77 $Jkg^{-1}K^{-1}$ with the higher value for the liganded one. Moreover, the nuclear receptor in the T3 deficient hypothyroid state loses specific heat capacity showing the symptoms of cold intolerance. Every value $c_V^p$ of THR isoforms (Table 13) lies within the experimental range, i.e. 1200-2300 $Jkg^{-1}K^{-1}$ of the native globular proteins at 298 K (Privalov, *et al.*, 1986). Privalov determined the heat capacities of the proteins in folding and unfolding states at the different temperatures. However, the specific heat $c_V^p$ that we calculated from the temperature rate of change of mean energy or from the internal energy fluctuations of THRs are slightly higher than the heat capacities of proteins in solution (6.5 ± 2.1 $kJmol^{-1}K^{-1}$ for myoglobin and 180 ± 35 $kJmol^{-1}K^{-1}$ for $Ca^{2+}$ ATP-ase) determined by Lervik *et al.* (2010) using MD simulations. In this way, we can compare the results of $c_V^p$ with the average specific heat of the hydrous globular proteins which is about 1500 $Jkg^{-1}K^{-1}$ at 300 K (Yu, *et al.* 2005; Yang, *et al.* 1979; Gomez, *et al.*, 1995; Cooper, 2000). According to Pandey *et al.* (2017), the partial heat capacity of dry state and hydrated proteins ranges from 0.494 to 0.606 cal $g^{-1}K^{-1}$ with the higher value in solution at 300 K. It is influenced by the protein-water H-bonds in the hydration state. Our results of $c_V^p$ also lie within the hydration limit of specific heat reported by the Pandey's study.

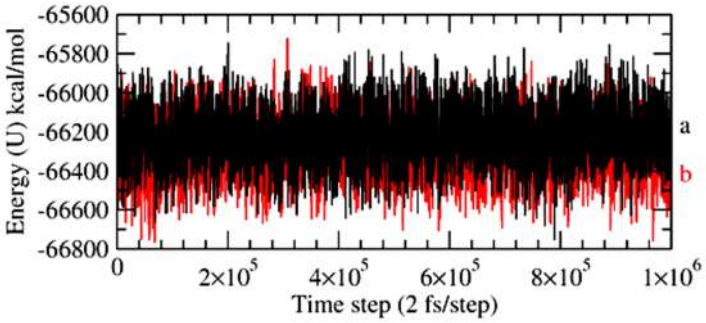


**Figure 49:** Energy fluctuations to obtain $< \delta U^2 >$ of the nanodroplets solvating (a) liganded THRT3-$\beta$ (black) and (b) unliganded THR-$\beta$ (red) during NVT production runs after the 20 ns equilibrations

Performing the temperature relaxation from 310 to 200 K and fitting the simulated data with the non-linear Equation 3.23 as shown in Figure 51, we obtain thermal diffusiviy $D$

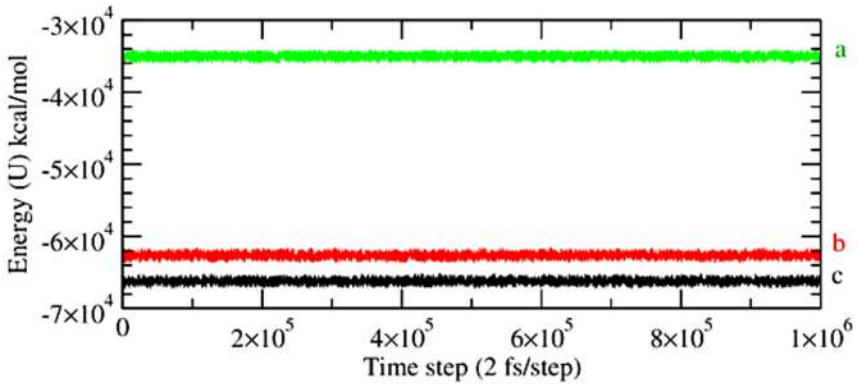


**Figure 50:** Fluctuating energy levels to obtain $< \delta U^2 >$ of the nanodroplets solvating (a) THRT3T4-$\alpha$ (green), (b) THRT3-$\beta$1 (red) and (c) THRT3-$\beta$ (black) during NVT production runs after the 20 ns equilibrations

of THR isoforms ranging from $1.28 \times 10^{-7}$ to $1.57 \times 10^{-7}$ m$^2$/s. Such values of $D$ are close to $D_w = 1.46 \times 10^{-7}$ m$^2$/s for water, $D_p = 2.11 \times 10^{-7}$ m$^2$/s for GFP protein and $1.87 \times 10^{-7}$ m$^2$/s for myoglobin (Yu, *et al.*, 2005); and $D_p = 0.4 \times 10^{-7}$ to $1.8 \times 10^{-7}$ m$^2$/s for the different proteins obtained by relaxing their temperature from 350 to 250 K (Lervik, *et al.*, 2010). By using computer simulations and thermal relaxation across the protein-water interface, we obtain slightly higher values of $D$ for THRT3-$\beta$ than THRT3-$\beta$1 and THRT3T4-$\alpha$ as depicted in the Table 13. The slightly changing heat conduction parameters $c_V^p$, $D$ and $k$ in the normal and diseased state THRs (Table 13) are related to the conformational changes by inter-residue H-bonding, energy transport channels and thermal boundary conductance (Xu, *et al.*, 2014). The protein-solution H-bondings also facilitate the transport of thermal vibrations across the boundary. Thermal conductivity $k$ of the hydrated THRs lies within the range of 0.26-0.30 W m$^{-1}$K$^{-1}$ with the standard error limit ± 0.02 W m$^{-1}$K$^{-1}$ which is lower than that of water, i.e. $k_w = 0.64$ W m$^{-1}$K$^{-1}$). The smaller $k$ signifies that THR isoforms support the principle of body temperature regulation. Here, $k$ of THRs that we obtained from the techniques of non-equilibrium thermodynamics are close to the values $k_p = 0.27$ W m$^{-1}$K$^{-1}$ determined by Yu *et al.* (2005) for both green fluorescent protein (GFP) and myoglobin., and $k_p = 0.13$ to 0.23 W m$^{-1}$K$^{-1}$ calculated by Lervik *et al.* (2010) for the different proteins at about 300 K. THRT3-$\beta$ has slightly higher thermal conductivity than THRT3-$\beta$1 and THRT3T4-$\alpha$ which is due to the effect of protein-surface curvature, hydrophilic or hydrophobic patches, and inter-residue or protein-water H-bondings (Lervik, *et al.*, 2010; Xu, *et al.*, 2014). The thermal perperties of T3/T4 liganded and unliganded THRs are significantly important to

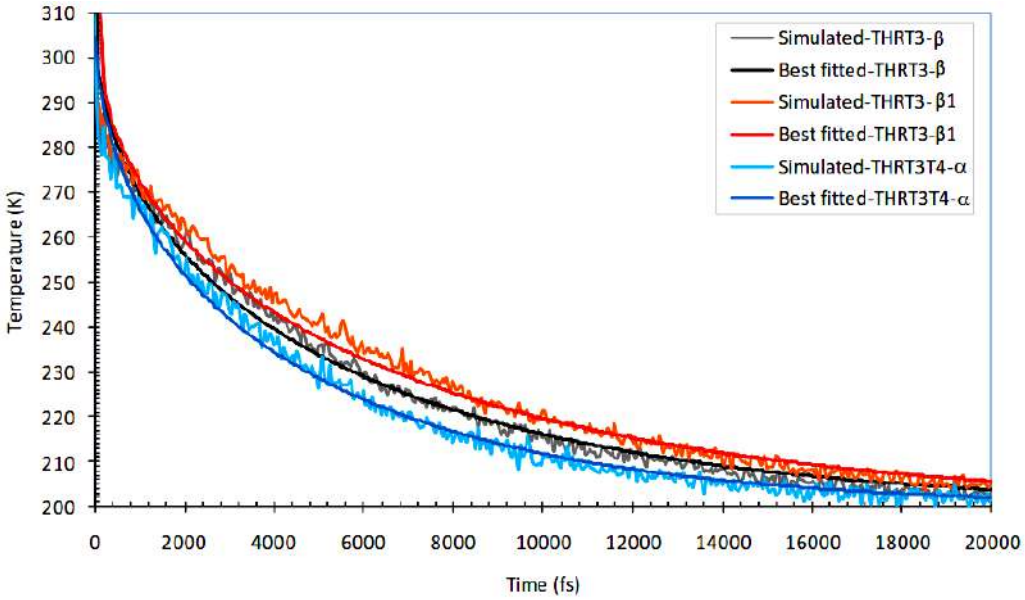


**Figure 51:** Cooling of THR isoforms in nanodroplets by relaxing the temperature from 310 to 200 K where the simulated datapoints are best fitted with the non-linear Equation 3.23 to obtain their thermal diffusivity $D$

**Table 12:** Partial heat capacities of THR-nanodroplets at $T$ = 310±1 K in NVT ensemble where $K_B$ = 0.00198657 kcal mol$^{-1}$K$^{-1}$ is Boltzmann constant

| THR-nanodroplets | Atoms $N$ | Mass $M$ (amu) | $\langle U^2 \rangle$ (kcal/mol)$^2$ |
|---|---|---|---|
| THR-$\beta$ | 21157 | 132213 | 4393896241.65 |
| THRT3-$\beta$ | 21192 | 132864 | 4384867565.23 |
| THRT3-$\beta$1 | 20266 | 127468 | 3925226341.90 |
| THRT3T4-$\alpha$ | 12249 | 79395.7 | 1225218557.93 |
| THR-nanodroplets | $\langle U \rangle^2$ (kcal/mol)$^2$ | $C_V = \frac{\langle U^2 \rangle - \langle U \rangle^2}{K_B T^2}$ kcal mol$^{-1}K^{-1}$ | $c_V$ J kg$^{-1}$K$^{-1}$ |
| THR-$\beta$ | 4393879748.25 | 86.39 ± 0.28** | 2736.42 ± 8.87 |
| THRT3-$\beta$ | 4384850985.47 | 86.85 ± 0.28 | 2737.51 ± 8.82 |
| THRT3-$\beta$1 | 3925210205.54 | 84.52 ± 0.27 | 2776.85 ± 8.87 |
| THRT3T4-$\alpha$ | 1225208975.47 | 50.19 ± 0.16 | 2647.36 ± 8.44 |

**Heat capacity $C_V = C_V(U,T)$, i.e. $\Delta C_V = C_V \sqrt{\left(\frac{\Delta U}{U}\right)^2 + \left(\frac{\Delta T}{T}\right)^2}$ where $\Delta C_V$, $\Delta U$ and $\Delta T$ are standard errors.

understand the body temperature regulation, energy or momentum transport mechanism and metabolic activities of the protein-hormone systems in euthyroid and hypothyroid states of the patients who suffer from thyroid gland abnormalities as reported in the Section 4.3. The heat conduction properties of THR-subtypes as explained above are also published in the paper by Lamichhane *et al.* (2018).

**Table 13:** Thermal conduction parameters of unliganded and liganded THR isoforms in solution where the partial specific heat $c_V^w$ of the solvent (water + ions) is 2928.75±39.70 $Jkg^{-1}K^{-1}$ and density $\rho$ of hydrated THRs is (950 ± 50) $kg/m^3$ at 310 K

| Molecule | $N$ | $M_p$(amu) | $c_V^p$ ($J\ kg^{-1}K^{-1}$)$^a$ | $D$ ($m^2/s$)$^b$ | $k$ ($W\ m^{-1}K^{-1}$)$^c$ |
|---|---|---|---|---|---|
| THR-$\beta$ | 3895 | 27640 | 2008.75 ± 107.77 | (1.56 ± 0.02) × $10^{-7}$ | 0.30 ± 0.02** |
| THRT3-$\beta$ | 3930 | 28291 | 2030.62 ± 105.32 | (1.57 ± 0.03) × $10^{-7}$ | 0.30 ± 0.02 |
| THRT3-$\beta$1 | 4014 | 29069 | 2244.53 ± 95.73 | (1.35 ± 0.05) × $10^{-7}$ | 0.29 ± 0.02 |
| THRT3T4-$\alpha$ | 3986 | 28853 | 2154.44 ± 46.32 | (1.28 ± 0.04) × $10^{-7}$ | 0.26 ± 0.02 |

**Thermal conductivity $k = k(c_V, D, \rho)$, i.e. $\Delta k = k\sqrt{\left(\frac{\Delta c_V}{c_V}\right)^2 + \left(\frac{\Delta D}{D}\right)^2 + \left(\frac{\Delta \rho}{\rho}\right)^2}$ where $\Delta k$, $\Delta c_V$, $\Delta D$ and $\Delta\rho$ are standard errors.
**a.** $c_V^p$ of native proteins varies from 1200 to 2300 $Jkg^{-1}K^{-1}$ at 298 K (Privalov, *et al.*, 1986).
**b.** $D_w$ = 14.6 Å$^2$/ps for water, $D_p$ = 21.1 Å$^2$/ps for GFP protein and 18.7 Å$^2$/ps for myoglobin (Yu, *et al.*, 2005); and $D_p$ = 4 to 18 Å$^2$/ps for the different proteins (Lervik, *et al.*, 2010).
**c.** $k_w$ = 0.64 W $m^{-1}K^{-1}$ for water and $k_p$ = 0.13-0.28 W $m^{-1}K^{-1}$ for proteins at 300 K (Yu, *et al.*, 2005; Lervik, *et al.*, 2010).

## 4.6 Structural Changes of THR-Beta Gene in Euthyroid, Hypothyroid and RTH or Mutational States

During the observation period, 48 patients with elevated FT3/FT4 without suppressed TSH were suspected of RTH. Genetic test is rquired to confirm the point mutations in THR-$\beta$ gene by means of which RTH arises. Since no patient was suggested for the genetic tests by the clinicians or endocrinologists, we took the cases of previously confirmed point mutations such as L330S and I431V in THR-$\beta$ gene (Azevedo, *et al.*, 2008; Pohlenz, *et al.*, 1997) as mentioned in the Subsections 2.2.3 and 3.2.2. Here, we analyze and compare the results obtained from the MD simulations of T3 liganded THR-$\beta$ (THRT3-WT), unliganded THR-$\beta$ (THR-WT) and mutated THR-$\beta$ (THRT3-MT) applicable to euthyroid, hypothyroid and RTH or mutational states of thyroid disorders. Basically, the structural and physical changes of THR-$\beta$ LBD by T3 binding and L330S like mutational interactions are explained below.

The protein structure of wild type THR-$\beta$ that we take for the simulation has 3895 atoms with total mass 27640 amu. The active ligand bound to THR-$\beta$ LBD is T3 hormone which has 35 atoms with mass 651 amu. In the point mutation L330S, LEU($C_6H_{13}NO_2$) of mass 131 amu is replaced by SER($C_3H_7NO_3$) of mass 105 amu. Similarly, in the point

mutation I431V, ILE($C_6H_{13}NO_2$) of mass 131 amu is replaced by VAL($C_5H_{11}NO_2$) of mass 117 amu.

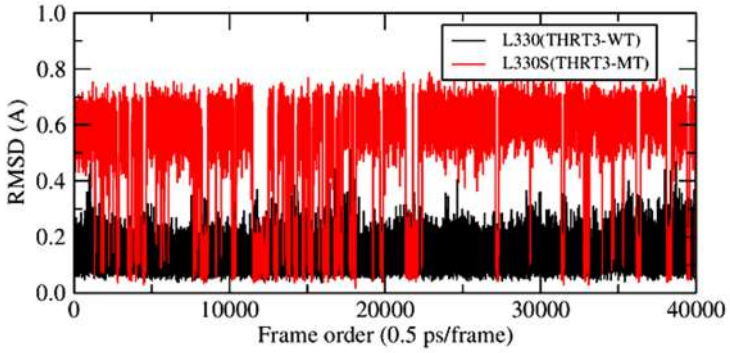


**Figure 52:** Fluctuating RMSDs of L330 and L330S during equilibrations of THRT3-WT and THRT3-MT systems

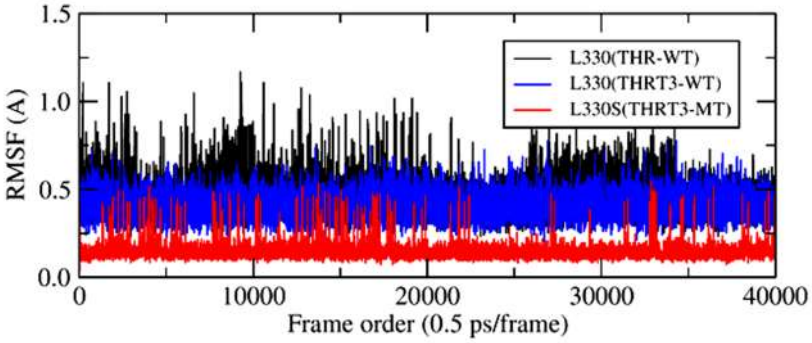


**Figure 53:** RMSFs of LEU and SER residues in 330-codon of unliganded, liganded and mutated THR-$\beta$ systems

The constancy of RMSD ($\leq$ 3 Å) and RG ($\approx$ 19 Å) of the protein backbone over the time frames of equilibration runs show the conformational stability and validity of force field topology and parameters used for MD simulations of wild type and mutated nuclear receptors. Some residues with more fluctuating RMSD/RG show their dynamic properties which are responsible for T3 binding and dissociation from THR-$\beta$ LBD. The values of RMSD and RG of the molecules with the standard deviations of the data are listed in the Table 14. During the 20 ns equilibration runs in neutral water-ion environment, RMSD of 330-residue in liganded THRT3-WT is smaller and less fluctuating than that in unliganded THR-WT and L330S-mutant THRT3-MT (Figure 52). T3 is more fluctuating due to smaller RG of L330S in mutated LBD than in wild type LBD. The RMSD/RG of the protein backbone is almost same with small fluctuations in these three cases (Table 14).

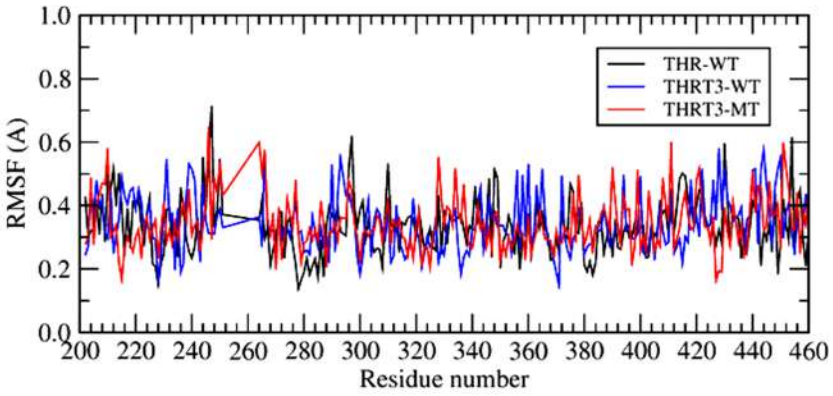


**Figure 54:** RMSFs of all residues in unliganded, liganded and L330S-mutant THR-$\beta$ systems during the last frame of 20 ns euilibrating simuations in the cellular environment

**Table 14:** Average RMSD and RG of unliganded THR-WT, liganded THRT3-WT and mutated THRT3-MT (L330S-mutant THR-$\beta$) included with standard deviations during the 20 ns equilibrations

| Molecule | *THR-WT* | | THRT3-WT | | | THRT3-MT | | |
|---|---|---|---|---|---|---|---|---|
| Residues | L330 | protein | L330 | T3 | protein | L330S | T3 | protein |
| RMSD(Å) | 0.56 ±0.44 | 2.60 ±0.50 | 0.13 ±0.05 | 0.40 ±0.11 | 2.72 ±0.41 | 0.52 ±0.20 | 1.63 ±0.25 | 2.88 ±0.27 |
| RG(Å) | 2.31 ±0.03 | 18.70 ±0.10 | 2.32 ±0.02 | 4.42 ±0.05 | 18.74 ±0.07 | 1.82 ±0.03 | 4.40 ±0.05 | 18.80 ±0.08 |

Root mean square fluctuation (RMSF) of the mutated residue L330S is smaller than the wild type L330 provided with larger fluctuations in the unliganded system as shown in the Figure 53. The RMSFs of all residues in unliganded, liganded and mutated THR-$\beta$ systems are small lying below 1.0 Å during their equlibrations as shown in the Figure 54. Related to the 330-codon, the RMSFs are 0.46 ± 0.10 Å for LEU of THR-WT, 0.41 ± 0.07 Å for LEU of THRT3-WT and 0.15 ± 0.04 Å for SER of THRT3-MT (Table 15).

The positions of L330S/I431V mutational sites and T3-hormone in THRT3-MT after their 20 ns equilibrations are shown in Figure 55. During the MD simulations of wild type and mutated THR-$\beta$ systems, distance between L330 and T3 in THRT3-WT varies as 6.36 ± 0.33 Å and the distance between L330S and T3 in THRT3-MT varies as 7.11 ± 0.28 Å. Such distance is smaller and more fluctuating in THRT3-WT than in THRT3-MT (Figure 56). This is one of the indicators of T3 resistant features of mutated nuclear receptor proteins that causes RTH.

Radial distribution function (RDF) or pair auto-correlation function (g(r)) in a system of particles measures probability of finding a particle at r distance away from the reference

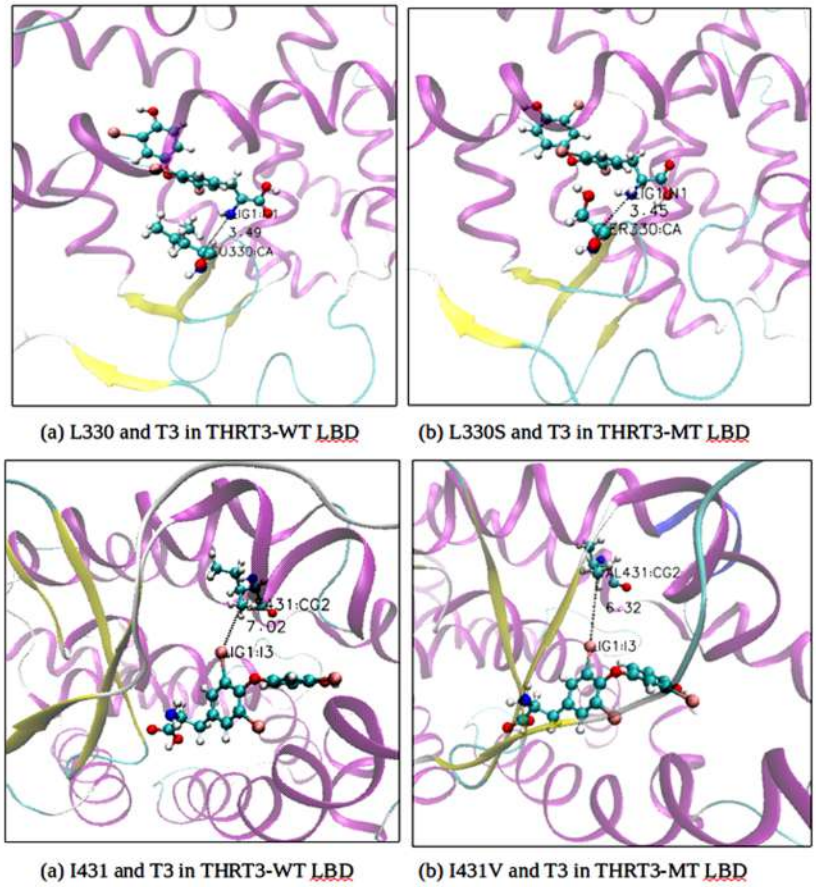


(a) L330 and T3 in THRT3-WT LBD (b) L330S and T3 in THRT3-MT LBD

(a) I431 and T3 in THRT3-WT LBD (b) I431V and T3 in THRT3-MT LBD

**Figure 55:** Positions of mutational sites (L330S and I431V) w.r.t. T3 in LBDs of THRT3-WT and THRT3-MT after their 20 ns equilibrations

particle (Fernández, *et al.*, 2007). The distribution function g(r) between the iodine atom I1(T3) and the oxygen atom OG(L330S) in THRT3-MT is shifted left from that in its wild type THRT3-WT within the range of 3.0-5.5 Å. In this way, the RDF between I3(T3) and CG2(I431V) in THRT3-MT has smaller height within the flat range of 4.5-8.5 Å than that in its wild type THRT3-WT as shown in the Figure 57. In other words, the number density of the mutant residue is less than that of the native wild type residue in order to respond for T3-hormone and TREs.

The plots of dihedral angles ($\phi$, $\psi$), i. e. Ramachandran plots for THR-WT, THRT3-WT and L330S/I431V mutant THRT3-MT in the last frame of 20 ns equilibrations are shown in Figure 58. In these plots, most of the amino acid residues of parallel, anti-parallel and right twisted $\beta$-sheets lie in the blue region of I-quadrant; that of right handed $\alpha$-helix lie in the blue region of II-quadrant and left handed $\alpha$-helix lie in the green region of III-quadrant (Hollingsworth, *et al.*, 2010; Ho, *et al.*, 2005). The residue GLY has no side chain so that it has no steric hindrance and it is allowed in the white region IV. The white

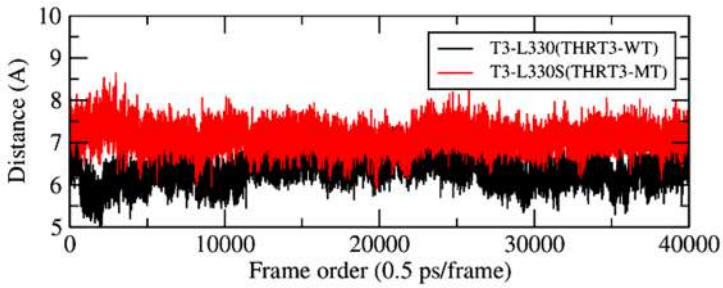


**Figure 56:** Fluctuating distances between T3 and L330/L330S during equilibrations of THRT3-WT and THRT3-MT systems

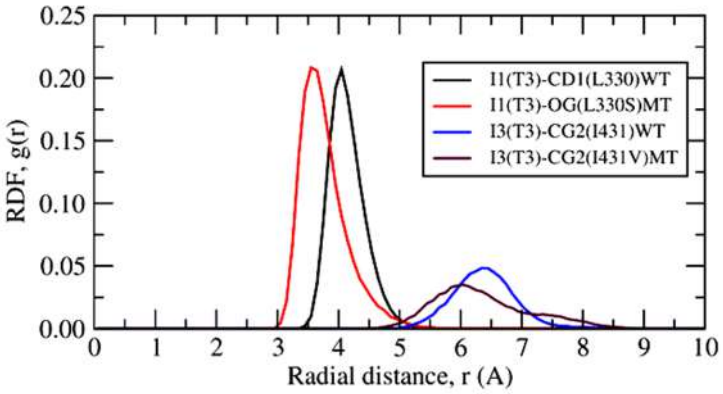


**Figure 57:** RDFs of some atoms in wild type and mutated residues (L330S and I431V) from I1 or I3 of T3-hormone during 20 ns equilibrations of THRT3-WT and THRT3-MT systems

region is sterically disallowed for all other amino acids except GLY. The blue regions are the most allowed regions for $\alpha$-helices and $\beta$-sheets. The green area is allowed for the shorter van der Waal radii of atoms and the related amino acids. By comparing the plots of Figure 58, we observe that the ($\phi$, $\psi$) values of L330S/I431V in THRT3-MT scatter more towards the disallowed regions than that of L330/I431 in THRT3-WT. This analysis verifies that the larger steric hindrances occur in the unliganded and mutated THR-$\beta$ resulting gene repressions and the related thyroid disorders. The clinical analysis shows that THRT3-WT, THR-WT and THRT3-MT are associated with normal thyroid functions, overt hypothyroidism and RTH, respectively.

Solvent accessible surface area (SASA) of 330-codon in THRT3-WT is observed to be different in the extension radius of 1.4 Å than that in THRT3-WT and THRT3-MT (Figure 59). As depicted in the Table 15, The SASA of the 330-codons in THR-WT, THRT3-WT and THRT3-MT are 290.96 ± 3.51, 285.62 ± 3.74 and 223.89 ± 3.41 Å$^2$, respectively which lie in the range of 0-300 Å$^2$ reported by Ausaf Ali *et al.* (2014). The lower SASA indicates the higher thermodynamic stability of the protein. The SASA of

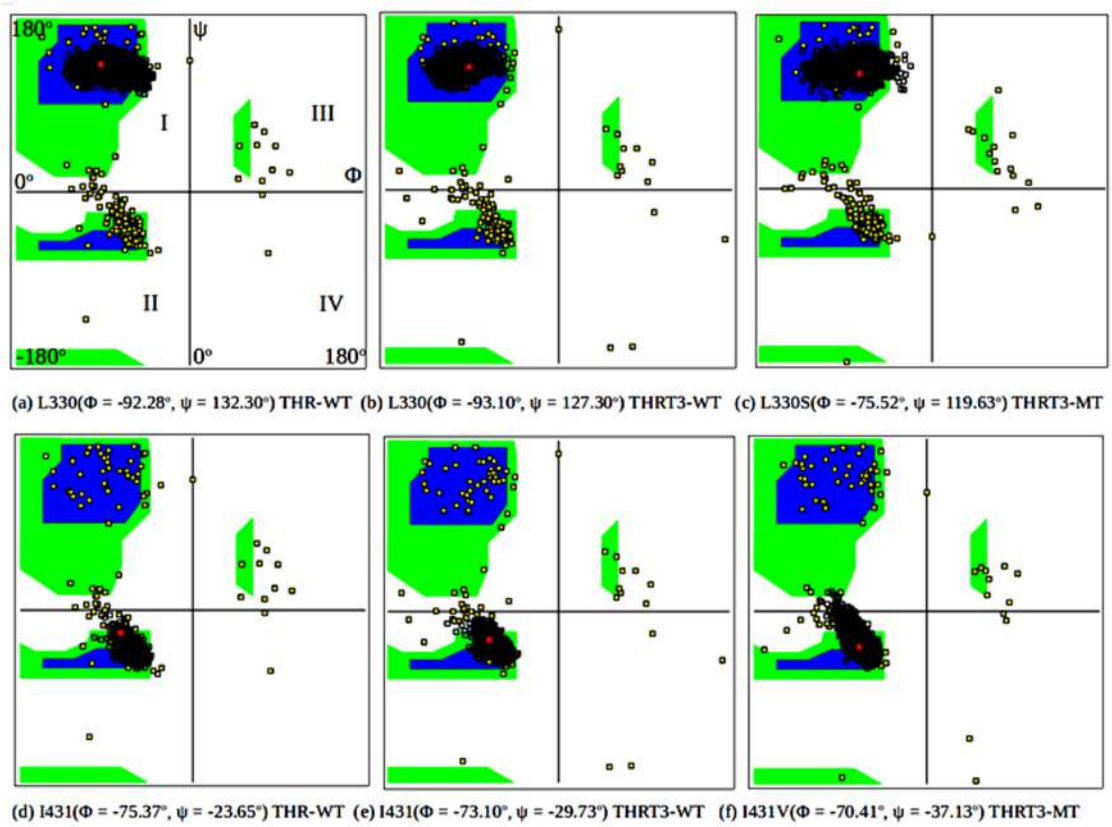


**Figure 58:** Ramachandran plots shown with darkline spots, i.e. the varying ($\phi$, $\psi$) values of residues: L330 (a,b), L330S (c), I431 (d,e) and I431V (f) in the related THR-WT, THRT3-WT and THRT3-MT systems during the last 1ns of their equilibration runs. The red spot with the given ($\phi$, $\psi$) values is related to the last time-step of simulations

T3-hormone is observed to be zero indicating the hydrophobicity of LBD of THR-$\beta$. The mutation on the solvent accessible residue causes the conformational change by partial unfolding of the protein (Gilis, *et al.*, 1996). Such effect is more intensive if the mutation occurs on the surface residue than on the interior of the protein. Since the SASA of L330/I431V has been found to be decreased relative to its wild type, such mutation is confirmed as a buried mutation of the THR-$\beta$ gene.

The IR spectral densities using total dipole moment of the atoms in the 330-residue are calculated in the frequency range of 0 to 2500 $cm^{-1}$ by adjusting the time interval between frame to frame calculations as 0.01 ps in the last 1 ns of the equilibrating simulations. Such spectral distributions are different for THRT3-WT and THRT3-MT as shown in Figure 60. The maximum IR-intensity of L330 in the wild type receptor is 0.0091 at 1228.56 $cm^{-1}$. Again, the maximum IR-intensity of L330S in the mutated receptor is 0.0081 at 1163.55 $cm^{-1}$. The distribution has larger number of high intensity peaks for L330 in THRT3-WT than for L330S in THRT3-MT.

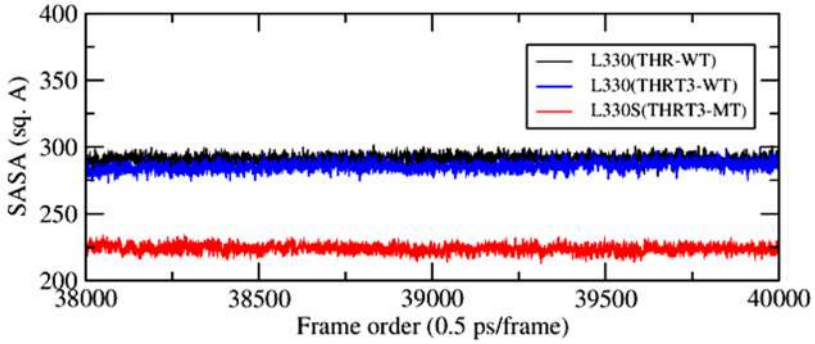


**Figure 59:** SASA of L330 and L330S residues in the last 1ns of equilibrations of unliganded, liganded and mutated THR-$\beta$ systems

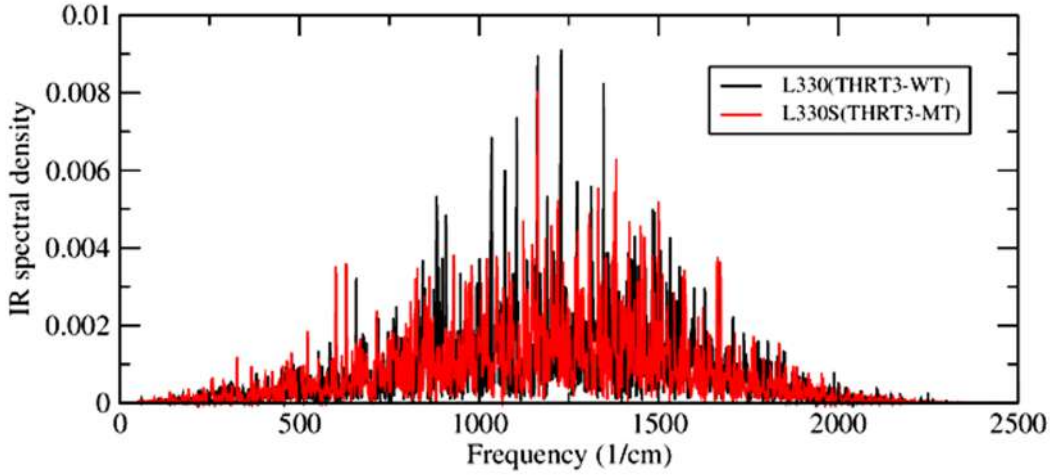


**Figure 60:** IR spectral density of L330 and L330S by adjusting the time interval between frame to frame calculations as 0.01 ps in the last 1 ns of the equilibrating simulations of THRT3-WT and THRT3-MT systems

Total non-bonding interaction energy is the sum of electrostatic and van der Waals interaction energies. The changing values of interaction energy between 330-codon and T3-hormone in wild type and L330S mutant THR-$\beta$ systems are plotted w.r.t. the frame order in the Figures 61 and 62. These are averaged over the time frames from the last 1 ns of the equilibrating simulations. The mean±SD of electrostatic ($E_{\text{elect}}$) and van der Waals ($E_{\text{vdw}}$) interaction energies are calculated by using the NAMD-Energy-GUI adjusted with switching and cut-off distances of 10 Å and 12 Å, respectively. As per the interactions between L330 and T3 in THRT3-WT, the values of $E_{\text{elect}}$ and $E_{\text{vdw}}$ are -1.58 ± 0.72 kcal/mol and -4.22 ± 0.84 kcal/mol whereas for the interactions between L330S and T3 in THRT3-MT, these are -2.37 ± 1.52 kcal/mol and -2.26 ± 0.85 kcal/mol, respectively (Table 15). The Figures 61 and 62 also demonstrate that $E_{\text{elect}}$ is more fluctuating with

larger negative value whereas $E_{\text{vdw}}$ is less fluctuating with smaller negative value when LEU is mutated with SER in 330-codon of the THR-$\beta$ gene. In this way, some changes observed for the interaction energies between 431-codon and T3 in wild type and I431V mutant THR-$\beta$ systems are depicted in the Table 15. Here, $E_{\text{elect}}$ has larger positive value and $E_{\text{vdw}}$ has smaller negative value when I431 is mutated to I431V. These factors are also significantly important to explore the insights into the RTH.

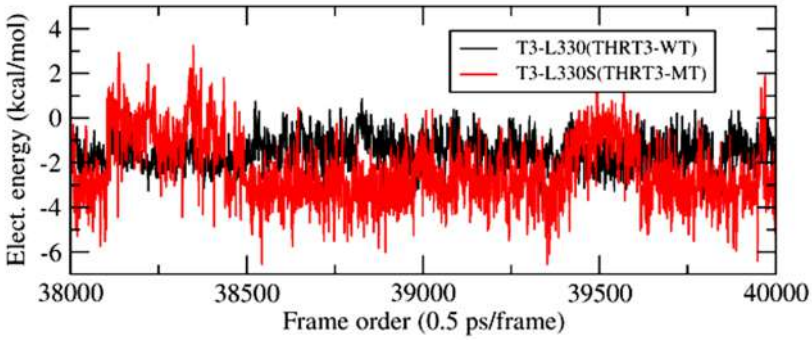


**Figure 61:** Electrostatic interaction energies between L330/L330S residue and T3 hormone in THRT3-WT and THRT3-MT in the last 1 ns of the equilibrating simulations

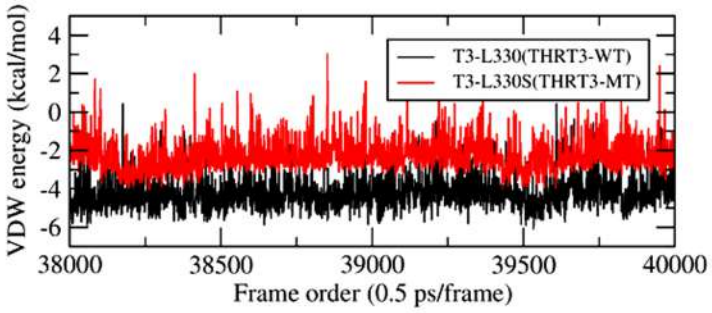


**Figure 62:** van der Waals interaction energies between L330/L330S residue and T3 hormone in THRT3-WT and THRT3-MT in the last 1 ns of the equilibrating simulations

Internal energy of the biomolecular system is the sum of bonding and non-bonding potentials. Coulomb energy is the largest and its fluctuation during MD simulations makes the total internal energy fluctuate about its mean value. Using NAMD-Energy-GUI with switching and cut-off distances of 10 Å and 12 Å, the internal energy ($U_i$) of 330-residue, bounded T3-hormone and protein of THR-WT, THRT3-WT and THRT3-MT are calculated from the last 1 ns of their equilibrations and the average values for the corresponding systems are listed in the Table 15. The variations of internal energy w.r.t. the simulation time are plotted in Figure 63. The plots for the individual potential terms

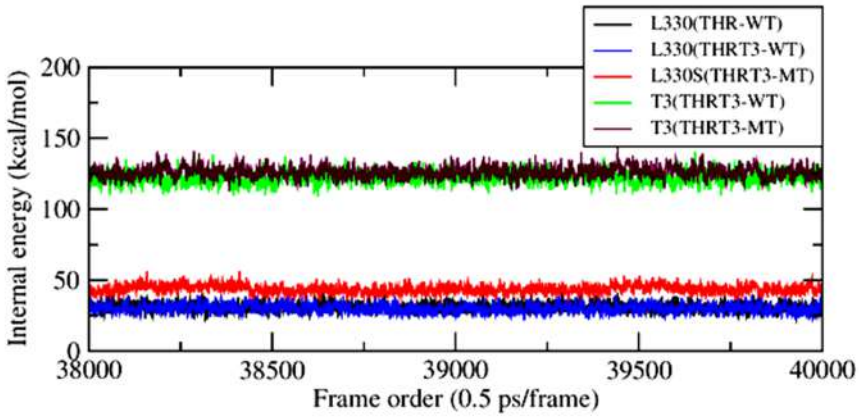


**Figure 63:** Fluctuating internal energies of L330, L330S and T3 in unliganded THR-WT, liganded THRT3-WT and mutated THRT3-MT in the last 1 ns of their equilibrations

**Table 15:** The mean±SD of RMSF (Å), SASA (Å$^2$), internal energy ($U_i$), and electrostatic ($E_{\text{elect}}$) and van der Waals ($E_{\text{vdw}}$) ineraction energies (kcal/mol) with T3 related to L330 and I431 residues in unliganded THR-WT, liganded THRT3-WT and mutated THRT3-MT where RMSF is averaged from the 20 ns equlibrations and the others are averaged from the last 1 ns of their equlibrations

| Molecule | Residue | RMSF | SASA | $U_i$ | $E_{\text{elect}}$ | $E_{\text{vdw}}$ |
|---|---|---|---|---|---|---|
| THR-WT | L330 | 0.46±0.10 | 290.96±3.51 | 30.93±3.09 | 0 | 0 |
| | I431 | 0.42±0.08 | 283.04±3.57 | 42.38±3.3.14 | 0 | 0 |
| THRT3-WT | L330 | 0.41±0.07 | 285.62±3.74 | 30.03±3.03 | -1.58±0.72 | -4.22±0.84 |
| | I431 | 0.44±0.08 | 284.41±3.64 | 42.71±3.17 | 0.17±0.07 | -0.25±0.09 |
| | T3 | - | 0 | 121.93±4.50 | - | - |
| THRT3-MT | L330S | 0.15±0.04 | 223.89±3.09 | 43.70±2.25 | -2.37±1.52 | -2.26±0.85 |
| | I431V | 0.43±.09 | 248.56±3.22 | 36.68±3.36 | 0.21±0.10 | -0.16±0.06 |
| | T3 | - | 0 | 126.07±4.43 | - | - |

show that the major contributor of fluctuations in internal energy is the electrostatic energy of the related system. The value of $U_i$ is 30.03 ± 3.03 kcal/mol for L330 in THRT3-WT and 43.70 ± 2.25 kcal/mol for L330S in THRT3-MT, i.e. the internal energy inceases when LEU is mutated with SER in the 330-codon of THR-$\beta$ LBD. However, the $U_i$ of 431-codon decreases from 42.71 ± 3.17 to 36.68 ± 3.36 kcal/mol when ILE is mutated with VAL in the THR-$\beta$ gene. The structural and physical changes in THR-$\beta$ by T3 binding and L330S mutational interactions related to normal and abnormal thyroid states are also published in the paper by Lamichhane *et al.* (2020). By using the MD simulations up to 2 ns under the periodic bounatary conditions, the results associated with the structural and biophysical changes of THR-$\beta$ gene due to the I431V mutation are described by Lamichhane *et al.* (2019).

# CHAPTER 5

## CONCLUSION AND RECOMMENDATIONS

Thyroid status has been evaluated statistically and graphically from the sufficient data of the hospital based subjects. Biochemical tests followed by ultrasonographic examinations of thyroid patients are important to develop the linear and non-linear relationships among FT3, FT4, TSH, thyroid size and thyroid gland abnormalities in thyroid dysfunction states. Age and gender dependent variations of TFT values and thyroid size of normal and abnormal thyroid have also been studied for the purpose of finding the new reference levels and the prevalence of thyroid disorders in central Nepal. Since the thyroid dysfunction pathways originate from the molecular levels, structural and biophysical properties of normal and diseased state THRs are explored by analyzing the results obtained after NAMD simulations. The conclusions of this research are listed below.

**1.** From the normal USG and TFT analysis in euthyroid subjects, the reference values with mean±SD of thyroid size, FT3, FT4 and TSH are recommended to be 4.74 ± 2.30 mL, 5.47 ± 0.83 pmol/L, 14.17 ± 2.82 pmol/L and 2.30 ± 0.98 mIU/L, respectively. The left lobe size has a strong positive linear correlation ($r = 0.73$, $p < 0.001$) with the right lobe size of the normal thyroid gland. The left lobe is almost equal in size for both genders, but the right lobe is larger for males. In menarche and menopause periods, the thyroid size has been found to be larger in females than that in males. The thyroid size increases from early age to adulthood and then decreases in elderly. Conversely, FT4 first decreases and then slightly increases with aging due to the fact of increased thyroid dysfunctions and prevalence of metabolic syndrome in the elderly.

**2.** The prevalence of hypothyroidism is higher than hyperthyroidism in which females are more vulnerable with greater impact in the elderly. Most of the hypothyroid patients

are related to the presence of goitrous, thyroiditic and nodular masses in somehow benign type, diffuse pattern of echogenicity and increased vascularity as shown by the USG findings. The features of overt thyroid dysfunction are more associated with family history of thyroid disease or genetics, insomnia, stressful lifestyle, smoking, alcoholism and pregnancy loss than in subclinical thyroid dysfunction. Some patients with normal TFTs also have abnormalities like cystic and/or hypoechoic and even malignant lesions in the thyroid gland.

**3.** FT3 and FT4 are linearly and strongly correlated in overt thyroid dysfunctions ($0.66 \leq r \leq 0.91$, $p < 0.001$) than in euthyroid and subclinical thyroid dysfunctions. There is a non-linear relation between ln(TSH) and FT4 which is better fitted with 4-P logistic model ($R^2 = 0.97$ and $p < 0.001$) in both hypothyroidism and hyperthyroidism on the basis of euthyroidism. The curvatures in the logistic curve are associated with the turning point of subclinical and overt thyroid dysfunctions from normal thyroid condition and vice-versa. Such logistic curves can be taken as the response trajectories of pituitary TSH by the deviation in serum FT4.

**4.** The nature of temperature auto-correlation as well as echo feature curve is significantly different in constrained and unconstrained dynamics of THRs. These curves are smoother in constrained vibrations and more distinct with shoulders in free vibrations resulting higher specific heat of the system in the later case. The partial heat capacities of native state THR (unliganded) and THRT3 (liganded) in free vibrations are $1763.63 \pm 74.24$ and $1807.43 \pm 41.44$ $\mathrm{Jkg^{-1}K^{-1}}$ at about 300 K, respectively which lie in the experimental range given by Privalov *et al.* (1986). The dephasing time of the echo pulses that ranges from 0.6 to 0.8 ps has inverse relations with anharmonicity diffusion and mobility. These are the important tools used to understand the regulation of gene expressions as a biomechanical function of hormone binding nuclear receptor.

**5.** The heat transfer properties of THRs in cellular environment differ from that of native globular forms in vacuo. The partial specific heat capacity of THRs ranges from 2000 to 2200 $\mathrm{Jkg^{-1}K^{-1}}$ in solution which is 15-20% higher than that in the dry state at about 300 K. In the case of overt hypothyroid disorder, THRs become almost free of T3. The lower heat capacity of THR than that of THRT3 is due to the change in degrees of freedom, protein-ligand interactions, H-bonding, and hydrophobic, vibrational and conformational

changes. Thermal diffusivity of THRs is around $1.46 \times 10^{-7}$ $m^2/s$ for water at 310 K where a little bit higher value for THRT3-$\beta$ than for THRT3-$\beta$1 and THRT3T4-$\alpha$ is associated with the effect of inter-residue and protein-water H-bonding, thermal transport channels and boundary conductance in the protein-water interface. Thermal conductivity of THRs ranges from 0.26-0.30 $Wm^{-1}K^{-1}$ with the higher value for THRT3-$\beta$ which is about half the value of water at 310 K. In euthyroidism, the THRT3 isoforms with lower thermal conductivity are responsible for the regulation of body scale temperature through thermogenesis and metabolism. The overt hypothyroid patients with weak hormone-receptor interactions have mixed symptoms of cold intolerance, autoimmune thyroiditis, vascular nodules and diffuse goitre.

**6.** Almost constant values of RMSD ($\leq$3 Å) and RG ($\approx$19 Å) of wild type as well as mutated THR-$\beta$ show their conformational stability during MD simulations. The point mutation L330S with largely fluctuating RMSD shows its resistive nature to the T3 binding in and dissociation from THR-$\beta$ LBD. The ($\phi$, $\psi$) values in Ramachandran plots of L330/I431 in unliganded THR-WT and L330S/I431V in mutated THRT3-MT scatter more towards the disallowed regions than that of L330/I431 in liganded THRT3-WT. This analysis verifies that the larger steric hindrances occur in the unliganded and mutated THR-$\beta$ resulting gene repressions and the related thyroid disorders. The smaller SASA of L330S mutation than its wild type residue indicates that it is stable buried-muation. The SASA of T3 is zero verifying its hydrophobicity upon binding to THR-$\beta$ LBD. Comparing RDFs between the atoms of T3 and L330/I431-codon, the probability of finding the atomic particles within the domain range of 3 to 10 Å is higher in THRT3-WT than in THRT3-MT. The IR spectral distributions in the range of 0-2500 $cm^{-1}$ suggest that the L330-residue in THRT3-WT has larger number of high spectral peaks with greater change in dipole moments than the L330S-residue in THRT3-MT. Related to the 330-codon of THR-$\beta$ LBD, electrostatic interaction energy is more fluctuating with larger negative value, van der Waals interaction energy is less fluctuating with smaller negative value and total internal energy is less fluctuating with larger positive value when LEU is mutated with SER. These are the strong parameters that explain the nature of point mutations in THR-$\beta$ gene resulting RTH and goitre.

Conclusively, the thyroid hormone levels in association with nuclear receptor interactions evaluate the thyroid dysfunction states. The readily distinguished strucural and

thermophysical properties of liganded, unliganded and mutated THRs are the byproducts of euthyroid, hypothyroid and RTH patients who have different features of thyroid USG scans. Euthyroidism, the state of normal thyroid functions, is the condition of normal THRT3 interactions refelcting almost same physical properties as that of other proteins. Hypothyroidism, the state of thyroid gland malfunctions, is the condition of T3 deficient THR interactions reflecting abnormal conformations with lower specific heat capacity. RTH diagnosed with goitre is a syndrome caused by THR-$\beta$ mutations resulting abnormal THRT3 interactions with changing conformations. Along with TFT evaluations followed by thyroid USG examinations, computational analysis of thyroid hormone binding nuclear receptors is equally important to explore the insights into thyroid disorders and medicinal practices for the patient safety and success of treatment modalities.

It is recommended that age and gender related new reference ranges of thyroid variables should be implemented to categorize the thyroid dysfunction states. The actual relationships among the thyroid variables in normal and abnormal thyroid states should be known first for the clinical diagnosis and medication of thyroid dysfunctions. The thyroid functions in the molecular levels being associated with hormone active biophysical role of THRs, one should know about conformational and spectroscopic changes, protein folding and unfolding states, free energy change, gene transcriptional activities after the heat energy or momentum transfer mechanism of such nuclear receptors. Some of these inherent properties such as structural and thermophysical properties of the protein-hormone systems in both normal and diseased states have been explored computationally in this study, and however, rest of them remain to discover as future research works which will be performed by using suitable software of classical as well as quantum computation in the supercomputers. Long MD simulations and quantum computations being costly and time consuming, the remaining work for investigating the role of T3 like ligands or drugs or inhibitors towards gene expressions will be continued in the near future. Furthermore, the mutational defects in THR-genes and their impacts on the thyroid functions will be studied experimentally as the next level of this research work.

# CHAPTER 6

## SUMMARY

Objective of this study is to explore the insights into thyroid disorders through biochemical (TFT) analysis followed by ultrasonographic (USG) examinations of thyroid patients and through molecular dynamics approach to thyroid hormone-receptor interactions. The observations were performed by taking informed consent to each patient and getting authority from Institutional Review Board at Tribhuvan University Teaching Hospital, Maharajgunj, Kathmandu, Nepal during January 2017 to December 2018. The TFTs include age- and gender-specific measurements of FT3, FT4 and TSH on the blood serum by enhanced chemiluminescence immunoassay technique. The thyroid scanning includes the examinations of thyroid lobe dimensions and gland abnormalities such as goitrous, cystic and nodular lesions, vascularity and echogenicity by USG technique. In a total of 3473 patients involved in TFT analysis, 270 of them were suggested for the USG examinations and 48 of them were isolated as a group of possibly resistance to thyroid hormones (RTH). The data set of 3425 patients was categorized into euthyroid, hypothyroid and hyperthyroid groups including subclinical and overt thyroid dysfunctions. The prevalence of goiter, nodule, cysts, hypo and hyperechogenic lesions and vascularity were noted down as the ultrasonographic findings in clinically euthyroid and hypothyroid patients. The observed data sets were analyzed statistically and graphically for each category of thyroid disorder using software packages: MS Excel-2007 and Origin-2017. The graphical analysis obtains empirical equations as the linear and non-linear relationships among thyroid variables such as thyroid size, FT3, FT4 and TSH in normal and abnormal conditions of thyroid. The results with $p$ <0.05 were taken to be statistically significant.

Normal thyroid analysis related to euthyroid subjects recommends new reference ranges

of the thyroid variables. The normal values of thyroid size, FT3, FT4 and TSH are 4.74 ± 2.30 mL, 5.47 ± 0.83 pmol/L, 14.17 ± 2.82 pmol/L and 2.30 ± 0.98 mIU/L, respectively. Normal thyroid size first increases and then decreases following parabolic nature with aging. It becomes maximum in the age group of 30-40 years. Left lobe size has significant linear correlation with right lobe size. The left lobe is almost same in size for both genders, but right lobe is greater in size for males. In menarche and menopause periods, the normal thyroid size of females exceeds that of males. In normal conditions, age and gender related variations of FT3 and TSH levels are not found to be significantly changed. However, FT4 concentration first decreases and then slightly increases with aging in both genders being minimum in the age group of 30-40 years. The prevalence of subclinical and overt hypothyroid patients is higher than that of hyperthyroid patients. FT3 and FT4 are more linearly correlated in overt thyroid dysfunctions than subclinical and normal thyroid functions. There is a non-linear negative correlation between FT4 and TSH following 4P-logistic model in both hypothyroidism and hyperthyroidism on the basis of euthyroidism. The hypothyroid patients mostly have Hashimoto's thyroiditis, benign goitres, cystic and nodular lesions, hypoechogenicity and vascularity in the thyroid gland. The rare cases of thyroid malignancy are diagnosed from FNA tests in both euthyroid and hypothyroid patients. The overt thyroid dysfunctions are found to be more associated with family history of thyroid disease, pregnancy loss, insomnia, stressful lifestyle, smoking and alcoholism.

The underactive thyroid conditions are associated with conformational, biophysical and physicochemical dysfunctions of triiodothyronine nuclear receptors called thyroid hormone receptors (THRs). In overt hypothyroidism, THRs become almost free of T3 so that gene transcription is not well regulated. The patients diagnosed with point mutations like L330S and I431V in THR-$\beta$ gene suffer from RTH and goitre resulting with FT3/FT4 elevation without TSH suppression (Azevedo, *et al.*, 2008; Pohlenz, *et al.*, 1997). The functions of liganded, unliganded and mutated THRs are the consequences of euthyroid, hypothyroid and RTH conditions, respectively. The structural analyses such as root mean square deviation (RMSD), radius of gyration (RG), root mean square fluctuation (RMSF), Ramachandran plot, radial distribution function (RDF) and hydrogen bonding, and thermophysical properties such as temperature and energy distributions, echo dephasing, heat capacity, thermal diffusivity and thermal conductivity of normal and abnormal

(unliganded and mutated) THRs were studied by means of nanoscale molecular dynamics (NAMD) simulations. The molecular structures of THRs were taken from 1XZX.pdb, 3GWS.pdb and 4LNX.pdb for MD simulations in cellular environments. Periodic as well as spherical boundary conditions were implemented for energy minimization and equilibration of the protein-hormone systems. The production runs were performed in different ensembles and the output data were analyzed to explore the structural and thermophysical differences between normal and diseased state THRs.

T3 binds to hydrophobic LBD of THRs, changes conformations by interacting with the side chains of the receptor protein and triggers DNA transcription. The echo dephasing patterns in the free atomic vibrations show that partial heat capacity of T3-liganded nuclear receptors is higher than unliganded THR-$\beta$. The heat capacity of these systems in hydrous state is 15-20% higher than that in anhydrous state. Thermal diffusivity of THRs is near to that of water. Thermal conductivity has been found to be about half the value of water that helps to regulate the body scale temperature. The mutated THR-$\beta$ loses T3 binding capacity by changing its conformations and by changing electrostatic and van der Waals interactions at the mutational sites in comparison with wild type THR-$\beta$. Conclusively, status of thyroid disorder, thyroid disorder pathways and physical impacts on molecular levels are explored in this research. The genetic experiments along with classical as well as quantum computations of T3 like ligands or drugs or inhibitors that stimulate biophysical phenomena associated with energy and momentum transfer mechanism of THRs towards gene expressions is referred as future work which will be a molecular basis of understanding the disorder pathways in the thyroid cycle.

# REFERENCES


Abalovich, M., Gutierrez, S., Alcaraz, G., Maccallini, G., Garcia, A., & Levalle, O. (2002). Overt and subclinical hypothyroidism complicating pregnancy. *Thyroid, 12*(1), 63-68.

Abraham-Nordling, M., Törring, O., Lantz, M., Hallengren, B., Ohrling, H., ..., & Wallin, G. (2008). Incidence of hyperthyroidism in Stockholm, Sweden, 2003–2005. *European Journal of Endocrinology*, *158*(6), 823–827.

Abu-Zidan, F. M., Hefny, A. F., & Corr, P. (2011). Clinical ultrasound physics. *Journal of Emergencies, Trauma and Shock , 4* (4), 501-503.

Almandoz, J. P., & Gharib, H. (2012). Hypothyroidism: etiology, diagnosis, and management. *Medical Clinics*, *96*(2), 203– 221.

Allen, M. P. (2004). Introduction to molecular dynamics simulation. *Computational Soft Matter: from Synthetic Polymers to Proteins, 23*, 1-28.

Almandoz, J. P., & Gharib, H. (2012). Hypothyroidism: etiology, diagnosis, and management. *Medical Clinics, 96*(2), 203-221.

Aoki, Y., Belin, R. M., Clickner, R., Jeffries, R., Phillips, L., & Mahaffey, K. R. (2007). Serum TSH and total T4 in the United States population and their association with participant characteristics: National Health and Nutrition Examination Survey (NHANES 1999–2002). *Thyroid, 17*(12), 1211-1223.

Ausaf Ali, S., Hassan, I., Islam, A., & Ahmad, F. (2014). A review of methods available to estimate solvent-accessible surface areas of soluble proteins in the folded and unfolded states. *Current Protein and Peptide Science, 15*(5), 456-476.

Azadeh, M., Gorovits, B., Kamerud, J., MacMannis, S., Safavi, A., Sailstad, J., & Sondag, P. (2018). Calibration curves in quantitative ligand binding assays: recommendations and best practices for preparation, design, and editing of calibration curves. *The AAPS Journal, 20*(1), 22-38.

Bacci, V., Schussler, G. C., & Kaplan, T. B. (1982). The relationship between serum triiodothyronine and thyrotropin during systemic illness. *The Journal of Clinical Endocrinology and Metabolism, 54*(6), 1229-1235.

Bahn, R. S., Burch, H. B., Cooper, D. S., Garber, J. R., Greenlee, M. C., ..., & Rivkees, S. A. (2011). Hyperthyroidism and other causes of thyrotoxicosis: management guidelines of the American Thyroid Association and American Association of Clinical Endocrinologists. *Thyroid*, *21*(6), 593–646.

Benhadi, N., Fliers, E., Visser, T., Reitsma, J., & Wiersinga, W. (2010). Pilot study on the assessment of the setpoint of the hypothalamus–pituitary– thyroid axis in healthy volunteers. *European Journal of Endocrinology*, *162*(2), 323–329.

Berberich, J., Dietrich, J. W., Hoermann, R., & Müller, M. A. (2018). Mathematical modeling of the pituitary–thyroid feedback loop: role of a TSH-T3-shunt and sensitivity analysis. *Frontiers in Endocrinology, 9*, 91-91.

Berendsen, H. J., Postma, J. V., van Gunsteren, W. F., DiNola, A. R. H. J., & Haak, J. R. (1984). Molecular dynamics with coupling to an external bath. *The Journal of Chemical Physics, 81*(8), 3684-3690.

Berghout, A., Wiersinga, W., Smits, N., & Touber, J. (1987). Determinants of thyroid volume as measured by ultrasonography in healthy adults in a non-iodine deficient area. *Clinical Endocrinology*, *26*(3), 273–280.

Biondi, B. (2013). The Normal TSH Reference Range: What Has Changed in the Last Decade?. *The Journal of Clinical Endocrinology and Metabolism, 98*(9), 3584–3587

Biondi, B., & Cooper, D. S. (2007). The clinical significance of subclinical thyroid dysfunction. *Endocrine Reviews*, *29*(1), 76–131.

Bochukova, E., Schoenmakers, N., Agostini, M., Schoenmakers, E., Rajanayagam, O., ... & Downes, K. (2012). A mutation in the thyroid hormone receptor alpha gene. *New England Journal of Medicine*, *366*(3), 243–249.

Bortolotto, E., Rousseau, R., Teodorescu, B., Wielant, A., and Debauve, G. (2015). Assessing Similarity with Parallel-Line and Parallel-Curve Models. *Bioprocess International, 13*(6), 26-37.

Brent, G. A. (1994). The molecular basis of thyroid hormone action. New England Journal of Medicine, 331 (13), 847–853.

Brent, G. A. (2012). Mechanisms of thyroid hormone action. *The Journal of Clinical*

*Investigation, 122*(9), 3035–3043.

Bunevicius, R., & Prange Jr, A. J. (2010). Thyroid disease and mental disorders: cause and effect or only comorbidity?. *Current Opinion in Psychiatry, 23*(4), 363-368.

Bussi, G., Donadio, D., & Parrinello, M. (2007). Canonical sampling through velocity rescaling. *The Journal of Chemical Physics, 126*(1), 014101-014107.

Canaris, G. J., Manowitz, N. R., Mayor, G., & Ridgway, E. C. (2000). The Colorado thyroid disease prevalence study. *Archives of Internal Medicine, 160*(4), 526-534.

Carlé, A., Pedersen, I. B., Knudsen, N., Perrild, H., Ovesen, L., ..., & Laurberg, P. (2009). Thyroid volume in hypothyroidism due to autoimmune disease follows a unimodal distribution: evidence against primary thyroid atrophy and autoimmune thyroiditis being distinct diseases. *The Journal of Clinical Endocrinology and Metabolism, 94*(3),833–839.

Casey, B. M., Dashe, J. S., Wells, C. E., McIntire, D. D., Byrd, W., ..., & Cunningham, F. G. (2005). Subclinical hypothyroidism and pregnancy outcomes. *Obstetrics and Gynecology, 105*(2), 239-245.

Caturegli, P., De Remigis, A., & Rose, N. R. (2014). Hashimoto thyroiditis: clinical and diagnostic criteria. *Autoimmunity Reviews, 13*(4), 391-397.

Chanoine, J. P., Toppet, V., Lagasse, R., Spehl, M., & Delange, F. (1991). Determination of thyroid volume by ultrasound from the neonatal period to late adolescence. *European Journal of Pediatrics, 150*(6), 395–399.

Chaudhary, V., & Bano, S. (2013). Thyroid ultrasound. *Indian Journal of Endocrinology and Metabolism, 17*(2), 219-227.

Chaurasia, P., Modi, B., Mangukiya, S., Jadav, P., & Shah, R. (2011). Variation in thyroid hormones level among people of different age, gender and seasons, piparia, gujarat. *National Journal of Medical Research, 1*(2), 57–9.

Chiamolera, M. I., & Wondisford, F. E. (2009). Thyrotropin-releasing hormone and the thyroid hormone feedback mechanism. *Endocrinology, 150*(3), 1091–1096.

Clark, P. M., Holder, R. L., Haque, S. M., Hobbs, F. R., Roberts, L. M., & Franklyn, J. A. (2012). The relationship between serum TSH and free T4 in older people. *Journal of Clinical Pathology, 65*(5), 463-465.

Cooper, A. (2000). Heat capacity of hydrogen-bonded networks: an alternative view of protein folding thermodynamics. *Biophysical Chemistry, 85*(1), 25-39.

Corrias, A., Mussa, A., Baronio, F., Arrigo, T., Salerno, M., ..., & Beccaria, L. (2010). Diagnostic features of thyroid nodules in pediatrics. *Archives of Pediatrics and Adolescent Medicine, 164(*8), 714-719.

Dangol, R. K., Lanjekar, P., & Pulipati, C. (2017). Thyroid function abnormalities among hospital patients of hilly Nepal. *Journal of Lumbini Medical College, 5*(1), 29–33.

De Vivo, A., Mancuso, A., Giacobbe, A., Moleti, M., Maggio Savasta, L., ..., & Vermiglio, F. (2010). Thyroid function in women found to have early pregnancy loss. *Thyroid, 20*(6), 633-637.

Ditudompo, S., Ongphiphadhanakul, B., Chanprasertyotin, S., & Rajatanavin, R. (1999). A de novo L330S point mutation in thyroid hormone receptor beta gene in a Thai female with resistance to thyroid hormone. *Endocrine Journal, 46*(6), 825-829.

Dix, D. (2019). Human carcinogenesis: the role of age and gender. *Anticancer Research, 39*(8), 4385-4391.

Eastwood, M. P., Stafford, K. A., Lippert, R. A., Jensen, M. Ø., Maragakis, P., ..., & Shaw, D. E. (2010). Equipartition and the calculation of temperature in biomolecular simulations. *Journal of Chemical Theory and Computation, 6*(7), 2045-2058.

Eftink, M. R., Anusiem, A. C., & Biltonen, R. L. (1983). Enthalpy-entropy compensation and heat capacity changes for protein-ligand interactions: general thermodynamic models and data for the binding of nucleotides to ribonuclease A. *Biochemistry, 22*(16), 3884-3896.

El Shafie, K., Ouhtit, A., Al Farsi, Y., Al Sayegh, A., & Al Shafaee, M. (2014). A rare thyroid hormone receptor beta (thr$\beta$) gene mutation in a 15-year-old girl with thyroid hormone resistance syndrome: a case report. *Journal of Medical Case Reports, 8*(1), 12.

Engum, A., Bjøro, T., Mykletun, A., & Dahl, A. A. (2002). An association between depression, anxiety and thyroid function–a clinical fact or an artefact?. *Acta Psychiatrica Scandinavica, 10*6(1), 27-34.

Evered, D. C., Clark, F., & Petersen, V. B. (1974). Thyroid function in euthyroid subjects with autonomous thyroid nodules. *Clinical Endocrinology, 3*(2), 149-154.

Fade, J. V., Franklyn, J. A., Cross, K. W., Jones, S. C., & Sheppard, M. (1991). Prevalence and follow-up of abnormal thyrotrophin (TSH) concentrations in the elderly in the United Kingdom. *Clinical Endocrinology, 34*(1), 77-84.

Fatourechi, V., Aniszewski, J. P., Fatourechi, G. Z. E., Atkinson, E. J., & Jacobsen, S. J. (2003). Clinical features and outcome of subacute thyroiditis in an incidence cohort: Olmsted county, minnesota, study. *The Journal of Clinical Endocrinology and Metabolism, 88*(5), 2100–2105.

Fayer, M. D. (2001). Fast protein dynamics probed with infrared vibrational echo experiments. *Annual Review of Physical Chemistry, 52*(1), 315– 356.

Feller, S. E., Zhang, Y., Pastor, R. W., & Brooks, B. R. (1995). Constant pressure molecular dynamics simulation: the Langevin piston method. *The Journal of Chemical Physics, 103*(11), 4613-4621.

Fereja, T. H., Hymete, A., & Gunasekaran, T. (2013). A recent review on chemiluminescence reaction, principle and application on pharmaceutical analysis. *ISRN Spectroscopy, 2013*, 1-12.

Fernández, M., Caballero, J., Fernández, L., Abreu, J. I., & Garriga, M. (2007). Protein radial distribution function (P-RDF) and Bayesian-regularized genetic neural networks for modeling protein conformational stability: chymotrypsin inhibitor 2 mutants. *Journal of Molecular Graphics and Modelling, 26*(4), 748-759.

Ferreira Azevedo, M., Barra, G. B., Medeiros, L. D. d., Simeoni, L. A., Naves, L. A., & Neves, F. d. A. R. (2008). A novel mutation of thyroid hormone receptor beta (I431V) impairs corepressor release, and induces thyroid hormone resistance syndrome. *Arquivos Brasileiros de Endocrinologia and Metabologia, 52*(8), 1304–1312.

Fontes, R., Coeli, C. R., Aguiar, F., & Vaisman, M. (2013). Reference interval of thyroid stimulating hormone and free thyroxine in a reference population over 60 years old and in very old subjects (over 80 years): comparison to young subjects. *Thyroid Research, 6*(1), 13-21.

Forrest, D., Hanebuth, E., Smeyne, R. J., Everds, N., Stewart, C. L., ..., & Curran, T. (1996). Recessive resistance to thyroid hormone in mice lacking thyroid hormone receptor beta: evidence for tissue- specific modulation of receptor function. *The EMBO Journal ,*

*15*(12), 3006–3015.

Fountoulakis, K. N., Iacovides, A., Grammaticos, P., St Kaprinis, G., & Bech, P. (2004). Thyroid function in clinical subtypes of major depression: an exploratory study. *BMC Psychiatry, 4*(1), 6-15.

Franklyn, J. A., Ramsden, D. B., & Sheppard, M. C. (1985). The influence of age and sex on tests of thyroid function. *Annals of Clinical Biochemistry, 22*(5), 502-505.

Frates, M. C., Benson, C. B., Doubilet, P. M., Kunreuther, E., Contreras, M., ..., & Alexander, E. K. (2006). Prevalence and distribution of carcinoma in patients with solitary and multiple thyroid nodules on sonography. *The Journal of Clinical Endocrinology and Metabolism, 91*(9), 3411-3417.

Fujisaki, H., Zhang, Y., & Straub, J. E. (2006). Time-dependent perturbation theory for vibrational energy relaxation and dephasing in peptides and proteins. *The Journal of Chemical Physics, 124*(14), 144910-144925.

Garber, J., Cobin, R., Gharib, H., Hennessey, J., Klein, I., ..., & Woeber, K. (2012). American thyroid association taskforce on hypothyroidism in adults. clinical practice guidelines for hypothyroidism in adults: cosponsored by the american association of clinical endocrinologists and the american thyroid association. *Endocrine Practice, 18*(6), 988–1028.

Gerendai, I., & Halász, B. (2001). Asymmetry of the neuroendocrine system. *Physiology, 16*(2), 92-95.

Gilis, D., & Rooman, M. (1996). Stability changes upon mutation of solvent accessible residues in proteins evaluated by database-derived potentials. *Journal of Molecular Biology, 257*(5), 1112-1126.

Gohlke, H., Hendlich, M., & Klebe, G. (2000). Knowledge-based scoring function to predict protein-ligand interactions. *Journal of Molecular Biology, 295*(2), 337-356.

Gómez, J., Hilser, V. J., Xie, D., & Freire, E. (1995). The heat capacity of proteins. *Proteins: Structure, Function, and Bioinformatics, 22*(4), 404-412.

Gromiha, M. M., Oobatake, M., Kono, H., Uedaira, H., & Sarai, A. (1999). Relationship between amino acid properties and protein stability: buried mutations. *Journal of Protein*

*Chemistry, 18*(5), 565-578.

Gromiha, M. M., Oobatake, M., Kono, H., Uedaira, H., & Sarai, A. (2002). Importance of mutant position in Ramachandran plot for predicting protein stability of surface mutations. *Biopolymers: Original Research on Biomolecules, 64*(4), 210-220.

Gupta, M., Gupta, S., & Gupta, V. B. (2010). Correlation of fine needle aspiration cytology with histopathology in the diagnosis of solitary thyroid nodule. *Journal of Thyroid Research*, 2010, 1-5.

Hadlow, N. C., Rothacker, K. M., Wardrop, R., Brown, S. J., Lim, E. M., & Walsh, J. P. (2013). The relationship between TSH and free T4 in a large population is complex and nonlinear and differs by age and sex. *The Journal of Clinical Endocrinology and Metabolism, 98*(7), 2936–2943.

Hardy, D. J., Wu, Z., Phillips, J. C., Stone, J. E., Skeel, R. D., & Schulten, K. (2015). Multilevel summation method for electrostatic force evaluation. *Journal of Chemical Theory and Computation, 11*(2), 766-779.

Hashimoto, K., Curty, F. H., Borges, P. P., Lee, C. E., Abel, E. D., ..., & Wondisford, F. E. (2001). An unliganded thyroid hormone receptor causes severe neurological dysfunction. *Proceedings of the National Academy of Sciences, 98*(7), 3998-4003.

Hegedüs, L. (2004). The thyroid nodule. *New England Journal of Medicine, 351*(17), 1764-1771.

Hegedüs, L., Perrild, H., Poulsen, L. R., Andersen, J. R., Holm, B., ..., & Hansen, J. M. (1983). The determination of thyroid volume by ultrasound and its relationship to body weight, age, and sex in normal subjects. *The Journal of Clinical Endocrinology and Metabolism, 56*(2), 260–263.

Helbing, J., Devereux, M., Nienhaus, K., Nienhaus, G. U., Hamm, P., & Meuwly, M. (2011). Temperature dependence of the heat diffusivity of proteins. *The Journal of Physical Chemistry A, 116*(11), 2620–2628.

Hendee, W. R., & Ritenour, E. R. (2003). *Medical imaging physics* (Ed. 4, pp.303-353). John Wiley and Sons.

Ho, B. K., and Brasseur, R. (2005). The Ramachandran plots of glycine and preproline.

*BMC Structural Biology, 5*(1), 14-25.

Hoermann, R., Eckl, W., Hoermann, C., & Larisch, R. (2010). Complex relationship between free thyroxine and TSH in the regulation of thyroid function. *European Journal of Endocrinology, 162*(6), 1123-1129.

Hoermann, R., Midgley, J. E., Giacobino, A., Eckl, W. A., Wahl, H. G., ..., & Larisch, R. (2014). Homeostatic equilibria between free thyroid hormones and pituitary thyrotropin are modulated by various influences including age, body mass index and treatment. *Clinical Endocrinology, 81*(6), 907–915.

Hollingsworth, S. A., & Karplus, P. A. (2010). A fresh look at the Ramachandran plot and the occurrence of standard structures in proteins. *Biomolecular Concepts, 1*(3), 271-283.

Hong, H. S., Lee, E. H., Jeong, S. H., Park, J., & Lee, H. (2015). Ultrasonography of various thyroid diseases in children and adolescents: a pictorial essay. *Korean Journal of Radiology, 16*(2), 419-429.

Hu, C. Y., Lynch, G. C., Kokubo, H., & Pettitt, B. M. (2010). Trimethylamine N-oxide influence on the backbone of proteins: an oligoglycine model. *Proteins: Structure, Function, and Bioinformatics, 78*(3), 695-704.

Humphrey, W., Dalke, A., & Schulten, K. (1996). VMD: visual molecular dynamics. *Journal of Molecular Graphics, 14*(1), 33-38.

Hwang, S. H., Kim, E. K., Moon, H. J., Yoon, J. H., & Kwak, J. Y. (2016). Risk of thyroid cancer in euthyroid asymptomatic patients with thyroid nodules with an emphasis on family history of thyroid cancer. *Korean Journal of Radiology, 17*(2), 255-263.

Ivanac, G., Rožman, B., Škreb, F., Brkljačić, B., & Pavić, L. (2004). Ultrasonographic measurement of the thyroid volume. *Collegium Antropologicum, 28*(1), 287–291.

Januś, D., Wójcik, M., Drabik, G., & Starzyk, J. (2018). Ultrasound variants of autoimmune thyroiditis in children and adolescents and their clinical implication in relation to papillary thyroid carcinoma development. *Journal of Endocrinological Investigation, 41*(3), 371–380.

Jonklaas, J., Kahric-Janicic, N., Soldin, O. P., & Soldin, S. J. (2009). Correlations of free thyroid hormones measured by tandem mass spectrometry and immunoassay with

thyroid-stimulating hormone across 4 patient populations. *Clinical Chemistry, 55*(7), 1380-1388.

Jonklaas, J., Nsouli-Maktabi, H., & Soldin, S. J. (2008). Endogenous thyrotropin and triiodothyronine concentrations in individuals with thyroid cancer. *Thyroid, 18*(9), 943–952.

Kayastha, P., Paudel, S., Shrestha, D., Ghimire, R., & Pradhan, S. (2010). Study of thyroid volume by ultrasonography in clinically euthyroid patients. *Journal of Institute of Medicine, 32*(2), 36–43.

Khan, F. I., Aamir, M., Wei, D. Q., Ahmad, F., & Hassan, M. I. (2017). Molecular mechanism of Ras-related protein Rab-5A and effect of mutations in the catalytically active phosphate-binding loop. *Journal of Biomolecular Structure and Dynamics, 35*(1), 105-118.

König, G., & Brooks, B. R. (2015). Correcting for the free energy costs of bond or angle constraints in molecular dynamics simulations. *Biochimica et Biophysica Acta (BBA)-General Subjects, 1850*(5), 932–943.

Kratzsch, J., Fiedler, G. M., Leichtle, A., Brugel, M., Buchbinder, S., ..., & Thiery, J. (2005). New reference intervals for thyrotropin and thyroid hormones based on National Academy of Clinical Biochemistry criteria and regular ultrasonography of the thyroid. *Clinical Chemistry, 51*(8), 1480-1486.

Kumar, T. R., Pradeep, P., & Ragavan, M. (2010). Bilobar thyroid agenesis presenting with adenomatous isthmus and hypothyroidism in a 13 year old girl: A case report. *Journal of Pediatric Sciences, 2*(2), e21-27.

Lamichhane, T. R., & Lamichhane, H. P. (2018). Heat conduction by thyroid hormone receptors. *AIMS Biophysics, 5*(4), 245-256.

Lamichhane, T. R., & Lamichhane, H. P. (2020). Structural changes in thyroid hormone receptor-beta by T3 binding and L330S mutational interactions. *AIMS Biophysics, 7*(1), 27-40.

Lamichhane, T. R., Pangeni, S., Paudel, S., & Lamichhane, H. P. (2015). Age and Gender Related Variations of Pituitary Gland Size of Healthy Nepalese People Using Magnetic

Resonance Imaging. *American Journal of Biomedical Engineering, 5*(4), 130-135.

Lamichhane, T. R., Pant, S. P., Lamichhane, B., Paudel, S., Yadav, B. K., & Lamichhane, H. P. (2020). Thyroid Hormones-Thyrotropin Interrelationships in Thyroid Dysfunction States. *bioRxiv*.

Lamichhane, T. R., Pant, S. P., Lamichhane, B., Gautam, C., Paudel, S., ..., & Lamichhane, H. P. (2018). Age- and gender-specific changes in thyroid Size and thyroid function test values of euthyroid subjects. *Journal of Biosciences and Medicines, 6*(11), 59-73.

Lamichhane, T. R., Paudel, S., Yadav, B. K., & Lamichhane, H. P. (2019). Echo dephasing and heat capacity from constrained and unconstrained dynamics of triiodothyronine nuclear receptor protein. *Journal of Biological Physics, 45*(1), 107-125.

Lamichhane, T. R., Paudel, S., Yadav, B. K., & Lamichhane, H. P. (2019). Molecular dynamics approach to the I431V mutational impact on thyroid hormone receptor-beta. *BIBECHANA, 16*, 79-91.

Larsen, P. R., Silva, J. E., & Kaplan, M. M. (1981). Relationships between circulating and intracellular thyroid hormones: physiological and clinical implications. *Endocrine Reviews, 2*(1), 87–102.

Lee, B., & Richards, F. M. (1971). The interpretation of protein structures: estimation of static accessibility. *Journal of Molecular Biology, 55*(3), 379-400.

Lee, J. H., & Kim, E. Y. (2014). Resistance to thyroid hormone due to a novel mutation of thyroid hormone receptor beta gene. *Annals of Pediatric Endocrinology and Metabolism, 19*(4), 229-231.

Leitner, D. M. (2008). Energy flow in proteins. *Annual Review of Physical Chemistry, 59*, 233–259.

Leoutsakos, V. (2004). A short history of the thyroid gland. *Hormones Athens*, 3, 268-271.

Leow, M. K. S. (2016). A review of the phenomenon of hysteresis in the hypothalamus–pituitary–thyroid axis. *Frontiers in Endocrinology, 7*, 64-72.

Leow, M. K. S. (2007). A mathematical model of pituitary–thyroid interaction to provide an insight into the nature of the thyrotropin–thyroid hormone relationship. *Journal of Theoretical Biology, 248*(2), 275–287.

Leppäluoto, J., Sikkilä, K., & Hassi, J. (1998). Seasonal variation of serum tsh and thyroid hormones in males living in subarctic environmental conditions. *International Journal of Circumpolar Health, 57*, 383–385.

Lervik, A., Bresme, F., & Kjelstrup, S. (2009). Heat transfer in soft nanoscale interfaces: the influence of interface curvature. *Soft Matter, 5*(12), 2407-2414.

Lervik, A., Bresme, F., Kjelstrup, S., Bedeaux, D., & Rubi, J. M. (2010). Heat transfer in protein–water interfaces. *Physical Chemistry Chemical Physics, 12*(7), 1610–1617.

Levine, B. G., Stone, J. E., & Kohlmeyer, A. (2011). Fast analysis of molecular dynamics trajectories with graphics processing units—Radial distribution function histogramming. *Journal of Computational Physics, 230*(9), 3556-3569.

Lewiński, A., Gerendai, I., Pawlikowski, M., & Halász, B. (1982). Unilateral posterior deafferentation of hypothalamus and mitotic activity of thyroid follicular cells under normal conditions and after hemithyroidectomy. *Endocrinologia Experimentalis, 16*(2), 75-80.

Lobanov, M. Y., Bogatyreva, N. S., & Galzitskaya, O. V. (2008). Radius of gyration as an indicator of protein structure compactness. *Molecular Biology, 42*(4), 623-628.

Lu, L., Zhan, T., Ma, M., Xu, C., Wang, J., ..., & Zhuang, S. (2018). Thyroid disruption by bisphenol s analogues via thyroid hormone receptor $\beta$: in vitro, in vivo and molecular dynamics simulation study. *Environmental Science and Technology, 52*(11), 6617–6625.

Machado, D. S., Sabet, A., Santiago, L. A., Sidhaye, A. R., Chiamolera, M. I., Ortiga-Carvalho, T. M., & Wondisford, F. E. (2009). A thyroid hormone receptor mutation that dissociates thyroid hormone regulation of gene expression in vivo. *Proceedings of the National Academy of Sciences, 106*(23), 9441–9446.

MacKerell Jr, A. D., Bashford, D., Bellott, M. L. D. R., Dunbrack Jr, R. L., Evanseck, J. D., ..., & Joseph-McCarthy, D. (1998). All-atom empirical potential for molecular modeling and dynamics studies of proteins. *The Journal of Physical Chemistry B, 102*(18), 3586-3616.

Mackerell Jr, A. D., Feig, M., & Brooks III, C. L. (2004). Extending the treatment of backbone energetics in protein force fields: Limitations of gas phase quantum mechanics

in reproducing protein conformational distributions in molecular dynamics simulations. *Journal of Computational Chemistry, 25*(11), 1400-1415.

Mahato, R., Jha, B., Singh, K., Yadav, B., Shah, S., & Lamsal, M. (2015). Status of thyroid disorders in central Nepal: A tertiary care hospital based study. *International Journal of Applied Sciences and Biotechnology, 3*(1), 119–122.

Małolepsza, E., & Straub, J. E. (2014). Empirical maps for the calculation of amide I vibrational spectra of proteins from classical molecular dynamics simulations. *The Journal of Physical Chemistry B, 118*(28), 7848-7855.

Manji, N., Carr-Smith, J. D., Boelaert, K., Allahabadia, A., Armitage, M., ..., & Franklyn, J. A. (2006). Influences of age, gender, smoking, and family history on autoimmune thyroid disease phenotype. *The Journal of Clinical Endocrinology and Metabolism, 91*(12), 4873-4880.

Marcocci, C., Vitti, P., Cetani, F., Catalano, F., Concetti, R., & Pinchera, A. (1991). Thyroid ultrasonography helps to identify patients with diffuse lymphocytic thyroiditis who are prone to develop hypothyroidism. *The Journal of Clinical Endocrinology and Metabolism, 72*(1), 209-213.

Mariotti, S., Franceschi, C., Cossarizza, A., & Pinchera, A. (1995). The aging thyroid. *Endocrine Reviews, 16*(6), 686-715.

Meng, Z., Liu, M., Zhang, Q., Liu, L., Song, K., ..., & Ren, X. (2015). Gender and age impacts on the association between thyroid function and metabolic syndrome in Chinese. *Medicine, 94*(50), e2193-2202.

Midgley, J. E., Hoermann, R., Larisch, R., & Dietrich, J. W. (2013). Physiological states and functional relation between thyrotropin and free thyroxine in thyroid health and disease: in vivo and in silico data suggest a hierarchical model. *Journal of Clinical Pathology, 66*(4), 335-342.

Mizokami, T., Wu Li, A., El-Kaissi, S., & Wall, J. R. (2004). Stress and thyroid autoimmunity. *Thyroid, 14*(12), 1047-1055.

Monaco, F. (2003). Classification of thyroid diseases: suggestions for a revision. *The Journal of Clinical Endocrinology and Metabolism, 88*(4), 1428–1432.

Nair, P. S., Sobhakumar, S., & Kailas, L. (2010). Diagnostic re-evaluation of children with congenital hypothyroidism. *Indian Pediatrics, 47*(9), 757–760.

Nascimento, A. S., Dias, S. M. G., Nunes, F. M., Aparício, R., Ambrosio, A. L., ..., & Togashi, M. (2006). Structural rearrangements in the thyroid hormone receptor hinge domain and their putative role in the receptor function. *Journal of Molecular Biology, 360*(3), 586-598.

Negro, R., Schwartz, A., Gismondi, R., Tinelli, A., Mangieri, T., & Stagnaro Green, A. (2010). Increased pregnancy loss rate in thyroid antibody negative women with TSH levels between 2.5 and 5.0 in the first trimester of pregnancy. *The Journal of Clinical Endocrinology and Metabolism, 95*(9), E44-48.

Nishihara, E., Amino, N., Ohye, H., Ota, H., Ito, M., ..., & Miyauchi, A. (2009). Extent of hypoechogenic area in the thyroid is related with thyroid dysfunction after subacute thyroiditis. *Journal of Endocrinological Investigation, 32*(1), 33–36.

Noid, W., Ezra, G. S., & Loring, R. F. (2004). Vibrational echoes: Dephasing, rephasing, and the stability of classical trajectories. *The Journal of Physical Chemistry B, 108*(21), 6536–6543.

Nosé, S. (1984). A molecular dynamics method for simulations in the canonical ensemble. *Molecular Physics, 52*(2), 255-268.

Oberhofer, R., Ober, A., Oberkofler, F., and Amor, H. (1989). Thyroid gland volumes of healthy adults in an area with endemic goiter. *Acta Medica Austriaca, 16*(2), 38-41.

Obregon, M. J., del Rey, F. E., & de Escobar, G. M. (2005). The effects of iodine deficiency on thyroid hormone deiodination. *Thyroid, 15*(8), 917–929.

Ortiga-Carvalho, T. M., Sidhaye, A. R., and Wondisford, F. E. (2014). Thyroid hormone receptors and resistance to thyroid hormone disorders. *Nature Reviews Endocrinology, 10*(10), 582-592.

Pandey, H. D., & Leitner, D. M. (2017). Thermodynamics of hydration water around an antifreeze protein: A molecular simulation study. *The Journal of Physical Chemistry B, 121*(41), 9498-9507.

Pearce, E. N., Farwell, A. P., & Braverman, L. E. (2003). Thyroiditis. *New England Journal*

*of Medicine, 348*(26), 2646-2655.

Peccin, S., De Castro, J. A. S., Furlanetto, T. W., Furtado, A. P. A., Brasil, B. A., & Czepielewski, M. A. (2002). Ultrasonography: is it useful in the diagnosis of cancer in thyroid nodules?. *Journal of Endocrinological Investigation, 25*(1), 39-43.

Pedersen, O. M., Aardal, N. P., Larssen, T. B., Varhaug, J. E., Myking, O., & Vik-Mo, H. (2000). The value of ultrasonography in predicting autoimmune thyroid disease. *Thyroid, 10*(3), 251-259.

Phillips, J. C., Braun, R., Wang, W., Gumbart, J., Tajkhorshid, E., ..., & Schulten, K. (2005). Scalable molecular dynamics with NAMD. *Journal of Computational Chemistry, 26*(16), 1781-1802.

Plastino, A. R., & Lima, J. A. S. (1999). Equipartition and virial theorems within general thermostatistical formalisms. *Physics Letters A, 260*(1-2), 46-54.

Pohlenz, J., Wildhardt, G., Zabel, B., & Willgerodt, H. (1997). Resistance to thyroid hormone in a family caused by a new point mutation L330S in the thyroid receptor (TR) beta gene. *Thyroid, 7*(1), 39-41.

Polyzos, S. A., Kita, M., Efstathiadou, Z., Poulakos, P., Slavakis, A., ..., & Avramidis, A. (2008). Serum thyrotropin concentration as a biochemical predictor of thyroid malignancy in patients presenting with thyroid nodules. *Journal of Cancer Research and Clinical Oncology, 134*(9), 953-960.

Prabhu, N. V., & Sharp, K. A. (2005). Heat capacity in proteins. *Annual Reiew of Physical Chemistry, 56*, 521–548.

Prisant, L. M., Gujral, J. S., & Mulloy, A. L. (2006). Hyperthyroidism: a secondary cause of isolated systolic hypertension. *The Journal of Clinical Hypertension, 8*(8), 596-599.

Privalov, P. L., & Dragan, A. I. (2007). Microcalorimetry of biological macromolecules. *Biophysical Chemistry, 126*(1-3), 16-24.

Privalov, P. L., & Potekhin, S. A. (1986). *[2] Scanning microcalorimetry in studying temperature-induced changes in proteins.* In Methods in enzymology (Vol. 131, pp. 4-51). Academic Press.

Privalov, P. L., Tiktopulo, E., Venyaminov, S. Y., Griko, Y. V., Makhatadze, G., &

Khechinashvili, N. (1989). Heat capacity and conformation of proteins in the denatured state. *Journal of Molecular Biology, 205*(4), 737–750.

Rabbiosi, S., Vigone, M. C., Cortinovis, F., Zamproni, I., Fugazzola, L., ..., & Weber, G. (2013). Congenital hypothyroidism with eutopic thyroid gland: analysis of clinical and biochemical features at diagnosis and after re-evaluation. *The Journal of Clinical Endocrinology and Metabolism, 98*(4), 1395-1402.

Rahat, O., Alon, U., Levy, Y., & Schreiber, G. (2009). Understanding hydrogen bond patterns in proteins using network motifs. *Bioinformatics, 25*(22), 2921-2928.

Raj, K. S. (2014). Thyroid function tests and its interpretation. J*ournal of Pathology of Nepal, 4*(7), 584–590.

Rajendran, V., Purohit, R., & Sethumadhavan, R. (2012). In silico investigation of molecular mechanism of laminopathy caused by a point mutation (R482W) in lamin A/C protein. *Amino Acids, 43*(2), 603-615.

Rector, K., Kwok, A., Ferrante, C., Tokmakoff, A., Rella, C., and Fayer, M. (1997). Vibrational anharmonicity and multilevel vibrational dephasing from vibrational echo beats. *The Journal of Chemical Physics, 106*(24), 10027–10036.

Reichlin, S., & Utiger, R. D. (1967). Regulation of the pituitary-thyroid axis in man: relationship of TSH concentration to concentration of free and total thyroxine in plasma. *The Journal of Clinical Endocrinology and Metabolism, 27*(2), 251-255.

Rekik, N., Suleiman, J., Blaise, P., & Wojcik, M. J. (2018). Equivalence between the classical and quantum IR spectral density approaches of weak H-bonds in the absence of damping. *The Journal of Physical Chemistry A, 122*(8), 2108-2115.

Rella, C., Kwok, A., Rector, K., Hill, J. R., Schwettman, H., ..., & Fayer, M. (1996). Vibrational echo studies of protein dynamics. *Physical Review Letters, 77*(8), 1648-1651.

Lee, B., & Richards, F. M. (1971). The interpretation of protein structures: estimation of static accessibility. *Journal of Molecular Biology, 55*(3), 379-400.

Riniker, S., Eichenberger, A. P., & van Gunsteren, W. F. (2012). Solvating atomic level fine-grained proteins in supra-molecular level coarse-grained water for molecular dynamics simulations. *European Biophysics Journal, 41*(8), 647-661.

Rohil, V., Mishra, A. K., Shrewastwa, M. K., Mehta, K. D., Lamsal, M., ..., & Majhi, S. (2010). Subclinical hypothyroidism in eastern Nepal: A hospital based study. *Kathmandu University Medical Journal*, 8(2), 231-237.

Rosen, M. D., & Privalsky, M. L. (2009). Thyroid hormone receptor mutations found in renal clear cell carcinomas alter corepressor release and reveal helix 12 as key determinant of corepressor specificity. *Molecular Endocrinology, 23*(8), 1183–1192.

Rosen, M. D., & Privalsky, M. L. (2011). Thyroid hormone receptor mutations in cancer and resistance to thyroid hormone: perspective and prognosis. *Journal of Thyroid Research, 2011*, 1-20.

Ryckaert, J. P., Ciccotti, G., & Berendsen, H. J. (1977). Numerical integration of the cartesian equations of motion of a system with constraints: molecular dynamics of n-alkanes. *Journal of Computational Physics, 23*(3), 327–341.

Safer, J. D., O'connor, M. G., Colan, S. D., Srinivasan, S., Tollin, S. R., & Wondisford, F. E. (1999). The thyroid hormone receptor-$\beta$ gene mutation R383H is associated with isolated central resistance to thyroid hormone. *The Journal of Clinical Endocrinology and Metabolism, 84*(9), 3099-3109.

Sandler, B., Webb, P., Apriletti, J. W., Huber, B. R., Togashi, M., ..., & others (2004). Thyroxine-thyroid hormone receptor interactions. *Journal of Biological Chemistry, 279*(53), 55801–55808.

Sawin, C. T., Chopra, D., Azizi, F., Mannix, J. E., & Bacharach, P. (1979). The aging thyroid: increased prevalence of elevated serum thyrotropin levels in the elderly. *Jama, 242*(3), 247-250.

Şeker, S., & Taş, İ. (2010). Determination of thyroid volume and its relation with isthmus thickness. *European Journal of General Medicine, 7*(2), 125-129.

Schulten, K., Lu, H., and Bai, L. (1997). *Probing protein motion through temperature echoes.* In Physics of biological systems (pp. 117–152). Springer.

Shivaraj, G., Prakash, B. D., Sonal, V., Shruthi, K., Vinayak, H., & Avinash, M. (2009). Thyroid function tests: a review. *European Review for Medical and Pharmacological Sciences, 13*(5), 341–349.

Souza, P., Puhl, A., Martinez, L., Aparicio, R., Nascimento, A. S., ..., & Polikarpov, I. (2014). Identification of a new hormone-binding site on the surface of thyroid hormone receptor. *Molecular Endocrinology, 28*(4), 534–545.

Shuto, Y., Wakabayashi, I., Amuro, N., Minami, S., & Okazaki, T. (1992). A point mutation in the 3, 5, 3'-triiodothyronine-binding domain of thyroid hormone receptor-beta associated with a family with generalized resistance to thyroid hormone. *The Journal of Clinical Endocrinology and Metabolism, 75*(1), 213-217.

Sturtevant, J. M. (1977). Heat capacity and entropy changes in processes involving proteins. *Proceedings of the National Academy of Sciences, 74*(6), 2236-2240.

Surks, M. I., Chopra, I. J., Mariash, C. N., Nicoloff, J. T., & Solomon, D. H. (1990). American Thyroid Association guidelines for use of laboratory tests in thyroid disorders. *Jama, 263*(11), 1529-1532.

Suurkuusk, J. (1974). Specific heat measurements on lysozyme, chymotrypsinogen, and ovalbumin in aqueous solution and in solid state. *Acta Chemica Scandinavica B, 28*(4), 409-417.

Szczepanek-Parulska, E., Woliński, K., Stangierski, A., Gurgul, E., & Rucha la, M. (2014). Biochemical and ultrasonographic parameters influencing thyroid nodules elasticity. *Endocrine, 47*(2), 519–527.

Trzepacz, P. T., Klein, I., Roberts, M., Greenhouse, J., & Levey, G. S. (1989). Graves' disease: an analysis of thyroid hormone levels and hyperthyroid signs and symptoms. *The American Journal of Medicine, 987*(5), 558–561.

Vagenakis, A. G., Rapoport, B., Azizi, F., Portnay, G. I., Braverman, L. E., & Ingbar, S. H. (1974). Hyperresponse to thyrotropin-releasing hormone accompanying small decreases in serum thyroid hormone concentrations. *The Journal of Clinical Investigation, 54*(4), 913-918.

Van Boxtel, M. P. J., Menheere, P. P. C. A., Bekers, O., Hogervorst, E., & Jolles, J. (2004). Thyroid function, depressed mood, and cognitive performance in older individuals: the Maastricht Aging Study. *Psychoneuroendocrinology, 29*(7), 891-898.

Van Gunsteren, W., & Berendsen, H. (1977). Algorithms for macromolecular dynamics and

constraint dynamics. *Molecular Physics, 34*(5), 1311– 1327.

Van Gunsteren, W. F., & Karplus, M. (1982). Effect of constraints on the dynamics of macromolecules. *Macromolecules, 15*(6), 1528-1544.

Vejbjerg, P., Knudsen, N., Perrild, H., Laurberg, P., Pedersen, I. B., ..., & Jørgensen, T. (2006). The association between hypoechogenicity or irregular echo pattern at thyroid ultrasonography and thyroid function in the general population. *European Journal of Endocrinology, 155*(4), 547-552.

Verlet, L. (1967). Computer experiments on classical fluids. I. Thermodynamical properties of Lennard-Jones molecules. *Physical Review, 159*(1), 98-103.

Walser, R., Hünenberger, P. H., & van Gunsteren, W. F. (2002). Molecular dynamics simulations of a double unit cell in a protein crystal: volume relaxation at constant pressure and correlation of motions between the two unit cells. *Proteins: Structure, Function, and Bioinformatics, 48*(2), 327-340.

Weeks, I., Sturgess, M. L., & Woodhead, J. S. (1986). Chemiluminescence immunoassay: an overview. *Clinical Science, 70*(5), 403–408.

Xu, D., Schulten, K., Becker, O. M., & Karplus, M. (1995). Temperature quench echoes in proteins. *The Journal of Chemical Physics, 103*(8), 3112–3123.

Xu, Y., & Leitner, D. M. (2014). Vibrational energy flow through the green fluorescent protein–water interface: communication maps and thermal boundary conductance. *The Journal of Physical Chemistry B, 118*(28), 7818-7826.

Yang, P. H., & Rupley, J. A. (1979). Protein-water interactions. Heat capacity of the lysozyme-water system. *Biochemistry, 18*(12), 2654-2661.

Yang, W., Yan, J., & Sang, Y. (2016). Resistance to thyroid hormone caused by a G344R mutation of thyroid hormone receptor beta gene: a case report study. *Endocrinology and Metabolic Syndrome, 5*(2), 231-235.

Ying, M., & Yung, D. M. (2009). Asymmetry of thyroid lobe volume in normal Chinese subjects: association with handedness and position of esophagus. *The Anatomical Record, 292*(2), 169-174.

Yu, X., & Leitner, D. M. (2005). Heat flow in proteins: computation of thermal transport

coefficients. *The Journal of Chemical Physics, 122*(5), 054902-054913.

Zhuang, S., Bao, L., Linhananta, A., & Liu, W. (2013). Molecular modeling revealed that ligand dissociation from thyroid hormone receptors is affected by receptor heterodimerization. *Journal of Molecular Graphics and Modelling, 44*, 155–160.

Zoete, V., Cuendet, M. A., Grosdidier, A., & Michielin, O. (2011). SwissParam: a fast force field generation tool for small organic molecules. *Journal of Computational Chemistry, 32*(11), 2359-2368.

Zou, J., Song, B., Simmerling, C., & Raleigh, D. (2016). Experimental and computational analysis of protein stabilization by Gly-to-d-Ala substitution: A convolution of native state and unfolded state effects. *Journal of the American Chemical Society, 138*(48), 15682-15689.

# APPENDIX

## 1. Publications

Lamichhane, T. R., & Lamichhane, H. P. (2020). Structural changes in thyroid hormone receptor-beta by T3 binding and L330S mutational interactions. *AIMS Biophysics, 7*(1), 27-40.

Lamichhane, T. R., & Lamichhane, H. P. (2020). Constant velocity pulling and unfolding of thyroid hormone receptor by steered molecular dynamics. *BIBECHANA, 17*, 50-57.

Lamichhane, T. R., Paudel, S., Yadav, B. K., & Lamichhane, H. P. (2019). Echo dephasing and heat capacity from constrained and unconstrained dynamics of triiodothyronine nuclear receptor protein. *Journal of Biological Physics, 45*(1), 107-125.

Lamichhane, T. R., Paudel, S., Yadav, B. K., & Lamichhane, H. P. (2019). Molecular dynamics approach to the I431V mutational impact on thyroid hormone receptor-beta. *BIBECHANA, 16*, 79-91.

Lamichhane, T. R., & Lamichhane, H. P. (2018). Heat conduction by thyroid hormone receptors. *AIMS Biophysics, 5*(4), 245-256.

Lamichhane, T. R., Pant, S., Lamichhane, B., Gautam, C., Paudel, S., Yadav, B. K., & Lamichhane, H. P. (2018). Age- and gender-specific changes in thyroid size and thyroid function test values of euthyroid subjects. *Journal of Biosciences and Medicines, 6*(11), 59-73.

## 2. Conferences

Lamichhane, T. R. (2019, Nov 17-22). *Thiocyanate-induced conformational changes on thyroid hormone receptor-beta by model ligand-T2SCN interactions* [Oral presentation]. 14th Asia-Pacific Physics Conference 2019 (APPC14), Borneo Convention Centre, Kuching, Sarawak, Malaysia.

Lamichhane, T. R. (2019, Feb 4-6). *Echo dephasing and heat capacity from constrained and*

*unconstrained dynamics of triiodothyronine nuclear receptor protein* [Oral presentation]. International Conference on Nanosciences and High Energy Physics (ICNHEP 2019), Central Department of Physics, Tribhuvan University, Kirtipur, Kathmandu, Nepal.

Lamichhane, T. R. (2019, Feb 4-6). *Biophysical analysis of thyroid function test reports of euthyroid subjects* [Best poster presentation]. International Conference on Nanosciences and High Energy Physics (ICNHEP 2019), Central Department of Physics, Tribhuvan University, Kirtipur, Kathmandu, Nepal.

Lamichhane, T. R. (2018, Dec 1-3). *Age and gender specific changes in thyroid size and thyroid function test values in euthyroid subjects*. The 4th Conference on Advances in Biochemistry and Molecular Biology (CABMB 2018), Asia Pacific Convention Center, Sanya, China.

Lamichhane, T. R. (2018, May 29-31). *Biophysical analysis of thyroid function test reports of euthyroid subjects* [Poster presentation]. International Conference on Explorations in Physics (ICEP 2018), Department of Physics, Amrit Science Campus, Tribhuvan University, Kathmandu, Nepal.

Lamichhane, T. R. (2017, Dec 27-28). *Non-equilibrium thermodynamic properties of thyroid hormone receptor-beta* [Best poster presentation]. International Conference on Nanomaterials and Computational Physics (ICNCP 2017), Central Department of Physics, Tribhuvan University, Kirtipur, Kathmandu, Nepal.

## Glossary of Medical Terms

| | |
|---|---|
| Autoimmunity | misdirected immune response that attacks body itself |
| Cyst | sac-like pocket of membranous tissue that contains fluid |
| DNA replication | process to make two identical DNA from a double stranded DNA |
| Echogenicity | ability to bounce an echo in ultrasound examination |
| Endocrine system | collection of glands that produce hormones to regulate body functions |
| Euthyroid | state of normal thyroid function |
| Goitre | swelling in neck resultinga enlarged thyroid gland |
| Hyperthyroid | state of overactive thyroid function |
| Hypothalamus | part of nervous system that links to endocrine system via pituitary gland |
| Hypothyroid | state of underactive thyroid function |
| Insomnia | sleep disorder in which people have trouble sleeping |
| Lesion | tissue which has suffered damage through injury or disease |
| Lymphocytic | autoimmune disorder where immune cells attack thyroid gland |
| Pituitary | master gland that controls the body functions by releasing hormones |
| Transcription | process of copying DNA sequence to make RNA |
| Thermogenesis | process of heat production in organisms |
| Thyroiditis | swelling or inflammation of thyroid gland |
| Thyrotoxicosis | clinical manifestation of excess thyroid hormone action at tissue level |
| Malignancy | state or presence of a malignant tumour or cancer |
| Metabolism | chemical reactions that maintain living state of cells and organism |
| Mutation | alteration in nucleotide or amino acid sequence |
| Neoplasia | uncontrolled growth of cells that is not under physiologic control |
| Nodule | growth of abnormal tissue |
| Vascularity | condition of having many highly-visible supericial veins |

# Published Papers

# &

# Conference Certificates

AIMS Biophysics, 7(1): 27–40.
DOI: 10.3934/biophy.2020003
Received: 04 February 2020
Accepted: 17 March 2020
Published: 23 March 2020

http://www.aimspress.com/journal/biophysics

*Research article*

# Structural changes in thyroid hormone receptor-beta by T3 binding and L330S mutational interactions

**Tika Ram Lamichhane and Hari Prasad Lamichhane***

Central Department of Physics, Tribhuvan University, Kirtipur, Kathmandu, Nepal

*** Correspondence:** Email: hlamichhane1@gmail.com; Tel: +9779843217767.

**Abstract:** The point mutations like L330S in the ligand binding domain (LBD) of thyroid hormone receptor-beta (THR-β) make the structural changes as reflected by Ramachandran plots, solvent accessible surface area, radial distribution functions, root mean square deviations and fluctuations, and interaction and internal energies of the LBD residues. By using nanoscale molecular dynamics (NAMD) simulations, the structural features of T3 liganded, unliganded and mutated THR-β LBD are compared to explore the molecular insights in euthyroid, hypothyroid and resistance to thyroid hormones (RTH) states, respectively. The L330S-mutant causes steric hindrance while binding T3 into THR-β LBD causing RTH in the thyroid patients.

**Keywords:** point mutation; thyroid hormone; thyroid hormone receptor-beta; hormone-receptor interactions; conformational changes

## 1. Introduction

The point mutations on thyroid hormone receptor-beta (THR-β) isoform of the nuclear receptor super family cause generalized resistance to thyroid hormones (RTH). The genetic disorder, RTH has the clinical features of elevating thyroid hormone levels without suppressing thyroid stimulating hormone (TSH) in the blood serum. The RTH patients suffer from inadequate secretions by hypothalamus-pituitary-thyroid (HPT) axis. The RTH reduces triiodothyronine (T3) binding affinity to THR-β ligand binding domain (LBD) and it further resists the binding affinity to DNA binding domain resulting in gene repressions. The wild type THR-β is able to select the coactivators for the basal transcription whereas mutated THR-β recruits corepressors inhibiting the transcription factors.

Thus, being linked with genetic defects, the THR-β mutations cause neoplasia and several endocrine disorders. Goitre formation, dizziness, speech disorder and tachycardia are common causes of RTH. All of these clinical facts are associated with the previously identified THR-β mutations [1–5]. L330S was identified in an 11-year-old boy with RTH showing the symptoms of both hypo- and hyperthyroidism, goitre and speech disorder [6]. The L330S mutation was also detected in a 19-year Thai woman with RTH and goitre [7].

To explore the mutational impacts on THR-β gene of the patients with RTH, it is necessary to compare the structural and physical properties of the mutated THR-β with that of wild type liganded and unliganded THR-β associated with euthyroid and hypothyroid states. For this purpose, we can perform MD simulations of each system and analyze root mean square deviation (RMSD), radius of gyration (RG), root mean square fluctuation (RMSF), classical as well as quantum IR spectral density (IRSD), radial distribution function (RDF), solvent accessible surface area (SASA), Ramachandran plots for the dihedral-angle distributions and interaction or internal energies. These types of analysis were also performed by Khan, et al., 2016 to explore the mutational effects in Ras-related protein [8] and by Rajendran, et al., 2012 to investigate the molecular mechanism of laminopathy due to a point mutation R482W in lamin A/C protein [9]. The SASA calculations of the residues in protein folding and unfolding states ranging from 0–300 $Å^2$ were reviewed by Ausaf Ali, et al., 2014 [10]. The protein stability influenced by buried and surface point mutations is due to physicochemical, energetic, and conformational properties of amino acid residues as reflected by the mutant positions on Ramachandran plots [11–13].

## 2. Methodology

The wild type (WT) native structure of T3-liganded thyroid hormone receptor-β (THRT3-WT) was taken from the crystal structure code: 3GWS.pdb [14]. The mutated (MT) nuclear receptor (THRT3-MT) was prepared after the point mutation on 330-codon replacing LEU by SER with the help of PyMOL-Mutagenesis. Topology and parameters required to prepare the complete simulated systems were used from the CHARMM force fields [14–17]. The T3 hormone being the hetero-molecule, it was suitably parameterized to define numerical constants, atomic masses and charges required to evaluate forces and energies [18]. Starting from the generation of protein structure files (psf), all the simulations for energy minimization, equilibration and production runs were performed with nanoscale molecular dynamics (NAMD-2.12) [19]. The simulated systems were analyzed with visual molecular dynamics (VMD-1.9.3) [20].

Each of the molecules, i.e. unliganded THR-WT, THRT3-WT and L330S-mutant THRT3-MT was solvated with 17220 water molecules (TIP3P) under the spherical boundary conditions and neutralized with $Na^+$ and $Cl^-$ ions in the concentration of 0.15 mol/L. Each system had the boundary conditions: radius 37.48 Å, center coordinates (4.14, 25.05, 20.60 Å), force constant 10 kcal $mol^{-1}Å^{-2}$, and exponent 2 for the first potential to be applied. The TCL script file called configuration file was prepared to provide the simulation details. The Langevin piston temperature is 310 K and damping coefficient is 1 $ps^{-1}$. The Langevin dynamics [21,22] was implemented with the integrator parameter of 2 fs/step keeping rigid bonds of all H-atoms. Multilevel summation method (MSM) was active with the grid spacing of 2.5 Å for the electrostatic force evaluation [23]. In order to evaluate the electrostatic and van der Waals interactions, the force field related terms such as 1–4 scaling, cut-off, switching and pair-list distances were set as 1.0, 12 Å, 10 Å and 14 Å, respectively. Then, the

energy of each system was minimized up to 3000 CG steps and its equilibration run was performed up to 20 ns at the body scale temperature 310 K. The new trajectories of the constituent atoms were calculated by using the velocity Verlet algorithm [24].

The conformational changes in the unliganded, T3-liganded and mutated THR-β were analyzed from the nature of RMSD, RG, RMSF and SASA plots related to their protein-backbone, T3-hormone and residues of interest, i.e. L330 and L330S. Ramachandran plots were used to observe the distributions of dihedral angles and the possible steric hindrances among α-helices, β-sheets, side chains and residues during the MD simulations. With the help of NAMD Energy Plugin (Version 1.4), the interaction energies (coulombic and van der Waals) between the native or mutated residues on the 330 codon and T3-hormone were observed in the related system. Furthermore, H-bond distribution, RDF, IRSD and internal energy of T3 and L330 codons were analyzed in both wild type and mutated systems.

As per analysis of the structural trajectory, RMSD vs time graph has been plotted to explain the conformational stability of the molecular system during the MD simulations. The RMSD is a numerical measure of the difference between the protein structures defined by Equation 1 [25,26].

$$RMSD = \sqrt{\frac{\sum_{i=1}^{N}(r_i - r_{i,ref})^2}{N}} \tag{1}$$

where N is the number of atoms whose positions are to be compared, $r_i$ is the position of atom i and $r_{i,ref}$ is the position of atom i in the reference configuration defined by X-ray structure of the protein system.

In addition to RMSD, the equilibrations of the system have been analyzed with RMSF and RG throughout the simulations. The RMSD from the average over time can be referred to as the RMSF. The RMSF of residue i is given by Equation 2 [26].

$$RMSF = \sqrt{\frac{\sum_{i=1}^{N_t}(r_i(t) - \langle r_i \rangle)^2}{N_t}} \tag{2}$$

where $N_t$ is the number of time steps giving new configurations in the simulations, $r_i(t)$ is the position of residue i, $\langle r_i \rangle = \frac{1}{N_t}\sum_{t_j=1}^{N_t} r_i(t_j)$ is the average position of residue i at time $t_j$.

The RG is a measure of compactness describing the extent of collapse or extension of the protein backbone [26,27]. It represents the deviation of atoms in a molecule from its centre of mass defined by the Equation 3.

$$RG = \sqrt{\frac{\sum_{i=1}^{N}(r_i - r_{cm})^2}{N}} \tag{3}$$

where N is the total number of protein atoms, $r_i$ is the position of atom i, $r_{cm} = \frac{1}{M}\sum_{t=1}^{N} m_i r_i$ is the centre of mass, $m_i$ is the mass of atom i and M is the total mass of the protein atoms.

Solvent accessible surface area (SASA) is the area described by the locus of the center of the water molecule when it rolls along the protein complex by making the maximum permitted van der Waals contacts without penetrating any other atom. The SASA is calculated by using the Equation 4 [10,28].

$$SASA = \sum_i \left( R \Big/ \sqrt{R^2 - Z_i^2} \right) . D . L_i \tag{4}$$

where D = ΔZ/2 + Δ'Z, R = r + $r_s$ = sum of van der Weals radius of the atom and chosen radius of the solvent molecule, $L_i$ = length of arc drawn on a given section i, $Z_i$ = the perpendicular distance from the center of the sphere to the section i, ΔZ = the spacing between the sections, and Δ'Z = ΔZ/2 or R−$Z_i$, whichever is smaller. The summation ranges over all of the arcs drawn for the given atom. Here, the solvent accessibility is defined by SA = 100.SASA/4π$R^2$.

In this way, NAMD calculates the spherical atomic radial distribution function (RDF/g(r)) between the atom coordinates in two selections over a given trajectory using GUI Plugin (Version 1.3) in VMD as explained by Levine, et al., 2011 [29]. The normalized distance-dependent RDF for the atom pairs with types i and j is defined by the Equation 5 [30].

$$g_{i,j}(r) = \frac{N_{i,j}(r)/4\pi r^2}{\sum_r (N_{i,j}(r)/4\pi r^2)} \tag{5}$$

where scaling to 4π$r^2$ accounts for the volume of the spherical shell of radius r and thickness dr. The number $N_{i,j}(r)$ of atom pairs i,j at a distance between r and r+dr is found by counting the occurrences $N_{i,j}(r) = \sum_i \sum_r \delta(|r_i - r_j|, r)$ where the delta function is δ = 1 if r ≤ $|r_i - r_j|$ ≤ r+dr and otherwise it is zero. Here, the bin size dr is chosen with high resolution between $r_{min}$ and $r_{max}$ including the atom pairs.

NAMD computes spectral densities from trajectories using time series data created with the measure dipole command in VMD-GUI, i.e. IR Spectral Density Calculator Plugin (Version 1.3). The details of theory and methods of NAMD simulations to calculate vibrational spectra of proteins were explained by Malolepsza, et al., 2014 [31]. The classical IR spectral density, $I_{cl}(\omega)$ is given by Fourier transform of the auto-correlation function $G_{cl}(t)$ of the dipole moment operator [32].

$$I_{cl}(\omega) = \Re\left[\int_0^\infty G_{cl}(t) e^{-i\omega t} dt\right] \tag{6}$$

where $G_{cl}(t) = tr\{\rho(\beta)\mu(0)\mu(t)\dagger\}$ . Here, μ(0) is the dipole moment operator at the initial time and μ(t) is the same operator at the time t, and ρ(β) is Boltzmann density operator with the statistical parameter β = 1/$K_B$T.

## 3. Results and discussion

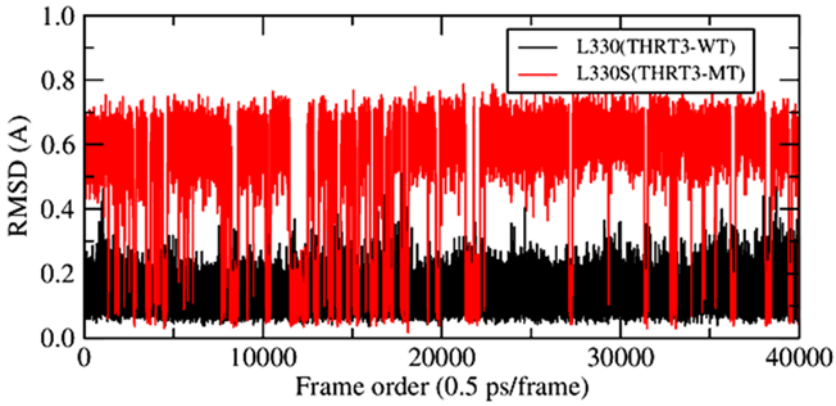


**Figure 1.** Fluctuating RMSDs of L330 and L330S during equilibrations of THRT3-WT and THRT3-MT systems.

**Table 1.** Average RMSD and RG of unliganded THR-WT, liganded THRT3-WT and mutated THRT3-MT (L330S-mutant THR-β) included with standard deviations during the 20 ns equilibrations.

| Molecule | THR-WT | | THRT3-WT | | | THRT3-MT | | |
|---|---|---|---|---|---|---|---|---|
| Residue | L330 | Protein | L330 | T3 | Protein | L330S | T3 | Protein |
| RMSD (Å) | 0.56 ±0.44 | 2.60 ±0.50 | 0.13 ±0.05 | 0.40 ±0.11 | 2.72 ±0.41 | 0.52 ±0.20 | 1.63 ±0.25 | 2.88 ±0.27 |
| RG (Å) | 2.31 ±0.03 | 18.70 ±0.10 | 2.32 ±0.02 | 4.42 ±0.05 | 18.74 ±0.07 | 1.82 ±0.03 | 4.40 ±0.05 | 18.80 ±0.08 |

The protein structure of wild type THR-β that we take for the simulation has 3895 atoms with total mass 27640 amu. The active ligand bound to THR-β LBD is T3 hormone which has 35 atoms with mass 651 amu. In the point mutation L330S, LEU ($C_6H_{13}NO_2$) of mass 131 amu is replaced by SER ($C_3H_7NO_3$) of mass 105 amu.

The constancy of RMSD ($\leq$ 3 Å) and RG ($\approx$ 19 Å) of the protein backbone over the time frames of equilibration runs show the conformational stability and validity of force field topology and parameters used for MD simulations of wild type and mutated receptor systems. Some residues with more fluctuating RMSD/RG show their dynamic properties which are responsible for T3 binding and dissociation from THR-β LBD. The values of RMSD and RG of the molecules with the standard deviations of the data are listed in the Table 1. During the 20 ns equilibration runs in neutral water-ion environment, RMSD of 330-residue in liganded THRT3-WT is smaller and less fluctuating than that in unliganded THR-WT and L330S-mutant THRT3-MT (Figure 1). T3 is more fluctuating due to smaller RG of L330S in mutated LBD than in wild type LBD. The RMSD/RG of the protein backbone is almost same with small fluctuations in these three cases (Table 1).

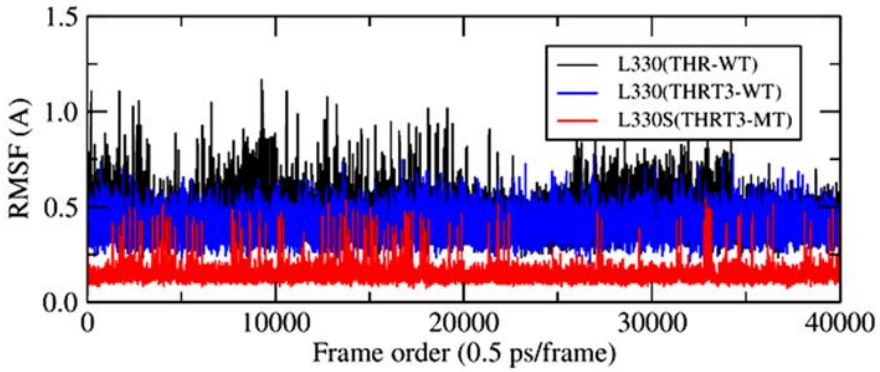


**Figure 2.** RMSFs of LEU and SER residues in 330-codon of unliganded, liganded and mutated THR-β systems.

Root mean square fluctuation (RMSF) of the mutated residue L330S is smaller than the wild type L330 provided with larger fluctuations in the unliganded system as shown in the Figure 2. The RMSFs of all residues in unliganded, liganded and mutated THR-β systems are small lying below 1.0 Å during their equlibrations as shown in the Figure 3. Related to the 330-codon, the RMSFs are 0.46 ± 0.10 Å for LEU of THR-WT, 0.41 ± 0.07 Å for LEU of THRT3-WT and 0.15 ± 0.04 Å for SER of THRT3-MT (Table 2). The positions of L330S mutational sites and T3-hormone in THRT3-MT after

their 20 ns equilibrations are shown in Figure 4. During the MD simulations of wild type and mutated THR-β systems, distance between L330 and T3 in THRT3-WT varies as 6.36 ± 0.33 Å and the distance between L330S and T3 in THRT3-MT varies as 7.11 ± 0.28 Å. Such distance is smaller and more fluctuating in THRT3-WT than in THRT3-MT (Figure 5). This is one of the indicators of T3 resistant features of mutated nuclear receptors causing RTH.

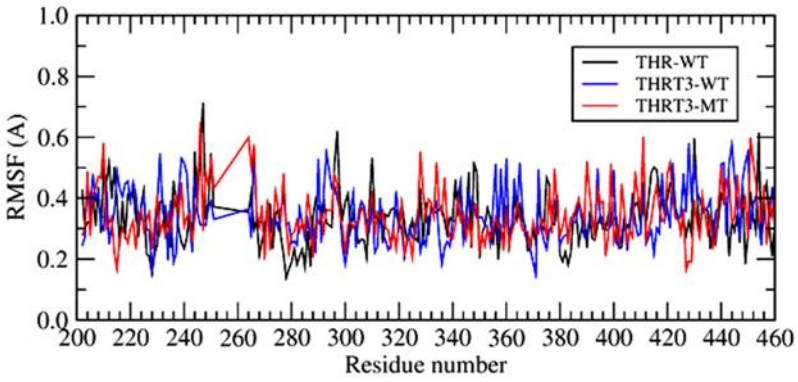


**Figure 3.** RMSFs of all residues in unliganded, liganded and L330S-mutant THR-β systems during the last frame of 20 ns equilibrating simulations in the cellular environment.

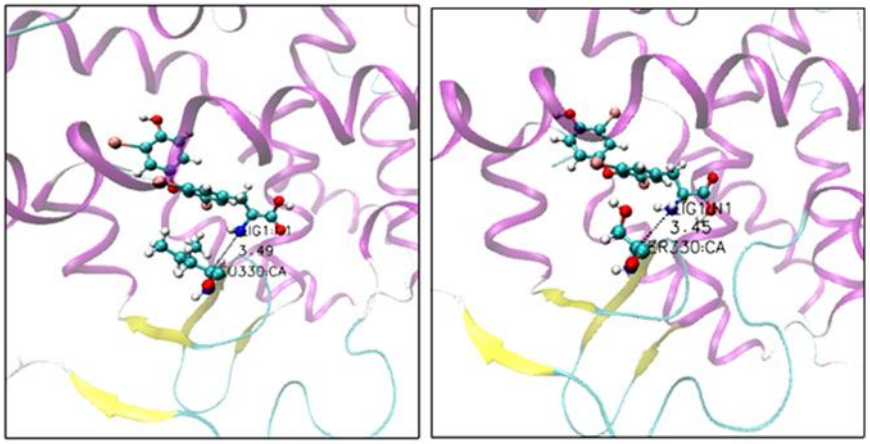


(a) (b)

**Figure 4.** Positions of (a) L330 in THRT3-WT and (b) L330S in THRT3-MT after their 20 ns equilibrations.

Radial distribution function (RDF) or pair auto-correlation function (g(r)) in a system of particles measures probability of finding a particle at r distance away from the reference particle [33]. The distribution function g(r) between the iodine atom I1 (T3) and the oxygen atom OG (L330S) in THRT3-MT is shifted left from that in its wild type THRT3-WT within the range of 3.0–5.5 Å. In this way, the RDF between I3 (T3) and CG2 (I431V) in THRT3-MT has smaller height within the flat range of 4.5–8.5 Å than that in its wild type THRT3-WT as shown in the Figure 6. In other words,

the number density of the mutant residue is less than that of the native wild type residue in order to respond for T3-hormone and TREs.

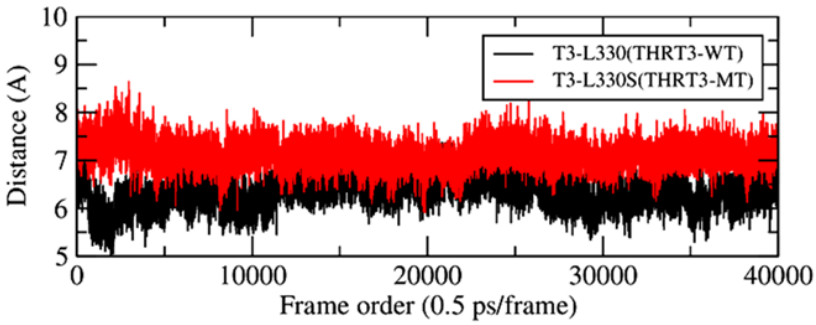


**Figure 5.** Fluctuating distances between T3 and L330/L330S during equilibrations of THRT3-WT/ THRT3-MT systems.

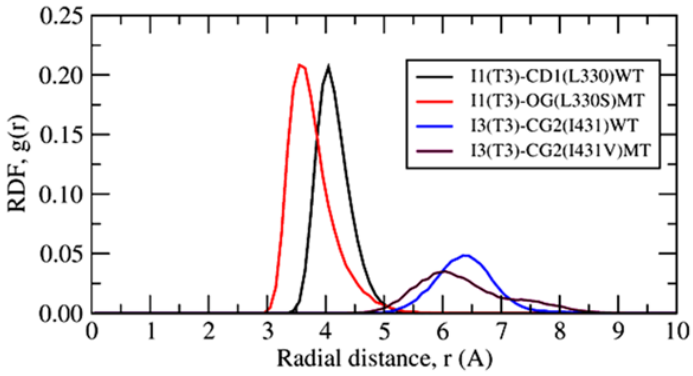


**Figure 6.** RDFs of some atoms in wild type and mutated residues (L330S and I431V) from I1 or I3 of T3-hormone during 20 ns equilibrations of THRT3-WT and THRT3-MT systems.

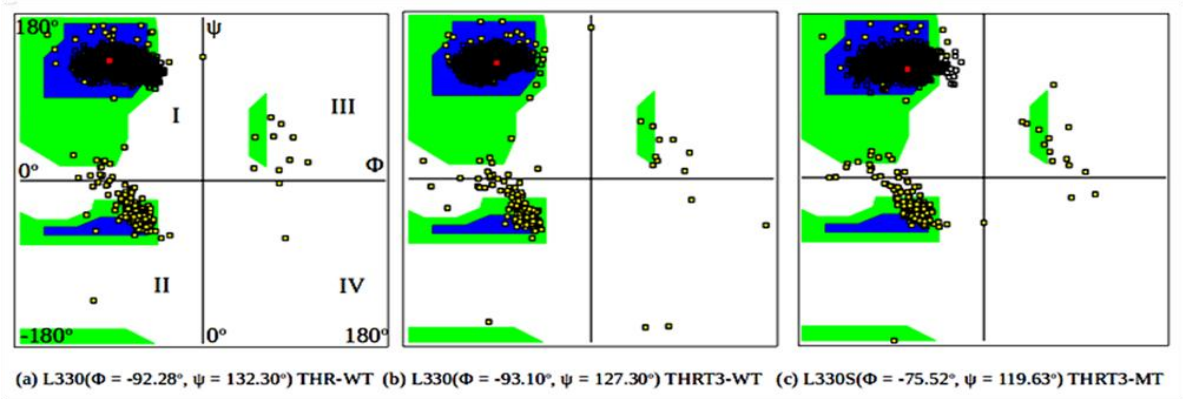


**Figure 7.** Ramachandran plots shown with dark line spots, i.e. the varying (φ, ψ) values of (a) L330 in THR-WT, (b) L330 in THRT3-WT, and (c) L330S in THRT3-MT during the last 1ns of their equilibration runs. The red spot with the given (φ, ψ) values is related to the last time-step of simulations.

Ramachandran plots of dihedral angles (φ, ψ) for THR-WT, THRT3-WT and L330S mutant THRT3-MT in the last frame of 20 ns equilibrations are shown in Figure 6. The residues of parallel, anti-parallel and right twisted β-sheets lie in the blue region of I; right handed α-helix lie in the blue region of II, and left handed α-helix lie in the green region of III quadrant [34,35]. The amino acid GLY existing without side chain has no steric hindrance so that it is allowed in the white region of IV quadrant. All the amino acids except GLY are sterically disallowed in the white regions. The most allowed regions for α-helices and β-sheets are the blue regions. The green region is allowed for those amino acids which consist of atoms with short van der Waals radii. By comparing the plots of Figure 7, we observe that the (φ, ψ) values of L330S in THRT3-MT scatter more towards the disallowed regions than that of L330 in THRT3-WT. This analysis verifies that the larger steric hindrances occur in the unliganded and mutated THR-β resulting gene repressions and the related thyroid disorders. The clinical evaluations show that THRT3-WT, THR-WT and THRT3-MT are associated with normal thyroid functions, overt hypothyroidism and RTH, respectively.

The SASA of 330-codon in THRT3-WT is observed to be different in the extension radius of 1.4 Å than that in THRT3-WT and THRT3-MT (Figure 8). As depicted in the Table 2, The SASA of the 330-codons in THR-WT, THRT3-WT and THRT3-MT are 290.96 ± 3.51, 285.62 ± 3.74 and 223.89 ± 3.41 $Å^2$, respectively which lie in the range of 0-300 $Å^2$ reported by Ausaf Ali, et al., 2014 [10]. The lower SASA indicates the higher thermodynamic stability of the protein. The SASA of T3-hormone is observed to be zero indicating the hydrophobicity of LBD of THR-β. The mutation on the solvent accessible residue causes the conformational change by partial unfolding of the protein [36]. Such effect is more intensive if the mutation occurs on the surface residue than on the interior of the protein. Since the SASA of L330 has been found to be decreased relative to its wild type, such mutation is confirmed as a buried mutation of the THR-β gene.

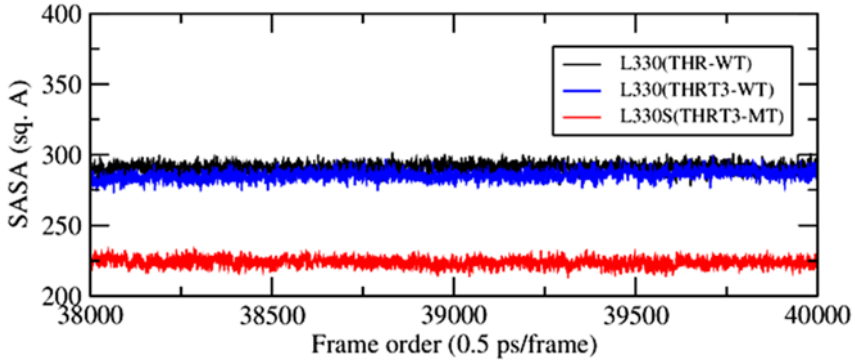


**Figure 8.** SASA of L330 and L330S in the last 1ns of equilibrations of unliganded, liganded and mutated THR-β systems.

The IR spectral densities using total dipole moment of the atoms in the 330-residue are calculated in the frequency range of 0 to 2500 $cm^{-1}$ by adjusting the time interval between frame to frame calculations as 0.01 ps in the last 1 ns of the equilibrating simulations. Such spectral distributions are different for THRT3-WT and THRT3-MT as shown in Figure 9. The maximum IR-intensity of L330 in the wild type receptor is 0.0091 at 1228.56 $cm^{-1}$. Again, the maximum IR-intensity of L330S in the mutated receptor is 0.0081 at 1163.55 $cm^{-1}$. The distribution has larger

number of high intensity peaks for L330 in THRT3-WT than for L330S in THRT3-MT.

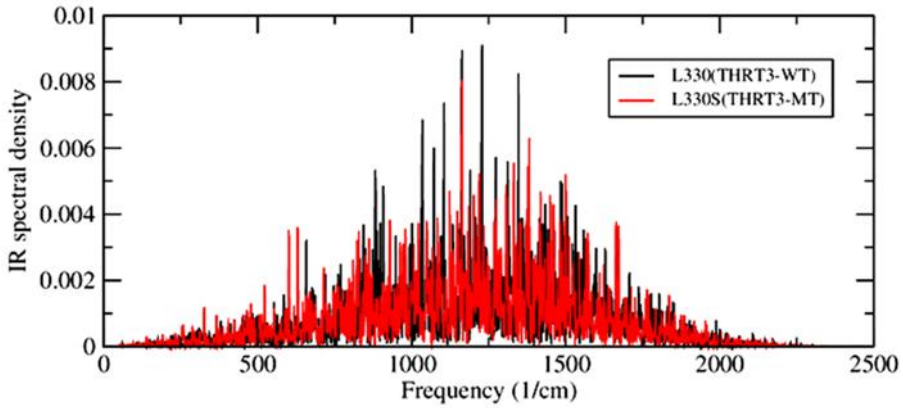


**Figure 9.** IR spectral density of L330 and L330S by adjusting the time interval between frame to frame calculations as 0.01 ps in the last 1 ns of the equilibrating simulations of THRT3-WT and THRT3-MT systems.

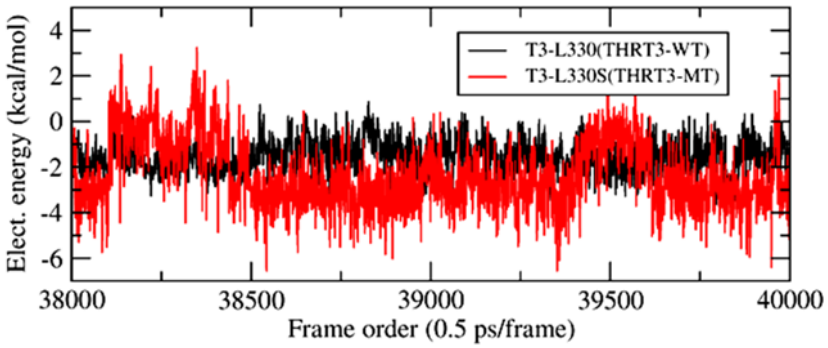


**Figure 10.** Electrostatic interaction energies between L330/L330S and T3 in THRT3-WT and THRT3-MT in the last 1 ns of the equilibrating simulations.

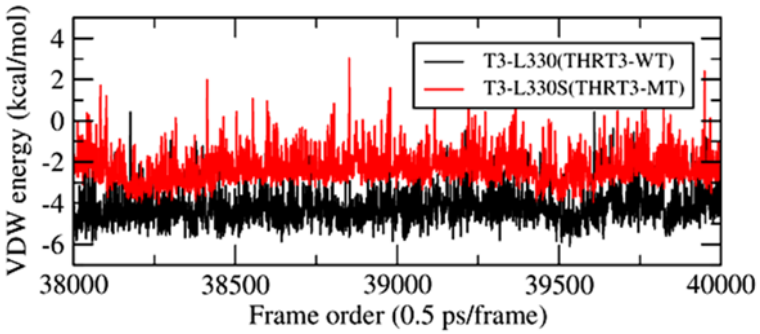


**Figure 11.** van der Waals interaction energies between L330/L330S and T3 in THRT3-WT and THRT3-MT in the last 1 ns of the equilibrating simulations.

Total non-bonding interaction energy is the sum of electrostatic and van der Waals interaction

energies. The changing values of interaction energy between 330-codon and T3-hormone in wild type and L330S mutant THR-β systems are plotted w.r.t. the frame order in the Figures 10 and 11. These are averaged over the time frames from the last 1 ns of the equilibrating simulations. The mean ± SD of electrostatic ($E_{elect}$) and van der Waals ($E_{vdw}$) interaction energies are calculated by using the NAMD-Energy-GUI adjusted with switching and cut-off distances of 10 Å and 12 Å, respectively. As per the interactions between L330 and T3 in THRT3-WT, the values of $E_{elect}$ and $E_{vdw}$ are −1.58 ± 0.72 kcal/mol and −4.22 ± 0.84 kcal/mol whereas for the interactions between L330S and T3 in THRT3-MT, these are −2.37 ± 1.52 kcal/mol and −2.26 ± 0.85 kcal/mol, respectively (Table 2). The Figures 9 and 10 also demonstrate that $E_{elect}$ is more fluctuating with larger negative value whereas $E_{vdw}$ is less fluctuating with smaller negative value when LEU is mutated with SER in 330-codon of the THR-β gene. These factors are also significantly important to explore the insights into the RTH.

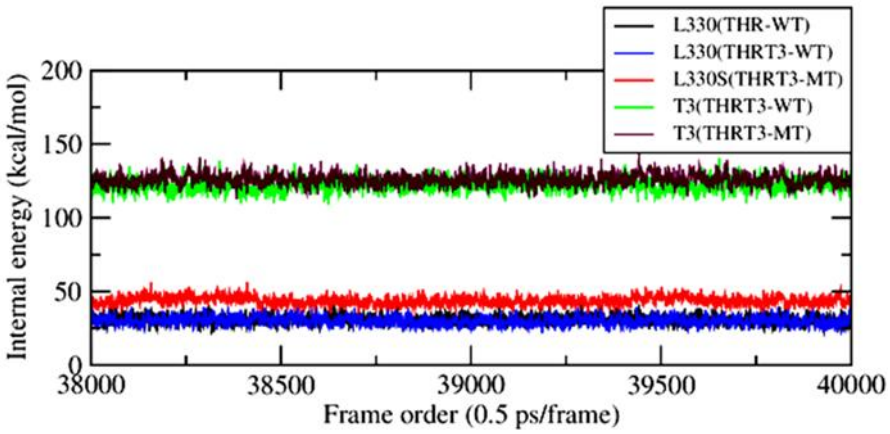


**Figure 12.** Fluctuating internal energies of L330, L330S and T3 in unliganded THR-WT, liganded THRT3-WT and mutated THRT3-MT in the last 1 ns of their equilibrations.

**Table 2.** The mean±SD of RMSF (Å), SASA (Å$^2$), internal energy ($U_i$), and electrostatic ($E_{elect}$) and van der Waals ($E_{vdw}$) interaction energies (kcal/mol) with T3 related to L330 residue in unliganded THR-WT, liganded THRT3-WT and mutated THRT3-MT. Here, RMSF is averaged from the 20 ns equilibrations and the others are averaged from the last 1 ns of their equilibrations.

| Molecule | Residue | RMSF | SASA | $U_i$ | $E_{elect}$ | $E_{vdw}$ |
|---|---|---|---|---|---|---|
| THR-WT | L330 | 0.46±0.10 | 290.96±3.51 | 30.93±3.09 | 0 | 0 |
| THRT3-WT | L330 | 0.41±0.07 | 285.62±3.74 | 30.03±3.03 | -1.58±0.72 | -4.22±0.84 |
| THRT3-MT | L330S | 0.15±0.04 | 223.89±3.09 | 43.70±2.25 | -2.37±1.52 | -2.26±0.85 |

Internal energy of the biomolecular system is the sum of bonding and non-bonding potentials. Coulomb energy is the largest and its fluctuation during MD simulations makes the total internal energy fluctuate about its mean value. Using NAMD-Energy-GUI with switching and cut-off distances of 10 Å and 12 Å, the internal energy ($U_i$) of 330-residue, bounded T3-hormone and

protein of THR-WT, THRT3-WT and THRT3-MT are calculated from the last 1ns of their equilibrations and the average values for the corresponding systems are listed in the Table 2. The variations of internal energy w.r.t. the simulation time are plotted in Figure 12. The plots for the individual potential terms show that the major contributor of fluctuations in internal energy is the electrostatic energy of the related system. The value of $U_i$ is 30.03 ± 3.03 kcal/mol for L330 in THRT3-WT and 43.70 ± 2.25 kcal/mol for L330S in THRT3-MT, i.e. the internal energy increases when LEU is mutated with SER in the 330-codon of THR-β LBD. In addition to these mutational impacts, thermophysical properties such as temperature echo, heat capacity, thermal diffusivity and thermal conductivity are also important to evaluate hormone-receptor interactions in different THR isoforms [37,38].

## 4. Conclusions

Almost constant values of RMSD (≤ 3 Å) and RG (≈ 19 Å) of wild type as well as mutated THR-β show their conformational stability during MD simulations. The point mutation L330S with largely fluctuating RMSD shows its resistive nature to the T3 binding in and dissociation from THR-β LBD. The (φ, ψ) values in Ramachandran plots of L330 in unliganded THR-WT and L330S in mutated THRT3-MT scatter more towards the disallowed regions than that of L330 in liganded THRT3-WT. This analysis verifies that the larger steric hindrances occur in the unliganded and mutated THR-β as the basis of gene repressions and the related thyroid disorders. The smaller SASA of L330S mutation than its wild type residue indicates that it is stable buried-muation. The SASA of T3 is zero verifying its hydrophobicity in THR-β LBD. Comparing RDFs between the atoms of T3 and mutational residues, the probability of finding the atomic particles within the domain range of 3 to 10 Å is shifted closer in THRT3-MT than in THRT3-WT. The IR spectral distributions in the range of 0-2500 $cm^{-1}$ suggest that the L330-residue in THRT3-WT has larger number of high spectral peaks with greater change in dipole moments than the L330S-residue in THRT3-MT. Related to the 330-codon of THR-β LBD, electrostatic interaction energy is more fluctuating with larger negative value, van der Waals interaction energy is less fluctuating with smaller negative value and total internal energy is less fluctuating with larger positive value when LEU is mutated with SER. These are the strong parameters that explain the nature of point mutations in THR-β gene.

## Acknowledgments

We are thankful to Prof. Dr. Raju Khanal, Central Department of Physics, Tribhuvan University for providing computing facility and to Nepal Academy of Science and Technology for the partial financial support to this research work.

## Conflict of interest

All authors declare no conflicts of interest in this paper.

## References


1. Forrest D, Hanebuth E, Smeyne RJ, et al. (1996) Recessive resistance to thyroid hormone in mice lacking thyroid hormone receptor beta: evidence for tissue-specific modulation of receptor function. *EMBO J* 15: 3006–3015.
2. Lee JH, Kim EY (2014) Resistance to thyroid hormone due to a novel mutation of thyroid hormone receptor beta gene. *Ann Pediatr Endocrinol Metab* 19: 229.
3. El Shafie K, Ouhtit A, Al Farsi Y, et al. (2014) A rare thyroid hormone receptor beta (thrβ) gene mutation in a 15-year-old girl with thyroid hormone resistance syndrome: a case report. *J Med Case Rep* 8: 12.
4. Safer JD, O'connor MG, Colan SD, et al. (1999) The thyroid hormone receptor-β gene mutation R383H is associated with isolated central resistance to thyroid hormone. *J Clin Endocrinol Metab* 84: 3099–3109.
5. Machado DS, Sabet A, Santiago LA, et al. (2009) A thyroid hormone receptor mutation that dissociates thyroid hormone regulation of gene expression in vivo. *Proc Natl Acad Sci* 106: 9441–9446.
6. Pohlenz J, Wildhardt G, Zabel B, et al. (1997) Resistance to thyroid hormone in a family caused by a new point mutation L330S in the thyroid receptor (TR) beta gene. *Thyroid* 7: 39–41.
7. Ditudompo S, Ongphiphadhanakul B, Chanprasertyotin S, et al. (1999) A de novo L330S point mutation in thyroid hormone receptor beta gene in a Thai female with resistance to thyroid hormone. *Endocrine J* 46: 825–829.
8. Khan FI, Aamir M, Wei DQ, et al. (2017) Molecular mechanism of Ras-related protein Rab-5A and effect of mutations in the catalytically active phosphate-binding loop. *J Biomol Struct Dyn* 35: 105–118.
9. Rajendran V, Purohit R, Sethumadhavan R (2012) In silico investigation of molecular mechanism of laminopathy caused by a point mutation (R482W) in lamin A/C protein. *Amino Acids* 43: 603–615.
10. Ausaf Ali S, Hassan I, Islam A, et al. (2014) A review of methods available to estimate solvent-accessible surface areas of soluble proteins in the folded and unfolded states. *Curr Protein Pept Sci* 15: 456–476.
11. Gromih MM, Oobatake M, Kono H, et al. (1999) Relationship between amino acid properties and protein stability: buried mutations. *J Protein Chem* 18: 565–578.
12. Gromiha MM, Oobatake M, Kono H, et al. (2002) Importance of mutant position in Ramachandran plot for predicting protein stability of surface mutations. *Biopolymers: Ori Res Biomol* 64: 210–220.
13. Zou J, Song B, Simmerling C, et al. (2016) Experimental and computational analysis of protein stabilization by Gly-to-d-Ala substitution: A convolution of native state and unfolded state effects. *J Am Chem Soc* 138: 15682–15689.
14. Nascimento AS, Dias SMG, Nunes FM, et al. (2006) Structural rearrangements in the thyroid hormone receptor hinge domain and their putative role in the receptor function. *J Mol Biol* 360: 586–598.

15. MacKerell AD, Feig M, Brooks CL (2004) Extending the treatment of backbone energetics in protein force fields: Limitations of gas-phase quantum mechanics in reproducing protein conformational distributions in molecular dynamics simulations. *J Comput Chem* 25: 1400–1415.
16. MacKerell AD, Bashford D, Bellott M, et al. (1998) All-atom empirical potential for molecular modeling and dynamics studies of proteins. *J Phys Chem B* 102: 3586–3616.
17. Jorgensen WL, Chandrasekhar J, Madura JD, et al. (1983) Comparison of simple potential functions for simulating liquid water. *J Chem Phys* 79: 926–935.
18. Zoete V, Cuendet MA, Grosdidier A, et al. (2011) SwissParam: a fast force field generation tool for small organic molecules. *J Comput Chem* 32: 2359–2368.
19. Phillips JC, Braun R, Wang W, et al. (2005) Scalable molecular dynamics with NAMD. *J Comput Chem* 26: 1781–1802.
20. Humphrey W, Dalke A, Schulten K (1996) VMD—visual molecular dynamics. *J Mol Graphics* 14: 33–38.
21. Feller SE, Zhang Y, Pastor RW, et al. (1995) Constant pressure molecular dynamics simulation: the Langevin piston method. *J Chem Phys* 103: 4613–4621.
22. Bussi G, Donadio D, Parrinello M (2007) Canonical sampling through velocity rescaling. *J Chem Phys* 126: 014101–014107.
23. Hardy DJ, Wu Z, Phillips JC, et al. (2015) Multilevel summation method for electrostatic force evaluation. *J Chem theory Comput* 11: 766–779.
24. Verlet L (1967) Computer "experiments" on classical fluids. I. Thermodynamical properties of Lennard-Jones molecules. *Phys Rev* 159: 98–103.
25. Walser R, Hünenberger PH, van Gunsteren WF (2002) Molecular dynamics simulations of a double unit cell in a protein crystal: volume relaxation at constant pressure and correlation of motions between the two unit cells. *Proteins Struct Funct Bioinf* 48*:* 327–340.
26. Riniker S, Eichenberger AP, van Gunsteren WF (2012) Solvating atomic level fine-grained proteins in supra-molecular level coarse-grained water for molecular dynamics simulations. *Eur Biophys J* 41: 647–661.
27. Hu CY, Lynch GC, Kokubo H, et al. (2010) Trimethylamine N-oxide influence on the backbone of proteins: an oligoglycine model. *Proteins Struct Funct Bioinf* 78: 695–704.
28. Lee B, Richards FM (1971) The interpretation of protein structures: estimation of static accessibility. *J Mol Biol* 55: 379–400.
29. Levine BG, Stone JE, Kohlmeyer, A (2011) Fast analysis of molecular dynamics trajectories with graphics processing units-radial distribution function histogramming. *J Comput Phys* 230: 3556–3569.
30. Gohlke H, Hendlich M, Klebe G (2000) Knowledge-based scoring function to predict protein-ligand interactions. *J Mol Biol* 295: 337–356.
31. Małolepsza E, Straub JE (2014) Empirical maps for the calculation of amide I vibrational spectra of proteins from classical molecular dynamics simulations. *J Phys Chem B* 118: 7848–7855.
32. Rekik N, Suleiman J, Blaise P, et al. (2018) Equivalence between the classical and quantum IR spectral density approaches of weak H-bonds in the absence of damping. *J Phys Chem A* 122: 2108–2115.

33. Fernández M, Caballero J, Fernández L, et al. (2007) Protein radial distribution function (P-RDF) and Bayesian-regularized genetic neural networks for modeling protein conformational stability: chymotrypsin inhibitor 2 mutants. *J Mol Graph Model* 26: 748–759.
34. Hollingsworth SA, Karplus PA (2010) A fresh look at the Ramachandran plot and the occurrence of standard structures in proteins. *Biomol Concepts* 1: 271–283.
35. Ho BK, Brasseur R (2005) The Ramachandran plots of glycine and pre-proline. *BMC Struct Biol* 5: 14.
36. Gilis D, Rooman M (1996) Stability changes upon mutation of solvent accessible residues in proteins evaluated by database-derived potentials. *J Mol Biol* 257: 1112–1126.
37. Lamichhane TR, Lamichhane HP (2018) Heat conduction by thyroid hormone receptors. *AIMS Biophysics* 5: 245–256.
38. Lamichhane TR, Paudel S, Yadav BK, et al. (2019) Echo dephasing and heat capacity from constrained and unconstrained dynamics of triiodothyronine nuclear receptor protein. *J Biol Phys* 45: 107–125.


AIMS Press

© 2020 the Author(s), licensee AIMS Press. This is an open access article distributed under the terms of the Creative Commons Attribution License (http://creativecommons.org/licenses/by/4.0)

VOLUME 17 January 2020 eISSN : 2382-5340 ISSN : 2091 - 0762


# Journal of Physical Sciences

# BIBECHANA

**Editor-in-Chief**

**Devendra Adhikari**

Professor, Physics

MMAMC, T.U.

Published by

Department of Physics

Mahendra Morang Adrash Multiple Campus

T.U., Biratnagar

www.nepjol.info/index.php/BIBECHANA

**BIBECHANA**
ISSN 2091-0762 (Print), 2382-5340 (Online)
Journal homepage: http://nepjol.info/index.php/BIBECHANA
**Publisher: Department of Physics, Mahendra Morang A.M. Campus, TU, Biratnagar, Nepal**

# Constant velocity pulling and unfolding of thyroid hormone receptor by steered molecular dynamics

**Tika Ram Lamichhane, Hari Prasad Lamichhane***
Central Department of Physics, Tribhuvan University, Kirtipur, Kathmandu, Nepal
*Email: tikaramlamichh@gmail.com

*Article Information:*
Received: July 06, 2019
Accepted: October 7, 2019

*Keywords*:
Steered molecular dynamics
Thyroid hormone receptor
Triiodothyronine
Ligand binding domain; Protein unfolding

***ABSTRACT***

Unfolding pathways of T3 liganded thyroid hormone receptor (THRT3) can be studied by using the protocols of steered molecular dynamics (SMD). Theory of constant velocity pulling has been implemented to the structure of THRT3 in a neutral water-ion solution equilibrated up to 20 ns. The globular form of THRT3 is completely unfolded extending N-C termini from 38 Å to 876 Å at a constant speed of 0.1 Å/ps by means of 8.5 ns long SMD simulations. The peak force measured in the intermediate conformations is related to a burst of backbone H-bonds among α-helices and β-hairpins. With decrease in H-bonds, electrostatic energy increases by losing gradually the secondary structure and separating α and β-strands in solution. The force at the end ($t > 8.5$ ns) increases steeply with the large increase in bond-angle and bond-length potentials when the system becomes completely unfolded. The hydrophobic ligand binding domain (LBD) of THR-β with load bearing H-bonds protects T3 from water attack. Even after complete unfolding of THR-β LBD, the position of T3 is not deviated more than 2.5 Å and a large number of water molecules remain in the surrounding of this domain area. This is a strong evidence for the mechanochemical stability of a receptor protein's LBD towards hormone activated gene expressions followed by ligand binding and dissociation.

DOI: https://doi.org/10.3126/bibechana.v17i0.25870
This work is licensed under the Creative Commons CC BY-NC License. https://creativecommons.org/licenses/by-nc/4.0/

## 1. Introduction

Steered molecular dynamics (SMD) is used to unfold the proteins and to study their elastic properties visualizing the different unfolding pathways [1]. The biophysical phenomena behind ligand binding, dissociation and conformational changes of thyroid hormone receptors (THR) are important in triiodothyronine (T3) stimulated gene expressions [2]. The physical properties such as echo dephasing, heat capacity, thermal diffusivity and thermal conductivity of liganded and/or unliganded THR-subtypes in folding states are previously studied [3, 4] by using MD simulations.

A point mutation in THR-β gene causes resistance to thyroid hormones. The mutational impacts are observed distinctly on the protein-hormone systems by analyzing conformations and interaction energies through molecular dynamics approach [5]. SMD is a technique to know the structure-function relationships of the protein-hormone complex through unbinding of hormone or unfolding of protein under the application of time-dependent external forces. The elastic properties of the biomolecular systems subjected to deformations by SMD are in close agreement with the experimental results obtained from atomic force microscopy (AFM) and optical tweezers [6-8].

The mechanical stability of thyroid hormone like heavy ligand receptors is governed by protein's secondary structure and pulling geometry [9]. Thyroid hormone dissociation or unfolding of THR strands proceeds a frictional path with constant velocity along x-direction defined by Langevin's equation [1]

$$\mu\dot{x} = -\frac{dU}{dx} + F(x,t) + \sigma f(t) \quad (1)$$

where μ is time dependent frictional coefficient having dimension of $[MT^{-1}]$, F(x, t) is deforming force, $U(x)$ is potential governing ligand dissociation or protein unfolding pathways and $f(t)$ is the stochastic or fluctuating force term having coupling coefficient $\sigma$. In SMD simulation, the SMD atom is attached to a dummy atom through a virtual spring. In one dimensional pulling, the dummy atom moves with constant velocity ($\vec{v} = d\vec{x}/dt$) so that the SMD atom experiences the force vector $\vec{F}(x,t) = k(\vec{v}t - \Delta\vec{x})$ depending on the linear distance between these atoms [10]. So, the external potential energy [11] is given by

$$U(x,t) = \frac{1}{2}k[(\vec{v}t - \Delta\vec{x}).\vec{n}]^2 \quad (2)$$

where $k$ is spring constant that specifies the stiffness of the applied harmonic restraining force, $\Delta\vec{x}(t) = \vec{x}(t) - \vec{x}_0$ is tagged group displacement with $\vec{x}(t)$ and $\vec{x}_0$ being actual and initial positions of the SMD atom and $\vec{n}$ is the direction of pulling.

## 2. Methodology

The initial structure of T3-liganded THR-β isoform of nuclear receptor super family was taken from the protein data bank code 3GWS [12]. The THR-β ligand binding domain (LBD) complex has the chain length of α-helices and β-forms with 259 amino acids and 3895 atoms. In the folding state or the globular form, end to end distance of THR-β LBD is 38 Å. The THR-β LBD actively binds T3 hormones having 35 atoms including 3 iodine atoms. The simulation packages such as protein structure file (psf) generation and solvation with water (TIP3P model) and ions providing cellular environment were prepared and structural and graphical analysis were performed by using visual molecular dynamics (VMD-1.9.3) [13]. In accordance with nanoscale molecular dynamics (NAMD-2.12) protocols [14], the topologies and parameters required for MD simulations of the THR-β LBD complex were obtained from CHARMM force fields for proteins [15, 16]. The T3-hormone was parameterized with the help of Zoete's force field generation tool [17].

The T3-liganded THR-β LBD (THRT3) was fully solvated into a water droplet of radius 37.5 Å consisting of 17245 water molecules neutralized with 26 $Na^+$ and 16 $Cl^-$ ions in the concentrations of 0.15 mol/L. The system's energy was minimized up to 3000 conjugate gradient steps and it was equilibrated up to 20 ns with NAMD protocols. Velocity Verlet algorithm [18] was used for the equilibration simulations with the integrator parameter of 2 fs/step, Langevin thermostat at 310 K and barostat at 1-atm and damping coefficient of 1 $ps^{-1}$. For the Lenard-Jones interactions, a 12 Å cut-off with smooth switching function starting at 10 Å was applied with 1-4 scaling 1.0. The final coordinates of the solvated THRT3 were extracted from the equilibrated droplet in order to perform SMD simulations.

The SMD simulation was conducted setting the $C_\alpha$ atom of the last residue-460 as the SMD atom and the $C_\alpha$ atom of the first residue-202 as the fixed

atom. The virtual spring between the SMD atom and the dummy atom was 7 kcal/mol/ $Å^2$. The one dimensional pulling was performed at constant velocity of 0.1 Å/ps in the direction along a vector connecting the fixed atom and the SMD atom. The THRT3 complex became completely unfolded at the simulation time of about 8.5 ns and the SMD was conducted up to 10 ns. The intermediate conformational states of the THRT3 structures were visualized and the images were generated by using the VMD software. The related physical parameters such as radius of gyration (RG), root mean square deviation (RMSD), extension or end-to-end distance (x), forces and energies were noted down and the graphical analysis was performed with the plotting program XMGRACE. The SMD simulation was repeated three times to check the accuracy of the obtained results.

## 3. Results and Discussion

In the folding state or completely stable globular form, N-C termini or end to end length of the THRT3 system is 38 Å. The receptor protein is unfolded smoothly with simulation time by breaking H-bonds among α-helices or β-sheets during the constant velocity (0.1 Å/ps) pulling of the SMD atom. The changing extension and RG of THRT3 over the course of simulation are shown in Figures 1-a & 1-b, respectively. The system becomes completely unfolded after the simulation time of 8.5 ns. At t = 8.5 ns, the end-to-end length is 876 Å and RG of about 258 Å.

The THRT3 conformations responsible for the peak force are B, C and D as indicated in force *vs* extension graph (Figure 2). The structure A is the initial folding state in equilibrated form whereas E is the final unfolding state extended to 1023 Å. The force at the end (t > 8.5 ns) of the simulation increases when THRT3 becomes completely unfolded due to stretching of the protein single strand. The structures (A, B, C, D and E) formed by sequential unzipping of H-bonds are shown in Figure 3 and the related physical parameters such as time, length, RG, RMSD, number of H-bonds (at 3 Å internal distance and 20° angle), force, kinetic energy (KE), potential energy (PE) and electrostatic energy are reported in Table 1. The resistance of H-bonds ruptures simultaneously causing the structural change and rapid extension of THRT3 LBD. Unfolding of native structures needs the maximum pulling force as they represent the bottom of the steep free energy well [19].

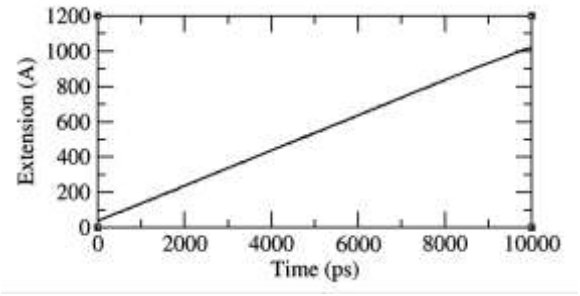


(a)

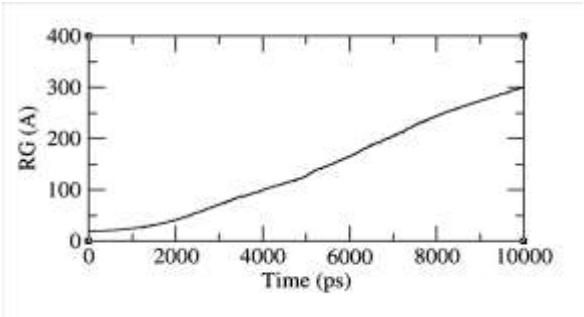


(b)

**Fig. 1**: End-to-end distance or extension and radius of gyration (RG) of THRT3 over the course of SMD simulation.

The T3 binding domain formed by α-helices and β-hairpins has been verified to be the most stable region, i.e. the hormone binds strongly in the LBD of THR-β because this region surrounded by a large mass of water remains almost unchanged (Figure 3-C) even up to 533 Å extension and 5 ns SMD simulation. Even after the T3 binding pocket is completely unfolded and the protein RMSD is raised up to 300 Å (Figure 4-a), the position of T3 does not shift more from its actual position as indicated by its RMSD (< 2.5 Å shown in Figure 4-

b). Abrupt breaking of hydrophobic contacts between helices 8 and 12 is required for the dissociation of T3 hormone from THR-β LBD. The ligand binding and dissociation pathways observed in THR-isoforms by using SMD simulations have been explained in the previous studies [10, 20, 21].

RMSD of T3 gets small step-up jump, i.e. the ligand/hormone becomes slightly unstable in the unfolding states of THRT3 responsible for the peak force generation as shown in the Figure 4-b.

Along with the elongating system, H-bonds decrease in number (Figure 5-a) whereas electrostatic energy increases up to the complete unfolding state of THRT3 (Figure 5-b). At the time of complete unfolding (t ≈ 8.5 ns), H-bonds reduce to 10 and the ranges of KE, PE and electrostatic energy are 13345, -5900 and -69000 kcal/mol, respectively. The actual data are reported in Table 1. After the complete unfolding state (t > 8.5 ns), H-bonds in a small number and electrostatic energy both remain almost constant as shown in Figure 5.

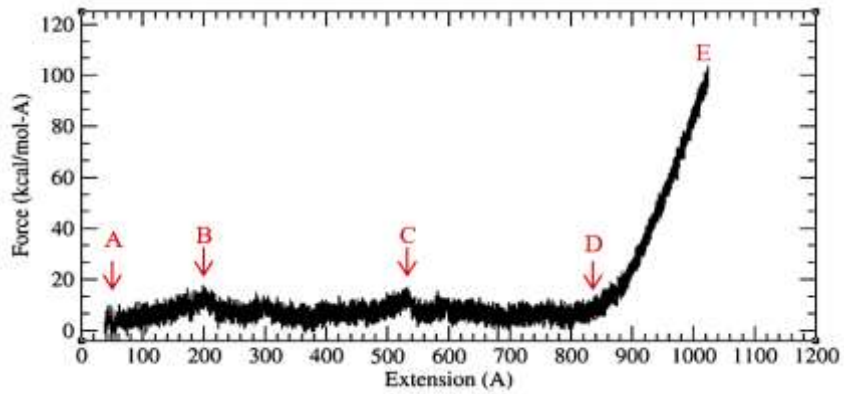


**Fig. 2**: Force *vs* extension plot showing initial folding state (A), intermediate states (B, C) having greater force associated with the breaking of H-bonds among α-helices or β-sheets and completely unfolding states (D, E). The force at the end (t > 8.5 ns) increases when THRT3 becomes completely unfolded.

**Table 1**: Physical parameters at different unfolding states of THRT3 protein responsible for peak force

| Unfolding states | Time (ps) | End-to-end distance (Å) | Force (kcal/mol-Å) | No. of H-bonds | RG (Å) | RMSD (Å) | KE (kcal/mol) | PE (kcal/mol) | Elect. energy (kcal/mol) |
|---|---|---|---|---|---|---|---|---|---|
| A | 0 | 38.00 | 0.00 | 60 | 18.86 | 0.61 | 13809.01 | -65680.75 | -75115.80 |
| B | 1673 | 203.64 | 15.40 | 54 | 34.06 | 23.75 | 13832.59 | -64576.79 | -74093.63 |
| C | 4964 | 532.87 | 17.17 | 31 | 125.17 | 121.28 | 13446.59 | -61668.09 | -71620.80 |
| D | 8404 | 875.90 | 17.10 | 10 | 257.22 | 254.02 | 13343.50 | -58944.43 | -69681.59 |
| E | 10000 | 1023.29 | 98.21 | 9 | 300.66 | 297.56 | 13273.46 | -50967.98 | -69695.32 |

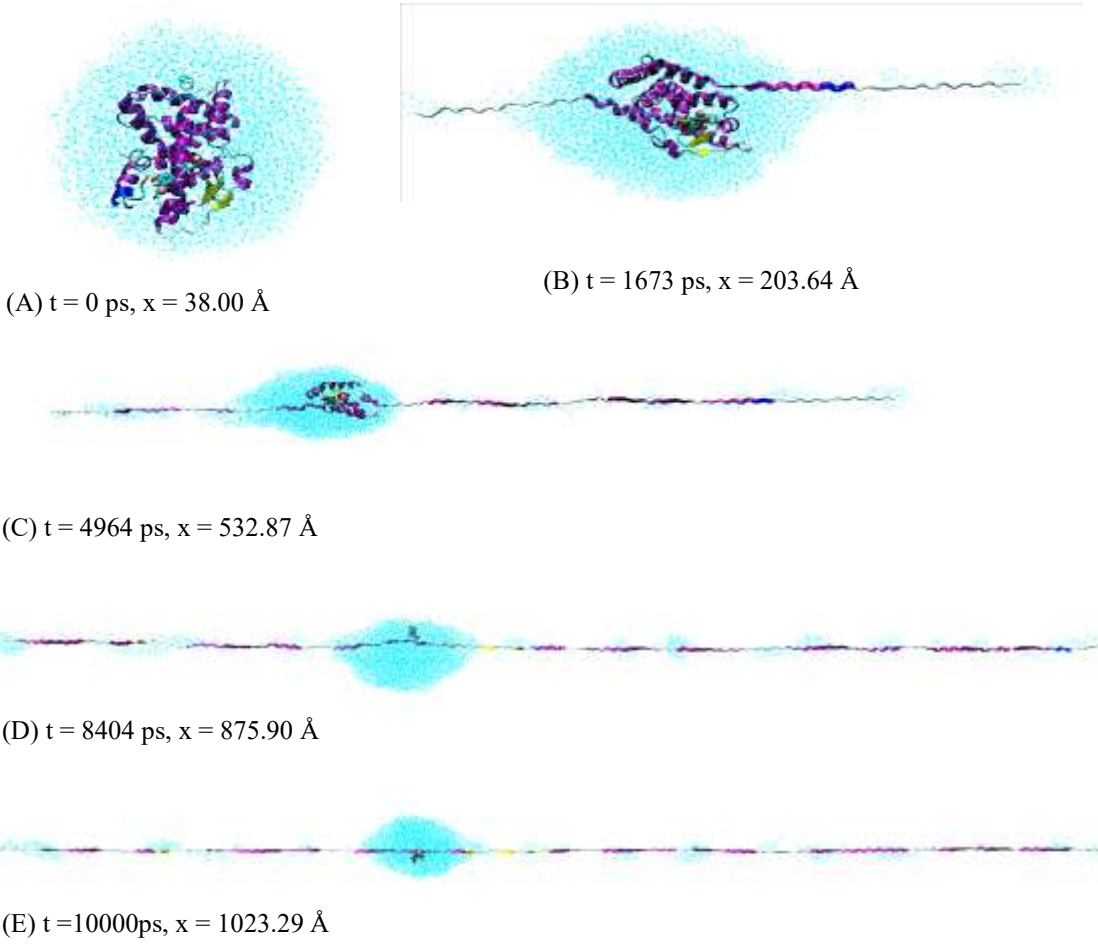

(A) t = 0 ps, x = 38.00 Å

(B) t = 1673 ps, x = 203.64 Å

(C) t = 4964 ps, x = 532.87 Å

(D) t = 8404 ps, x = 875.90 Å

(E) t =10000ps, x = 1023.29 Å

**Fig. 3**: Different unfolding states responsible for peak force provided with the simulation time (t) and end-to-end distance (x) during the constant velocity (0.1 Å/ps) stretching of THRT3.

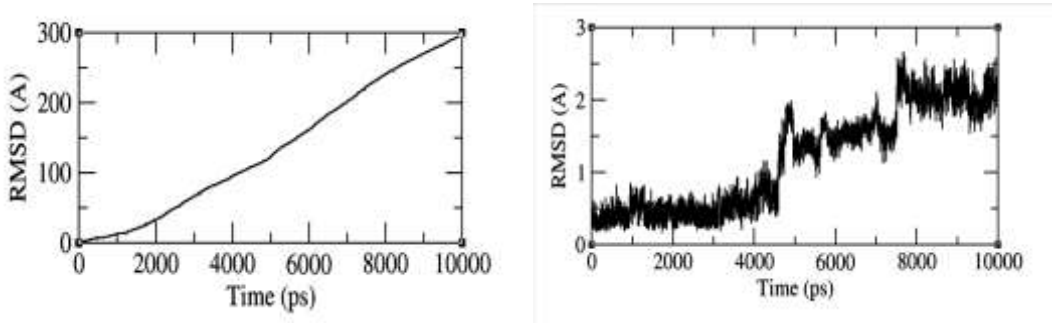


**Fig. 4:** Root mean square deviation (RMSD) of (a) receptor protein and (b) T3-hormone during unfolding of THRT3.

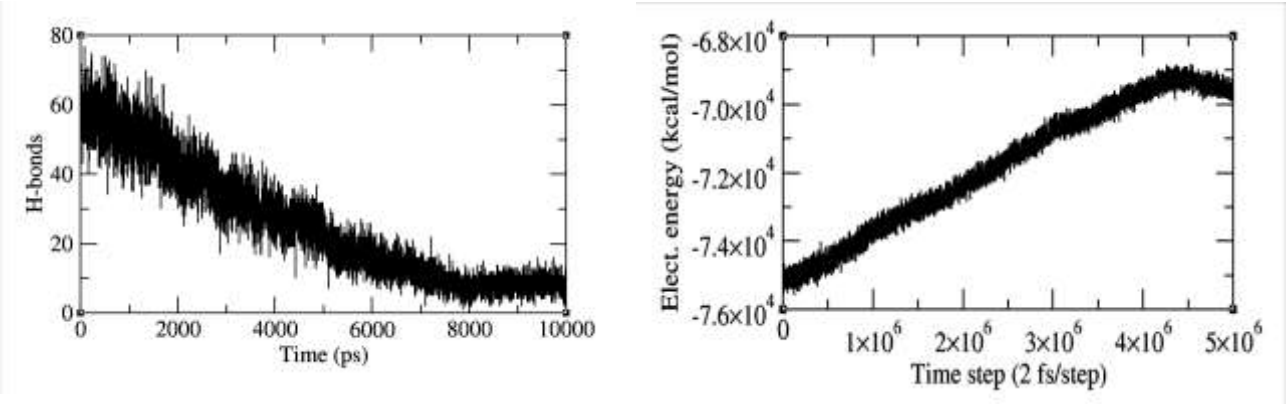


**Fig. 5:** Variation of (a) H-bonds and (b) electrostatic energy over the course of 10 ns SMD simulation at constant velocity (0.1 Å/ps) pulling of THRT3.

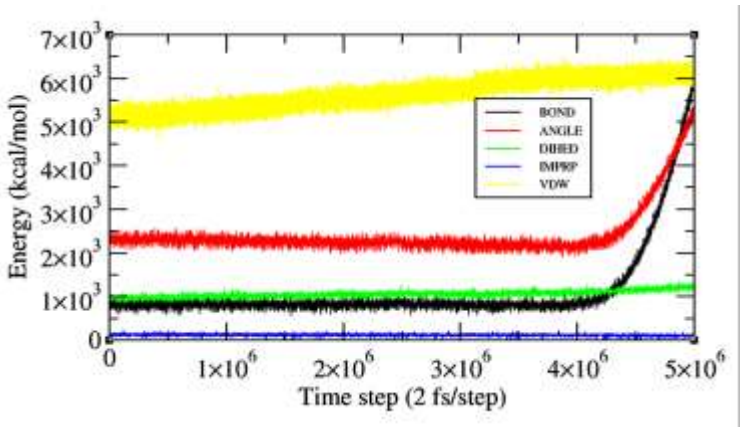


**Fig. 6:** Energy profile diagram during unfolding of THRT3 by SMD at constant velocity (0.1 Å/ps ) pulling.

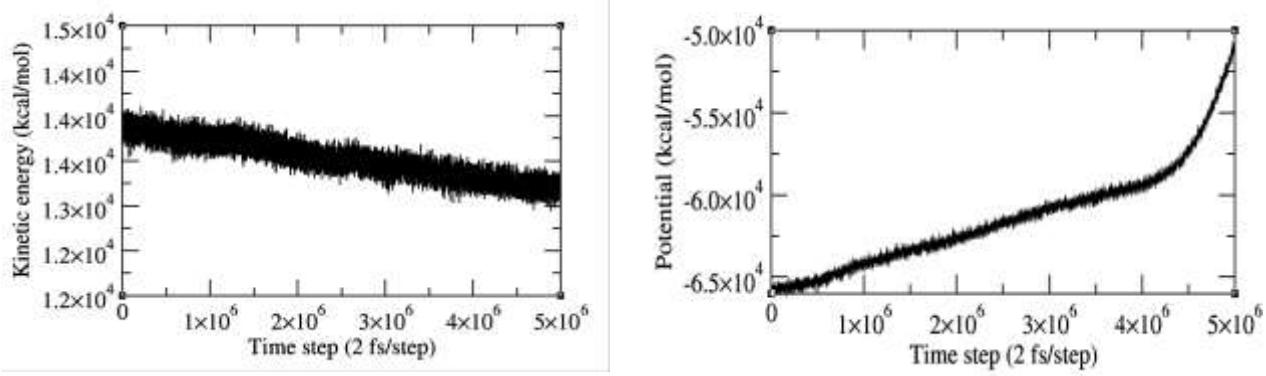


**(a)** **(b)**

**Fig. 7:** Variation of (a) kinetic and (b) internal potential energies over the course of 10 ns SMD simulation at constant velocity (0.1 Å/ps) pulling of energy.

The Linard Jones potential is getting raised linearly with small slope and the energy terms: dihedral and improper remain almost constant throughout the SMD simulation. Bond-angle and bond-length energies are almost constant before 8.5 ns and they rise up steeply after 8.5 ns when THRT3 is completely unfolded as shown in Figure 6.

Figures 7-a & 7-b show that KE decreases slowly and linearly throughout the simulation, and conversely, PE increases slightly up to the state of complete unfolding of THRT3. When the system is completely unfolded (t > 8.5 ns), PE increases steeply. The cause behind the steeply changed PE is the fast increasing force generated after unwinding the molecular system.

The load bearing strands are shielded by water and it interacts with bond-breaking events between such strands [9]. Even if the strand is fully dissociated, water makes H-bonding to the exposed sites as in Figure 3. The hydrophobic LBD of THR-β with load bearing H-bonds is protected from water attack so that T3 is not dragged away from its pocket position even if the system is completely unfolded. In order to employ the reversible work comparable to AFM experiments, very low speed pulling is to be implemented while unwinding the molecular system which is practically difficult due to computational limits. However, higher pulling velocities do not influence the reliability of the SMD results [22]. Continuous breaking of H-bonds up to the complete unfolding of THRT3 (Figure 5-a) and force *vs* extension graph (Figure 2) are comparable to AFM results even at this pulling speed of 0.1 Å/ps. The SMD technique of crack propagation allows the identification of intermediate conformations of THRT3 responsible for the gene transcriptional activities.

## 4. Conclusion

Triiodothyronine nuclear receptor (THRT3) is completely unfolded resulting end-to-end length of 876 Å by 8.5 ns long SMD simulations performed at constant velocity of 0.1 Å/ps. The peak force associated with the intermediate conformations is due to breaking of H-bonds among α-helices and β-hairpins. Though RMSD of T3 does not exceed 2.5 Å throughout the simulation, T3 is deviated more from its mean position in the conformational states of peak force generation. Hydrophobic LBD, i.e. T3 binding pocket of the receptor that gets surrounded by water is unfolded only in the last of the simulation. It is an evidence for the stability of THR-β LBD towards ligand (T3) binding and dissociation. Even after complete stretching of the protein strand LBD, the position of T3 remains almost constant surrounded by water molecules. Along with decrease in H-bonds, electrostatic energy increases gently during unfolding. There are linear changes with slightly decreased kinetic energy and slightly increased van der Waals energy at this constant velocity pulling. However, force or net potential of the system increases rapidly at the end (t > 8.5 ns) of the simulation. Dihedral and improper energies remain almost unchanged throughout the SMD simulations, but bond-angle and bond-length energies increase steeply after complete unfolding (t > 8.5 ns) of the system. Thus, one dimensional mechanical pulling at constant velocity is important technique to better understand the unfolding pathways of THRT3 like nuclear receptors.

## Acknowledgements

We would like to acknowledge the computing resources provided by Prof. Dr. Raju khanal at his Plasma Lab, Central Department of Physics, Tribhuvan University, Kathmandu, Nepal. The partial financial support for this research has been provided by Nepal Academy of Science and Technology as the PhD fellowship to the first author.

## References

[1] S. Izrailev, S. Stepaniants, B. Isralewitz, D. Kosztin, H. Lu, F. Molnar, W. Wriggers, K. Schulten, Steered molecular dynamics, Computational molecular dynamics: challenges, methods, ideas, (1999) 39-65, Springer, Berlin, Heidelberg.

[2] T. M. Ortiga-Carvalho, A. R. Sidhaye, F. E. Wondisford, Thyroid hormone receptors and resistance to thyroid hormone disorders, Nature Rev. Endocrinol 10 (2014) 582. doi.org/10.1038/nrendo.2014.143

[3] T. R. Lamichhane, S. Paudel, B. K. Yadav, H. P. Lamichhane, Echo dephasing and heat capacity

from constrained and unconstrained dynamics of triiodothyronine nuclear receptor protein, J. Biol. Phys. 45(2019) 107-135. doi.org/10.1007/s10867-018-9518-3

[4] T. R. Lamichhane, H. P. Lamichhane, Heat conduction by thyroid hormone receptors, AIMS Biophys. 5(2018) 245-256. doi.org/10.3934/biophy.2018.4.245

[5] T. R. Lamichhane, S. Paudel, B. K. Yadav, H. P. Lamichhane, Molecular dynamics approach to the I431V mutational impact on thyroid hormone receptor-beta, BIBECHANA, 16 (2019) 79-91. doi.org/10.3126/bibechana.v16i0.21109

[6] J. J. Booth, D. V. Shalashilin, Fully atomistic simulations of protein unfolding in low speed atomic force microscope and force clamp experiments with the help of boxed molecular dynamics, J. Phys. Chem. B 120 (2016) 700-708. doi.org/10.1021/acs.jpcb.5b11519

[7] Z. Mártonfalvi, P. Bianco, K. Naftz, G. G. Ferenczy, M. Kellermayer, Force generation by titin folding, Protein Sci 26 (2017) 1380-1390. https://doi.org/10.1002/pro.3117

[8] J. Schönfelder, D. De Sancho, R. Perez-Jimenez, The power of force: insights into the protein folding process using single-molecule force spectroscopy, J. Mol. Biol. 428 (2016) 4245-4257. doi.org/10.1016/j.jmb.2016.09.006

[9] D. L. Guzmán, A. Randall, P. Baldi, P., Z. Guan, Computational and single-molecule force studies of a macro domain protein reveal a key molecular determinant for mechanical stability. Proc. Natl. Acad. Sci. U. S. A. 107(2010) 1989-1994. doi.org/10.1073/pnas.0905796107

[10] L. Martínez, I. Polikarpov, M. S. Skaf, Only subtle protein conformational adaptations are required for ligand binding to thyroid hormone receptors: simulations using a novel multipoint steered molecular dynamics approach, J. Phys. Chem. B 112(2008) 10741-10751. doi.org/10.1021/jp803403c

[11] J. R. Gullingsrud, R. Braun, K. Schulten, Reconstructing potentials of mean force through time series analysis of steered molecular dynamics simulations, J. Comp. Phys. 151(1999) 190-211. doi.org/10.1006/jcph.1999.6218

[12] A.S. Nascimento, S. M. G. Dias, F. M. Nunes, R. Aparício, A. L. Ambrosio, Bleicher, L., A. C. M. Figueira, M. A. M. Santos, M. de Oliveira Neto, H. Fischer, M. Togashi, Structural rearrangements in the thyroid hormone receptor hinge domain and their putative role in the receptor function, J. Mol. Biol. 360 (2006) 586-598. doi.org/10.1016/j.jmb.2006.05.008

[13] W. Humphrey, A. Dalke, K. Schulten, VMD—Visual Molecular Dynamics, J. Mol. Graphics 14 (1996) 33–38. doi.org/10.1016/0263-7855(96)00018-5

[14] W. Humphrey, A. Dalke, K. Schulten, VMD—Visual Molecular Dynamics, J. Mol. Graphics 14 (1996) 33–38. doi.org/10.1016/0263-7855(96)00018-5

[15] A. D. MacKerell, M. Feig, C. L. Brooks, Extending the treatment of backbone energetics in protein force fields: Limitations of gas-phase quantum mechanics in reproducing protein conformational distributions in molecular dynamics simulations, J. Comp. Chem. 25(2004) 1400-1415. doi.org/10.1002/jcc.20065

[16] A. D. MacKerell, D. Bashford, M. Bellott, R. L. Dunbrack, J. D. Evanseck, M. J. Field, S. Fischer, J. Gao, H. Guo, S. Ha, D. Joseph-McCarthy, All-atom empirical potential for molecular modeling and dynamics studies of proteins, J. Phys. Chem. B 102 (1998) 3586–3616. doi.org/10.1021/jp973084f

[17] V. Zoete, M. A. Cuendet, A. Grosdidier, O. Michielin, SwissParam: a fast force field generation tool for small organic molecules, J. Comp. Chem. 32 (2011) 2359-2368. doi.org/ 10.1002/jcc.21816

[18] L. Verlet, Computer "experiments" on classical fluids. I. Thermodynamical properties of Lennard-Jones molecules, Phy. Rev. 159 (1967) 98. doi.org/10.1103/PhysRev.159.98

[19] J. J. Booth, D. V. Shalashilin, Fully atomistic simulations of protein unfolding in low speed atomic force microscope and force clamp experiments with the help of boxed molecular dynamics, J. Phys. Chem. B 120(2016) 700-708. doi.org/10.1021/acs.jpcb.5b11519

[20] D. Kosztin, S. Izrailev, K. Schulten, Unbinding of retinoic acid from its receptor studied by steered molecular dynamics, Biophys. J. 76(1999) 188-197. doi.org/10.1016/S0006-3495(99)77188-2

[21] L. Martínez, P. Webb, I. Polikarpov, M. S. Skaf, Molecular dynamics simulations of ligand dissociation from thyroid hormone receptors: evidence of the likeliest escape pathway and its implications for the design of novel ligands, J. Med. Chem. 49(2006) 23-26. doi.org/10.1021/jm050805n

[22] J. L. Zhang, Q. C. Zheng, H. X. Zhang, Unbinding of glucose from human pulmonary surfactant protein D studied by steered molecular dynamics simulations, Chem. Phys. Lett. 484(2010) 338-343. doi.org/10.1016/j.cplett.2009.12.022

Journal of Biological Physics
https://doi.org/10.1007/s10867-018-9518-3

ORIGINAL PAPER

# Echo dephasing and heat capacity from constrained and unconstrained dynamics of triiodothyronine nuclear receptor protein

Tika Ram Lamichhane[1] · Sharma Paudel[2] · Binod Kumar Yadav[2] · Hari Prasad Lamichhane[1]

Received: 19 April 2018 / Accepted: 20 December 2018/Published online: 27 February 2019
© Springer Nature B.V. 2019

## Abstract

The objective of this study is to observe the echo feature curves, vibrational dephasing, and heat capacity of a protein–hormone system taking thyroid hormone receptor-beta (THR-β) as an example. Constrained and unconstrained molecular dynamics simulations are performed by implementing the theory of velocity reassignments to probe the phase coherent state in terms of echo pulses. The constrained vibrations are incorporated by adjusting rigid bonds to all hydrogen atoms with an integrator parameter of 2 fs/step in order to reduce the degrees of freedom whereas 1 fs/step is used in the free vibrations of the atomic cluster. The nature of temperature auto-correlation functions changes so that echo feature curves also show a distinct nature in the cases of constrained and unconstrained vibrations. There is a large variation in kinetic temperature and internal potential energy in the echo time zone. The temperature rate of change of internal potential energy is the main contributor to the heat capacity of the native state protein–hormone system. The heat capacity of proteins estimated from this technique is in good agreement with the values from experiments. This study shows that triiodothyronine (T3) hormone makes some differences in heat capacity upon binding to the THR-β ligand binding domain (LBD). The physical properties of unliganded THR-β and T3-bound THR-β LBD in the cases of constrained and unconstrained dynamics are observed distinctly under the effect of anharmonicity on the phase coherent state of normal modes and the dephasing time lies in a range of 0.6–0.8 ps when the systems are perturbed suddenly.

**Keywords** Thyroid hormone receptor · Triiodothyronine · Temperature echo · Heat capacity · Dephasing · Anharmonicity

✉ Hari Prasad Lamichhane
hlamichhane1@gmail.com

[1] Central Department of Physics, Tribhuvan University, Kirtipur, Kathmandu, Nepal

[2] Institute of Medicine, Tribhuvan University Teaching Hospital, Maharajgunj, Kathmandu, Nepal

## 1 Introduction

The major form of thyroid hormones secreted by the thyroid gland is 3,5,3′,5′-tetraiodo-L-thyronine (thyroxin, T4). T4 is converted into 3,5,3′-triiodo-L-thyronine (T3) after intracellular activity called local deiodination [1]. T3 actively binds to the ligand binding domain (LBD) of the thyroid hormone receptor (Fig. 1) that has two subtypes: THR-α and THR-β. These are members of the nuclear receptor superfamily of ligand activated transcription factors. T3-activated nuclear receptors regulate gene expression involved in cell differentiation, growth, and homeostasis. Since the total serum concentration of T4 is 40-fold higher than T3, T4 can also bind and modulate the receptor's activity in lower affinity [2].

Due to a negative feedback mechanism, an increase in the thyroid stimulating hormone (TSH) level generally causes a decrease in T3/T4 concentrations and vice versa. The decrease in serum T3/T4 levels from the normal range is an indicator of clinical or subclinical hypothyroidism. In contrary, a decrease in TSH, i.e., an increase in T3/T4 concentration is related to hyperthyroidism [3]. THR-β is found in the liver, which is involved in the regulation of metabolic rate. The T3-bound THR-β LBD (THRT3) plays a key regulatory role on the negative feedback mechanism of circulating thyroid hormone levels for the production of the hypothalamic thyrotropin releasing hormone (TRH) and hypophyseal TSH [4]. Any mutation in THR-β can cause a resistance to thyroid hormones (RTH), which results in a disorder characterized by elevated levels of serum T3/T4 and normal or elevated thyroid stimulating hormone (TSH). The genetic disease RTH has a complex range of symptoms such as pituitary malfunction, goiter, and neurological disorder [5]. The unliganded THR-β (THR) functions as a transcriptional repressor of the target genes. The carboxyl terminal of LBD obtains the conformational change through an activation function (AF-2) when bound to T3 and this further alters the position of helix 12 [2, 6]. Even a mutation in the helix 12 region can block the recruitment of cofactors to the AF-2 domain resulting in the inhibition of both T3-mediated activation and repression of gene transcription [7]. There are seven pathways of T3 dissociation; most of which are significantly affected by THR-β heterodimerization [8]. The molecular interaction of 4-hydroxyphenyl sulphone (BPS used as a BPA alternative) toward THR-β LBD makes a structural disruption, which is a type of potential endocrine effect on the biological systems [9].

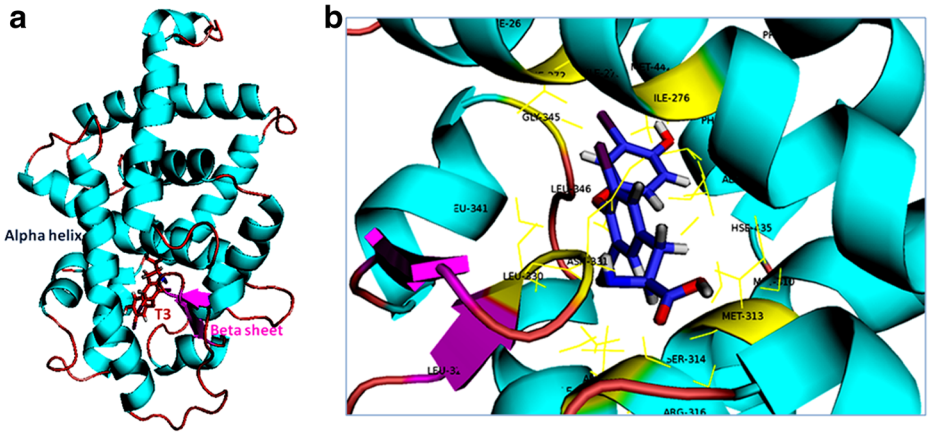


**Fig. 1** Structure of triiodothyronine (T3)-liganded thyroid hormone receptor-beta (THR-β) showing **a** alpha-helices and beta-sheets in cartoon view and **b** T3 binding domain (*yellow region*: 4 Å around T3) in THR-β prepared with the PyMOL molecular graphics system

Constraints are imposed in the biomolecular systems to remove the associated rapid vibrational modes by reducing the internal degrees of freedom [10–13]. A longer time step can be used for integrating Newton's equations of motion without distorting the system. The constrained vibrations save computer time while finding the physical properties of the atomic clusters by means of computational techniques.

In the vibrational echo experiments used to study protein dynamics [14–16], the echo decay provides dephasing time under the effect of anharmonicity. The classical dynamics of atomic particles in defining the vibrational echoes can be interpreted as a probe of stability of atomic trajectories [17].

The structural and physical properties of bio-atomic clusters reflect some intrinsic features such as the temperature echo after the application of sudden perturbations and monitoring their response. We used the theory of temperature quenching and echo formation described by Xu et al. with some modifications to calculate heat capacity and diffusion and mobility constants of anharmonicity [18]. The temperature quench echo and the velocity replacement echo can be visualized through molecular dynamics (MD) simulations. In analogy with the phonons in a crystalline solid, the internal dynamics of atoms in a globular protein in a high-frequency range can also be described as the normal modes of vibration. The normal modes oscillate in a phase coherent state leading to resonances referred to as echoes in response to a suitable signal or perturbation [18, 19]. The decay of coherent states of atomic motions can be analyzed in terms of dephasing time by employing MD simulations. In the temperature echo method, the coherence of atomic motions is probed by reassigning the atomic velocities to a fixed temperature distribution ranging from zero to that of the equilibrated system.

## 2 Materials and methods

### 2.1 Theory

The time evolution of the kinetic temperature [18, 19] in a molecular system is given by

$$T(t) = \frac{2}{(3N-6)K_B} E_k(t) = \frac{2}{(3N-6)K_B} \sum_{i=1}^{(3N-6)} \frac{1}{2} m_i v_i^2 \tag{1}$$

where N refers to the number of atoms in the system and $T(t)$ acquires sharp features during the synchronization signal, probing the signal and temperature echoes. In a normal mode analysis of the protein–hormone system, the Hamiltonian associated with the $i^{th}$ normal mode describing the echoes by kinetic energy (temperature) and potential energy is

$$H_i = \frac{p_i^2}{2m_i} + \frac{1}{2} m_i \omega_i^2 y_i^2 \tag{2}$$

The position of the $i^{th}$ normal mode under harmonic approximation is $y_i(t) = A_i \cos(\omega_i t + \delta_i)$ and the momentum is $p_i(t) = -m_i A_i \omega_i \sin(\omega_i t + \delta_i)$. The total kinetic energy of the system is given by

$$E_K(t) = \sum_i \frac{1}{2} m_i A_i^2 \omega_i^2 \sin^2(\omega_i t + \delta_i) \tag{3}$$

Temperature autocorrelation function [19] before quenching or before velocity reassignment is given by:

$$C_{T,T}(t) = \frac{\langle E_k(t)E_k(0)\rangle - \langle E_k(0)\rangle^2}{\left\langle [E_k(t)]^2 \right\rangle - \langle E_k(0)\rangle^2} = \frac{\langle T(t)T(0)\rangle - \langle T(0)\rangle^2}{\left\langle [T(t)]^2 \right\rangle - \langle T(0)\rangle^2} = \frac{\left\langle \sum_i m_i^2 A_i^4 \omega_i^4 \cos(2\omega_i t)\right\rangle}{\left\langle \sum_i m_i^2 A_i^4 \omega_i^4 \right\rangle} \quad (4)$$

The $C_{T,T}(t)$ function can be approximated to a single exponential function with decay time $\tau_d$, i.e., $C_{T,T}(t) \approx e^{-t/\tau_d}$.

At the first velocity reassignment, i.e., at $t = 0$ (say), $v_i(0) = \lambda_1 u_i$ synchronizes the atomic oscillators or it makes them oscillate in phase. After some delay time ($\tau$), $v_i(\tau) = \lambda_2 u_i$ probe the degree of coherence of the system. Here, $\lambda_i$ are the numbers multiplied with the initial velocities $u_i$. The degree of coherence is characterized by time of appearance and depth of echoes. If $\lambda_1 = \lambda_2 = 0$, the system has a temperature quench echo; if $\lambda_1 = \lambda_2 = 1$, it has a constant velocity replacement echo and if $\lambda_1 \neq \lambda_2 \neq 1$, it has a velocity replacement echo. The temperature echo can be detected at $t = 2\tau$ in the first case and at $t = 3\tau/2$ in the second and third cases. In each of these cases, the depth of echo differs from its value. The largest depth of the temperature quench echo in the first case is $\Delta T = T_0/8$ where $T_1 = \lambda_1^2 T_0$ and $T_2 = \lambda_2^2 T_0$ with $\lambda_1 = \lambda_2 = 0$ having $T_0$ as the equilibrium temperature [18, 19].

From harmonic approximation, the temperature response function [18, 19] for the time interval, $t > \tau >> \tau_d$, is

$$T(t) \approx T_0 \left[ \frac{1 + \lambda_1^2 + 2\lambda_2^2}{4} - \frac{1 + \lambda_1^2 - 2\lambda_2^2}{4} C_{T,T}(t-\tau) - \frac{\lambda_1 \lambda_2}{2} C_{T,T}\left( \left| t - \frac{3\tau}{2} \right| \right) - \frac{1-\lambda_1^2}{8} C_{T,T}(|t-2\tau|) \right] \quad (5)$$

In Eq. (5), the first term on the right side represents the average temperature after the second velocity reassignment, the second term is the recovery of temperature and the third and final terms represent for $\frac{3\tau}{2}$ -echo pulse and $2\tau$ -echo pulse, respectively. The respective echo pulses have a depth of $\Delta T(3\tau/2) = \frac{T_0}{2}\lambda_1\lambda_2$ and of $\Delta T(2\tau) = \frac{T_0}{8}(1-\lambda_1^2)$.

For the temperature quench echo with $T_1 = T_2 = 0$, the temperature response function deals only with the $2\tau$-echo pulse [18, 19], which is given by

$$T(t) \approx \frac{T_0}{4} \left[ 1 - C_{T,T}(t-\tau) - \frac{1}{2} C_{T,T}(|t-2\tau|) \right] \quad (6)$$

The depth of this echo pulse under harmonic approximation is $\Delta T(2\tau) = T_0/8$.

Along with the time evolution of temperature, kinetic energy ($E_K$) as well as internal potential energy ($U$) change greatly with temperature in the echo time zone. As the total energy remains almost constant throughout the simulation in the NVE ensemble, i.e., $E_K(t) + U(t) = E_T \approx$ constant [19], we can define heat capacity in two ways. If

$$\Delta E_k(t) = \frac{(3N-6)K_B}{2} \Delta T(t) \approx -\Delta U(t)$$

then

$$C_{V1} = \left( \frac{\partial E_k}{\partial T} \right)_{N,V,E} = \frac{(3N-6)K_B}{2} \approx C_{V2} = -\frac{dU(t)}{dT(t)} = -\left( \frac{\partial U}{\partial T} \right)_{N,V,E} \quad (7)$$

where $\mathcal{C}_{V1}$ is the heat capacity in terms of kinetic energy that depends only on degrees of freedom of the system and $C_{V2}$ is the heat capacity in terms of internal potential energies (e.g., electrostatic, van der Waal, bond, angle, dihedral, etc.) with the expense of kinetic energy (macroscopic mass motion) as indicated by the negative sign. In other words, $C_{V2}$ is temperature dependent but not $\mathcal{C}_{V1}$.

If we implement some constrained degrees of freedom ($N_C$) during the simulation of the molecular system, the echo depth in kinetic energy in terms of echo depth in temperature can be expressed as

$$\Delta E_K = \left(\frac{3N-N_C-6}{2}\right) K_B \Delta T = \mathcal{C}_{V1}\, \Delta T \tag{8}$$

The small fluctuation observed in the total energy of the system in its NVE ensemble is only due to fluctuations in the internal potential energy terms by means of kinetic temperature. Thus, being a function of temperature, the potential energy is the major contributor of heat capacity. It has also been verified by the results obtained after simulations. In most of the MD simulations of macromolecules, vibrations of H-atoms are constrained ($N_C \neq 0$) with their rigid bonds and a time step of 2 fs and all atomic vibrations are made free ($N_C = 0$) with the time step of 1 fs. The results obtained from these two methods are compared with the experimental values.

In case of complex thermodynamic systems like proteins, the heat capacity components can be separated regarding the different physical contributions such as internal potential energy terms (atomic and covalent bonding and all other non-covalent contributions), folding and unfolding states and interaction with solvents [20, 21]. For a native state protein in vacuo, the temperature echoes and heat capacity can be observed from the potential function describing the system [19, 20].

According to Xu et al. [18], the depth of echo decays exponentially with delay time ($\tau$) due to the anharmonic contributions that arise from electrostatic, torsional and van der Waals interactions, i.e., $\Delta T \propto \exp(-\tau/\tau_0)$ where $\tau_0$ is the dephasing time. So, the correct form of echo depth is given by

$$\Delta E_K = \mathcal{C}_{V1}\, \Delta T = \mathcal{C}_{V1}\, \Delta T_0 e^{-\tau/\tau_0} = \Delta E_{K0} e^{-b_0 \tau} \tag{9}$$

where $b_0$ is the echo damping coefficient of the protein. Friction and fluctuating forces result anharmonicity in the normal modes of vibrations. The anharmonic terms in the internal energy of the system make the normal modes dephase. In MD simulations, vibrational energy relaxation and dephasing are important to study energy transfer and reactivity in peptides and proteins [18, 22]. The diffusion coefficient ($D_i$) and mobility constant ($\mu_i$) for the anharmonic interactions in the $i^{th}$ normal mode of vibration of the system can be connected by Einstein's diffusion equation with $D_i = \mu_i K_B T$. For the process of temperature quenching and large delay time ($\tau$), the echo depth [18] at $t = 2\tau$ can be expressed as

$$\Delta T(\tau) \approx \frac{T_0}{8}\left\langle e^{-(3\mu_i K_B T_0 \tau)} \right\rangle = \frac{T_0}{8}\left\langle e^{-(3D_i \tau)} \right\rangle = \Delta T_0 \left\langle e^{-(3D_i \tau)} \right\rangle \tag{10}$$

In the case of constant velocity reassignment echo, $\Delta T_0 = T_0/2$. If the diffusion constant ($D_0$) and mobility constant ($\mu_0$) are assumed to be the same for each of the normal modes, the echo depths for the temperature and kinetic energy are related as

$$\Delta E_K(\tau) = \mathcal{C}_{V1}\,\Delta T(\tau) \approx \mathcal{C}_{V1}\,\Delta T_0 e^{-(3\mu_0 K_B T_0 \tau)} = \Delta E_{K0} e^{-(3D_0\tau)} \tag{11}$$

Thus, the dephasing time and the anharmonic constants are

$$D_0 = \frac{1}{3\tau_0} = \frac{b_0}{3} = \mu_0 K_B T_0 \tag{12}$$

Rearranging and taking the natural log of both sides gives

$$ln(\Delta E_K) = A - b_0 \tau \tag{13}$$

Then, we can obtain $\mathcal{C}_{V1}$ from the intercept: $\mathbf{A} = \ln(\mathcal{C}_{V1}\Delta T_0)$; and $b_0$, $D_0$ and $\tau_0$ from the slope.

### 2.2 Simulation details

The crystal structure of T3-bound THR-β isoform (THRT3) was taken from the protein data bank (pdb) code 3GwS at 2.2-Å resolution [23]. The topologies and parameters required to prepare the complete simulated systems were used from the CHARMM force field [24–26]. As the ligand (T3) is a hetero-molecule, it was parameterized to describe its molecular geometry, partial atomic charges, atomic masses, theoretical and experimental torsion barriers [26]. All the simulations starting from the generation of the protein structure file (psf) and energy minimization, equilibration run and production run were performed with nanoscale molecular dynamics (NAMD-2.12) [27]. The simulated systems were analyzed with visual molecular dynamics (VMD-1.9.3) [28]. Both systems, i.e., THR and THRT3, were simulated by the same procedures in a water-ion environment and then in vacuo to study the physical role of T3 in its receptor proteins by the echo method.

Each of the THR and THRT3 molecules was solvated fully in a neutral water-droplet (TIP3P) of radius 37.5 Å by adding $Na^+$ and $Cl^-$ ions with a concentration of 0.15 mol/l providing the cellular environment so that the complexes have 21,157 and 21,192 atoms, respectively. The prepared systems were geometrically optimized by 3000 conjugate gradient steps and equilibrated up to 7-ns coupling to the heat bath at 310 K under non-periodic boundary conditions. Furthermore, the final coordinates of each system were extracted to equilibrate separately again in vacuo up to 1 ns because the echo features are more distinct and observable in an anhydrous state rather than in a solution. In defining the force-field parameters in the configuration systems, 1–4 scaling for the electrostatic interactions was 1.0, cut-off distance for the electrostatic and van der Waal interactions was 12.0 Å with the smooth switching function starting at 10.0 Å and the pair list distance was 14.0 Å. The integrator parameter for the simulation of solvated THR and THRT3 systems was 2.0 fs/step providing a command for the rigid bonds to all H-atoms. However, all of the simulations in vacuo were performed in both cases: constrained vibrations with rigid bonds of H-atoms (2 fs per time step) and free vibrations of all atoms (1 fs per time step) and finally the results obtained were

compared. During the simulation, the Langevin temperature and damping coefficient were 310 K and 1.0/ps, respectively. The velocity Verlet algorithm [29] was used to calculate the trajectory of atomic particles by integrating Newton's equations of motion. The conformational stability of the protein–hormone systems was tested by analyzing their trajectories during the simulations and by plotting the root mean square deviation (RMSD) and radius of gyration ($R_g$) of the protein backbone.

After employing MD simulations for energy minimization and equilibration in the TIP3P explicit solvent and then in vacuo at 310 K, both the THR and THRT3 systems were simulated up to 5 ps removing the thermostat in the NVE ensemble. The temperature autocorrelation functions were plotted using Eq. (4) and best fitted with the single exponential function to approximate the decay time related to the systems.

To observe and compare the physical phenomena during the formation of temperature echoes in the protein–hormone systems, i.e., THR and THRT3, we used the theory of temperature quench echoes by reassigning twice the atomic velocities to zero and by using the constant velocity replacement method. We performed 15–20 different simulations for both systems in each case of 1 fs/step and 2 fs/step in the NVE ensemble with the values of delay time ($\tau$) ranging from 0.1 to 2 ps. Using the resulting data, different graphs relating the physical variables such as temperature, energies and delay time were plotted and analyzed. The vicinity of the echo was also compared with the harmonic approximation (Eq. 6). From the different sets of numerical data for the temperature echoes, we analyzed the dephasing behavior of the systems by plotting echo depths vs. delay time.

The variations of internal potential energies in the echo time zone were plotted to analyze the impacts on bonding and non-bonding terms. Also, the plots for the number of H-bonds vs. radius of gyration were analyzed to know more about the temperature changing conformations of the protein–hormone systems. The changes in internal potential energy with respect to echo minimum temperature were used to obtain the heat capacity of the native globular proteins. Even with large fluctuations of temperature in the echo time zone, we can see the particular section of energy vs. temperature curves to obtain the heat capacity at that particular temperature. The anharmonicity coefficients such as dephasing time constant, diffusion and mobility constants were also estimated for THR and THRT3 by fitting a straight line (Eq. 13) in both cases: rigid bonds of H-atoms (2 fs/step) and free vibrations of all atoms (1 fs/step). The plotting programs used were Xmgrace, Origin-2017, and MS-Excel-2007. The validity of the results was tested by revising the simulations at least three times each.

## 3 Results and discussion

The THR-β isoform consists of a chain length of 259 amino acids. The unliganded THR has 3895 atoms, mass of 27,640 amu and 1952 bonds of H-atoms. The THRT3 system has 3930 atoms, mass of 28,291 amu and 1964 bonds of H-atoms. The number of atoms, charges, bonds, angles, dihedrals, impropers, cross-terms, and force field parameters yield total bonded and nonbonded potential functions in the molecular system.

RMSDs of both the THR and THRT3 systems are below 2.5 Å (Fig. 2) while simulating them separately in the explicit TIP3P water-ion environment. During geometrical optimization, equilibration and production runs, each of these molecules is conformationally stable. Although the major fold is conserved, the small peaks found in RMSD curves indicate the

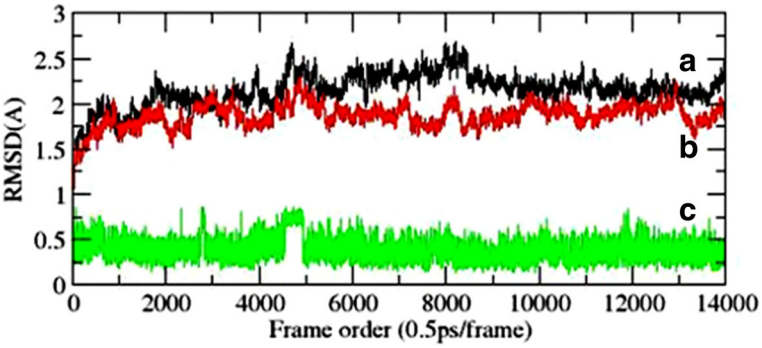


**Fig. 2** Root mean square deviation (RMSD) excluding H-atoms of **a** THR protein, **b** THRT3 protein, and **c** T3 hormone during the separate equilibration runs in a neutral water-ion environment at 310 K

breaking and reforming of H-bonds among the free and more stable residues, α-helix and β-sheets of the molecules during the simulations [30].

During the separate 7-ns equilibration runs of the THR and THRT3 systems solvated each in a water droplet of radius 37.48 Å, the radius of gyration ($R_g$) of the protein–hormone system is (18.33 ± 0.40)Å. Such a value of $R_g$ remains almost constant (Fig. 3) indicating the continuity of conformational stability when the systems are subjected to the equilibration run in vacuo too. It is to be noted that the echo features are more distinct and observable in the native state protein in vacuo than in water because there is a higher effect of anharmonicity in a solution. As the radius of gyration indicates the protein structure compactness [31], the average values of $R_g$ are (18.04 ± 0.09) Å, (18.35 ± 0.08) Å and (4.50 ± 0.05) Å for the THRT3, THR and T3 hormone, respectively during their equilibration runs in vacuo. The fluctuating nature of kinetic temperature of about 310 K indicates the dynamic properties of the protein atoms.

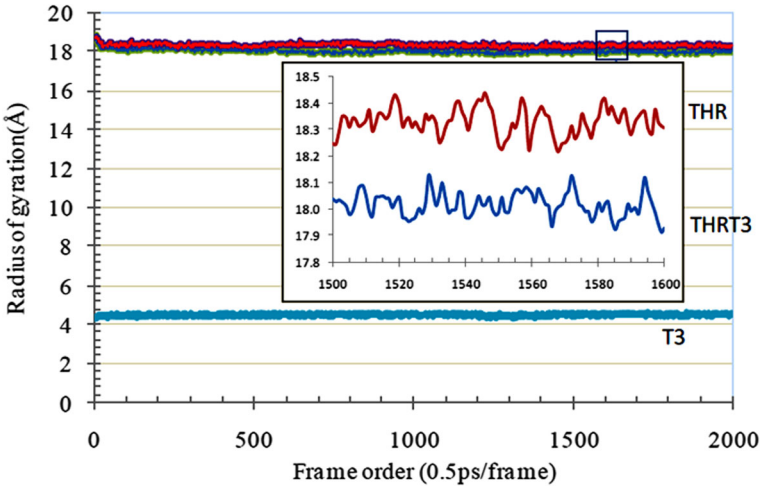


**Fig. 3** Radius of gyration of both the THR and THRT3 systems during the separate 1-ns equilibration runs in the NVT ensemble in vacuo after obtaining their final coordinates from 7-ns equilibration in the neutral water-ion environment at 310 K. A small part of the graph has also been highlighted

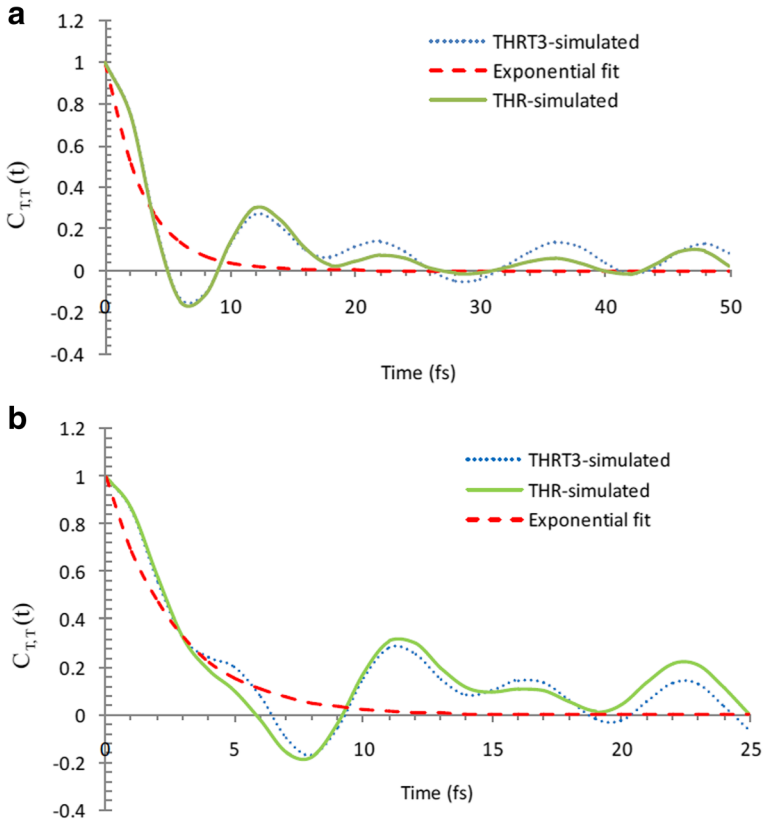


**Fig. 4** Temperature auto-correlations for THR and THRT3 simulated in the NVE ensemble **a** with 2 fs/step and rigid bonds to all H-atoms resulting in the decay time $\tau_d = 3.00 \pm 0.03$ fs and **b** with 1 fs/step and non-rigid bonds to all atoms resulting in the decay time $\tau_d = 2.80 \pm 0.15$ fs

The temperature autocorrelation function $C_{T,T}(t)$ shows the distinct nature for the simulations in the NVE ensemble with constrained rigid bonds of H-atoms (2 fs/step) and free vibration of all atoms (1 fs/step) of the THR and THRT3 molecules in vacuo. The free vibrations of H-atoms result in shoulder like features (Fig. 4-b) in the plots of autocorrelation functions with the effect of anharmonicity being clearer. The function $C_{T,T}(t)$ has been fitted with the exponential function $e^{-t/\tau_d}$ taking the data for $C_{T,T}(t)$ from 5-ps simulation in the NVE-ensemble of the equilibrated THR and THRT3 systems as shown by the dashed (red) curves in Fig. 4a, b. The decay time for both THR and THRT3 lies within the given error limit, i.e., $(3.00 \pm 0.03)$ fs for 2 fs/step and $(2.80 \pm 0.15)$ fs for 1 fs/step simulations. These values are slightly higher than the decay time (2.67 fs) of the trans-membrane protein bacteriorhodopsin found by Schulten et al. [19].

When the temperature is quenched twice to zero at a particular delay time, the echo depth as well as the nature of the echo feature curve change for the molecules THR and THRT3 and also for the cases of constrained and unconstrained normal modes of vibrations in the separate NVE simulations. Figure 5 shows the kinetic temperature distributions and the response (echo) of perturbation (quenching) in the molecular

systems that appear in the same way as explained in the theory. Here, the plots of temperature vs. time follow the same pattern as that of kinetic energy as shown in Fig. 6. The temperature $T(t)$ vs. time plots during simulations at the NVE-ensemble of the THR and THRT3 systems in equilibrium up to 5 ps show almost a constant nature about 310 K. The reassignment of atomic velocities is set to zero at $t_0 = 5$ ps and $t_1 = 5.2$ ps (delay time $\tau = t_1 - t_0 = 200$ fs). The temperature quench echo was observed at $t = t_0 + 2\tau = 5.4$ ps, i.e., at 0.4 ps after the first point of temperature quenching. At the vicinity of the echo, the mean of the temperature fluctuation is best fitted with the harmonic approximation. In the case of Figs. 5 and 6, the echo depths in terms of temperature and kinetic energy are: $\Delta T = 31.86$ K and $\Delta E_K = 311.05$ kcal/mol for THRT3. Similar calculations for THR result in $\Delta T = 33.92$ K and $\Delta E_K = 327.96$ kcal/mol. In this way, we can observe all cases of echo formation by temperature quenching and constant velocity replacement for both molecules: THR and THRT3 taking rigid bonds of H-atoms with 2 fs/step and free vibrations of all atoms with 1 fs/step simulations through the thermal equilibrium to non-equilibrium in the NVE ensembles as explained in the methodology.

The echo pulses in THRT3 are also reflected by energy profile diagrams (Figs. 6, 11 and 12) in which the total change in potential energy is equal and negative to the change in kinetic energy with the total energy remaining constant in the respective NVE ensembles of the protein–hormone system. The total energy gets a step jump along with kinetic and potential energies at the temperature quenching points, i.e., at $t_1 = 5$ ps and then $t_2 = 5.2$ ps as shown in Fig. 6. The amount of step jump in the total energy is equal to the sum of change in kinetic and potential energies and it depends on the nature of protein molecules and also on the cases of constraints imposed during the simulations.

H-bonds among N and O atoms are observed for donor-acceptor distance = 4 Å and cut-off angle = 40°. The number of H-bonds gets a step up jump and the size of the globular proteins tend to shrink at the temperature quenching points where the temperature is set to zero. Figure 7 shows the H-bond distributions for THR and THRT3 in the NVE ensembles taking rigid bonds to all H-atoms with a delay time $\tau = 2$ ps and a time step of 2 fs. The molecular

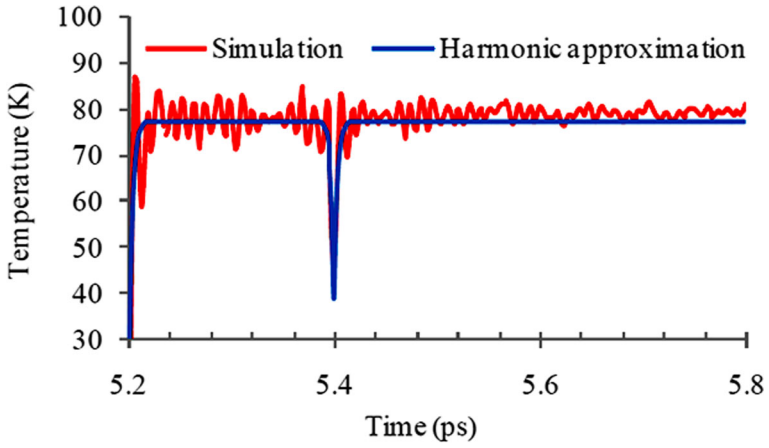


**Fig. 5** Temperature echo pulse for THRT3 fitted with harmonic approximation after quenching the temperature to zero at 5.0 ps and then at 5.2 ps with the delay time $\tau = 0.2$ ps and 2 fs/step simulation in the NVE ensembles constrained with rigid bonds to all H-atoms

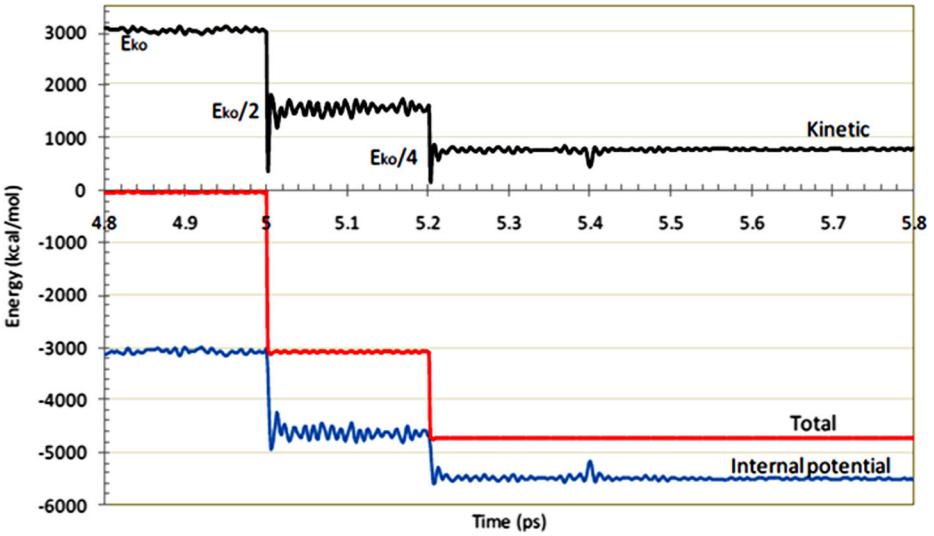


**Fig. 6** Perturbed kinetic, internal potential, and total energy distributions parallel to the temperature distribution with delay time $\tau = 0.2$ ps and 2 fs/step simulations in the respective NVE ensembles of THRT3 keeping rigid bonds to all H-atoms

conformations change along with the formation of new H-bonds [30]. The protein becomes more globular and stable when it is perturbed under the temperature quenching and released. The THRT3 system may get jiggled to return to its original conformation at the point of second quenching (at $t = 7$ ps as shown in Fig. 8) in the presence of a heavy ligand (T3) in its LBD. The mean values of temperature, total energy, H-bonds ($N_H$) and radius of gyration ($R_g$) at the different time frames listed in Table 1 and the $N_H$ vs. $R_g$ plot in Fig. 9 verify that the proteins become more globular (smaller $R_g$) with increasing $N_H$ while decreasing the temperature. We observe a strong negative correlation ($r = -0.86$) between $R_g$ and $N_H$.

While observing the plots of individual potential energies (Fig. 10), the bigger peak (echo) in bond angle energy shows the skeletal motion of the normal modes in the proteins. In the

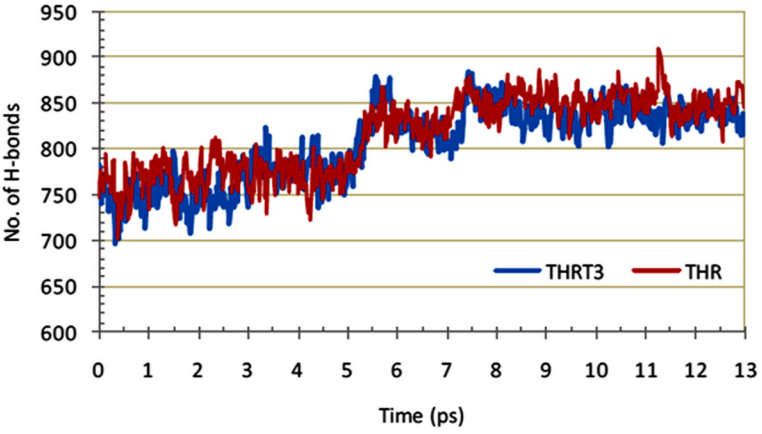


**Fig. 7** Variations in the number of H-bonds along with time of simulations in NVE ensembles for THR and THRT3 constrained with rigid bonds to all H-atoms with a time step of 2 fs and with a delay time $\tau = 2$ ps during the formation of temperature echo by quenching

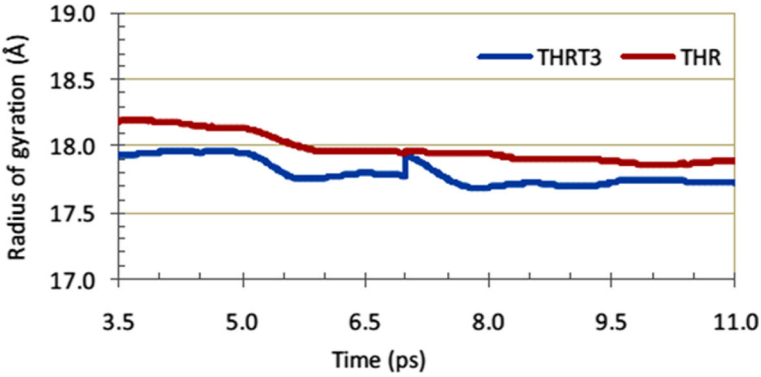


**Fig. 8** Variations in the radius of gyration of THR and THRT3 at the points of temperature quenching with a step jump at the point of second quenching (t = 7 ps) for THRT3

case of the constant velocity replacement echo (Fig. 11), the total energy almost remains conserved even if the large fluctuation in kinetic temperature occurs in the echo time zone.

In the case of a constant velocity ($T = 310$ K) replacement echo observed in the protein–hormone systems with rigid bonds to H-atoms, the maximum energy fluctuations in the echo time zone ($t = 5.400 \pm 0.008$ ps) are $\Delta E_K$ (kinetic) = 1415.68 kcal/mol and $\Delta E_{BP}$ (bond angle potential) = 987.73 kcal/mol for THR but $\Delta E_K = 1552.84$ kcal/mol and $\Delta E_{BP} = 1025.85$ kcal/mol for THRT3. The significant change in bond angle potential suggests that the T3-hormone provides much more skeletal motion to its nuclear receptor protein.

The echo features in the internal potential energy ($U$) and the temperature ($T$) of THR and THRT3 are plotted with respect to time ($t$) in Fig. 12. The internal potential energies of THR and THRT3 are changing smoothly when bonds of H-atoms are made rigid resulting in a larger value of $U(t)$ for THRT3 than that of THR. However, on releasing the constrained bonds of H-atoms, the nature of $U(t)$ curves for both THR and THRT3 has changed from the constrained case and there are shoulders at many places. The shoulders appear by means of free H-atoms (larger degrees of freedom) and increasing anharmonic interactions [18]. From these echo feature curves, the heat capacity of the protein–hormone systems contributed by the internal potential energy terms can be estimated in the different temperature range. The value of the echo depth can be varied in two ways: i) by changing the delay time and ii) by changing the temperature of quenching or the velocity rescaling. The depth of the echo increases with the increase in temperature of quenching (0 to 310 K), which is verified by comparing Figs. 6 and 11. Such depth decays exponentially with delay time due to the impact of anharmonicity.

**Table 1** Average values of temperature, total energy, number of H-bonds ($N_H$) and radius of gyration ($R_g$) for THR and THRT3 in NVE ensembles with rigid bonds to all H-atoms with a delay time $\tau = 2$ ps and a time step of 2 fs

| Time frame | Molecule | T(K) | $E_T$ (kcal/mol) | $N_H$ | $R_g$ (Å) |
|---|---|---|---|---|---|
| $0 \le t \le 5$ ps | THR | 312.52 | − 150.44 | 770 | 18.14 |
| | THRT3 | 311.12 | − 43.17 | 761 | 17.95 |
| $5 \le t \le 7$ ps | THR | 153.55 | − 3331.33 | 821 | 18.00 |
| | THRT3 | 160.43 | − 3095.94 | 824 | 17.81 |
| $7 \le t \le 13$ ps | THR | 77.29 | − 4854.71 | 852 | 17.91 |
| | THRT3 | 78.77 | − 4743.17 | 840 | 17.73 |

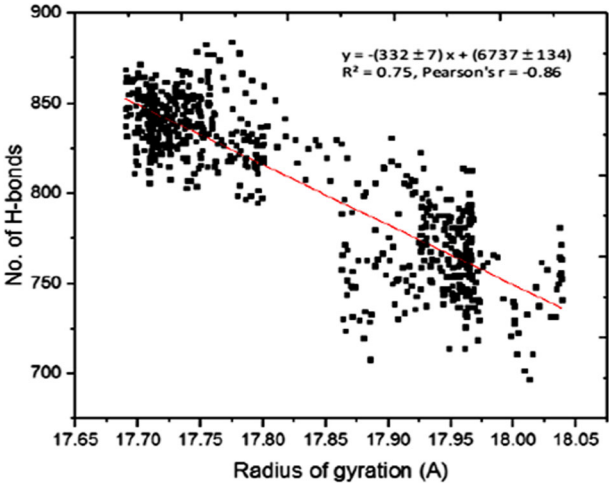


**Fig. 9** Negative correlation between the number of H-bonds and radius of gyration of the protein obtained from the temperature quenching simulations of THRT3 in NVE ensembles in a time step of 2 fs

In the case of constrained or rigid bonds of H-atoms with 2 fs/step, the echo minimum temperature changes exponentially with the delay time as shown in Fig. 13. Also, the variations of kinetic energy, internal potential energy and total energy of THR and THRT3 with respect to the echo minimum temperature have been studied. In all of the cases for the constrained and free atomic vibrations of both THR and THRT3 molecules, the square of the correlation coefficient ($R^2$) between kinetic energy and echo minimum temperature is found to be unity, showing a very exact positive linear correlation. On the other hand, the internal potential energy has $R^2 = 0.98 \pm 0.1$ with the echo minimum temperature resulting in a negative linear correlation. The total energy almost remains constant with changing the echo minimum temperature during the dephasing of normal modes of vibrations in the molecular systems. As the kinetic energy smoothly varies with echo minimum temperature, the slightly fluctuating internal potential energy results in a temperature dependent change on heat capacity (Fig. 14). We estimated the heat capacity, dephasing time, anharmonicity diffusion and

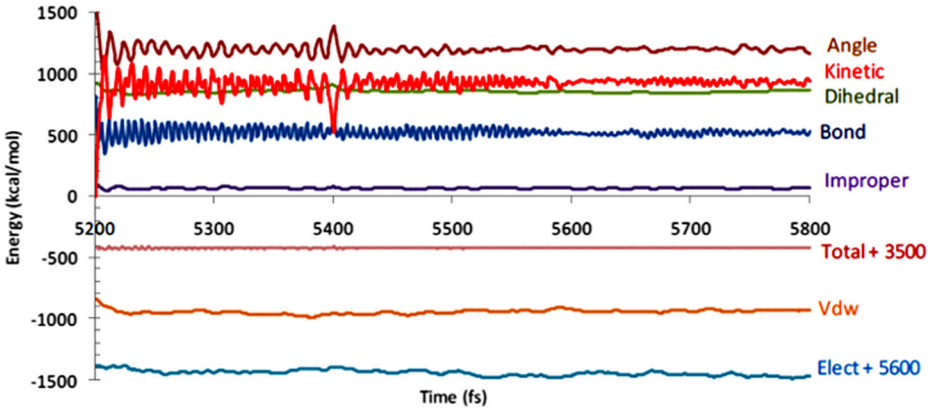


**Fig. 10** Energy distributions for THRT3 in the vicinity of the echo (temperature quenching twice to zero) with a delay time $\tau = 0.2$ ps and 1 fs/step simulation in NVE ensembles by releasing all bonds to free vibration

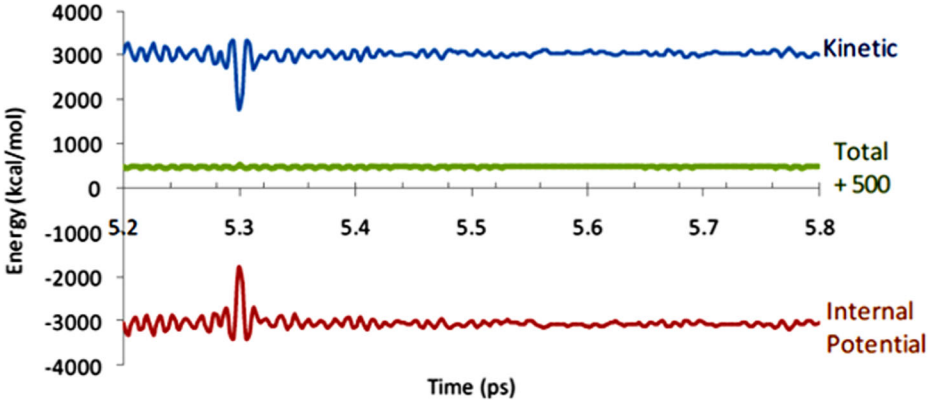


**Fig. 11** Energy distributions for THRT3 in the vicinity of the constant velocity (T = 310 K) reassignment echo with a delay time τ = 0.2 ps and 2 fs/step simulation in NVE ensembles constrained with rigid bonds to all H-atoms

mobility constants by analyzing the different graphs (Figs. 14 and 15) in the echo time-zone of THR and THRT3 utilizing proteins as listed in Table 2. As the heat capacity $\mathcal{C}_{V1}$ depends on the number of degrees of freedom, its value given by the theoretical formula from Eq. (7) and (8) is 11.60 kcal mol$^{-1}$ K$^{-1}$ for THR and 11.70 kcal mol$^{-1}$ K$^{-1}$ for THRT3 with unconstrained vibrations, i.e., $N_C = 0$. In the case of rigid bonds of H-atoms, $N_C = 1952$ for THR and 1964 for THRT3 and the value of $\mathcal{C}_{V1}$ is 9.66 kcal mol$^{-1}$ K$^{-1}$ for THR and 9.75 kcal mol$^{-1}$ K$^{-1}$ for THRT3. These values (within the error limit of ±0.01 kcal mol$^{-1}$ K$^{-1}$) are the same as the slope of the straight line fitted for the kinetic energy distribution and nearly equal to the slope ($C_{V2}$)

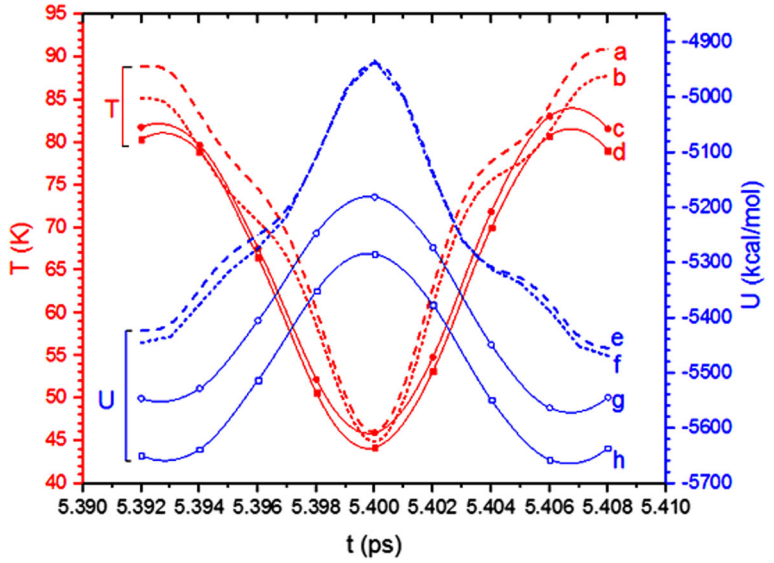


**Fig. 12** Variations of internal potential energy (THR: curves 'f and h' and THRT3: 'e and g') and temperature (THR: curves 'a and d' and THRT3: 'b and c') in the echo time zone (t = 5.400 ± 0.008 ps). These echo feature curves are related to the temperature quenching twice to zero and the delay time τ = 0.2 ps with rigid bonds to all H-atoms (2 fs/time step simulations shown by *smooth lines*: 'c, d, g and h') and with non-rigid bonds to all atoms (1 fs/time step simulations shown by *dotted lines*: 'a, b, e and f')

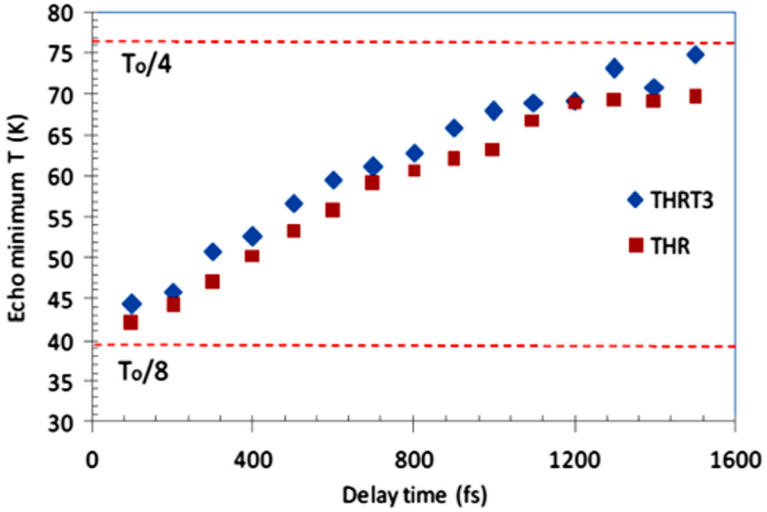


**Fig. 13** Variation of echo-minimum temperature with the delay time while dephasing THR and THRT3 after temperature quenching with the time step of 2 fs constrained with rigid bonds to all H-atoms

of the internal potential energy distribution w.r.t. the echo minimum temperature as shown in Fig. 14 during the respective dephasing simulations in the NVE ensemble of THR and THRT3. The results obtained from fitting the data after many simulations are presented in Table 2. Due to the lack of space and similarity in the graphs, a few sample graphs are shown in this paper. As the heat capacity is temperature dependent, its value has been found to increase by increasing the temperature in the echo time zone.

The average values of heat capacity $C_{V2}$ of THR and THRT3 systems in the echo-temperature range $160 \leq T \leq 310$ K are $11.64 \pm 0.49$ and $12.21 \pm 0.28$ kcal mol$^{-1}$ K$^{-1}$, respectively, as given by

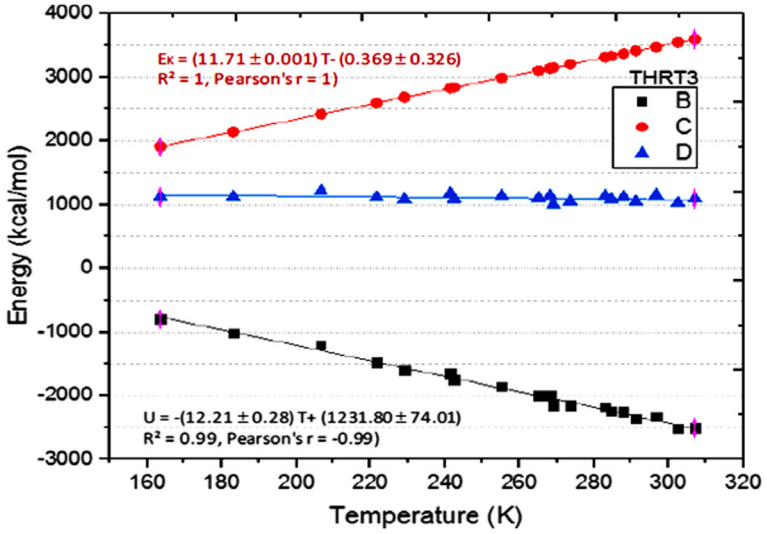


**Fig. 14** Change in potential energy U(B), kinetic energy $E_K$(C) and total energy $E_T$(D) with echo-minimum temperature during the vibrational dephasing of THRT3 after the constant velocity ($T = 310$ K) reassignment where the simulation is performed in the NVE ensemble with free vibrations of all atoms and a time step of 1 fs

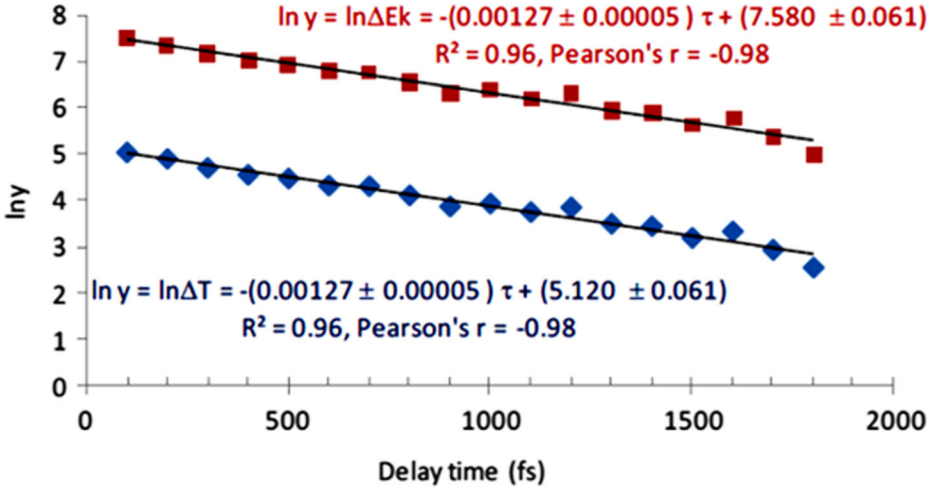


**Fig. 15** Linear fit in the logarithm of echo depth with the delay time during the process of the constant velocity (at $T = 310$ K) reassignment echo of the THRT3 system with 1 fs per time step simulations taking free vibrations of all atoms

the negative slope of the U vs. T straight line (Fig. 14). Such values of $C_{V2}$ are slightly higher than the respective values 11.24 ± 0.65 and 11.62 ± 0.66 kcal mol$^{-1}$ K$^{-1}$ in the echo-temperature range $40 \leq T \leq 80$ K. These results are taken from the case of free vibrations of all atoms with 1 fs/step simulations, which are different from the case of constrained or rigid bonds of H-atoms with 2 fs/step simulations of the systems as presented in Table 2. Here, we observe that the heat capacity difference between THR and THRT3 at about 300 K is 0.57 kcal mol$^{-1}$ K$^{-1}$ and it is supplied by the T3 hormone to its nuclear receptor protein. According to Privalov and Potekhin, the partial

**Table 2** Dephasing time ($\tau_0$), damping constant ($b_0$), anharmonicity diffusion constant ($D_0$), anharmonicity mobility ($\mu_0$) and heat capacity ($C_{V2}$) of unliganded thyroid hormone receptor-beta (THR) and liganded receptor-hormone system (THRT3) in the form of native globular proteins[§§] calculated for the constrained bonds of H-atoms simulated with 2 fs/step and for the free vibrations of all atoms simulated with 1 fs/step related to this work [$C_{V2}$ has been reported in the given echo-temperature range ($\Delta$T) and others are at 310 K and the errors included are the standard errors of the corresponding data]

| Physical parameters | Constrained vibrations with rigid bonds of H-atoms (2 fs/step) | | | | Free vibrations of all atoms (1 fs/step) | | | |
|---|---|---|---|---|---|---|---|---|
| Molecule | THR | | THRT3 | | THR | | THRT3 | |
| $\tau_0$ (ps) | 0.826 ± 0.034 | | 0.625 ± 0.040 | | 0.813 ± 0.020 | | 0.787 ± 0.031 | |
| $b_0$ (ps$^{-1}$) | 1.21 ± 0.05 | | 1.60 ± 0.10 | | 1.23 ± 0.03 | | 1.27 ± 0.05 | |
| $D_0$ (rad ps$^{-1}$) | 0.40 ± 0.02 | | 0.53 ± 0.03 | | 0.41 ± 0.01 | | 0.42 ± 0.02 | |
| $\mu_0$ (mol kcal$^{-1}$ ps$^{-1}$) | 0.65 ± 0.03 | | 0.86 ± 0.05 | | 0.66 ± 0.02 | | 0.68 ± 0.03 | |
| $\Delta$T(K) | 40–80 | 160–310 | 40–80 | 160–310 | 40–80 | 160–310 | 40–80 | 160–310 |
| $C_{V2}$ (kcal mol$^{-1}$ K$^{-1}$) | 8.89 ± 0.79 | 10.18 ± 0.46 | 9.09 ± 0.72 | 10.78 ± 0.60 | 11.24 ± 0.65 | 11.64 ± 0.49 | 11.62 ± 0.66 | 12.21 ± 0.28 |
| $C_{V2}$ (Jkg$^{-1}$ K$^{-1}$) | 1347.97 ± 119.69 | 1542.42 ± 69.69 | 1345.58 ± 106.58 | 1595.75 ± 88.81 | 1703.03 ± 98.48 | 1763.63 ± 74.24 | 1720.09 ± 97.69 | 1807.43 ± 41.44 |

[§§] From Privalov and Potekhin [32], $C_{V2}$ for different native proteins lies in the range of 1200 to 2300 Jkg$^{-1}$ K$^{-1}$ at 298 K, from Xu et al. [18], $\tau_0 = 884$ fs for pancreatic trypsin inhibitor (BPTI) and from Schulten et al. [19], $\tau_0 = 700$ fs and $b_0 = 1.43$ ps$^{-1}$ for bacteriorhodopsin

specific heat capacity of the different native proteins at 298 K varies within the range of 1200 to 2300 $Jkg^{-1}$ $K^{-1}$ and increases linearly with a slope of 1 $Jkg^{-1}$ $K^{-1}$ when raising the temperature [32]. In our study of the echo method in unconstrained dynamics of native globular proteins, the specific heat capacities at about 300 K are 1763.63 ± 74.24 $Jkg^{-1}$ $K^{-1}$ for THR and 1807.43 ± 41.44 $Jkg^{-1}$ $K^{-1}$ for THRT3, which lie within the range given by Privalov's study. Furthermore, the values of $C_{V2}$ that we found in the case of constrained dynamics, 1542.42 ± 69.69 $Jkg^{-1}$ $K^{-1}$ for THR and 1595.75 ± 88.81 $Jkg^{-1}$ $K^{-1}$ for THRT3 at about 300 K are a little bit higher than the average value for the anhydrous proteins, i.e., 1250 ± 13 $Jkg^{-1}$ $K^{-1}$ at 298 K studied by Gomez et al. [21].

The dephasing times ($\tau_0$) for THR and THRT3 in the case of free vibrations are 813 ± 20 fs and 787 ± 31 fs, respectively, which are calculated from the reciprocal of the slope of the linear fit for the logarithm of echo depth vs. delay time as shown in Fig. 15. Also, in the case of constrained vibrations, the values of $\tau_0$ are 826 ± 34 fs for THR and 625 ± 40 fs for THRT3. Thus, the dephasing time of these systems lies in a range of 0.6–0.8 ps, which is a valid range for the echo dephasing of the native globular proteins as observed in the previous studies [18, 19]. In the study performed by Xu et al. [18] $\tau_0$ is 884 fs for pancreatic trypsin inhibitor (BPTI) and for a similar study carried out by K. Schulten et al. 1997 for bacteriorhodopsin, it is 700 fs. In addition, the diffusion and mobility constants of anharmonicity related to $\tau_0$ are listed in Table 2. As observed in Table 2, the dephasing time for THRT3 is a little bit smaller than that of THR. The faster dephasing of hormone binding nuclear receptors means the higher effect of anharmonicity on the normal modes of vibrations when the systems are perturbed suddenly. These parameters help to explore the energy transfer mechanism through the atoms of THRT3 to TREs probing T3-stimulated gene transcription.

## 4 Conclusions

We used the theory of velocity reassignments and temperature echo to study the physical properties of a native globular protein including thyroid hormone responsive features when bounded to thyroid hormone receptors. Performing MD simulations, unliganded THR-β (THR) and T3-bound THR-β LBD (THRT3) were equilibrated up to 7 ns in a cellular environment and then to 1 ns in vacuo at 310 K for the purpose of observing echo features and energy changing patterns with time and temperature in NVE ensembles. The production runs were performed in the microcanonical ensembles under constrained and unconstrained atomic vibrations to explore thermophysical properties such as temperature auto-correlations, temperature dependent hydrogen bonding and radius of gyration, heat capacity, dephasing time constant and constants of diffusion and mobility of anharmonicity. We also evaluated the simulation discrepancies by comparing the results between (a) case of constrained vibrations of H-atoms with 2 fs/step and (b) case of free vibrations of all atoms with 1 fs/step. The estimated decay times of temperature auto-correlation for THR and THRT3 are 3.00 ± 0.03 fs for case (a) and 2.80 ± 0.15 fs for case (b), which are slightly higher than 2.67 fs for bacteriorhodopsin in K. Schulten et al. 1997 [19]. The number of H-bonds of the protein gets a step up jump along with a decrease in radius of gyration at the points of temperature quenching twice to 0 K. The nature of the temperature auto-correlation function as well as echo feature curves is significantly different in cases (a) and (b). The curves are smoother in case (a) and more distinct with shoulders in case (b). Here, we focus on the analysis of changes in temperature and energy because these samples of the molecular systems transform energy from NVT to NVE

ensembles. Due to the change in internal potential energy being a function of temperature, the small fluctuation found in the total energy of the system in the NVE ensemble is only due to the fluctuating values in potential energy terms but not from kinetic energy during the conservation of total energy. It has been verified from graphical analysis that the temperature rate of change of kinetic energy, i.e., heat capacity defined in terms of it, is only the function of degrees of freedom but not of temperature in the molecular system. Thus, the potential energy is the major contributor of heat capacity. In the case of constrained or rigid bonds of H-atoms, the potentials due to bonded terms of H-atoms are not added to the net potential of the system. As a result, the heat capacity found by the temperature echo method is significantly different between cases (a) and (b) that are listed in Table 2. Since the calculations in the case of free vibration of all atoms with 1 fs/step (case-b) are more accurate, the heat capacities ($C_{V2}$) for THR and THRT3 are observed as $11.64 \pm 0.49$ kcal $mol^{-1}$ $K^1 = 1763.63 \pm 74.24$ $Jkg^{-1}$ $K^{-1}$ and $12.21 \pm 0.28$ kcal $mol^{-1}$ $K^{-1} = 1807.43 \pm 41.44$ $Jkg^{-1}$ $K^{-1}$, respectively at about 300 K. These values lie within the range of experimentally observed heat capacities, i.e., 1200 to 2300 $Jkg^{-1}$ $K^{-1}$ for the native proteins studied by Privalov and Potekhin [32] and a little bit higher than $0.298 \pm 0.003$ $ca1g^{-1}$ $K^{-1}$ for the anhydrous proteins studied by Gomez et al. [21]. The results of the heat capacity ($\tilde{C}_{V1}$) obtained from the theory and the simulations match each other with a very strong positive correlation between kinetic energy and temperature ($R^2 = 1$). The dephasing time of the echo pulses has an inverse relation with diffusion and mobility of anharmonicity of the atomic vibrations and ranges from 0.6 to 0.8 ps for THR and THRT3. These parameters are valuable tools for the analytical study of biophysical phenomena associated with echo formation and dephasing, which is important in order to understand the functions of hormone binding nuclear receptors towards the regulation of gene expression.

**Acknowledgements** This work was partially supported by the Nepal Academy of Science and Technology (NAST) through a grant of PhD fellowship to the first author.

## Compliance with ethical standards

**Conflict of interest** The authors declare that they have no conflicts of interest.

**Publisher's note** Springer Nature remains neutral with regard to jurisdictional claims in published maps and institutional affiliations.

## References

1. Álvarez, R.M.S., Cutin, E.H., Farías, R.N.: Conformational changes of 3, 5, 3′-triiodo L-thyronine induced by interactions with phospholipid: physiological speculations. J. Membr. Biol. **205**(2), 61–69 (2005)
2. Souza, P.C.T., Puhl, A.C., Martínez, L., Aparício, R., Nascimento, A.S., Figueira, A.C.M., Nguyen, P., Webb, P., Skaf, M.S., Polikarpov, I.: Identification of a new hormone-binding site on the surface of thyroid hormone receptor. Mol. Endocrinol. **28**(4), 534–545 (2014)
3. Obregon, M.J., del Rey, F.E., de Escobar, G.M.: The effects of iodine deficiency on thyroid hormone deiodination. Thyroid **15**(8), 917–929 (2005)
4. Chiamolera, M.I., Wondisford, F.E.: Thyrotropin-releasing hormone and the thyroid hormone feedback mechanism. Endocrinol. **150**(3), 1091–1096 (2009)
5. Forrest, D., Hanebuth, E., Smeyne, R.J., Everds, N., Stewart, C.L., Wehner, J.M., Curran, T.: Recessive resistance to thyroid hormone in mice lacking thyroid hormone receptor beta: evidence for tissue-specific modulation of receptor function. EMBO J. **15**(12), 3006–3015 (1996)

6. Sandler, B., Webb, P., Apriletti, J.W., Huber, B.R., Togashi, M., Lima, S.T.C., Juric, S., Nilsson, S., Wagner, R., Fletterick, R.J., Baxter, J.D.: Thyroxine-thyroid hormone receptor interactions. J. Biol. Chem. **279**(53), 55801–55808 (2004)
7. Ortiga-Carvalho, T.M., Sidhaye, A.R., Wondisford, F.E.: Thyroid hormone receptors and resistance to thyroid hormone disorders. Nature Rev. Endocrinol. **10**(10), 582 (2004)
8. Zhuang, S., Bao, L., Linhananta, A., Liu, W.: Molecular modeling revealed that ligand dissociation from thyroid hormone receptors is affected by receptor heterodimerization. J. Mol. Graph. Model. **44**, 155–160 (2013)
9. Lu, L., Zhan, T., Ma, M., Xu, C., Wang, J., Zhang, C., Liu, W., Zhuang, S.: Thyroid disruption by bisphenol S analogues via thyroid hormone receptor β: in vitro, in vivo and molecular dynamics simulation study. Environ. Sci. Technol. **52**(11), 6617–6625 (2018)
10. König, G., Brooks, B.R.: Correcting for the free energy costs of bond or angle constraints in molecular dynamics simulations. Biochim. Biophy. Acta **1850**(5), 932–943 (2015)
11. Van Gunsteren, W.F., Berendsen, H.J.C.: Algorithms for macromolecular dynamics and constraint dynamics. Mol. Phys. **34**(5), 1311–1327 (1977)
12. Ryckaert, J.P., Ciccotti, G., Berendsen, H.J.: Numerical integration of the Cartesian equations of motion of a system with constraints: molecular dynamics of n-alkanes. J. Comp. Phys. **23**(3), 327–341 (1977)
13. Van Gunsteren, W.F., Karplus, M.: Effect of constraints on the dynamics of macromolecules. Macromolecules **15**(6), 1528–1544 (1982)
14. Fayer, M.D.: Fast protein dynamics probed with infrared vibrational echo experiments. Annu. Rev. Phys. Chem. **52**(1), 315–356 (2001)
15. Rector, K.D., Kwok, A.S., Ferrante, C., Tokmakoff, A., Rella, C.W., Fayer, M.D.: Vibrational anharmonicity and multilevel vibrational dephasing from vibrational echo beats. J. Chem. Phys. **106**(24), 10027–10036 (1997)
16. Rella, C.W., Kwok, A., Rector, K., Hill, J.R., Schwettman, H.A., Dlott, D.D., Fayer, M.D.: Vibrational echo studies of protein dynamics. Phys. Rev. Lett. **77**(8), 1648 (1996)
17. Noid, W.G., Ezra, G.S., Loring, R.F.: Vibrational echoes: dephasing, rephasing, and the stability of classical trajectories. J. Phys. Chem. B **108**(21), 6536–6543 (2004)
18. Xu, D., Schulten, K., Becker, O.M., Karplus, M.: Temperature quench echoes in proteins. J. Chem. Phys. **103**(8), 3112–3123 (2004)
19. Schulten, K., Lu, H., Bai, L.: Probing protein motion through temperature echoes. In: Phys. Biol. Systems, pp. 117–152. Springer, Heidelberg (1997)
20. Prabhu, N.V., Sharp, K.A.: Heat capacity in proteins. Annu. Rev. Phys. Chem. **56**, 521–548 (2005)
21. Gomez, J., Hilser, V.J., Xie, D., Freire, E.: The heat capacity of proteins. Proteins **22**(4), 404–412 (1995)
22. Fujisaki, H., Zhang, Y., Straub, J.E.: Time-dependent perturbation theory for vibrational energy relaxation and dephasing in peptides and proteins. J. Chem. Phys. **124**(14), 144910 (2006)
23. Nascimento, A.S., Dias, S.M.G., Nunes, F.M., Aparício, R., Ambrosio, A.L., Bleicher, L., Figueira, A.C.M., Santos, M.A.M., de Oliveira Neto, M., Fischer, H., Togashi, M.: Structural rearrangements in the thyroid hormone receptor hinge domain and their putative role in the receptor function. J. Mol. Biol. **360**(3), 586–598 (2006)
24. MacKerell, A.D., Feig, M., Brooks, C.L.: Extending the treatment of backbone energetics in protein force fields: limitations of gas-phase quantum mechanics in reproducing protein conformational distributions in molecular dynamics simulations. J. Comp. Chem. **25**(11), 1400–1415 (2004)
25. MacKerell Jr., A.D., Bashford, D., Bellott, M.L.D.R., Dunbrack Jr., R.L., Evanseck, J.D., Field, M.J., Fischer, S., Gao, J., Guo, H., Ha, S.: Joseph-McCarthy, D.: all-atom empirical potential for molecular modeling and dynamics studies of proteins. J. Phys. Chem. B **102**(18), 3586–3616 (1998)
26. Zoete, V., Cuendet, M.A., Grosdidier, A., Michielin, O.: Swiss Param: a fast force field generation tool for small organic molecules. J. Comp. Chem. **32**(11), 2359–2368 (2011)
27. Phillips, J.C., Braun, R., Wang, W., Gumbart, J., Tajkhorshid, E., Villa, E., Chipot, C., Skeel, R.D., Kale, L., Schulten, K.: Scalable molecular dynamics with NAMD. J. Comp. Chem. **26**(16), 1781–1802 (2005)
28. Humphrey, W., Dalke, A., Schulten, K.: VMD: visual molecular dynamics. J. Mol. Graph. **14**(1), 33–38 (1996)
29. Verlet, L.: Computer "experiments" on classical fluids. I. Thermodynamical properties of Lennard–Jones molecules. Phys. Rev. **159**(1), 98–103 (1996)
30. Rahat, O., Alon, U., Levy, Y., Schreiber, G.: Understanding hydrogen-bond patterns in proteins using network motifs. Bioinformatics **25**(22), 2921–2928 (2009)
31. Lobanov, M.Y., Bogatyreva, N.S., Galzitskaya, O.V.: Radius of gyration as an indicator of protein structure compactness. Mol. Biol. **42**(4), 623–628 (2008)
32. Privalov, P.L., Potekhin, S.A.: Scanning microcalorimetry in studying temperature-induced changes in proteins. In: Methods Enzymol., pp. 4–51. Academic Press (1986)

**BIBECHANA**
A Multidisciplinary Journal of Science, Technology and Mathematics
ISSN 2091-0762 (Print), 2382-5340 (0nline)
Journal homepage: http://nepjol.info/index.php/BIBECHANA
**Publisher: Research Council of Science and Technology, Biratnagar, Nepal**

# Molecular dynamics approach to the I431V mutational impact on thyroid hormone receptor-beta

**Tika Ram Lamichhane[1], Sharma Paudel[2], Binod Kumar Yadav[2], Hari Prasad Lamichhane[1*]**

[1]Central Department of Physics, Tribhuvan University, Kirtipur, Kathmandu, Nepal
[2]Institute of Medicine, Tribhuvan University, Teaching Hospital, Maharajgunj, Kathmandu, Nepal
*Email: hlamichhane1@gmail.com

***Article history: Received 15 March, 2018; Accepted 16 September, 2018***
DOI: http://dx.doi.org/10.3126/bibechana.v13i0.21109

This work is licensed under the Creative Commons CC BY-NC License.
https://creativecommons.org/licenses/by-nc/4.0/

**Abstract**

The point mutations like I431V on thyroid hormone receptor-beta (THR-β) gene cause resistance to thyroid hormones (RTH) with the clinical diagnosis of elevated free triiodothyronine (T3) and free thyroxin (T4) but not suppressed thyroid stimulating hormone (TSH) on the blood serum. Some ultrasonographic (USG) reports of the patients with RTH show thyroid gland disorder with goiter or nodule(s) or cyst(s) and some USG reports even with RTH are normal. I431V-mutant causes more steric hindrance while binding T3 into THR-β than the native wild type THRT3. The residue on the 431-codon is dynamic in nature showing its flexibility over the course of entry and release of T3-hormone into/from the ligand binding pocket. The more increased solvent accessible surface area of I431V-mutant than that of native I431-residue makes the partial unfolding of the globular THR-β protein. The smaller height of radial distribution function between I431-mutant and T3 shows the decrease in probability of finding the atomic particles nearby T3-hormone in THRT3-MT than in THRT3-WT. The electrostatic interaction energy between native I431 and T3 is negative, but it is positive between I431V and T3. Moreover, the internal energy of I431V-mutant has been found smaller than that of native I431-residue in THRT3 systems.

**Keywords:** Thyroid hormone receptor; resistance to thyroid hormones; point mutation; interaction energy; internal energy.

## 1. Introduction

Thyroid hormone receptors (THRs) are the nuclear receptor proteins that actively bind triiodothyronine (T3: hormone secreted by thyroid gland) to mediate the biological activities associated with gene transcription. THRs regulate gene expressions upon binding to the DNA sequences called as thyroid response elements (TREs). THRs have two isoforms THR-α and THR-β that are in hetero-diversity in the different organs. T3 has the higher affinity to bind into both isoforms than thyroxin (T4). While T3

binds to the ligand binding domain (LBD) of hydrophobicity, THR shows its structural change [1-4]. The carboxy-terminal activation domain forms an amphi-pathic helix[2, 3] as a part of cavity or LBD. The dynamic nature of helix-12 (H12 in Fig. 2-c) of THR is is important for the hormone binding, ligand dissociation, activation mechanism and regulation of transcription activity [5].

The mutational impact on THR reduces the hormone binding affinity and gene expression activity. Ultimately, the mutations leading to the resistance to thyroid hormone (RTH) cause the endocrine disorder. The inactivated THR-β gene by means of homozygous mutant (*Thrb*$^{-/-}$) in mice results in a goiter and elevated levels of thyroid hormones [6]. The mutant T327I found in THR-β gene shows the paucity of symptoms and signs of thyroid dysfunction suggesting RTH despite the increased serum levels of T3, T4 and thyroid stimulating hormone (TSH) [7]. A rare mutation A268G found in axon 9 of THR-β gene results RTH with elevated serum T3 and T4, TSH in the normal range and the episodic palpitations associated with mild dizziness [8]. A heterogeneous mutation G344R is identified in axon 10 of THR-β gene of 10-month-old-female resulting in paucity of symptoms of RTH with normal T3, T4 and TSH levels [9]. Also, R383H mutation is found in THR-β gene of a woman with inappropriate central secretion of TSH despite of elevated T3 and T4 [10]. The RTH patients are clinically euthyroid or hypothyroid depending on severity of mutation. A point mutation R429Q found in mice has the elevated serum thyroid hormones but the inappropriate TSH consistent with hypothalamic-pituitary RTH [11]. The active sites of these point mutations along with the site of I431V-mutant [12] in the THR-β gene are indicated in Fig. (2-c). The helix-12 serves as a selective gatekeeper which is responsible for corepressor specificity by the wild type receptor (THR-WT). The point mutations in THR are all positioned to impact the gatekeeper functions and then to change corepressor specificity by the mutated receptor (THR-MT) [13, 14]. THR-WTs regulate normal physiological and developmental pathways, but THR-MTs result neoplastic and endocrine diseases.

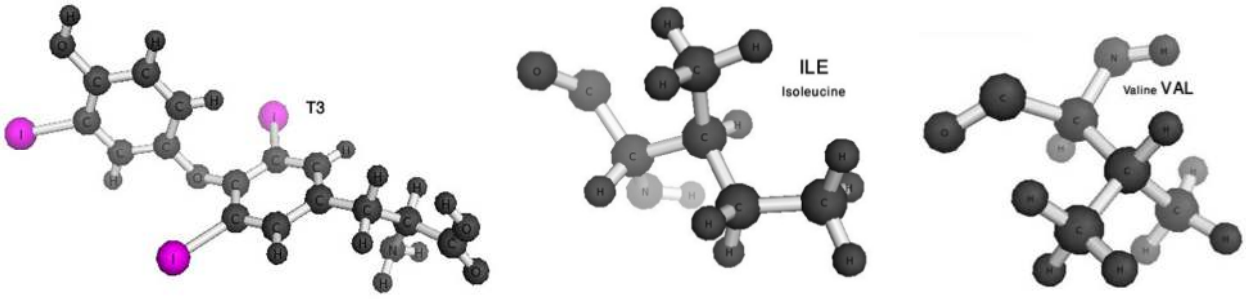


(a) (b) (c)

**Fig. 1:** Chemical structures of (a) triiodothyronine (T3): $C_{15}H_{12}I_3NO_4$ with molar mass = 650.98 g/mol, (b) isoleucine (ILE): $C_6H_{13}NO_2$ with molar mass = 131.17 g/mol and (c) valine (VAL): $C_5H_{11}NO_2$ with molar mass = 117.15 g/mol[prepared from PyMOL molecular graphics system].

The I431V point mutation is detected experimentally in THR-β gene of a 14-year-old Brazilian girl with elevated T3 and T4 but unsuppressed TSH showing RTH with goiter [12]. This mutation occurs

by replacing isoleucine (ILE) amino acid residue by valine (VAL) in 431 codon of THR-β gene. I431V mutation exerts impairment of ligand-dependent release of corepressor, silencing mediator for retinoid and thyroid receptors (SMRT) with dominant negative effects on THR-WT and reducing potency. The chemical structures of T3, ILE and VAL are shown in Fig. 1. ILE is heavier and larger in size than VAL. T3 binding assay [12] shows that the hormone binding affinity of I431V-mutant THR-β is 2.6 times lower than that in wild type THR-β. THR-WT, THRT3-WT and THRT3-MT show the distinct features reflecting in terms of root mean square deviation (RMSD), radius of gyration ($R_g$), root mean square fluctuation (RMSF), IR spectra, radial distribution functions, solvent accessible surface area (SASA), interaction energy, internal energy, etc. The structural and physical properties of the wild type and the mutated protein-hormone systems can be studied by using molecular dynamics simulations (MDS).

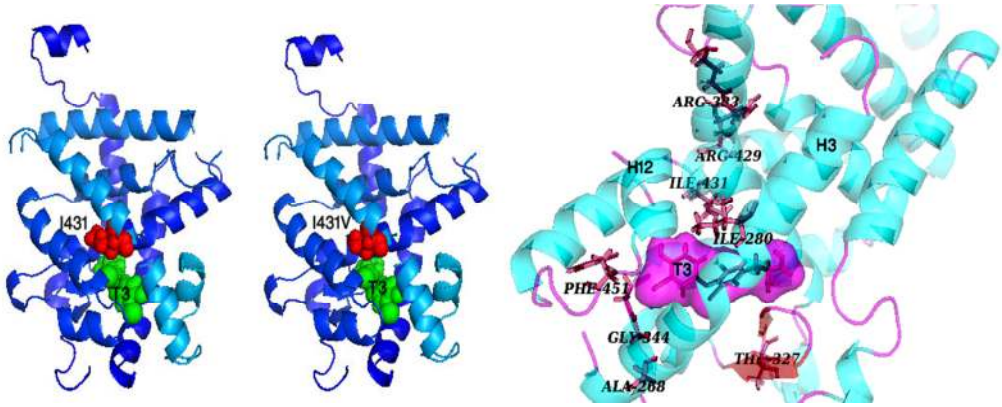


(a) (b) (c)

**Fig.2:** (a) Wild type THR-β highlighting with I431 codon and T3 hormone, (b) I431V-mutant on THR-β gene and (c) experimentally observed mutational sites on THR-β gene [7-12]. The images are prepared from PyMOL molecular graphics system.

## 2. Methodology

The structure of wild type THRT3 was taken from the x-ray crystallographic data of protein data bank code-3GwS [15]. The CHARMM force field topologies and parameters [16, 17, 18, 19] were used for MDS of the protein-hormone systems. The hetero-atomic T3-hormone was parameterized first to describe its molecular geometry, atomic masses, charges and torsion barriers [19]. The generation of the complete systems of THR-WT, THRT3-WT and THRT3-MT starting from their protein structure files to the solvation in neutral water-ion environment, equilibration, production runs and analysis of the results were performed by using the interfaces of visual molecular dynamics (VMD) [20] and nanoscale molecular dynamics (NAMD) [21] computational packages.

From the wild type native structure of THRT3, the mutated THRT3 was made after the point mutation on 431-codon replacing ILE by VAL with the help of VMD-Mutagenesis. Unliganded THR-WT, T3-liganded THRT3-WT and I431V-mutant THRT3-MT were solvated separately in the TIP3P water-box

which was neutralized with $Na^+$ & $Cl^-$ ions in the concentration of 0.15 mol/L. Each water-box has the periodic cell basis vectors 50.35, 61.92 and 74.78 Å along x, y and z-axes, respectively.

Configuration files were prepared by writing TCL-scripts to simulate the systems for which Langevin piston temperature, pressure and damping coefficient are 310 K, 1 bar and 1 $ps^{-1}$, respectively. Oscillation period of the piston was 100 fs with decay time of 50 fs and periodic cell fluctuation was isotropic. The Langevin dynamics [22, 23] was applied for all atoms except hydrogens of the systems. Particle mesh Ewald (PME) was active with the grid dimensions of (54, 64, 80Å) and the PME coefficient of 0.258 for the electrostatic force evaluation [24]. In adjusting the force field parameters used in MDS, 1-4 scaling was 1.0; cut-off, switching and pair-list distances for the electrostatic and van der Waals interactions were 12, 10 and 14 Å, respectively. Finally, each system was geometrically optimized with 3000 conjugate gradient steps and then it was equilibrated up to 2ns at 310 K. To calculate the trajectory of atomic particles, the velocity Verlet algorithm [25] was used during MDS of the systems. All the simulations were performed adjusting integrator parameters of 2 fs/step constrained with rigid bonds of H-atoms.

Conformational stability of the protein-hormone systems was tested by plotting RMSD, RG, RMSF and SASA of protein backbone, T3-hormone and residues of interest: I431 and I431V of THR-WT, THRT3-WT and THRT3-MT. The dihedral angle distributions were analyzed from Ramachandran plots to test the steric hindrance among α-helices, β-sheets and side chains and residues of the systems. The electrostatic and van der Waals interactions were observed between the native or mutated residue on 431-codon and T3-hormone by using NAMD-Energy-GUI. Also, number of H-bonding, probability density from radial distribution functions, IR spectral densities, internal energies of the native wild type and mutated systems were calculated, analyzed and compared by plotting the corresponding results over the simulation time.

## 3. Result and Discussion

THR-β nuclear receptor isoform consists of a chain length of 259 amino acid residues. The protein structure of wild type THR-β that we take for the simulation has total mass of 27640 amu and 3895 atoms. The active ligand bound to the LBD of THR-β is the thyroid hormone (T3) which has mass of 651 amu and 35 atoms. The plots of dihedral angles (ϕ,ψ), i. e. Ramachandran plots for THR-WT, THRT3-WT and I431V mutant THRT3-MT are shown in Fig. 3. In these plots, most of the amino acid residues of parallel, anti-parallel and right twisted β-sheets lie in the blue region of I-quadrant; that of right handed α-helix lie in the blue region of II-quadrant and left handed α-helix lie in the green region of III-quadrant [26, 27]. The residue GLY has no side chain so that it has no steric hindrance and it is allowed in the white region. The white region is sterically disallowed for all other amino acids except GLY. The blue regions are the most allowed regions for α-helices and β-sheets. The green area is allowed for the shorter van der Waal radii of atoms and the related amino acids. By comparing three plots of Fig. 2, we observe that smaller number of amino acid residues lies in the disallowed region for THRT3-WT than for THR-WT and THRT3-I431V. Thus, the larger steric hindrances occur for the unliganded and mutated THR-β. The clinical analysis shows that THRT3-WT is related to euthyroid or normal thyroid functions, THR-WT is related to overt thyroidism and THRT3-MT is related to RTH [6-14].

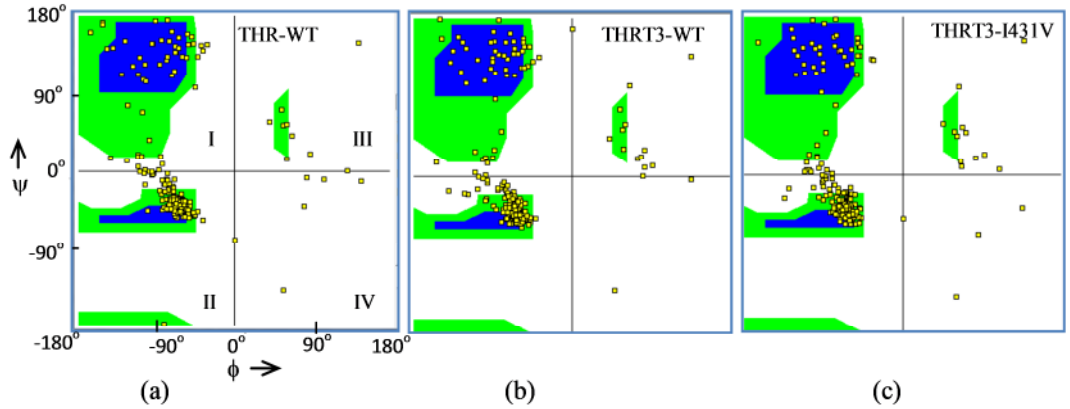


**Fig. 3:**Ramachandran plots for (a) wild type THR-β, (b) T3-liganded wild type THR-β and (c) I431V-mutant THRT3.

The constancy of root mean square deviation (RMSD) and radius of gyration (RG) of the molecules THR-β protein and T3-hormone over the time frames of equilibration run (Fig. 4, 5) show the conformational stability and validity of force field topology and parameters used for MDS of wild type and mutated nuclear receptors. The more fluctuating RMSD and RG of residue ID-431 show its dynamic property. This dynamic property of the residues is significantly important while trapping T3 in and releasing T3 from the LBD of thyroid hormone receptors.

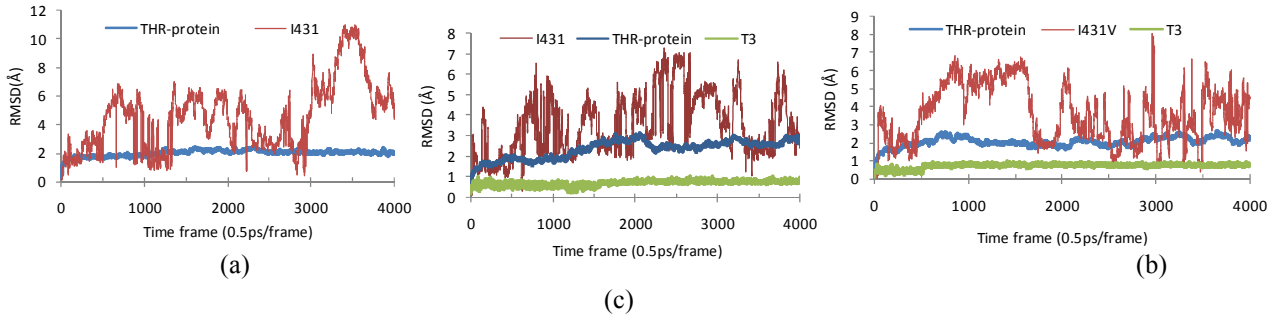


**Fig.4:** RMSD-plots of 431 residue, THR-protein and T3-hormone during equilibration of (a) wild type THR, (b) wild type THRT3 and (c) I431V-mutant THRT3.

The values of RMSD and RG of the molecules with the standard deviations of the data are listed in the Table 1. During their 2 ns equilibration run in neutral water-ion environment, RG of 431-residue of THR-WT is being smaller with larger RMSD, i.e. it is bending more towards the center of mass of the system than that of THRT3-WT and THRT3-MT. In other words, the nature of RMSD of 431-residue change from unliganded to liganded as well as wild type to mutated THR-β. The RMSD or RG of the protein is almost same with small fluctuations for these three cases. The protein RMSD is about 2 Å and the protein RG is about 19 Å for the wild type and the mutated THR-β systems. The RMSD

and RG of T3-hormone while bounded in the LBD of nuclear receptors are 0.7 Å and 4.3 Å respectively.

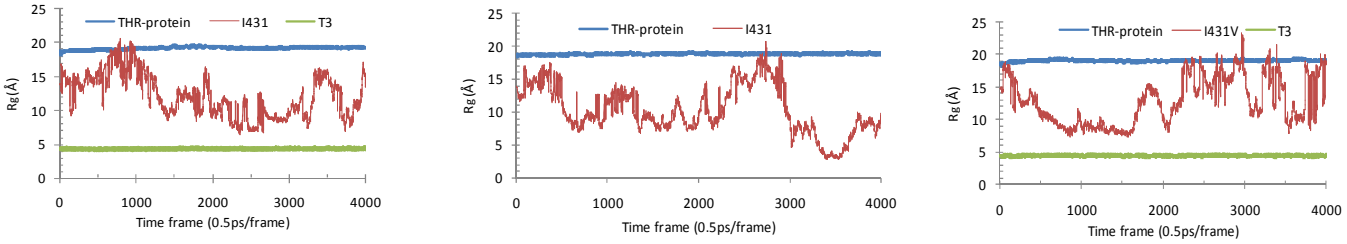


(a) (b) (c)

**Fig. 5:** RG-plots of 431 residue, THR-protein and T3-hormone during equilibration of (a) wild type THR, (b) wild type THRT3 and (c) I431V-mutant THRT3.

**Table 1:** Average values of root mean square deviation (RMSD) and radius of gyration (RG) of unliganded wild type and T3-liganded wild type and I431V-mutant THR-β including with the standard deviation of the data obtained after MDS by their equilibration runs.

| Molecule | THR-WT | | THRT3-WT | | | THRT3-MT | | |
|---|---|---|---|---|---|---|---|---|
| | I431 | protein | I431 | T3 | protein | I431V | T3 | protein |
| RMSD(Å) | 4.6 ± 2.4 | 2.0 ± 0.2 | 3.6 ± 1.6 | 0.7 ± 0.1 | 2.0 ± 0.3 | 3.5 ± 1.5 | 0.7 ± 0.1 | 2.3 ± 0.4 |
| RG(Å) | 10.3 ± 3.7 | 18.8 ± 0.1 | 12.1 ± 3.1 | 4.3 ± 0.1 | 19.2 ± 0.2 | 12.8 ± 3.6 | 4.3 ± 0.1 | 19.1 ± 0.1 |

In this study, the root mean square fluctuations (RMSF) of most of the residues of THRT3-WT are observed to be a little bit larger than that of THR-WT and THRT3-MT as shown in Fig. 6. In the I431V mutational site, the values of RMSF are 3.2 Å for ILE of THR-WT, 4.1 Å for ILE of THRT3-WT and 3.0 Å for VAL of THRT3-MT. The residues in helix-1 have the highest RMSF so that the helix-1in THRT3-WT is more flexible.

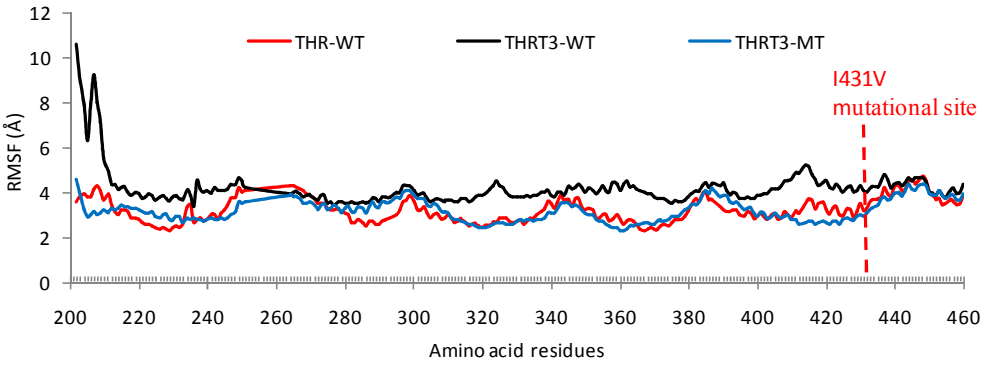


**Fig. 6:** RMSF of amino acid residues of THR-WT, THRT3-WT and I431V-mutant THRT3-MT during their 2 ns equilibration run.

Solvent accessible surface area (SASA) of THR-WT, THRT3-WT and THRT3-MT are observed to be slightly different in the extension radius of 1.4 Å. After 500 frames of energy minimization and equilibration, the SASA with the standard deviation of the data from frame to frame simulation up to 2 ns is 13620.1 ± 253.07 $Å^2$ for THR-WT, 13952.4 ± 130.9 $Å^2$ for THRT3-WT and 13721.0 ± 147.9 $Å^2$ for THRT3-MT. In this way, the SASA of 431-residue is 14.8 ± 9.0 $Å^2$ for THR-WT, 12.6 ± 10.1 $Å^2$ for THRT3-WT and 17.4 ± 8.1 $Å^2$ for THRT3-MT. The lower SASA indicates the higher thermodynamic stability of the protein. The SASA of T3-hormone is observed to be zero indicating the hydrophobicity of LBD of THR-β. The mutation on the solvent accessible residue causes the conformational change by partial unfolding of the protein with increasing SASA [28]. Such effect is more intensive if the mutation occurs on the surface residue than on the interior of the protein. The I431V mutation is the interior one so that no significant change in SASA of wild type and mutated THR-β has been observed after their 2 ns equilibration. However, the total SASA of THR-WT and THRT3-MT are more fluctuating than that of THRT3-WT up to 3000 frames of the equilibration runs (Fig. 7-a). Furthermore, SASA of I431V-mutant is higher and less fluctuating than that of native and wild type I431-rsidue of THR-β (Fig.7-b).

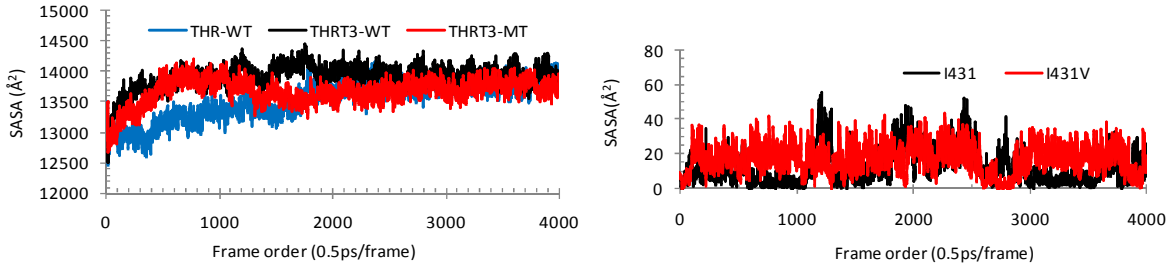


(a) (b)

**Fig. 7:** (a) SASA of protein in wild type THR, THRT3 and mutated-THRT3, (b) SASA of I431 residue in THRT3-WT and I431V mutant in THRT3-MT during their equilibration runs.

The distributions of number of H-bonds along with the frame order of the simulations up to 2 ns equilibrations are shown in Fig. 8. Here, the average values of H-bond number with the standard deviation of the data after 500 frames with the donor-acceptor distance 4.0 Å and cut-off angle 40° among N and O atoms are 5 ± 2 for I431-THR(WT), 16 ± 4 for T3-THR(WT), 4 ± 2 for I431-THR(MT) and 15 ± 4 for T3-THR(MT).

During MDS of the wild type and mutated THR-β systems, the distance between I431 and T3 in THRT3-WT varies as 10.2 ± 2.6 Å and the distance between I431V and T3 in THRT3-MT varies as 13.1 ± 2.0 Å as shown in Fig. 9-b. Such distance is smaller and more fluctuating in THRT3-WT than in THRT3-MT. This is one of the indicators of T3 resistant features of mutated nuclear receptor proteins that cause RTH.

Radial distribution function [29] or pair auto-correlation function g(r) in a system of particles measures probability of finding a particle at r distance away from the reference particle. The distribution function g(r) between I431-residue and T3-hormone has the higher value than that between I431V and T3

and it lies in the range of 5 Å and 18 Å as shown in Fig. 9-c. In other words, the number density of mutated residue is less than that of the native wild type residue to respond for T3-hormone and TREs.

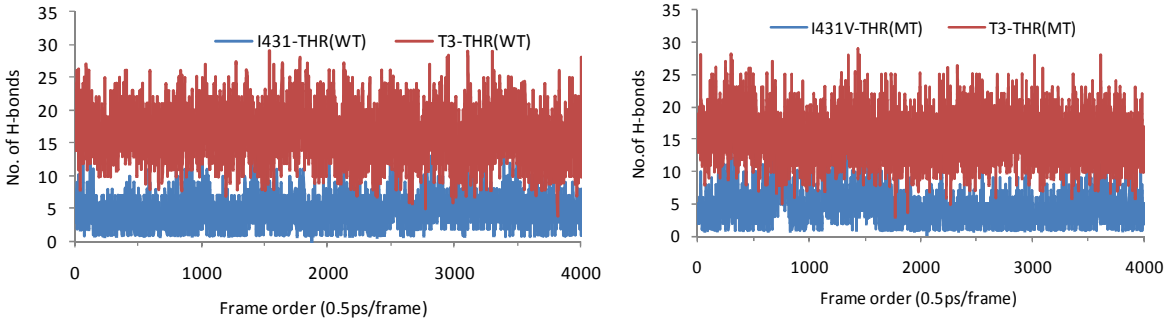


(a) (b)

**Fig. 8:** Variation of number of H-bonds between 431-residue and protein vs. simulation time in case of (a) wild type and (b) I431V-mutant THRT3 systems.

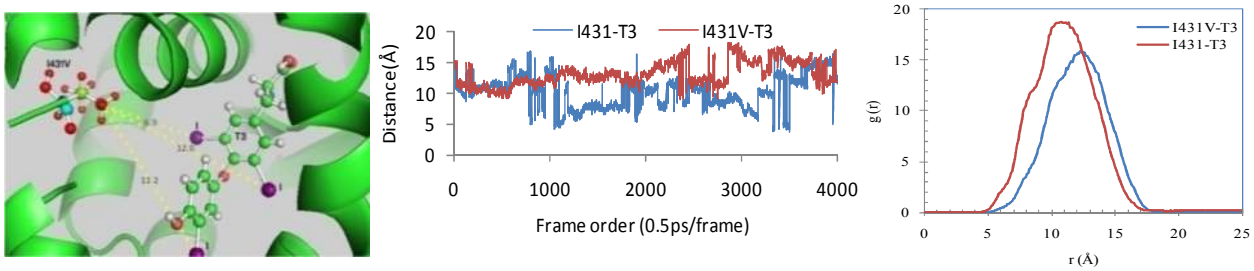


(a) (b) (c)

**Fig. 9:** (a) Positions of I431V-mutant and T3-hormone in THRT3-MT, (b) changing distance between 431-codon and T3 while equilibrating THRT3-WT and THRT3-MT systems and (c) radial distribution functions between 431-residue and T3-hormone in case of wild type and mutated THRT3.

IR spectral densities using total dipole moment of the atoms in 431-residue and T3 are calculated in the frequency range of 0 to 2000 $cm^{-1}$ and their plots are different for THRT3-WT and THRT3-MT as shown in Fig. 10. The maximum IR-intensity of T3 in the wild type receptor is 0.041 at 1837.42 $cm^{-1}$ and that of I431 (wild type) is 0.027 at 1637.88 $cm^{-1}$. Again, the maximum IR-intensity of T3 in the mutated receptor is 0.037 at 1313.63 $cm^{-1}$ and that for I431V-mutant is 0.029 at 1571.37 $cm^{-1}$. The distribution has larger number of high intensity peaks for T3 and I431V in THRT3-MT than in THRT3-WT.

Total non-bonding interaction energy is the sum of electrostatic and van der Waal's interaction energy. The changing values of interaction energy between 431-residue and T3-hormone in wild type and mutated THR-β systems are plotted with respect to the frame order in Fig. 11 and these are averaged

over the time frames from 500 to 4013. The average values of electrostatic and van der Waals interaction energy (from NAMD-Energy-GUI using switching and cut-off distances of 10 Å and 12 Å, respectively) with their standard deviations are -0.25 ± 0.17 kcal/mol and -0.18 ± 0.07 kcal/mol between I431 and T3 of THRT3-WT and 0.21 ± 0.08 kcal/mol and -0.07 ± 0.05 kcal/mol between I431V and T3 of THRT3-MT, respectively. Thus, the electrostatic energy between I431 and T3 in THRT3-WT is negative and more fluctuating and that between I431V and T3 in THRT3-MT is positive and less fluctuating over the simulation time.

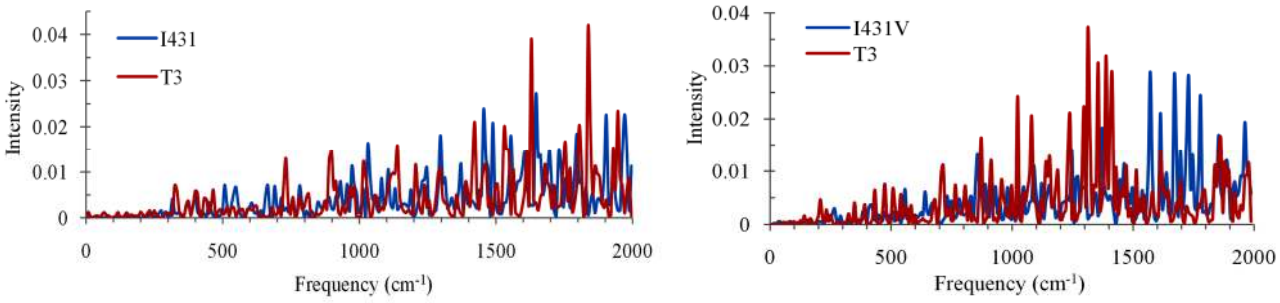


(a) (b)

**Fig. 10:** IR spectra of (a) I431 residue and T3-hormone in wild type THRT3 and (b) I431V-mutant and T3-hormone in mutated THRT3.

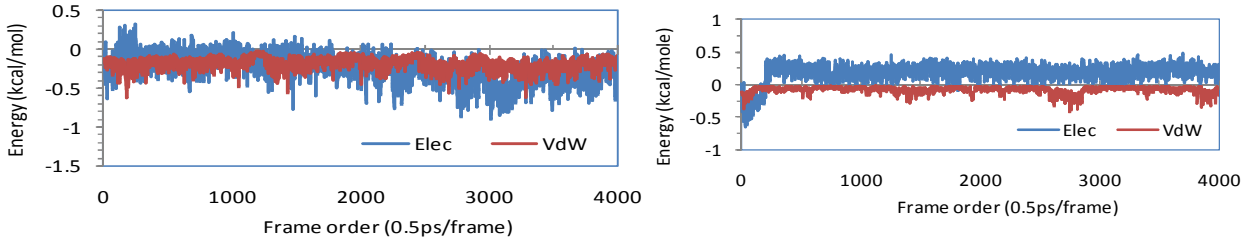


(a) (b)

**Fig. 11:** Electrostatic and van der Waals interaction energies (a) between I431 and T3 in wild type THRT3 and (b) between I431V and T3 in mutated THRT3.

Internal energy of the biomolecular system is the sum of bonding and non-bonding potentials. Coulomb energy is the largest and its fluctuation during SMD makes the total internal energy fluctuate about its mean value. Using NAMD-Energy-GUI with switching and cut-off distances of 10 Å and 12 Å, the internal energy of 431-residue, bounded T3-hormone and protein of THR-WT, THRT3-WT and THRT3-MT are calculated and the average values for the corresponding systems are listed in the Table 2. The variations of the related internal energy with respect to the simulation time are plotted in the Fig. 12. The plots for the individual potential terms show that the major contributor of fluctuations in the internal energy is the electrostatic energy of the related system.

**Table 2:** Internal energy of the components of unliganded wild type, T3-liganded wild type and I431V-mutant THR-β systems averaged over the values from the last 0.25 ns of their equilibrations where the including error represents standard deviation of the data.

| Molecule | THR-WT | | THRT3-WT | | | THRT3-MT | | |
|---|---|---|---|---|---|---|---|---|
| | I431 | protein | I431 | T3 | protein | I431V | T3 | protein |
| Int. energy (kcal/mol) | 42.82 ± 3.21 | -822.38 ± 67.67 | 42.88 ± 3.18 | 128.73 ± 4.52 | -644.21 ± 109.87 | 36.13 ± 3.07 | 124.41 ± 4.63 | -756.54 ± 104.22 |

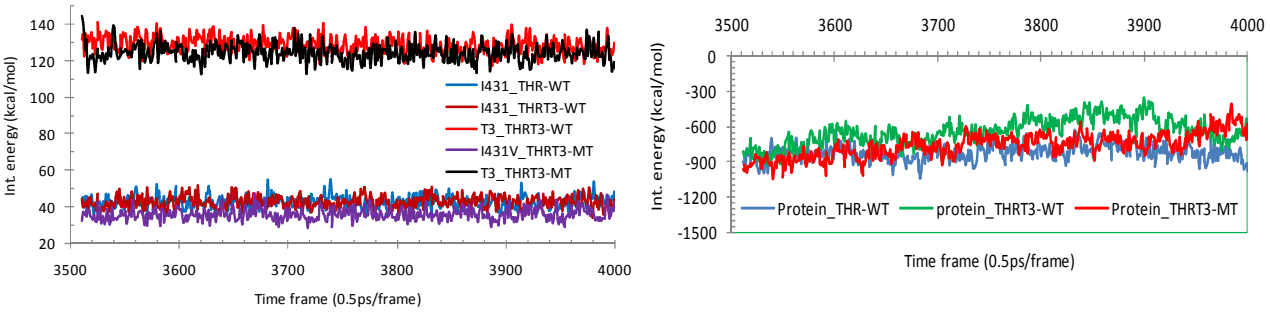


(a) (b)

**Fig. 12:** Fluctuating total internal energy along the frame order of (a) I431-residue and T3, and (b) THR-proteins for unliganded as well as T3-liganded wild type and I431V-muatant THR-β systems in the last 0.25 ns of their equilibrations.

## 4. Conclusion

Conformational properties and interactions of mutational residues and T3-hormone of unliganded and T3-liganded thyroid hormone receptor-beta (THR-β) can be studied by means of molecular dynamics simulations (MDS). The almost constant values of root mean square deviation (RMSD ≈ 2 Å) and radius of gyration (RG ≈ 19 Å) of native and I431-mutant THR-β proteins show their conformational stability during MDS. The native I431-residue has largely fluctuating RMSD and RG showing its dynamic property in adapting and releasing T3-hormone. The experimentally verified I431V mutation on THR-β gene (Ferreira *et al.*, 2010) is the subject of this computational study. This mutation causes resistance to thyroid hormones [12]. Solvent accessible surface area (SASA) is larger for the I431V-mutant indicating partial unfolding of the globular protein. However, the root mean square fluctuation of I431V-mutant is smaller in comparison with that of native wild type I431. The SASA of T3 is zero verifying the hydrophobicity upon binding to the ligand binding domain (LBD) of THR-β.

Comparing the radial distribution functions g(r) for the atomic particles between I431 and T3 as well as I431V and T3, the probability density is higher in the former wild type than the latter mutated type for which g(r) covers the distance of 5 Å to 18 Å. IR spectral density calculations for I431-residue and T3-hormone in the frequency range of 0-2000 $cm^{-1}$ imply that greater number of intensity maxima is found in THRT3-MT than in THRT3-WT. This signifies higher dipole moment distributions by supporting less globular stability of the mutated THR-β than that of the wild type THR-β. Furthermore, electrostatic interaction energy between I431V-mutant and T3 is positive whereas it is negative between

native I431-residue and T3. In this study, internal energy of the native I431-residue is 42.88 ± 3.18 kcal/mol and that of wild type I431V-mutant is 36.13 ± 3.07 kcal/mol in THRT3 systems. The major contributor of such change in the internal energy is the electrostatic energy.

## Acknowledgement

This work was partially supported by Nepal Academy of Science and Technology (NAST) as the Ph. D. fellowship grant to the first author. The computing facility was provided by Central Department of Physics, Tribhuvan University, Kathmandu, Nepal.

## References

[1] L. Martínez, I. Polikarpov, M. S. Skaf, Only subtle protein conformational adaptations are required for ligand binding to thyroid hormone receptors: simulations using a novel multipoint steered molecular dynamics approach,J. Phys. Chem. B 112 (2008) 10741–10751. doi.org/10.1021/jp803403c.

[2] L. Martínez, P. C. T. Souza, W. Garcia, F. A. Batista, R. V. Portugal, A. S. Nascimento, M. Nakahira, L. M. Lima, I. Polikarpov, M. S. Skaf, On the denaturation mechanisms of the ligand binding domain of thyroid hormone receptors, J. Phys. Chem. B 114 (2010) 1529–1540. doi.org/ 10.1021/jp911554p.

[3] R. L. Wagner, J. W. Apriletti, M. E. McGrath, B. L. West, J. D. Baxter, R. J. Fletterick, A structural role for hormone in the thyroid hormone receptor, Nature 378 (1995) 690–697.doi.org/0.1038/378690a0.

[4] R. V. Weatherman, R. J. Fletterick, T. S. Scanlan, Nuclear-receptor ligands and ligand-binding domains, Annu. Rev. Biochem. 68 (1999) 559–581.doi.org/10.1146/annurev.biochem.68.1.559.

[5] B. C. Kallenberger, J. D. Love, V. K. Chatterjee, J. W. Schwabe, A dynamic mechanism of nuclear receptor activation and its perturbation in a human disease, Nat. Struct. Biol.10 (2003) 136–140.doi.org/10.1038/nsb892.

[6] D. Forrest, E. Hanebuth, R. J. Smeyne, N. Everds, C. L. Stewart, J. M. Wehner, T. Curran, Recessive resistance to thyroid hormone in mice lacking thyroid hormone receptor beta: evidence for tissue-specific modulation of receptor function, EMBO J. 15 (1996) 3006-3015.doi.org/10.1002/j.1460-2075.1996.tb00664.x.

[7] J. H. Lee, E. Y. Kim, Resistance to thyroid hormone due to a novel mutation of thyroid hormone receptor beta gene, *Ann. Pediatr. Endocrinol. Metab.*19 (2014) 229-231. doi.org/10.6065/apem.2014.19.4.229.

[8] K. El Shafie, A. Ouhtit, Y. Al Farsi, A. Al Sayegh, M. Al Shafaee, A rare thyroid hormone receptor beta (THRβ) gene mutation in a 15-year-old girl with thyroid hormone resistance syndrome: a case report, J. Med. Case Rep. 8 (2014) 12. doi.org/ 10.1186/1752-1947-8-12.

[9] W. Yang, J. Yan, Y. Sang , Resistance to thyroid hormone caused by a G344R mutation of thyroid hormone receptor beta gene: A case report study,Endocrinol. Metab.Synd. 5 (2016) 231.doi.org/10.4172/2161-1017.1000231.

[10] J. D. Safer, M. G. O'connor, S. D. Colan, S. Srinivasan, S. R. Tollin, F. E. Wondisford, The thyroid hormone receptor-β gene mutation R383H is associated with isolated central resistance to thyroid hormone, J. Clin. Endocrinol.Metab. 84 (1999) 3099-3109.doi.org/10.1210/jcem.84.9.5985.

[11] D. S. Machado, A. Sabet, L. A. Santiago, A. R. Sidhaye, M. I. Chiamolera, T. M. Ortiga-Carvalho, F. E. Wondisford, A thyroid hormone receptor mutation that dissociates thyroid hormone regulation of gene expression in vivo, Pro. Natl. Acad. Sci. 106 (2009) 9441-9446.doi.org/10.1073/pnas.0903227106.

[12] M. Ferreira Azevedo, G. B. Barra, L. D. D. Medeiros, L. A. Simeoni, L. A. Naves, F. D. A. R. Neves, A novel mutation of thyroid hormone receptor beta (I431V) impairs corepressor release, and induces thyroid hormone resistance syndrome, Arq. Bras.Endocrinol.Metab. 52 (2008) 1304-1312. doi.org/10.1590/S0004-27302008000800016.

[13] M. D. Rosen, M. L. Privalsky, Thyroid hormone receptor mutations in cancer and resistance to thyroid hormone: perspective and prognosis, J. Thyroid Research, 2011 (2011) 20.doi.org/10.4061/2011/361304.

[14] M. D. Rosen, M. L. Privalsky,Thyroid hormone receptor mutations found in renal clear cell carcinomas alter corepressor release and reveal helix 12 as key determinant of corepressor specificity, Mol. Endocrinol. 23 (2009) 1183-1192. doi.org/10.1210/me.2009-0126.

[15] A.S. Nascimento, S. M. G. Dias, F. M. Nunes, R. Aparício, A. L. Ambrosio, Bleicher, L., A. C. M. Figueira, M. A. M. Santos, M. de Oliveira Neto, H. Fischer, M. Togashi, Structural rearrangements in the thyroid hormone receptor hinge domain and their putative role in the receptor function, J. Mol. Biol. 360 (2006) 586-598.doi.org/10.1016/j.jmb.2006.05.008.

[16] A. D. MacKerell, M. Feig, C. L. Brooks, Extending the treatment of backbone energetics in protein force fields: Limitations of gas-phase quantum mechanics in reproducing protein conformational distributions in molecular dynamics simulations, J. Comp. Chem. 25(2004) 1400-1415. doi.org/10.1002/jcc.20065.

[17] A. D. MacKerell, D. Bashford, M. Bellott, R. L. Dunbrack, J. D. Evanseck, M. J. Field, S. Fischer, J. Gao, H. Guo, S. Ha, D. Joseph-McCarthy, All-atom empirical potential for molecular modeling and dynamics studies of proteins, J. Phys. Chem. B 102 (1998) 3586–3616. doi.org/10.1021/jp973084f.

[18] W. L. Jorgensen, J. Chandrasekhar, J. D. Madura, R. W. Impey, M. L. Klein, Comparison of simple potential functions for simulating liquid water, J. Chem. Phys. 79 (1983) 926–935. doi.org/10.1063/1.445869.

[19] V. Zoete, M. A. Cuendet, A. Grosdidier, O. Michielin, SwissParam: a fast force field generation tool for small organic molecules, J. Comp. Chem.32(2011) 2359-2368. doi.org/ 10.1002/jcc.21816.

[20] W. Humphrey, A. Dalke, K. Schulten, VMD—Visual Molecular Dynamics, J. Mol. Graphics 14 (1996) 33–38. doi.org/10.1016/0263-7855(96)00018-5.

[21] J. C. Phillips, R. Braun, W. Wang, J. Gumbart, E. Takhorshid, E. Villa, C. Chipot, R. D. Skeel, L. Kale, K. Schulten,Scalable molecular dynamics with NAMD, J. Comput. Chem. 26 (2005) 1781–1802. doi.org/10.1002/jcc.20289.

[22] S. E. Feller, Y. Zhang, R. W. Pastor, B. R. Brooks, Constant pressure molecular dynamics simulation: the Langevin piston method, J. Chem. Phys. 103 (1995) 4613-4621.doi.org/10.1063/1.470648.

[23] G. Bussi, D. Donadio, M. Parrinello, Canonical sampling through velocity rescaling, J. Chem Phys. 126(2007) 014101.doi.org/10.1063/1.2408420.

[24] T. Darden, D. York, L. Pedersen, Particle mesh Ewald: an N·log(N) method for Ewald sums in large systems, J. Chem. Phys. 98 (1993) 10089–10092. doi.org/10.1063/1.464397.

[25] L. Verlet, Computer "experiments" on classical fluids. I. Thermodynamical properties of Lennard-Jones molecules, Phy. Rev. 159 (1967) 98.doi.org/10.1103/PhysRev.159.98.

[26] S. A. Hollingsworth, P. A. Karplus, A fresh look at the Ramachandran plot and the occurrence of standard structures in proteins, Biomol. concepts 1(2010) 271-283. doi.org/10.1515/bmc.2010.022.

[27] B. K. Ho, R. Brasseur, The Ramachandran plots of glycine and pre-proline, BMC Struct. Biol. 5 (2005) 14.doi.org/10.1186/1472-6807-5-14.

[28] D. Gilis, M. Rooman, Stability changes upon mutation of solvent-accessible residues in proteins evaluated by database-derived potentials, J. Mol. Biol. 257(1996) 1112-1126. doi.org/10.1006/jmbi.1996.0226.

[29] M. Fernández, J. Caballero, L. Fernández, J. I. Abreu, M. Garriga, Protein radial distribution function (P-RDF) and Bayesian-Regularized Genetic Neural Networks for modeling protein conformational stability: Chymotrypsin inhibitor 2 mutants, J. Mol. Graph. Modl. 26(2007) 748-759. doi.org/10.1016/j.jmgm.2007.04.011.

AIMS Biophysics, 5(4): 245–256.
DOI: 10.3934/biophy.2018.4.245
Received: 10 August 2018
Accepted: 16 October 2018
Published: 25 October 2018

http://www.aimspress.com/journal/biophysics

*Research article*

# Heat conduction by thyroid hormone receptors

**Tika Ram Lamichhane and Hari Prasad Lamichhane***

Central Department of Physics, Tribhuvan University, Kirtipur, Kathmandu, Nepal

* **Correspondence:** Email: hlamichhane1@gmail.com; Tel: +9779843217767.

**Abstract:** Thyroid hormone receptors (THRs) together with hormone binding and dissociation are important in gene expressions. The heat conduction properties such as heat capacity, thermal diffusivity and thermal conductivity of THR isoforms are determined by means of molecular dynamics simulations. Mean energy fluctuations in canonical ensemble at 310 K and theory of mole fraction are used to find the heat capacity of THRs in solution. The larger heat capacity of liganded THR-β than that of unliganded THR-β signifies the effect of receptor-ligand interactions, and hydrophobic, vibrational and conformational changes. The specific heats of THR isoforms in solution range from 2000 to 2200 $Jkg^{-1}K^{-1}$ at 310 K which lie within the experimental range for the native globular proteins. Providing temperature relaxation from 310 K to 200 K across protein-water interface in nano-droplets, the thermal diffusivity of THRs ranges from $1.28 \times 10^{-7}$ to $1.57 \times 10^{-7}$ $m^2/s$ which is around $1.46 \times 10^{-7}$ $m^2/s$ for water. The thermal conductivity of THRs lies in the range 0.26–0.30 $Wm^{-1}K^{-1}$ which is about half the value, 0.64 $Wm^{-1}K^{-1}$ for water at 310 K.

**Keywords:** thyroid hormone receptors; heat capacity; thermal diffusivity; thermal conductivity

## 1. Introduction

Thyroid signaling defects broadly depend on the action of thyroid hormone receptors (THRs), local ligands, thyroid hormone (TH) carrier proteins, coactivators, corepressors, neural development and metabolism [1]. There are two THR subtypes (THR-α and THR-β) consisting of ligand binding domain (LBD) and homogeneous DNA-binding domain (DBD). The LBDs of these subtypes differ only by a single amino acid residue: Ser277 in THR-α and Asn331 in THR-β [2]. THR isoforms differ in chain length by amino as well as carbxy termini. THR-α1 (triiodothyronine: T3-binding splice product of THR-α) is expressed in skeletal muscle, heart and brain. THR-β has three

T3-binding splice products: THR-β1 is expressed in wide regions of body tissues; THR-β2 is in retina, brain and inner ear; and THR-β3 is predominant in liver, kidney and lung [1]. THs interact with different signalling pathways and their fuction is based on iodine and nutritional status. The TH-liganded isoforms: THR-β, THR-β1 and THR-α in cartoon view of globular forms are shown in Figure 1. The mutational evidances found in THR isoforms indicate thyroid disorders with resistance to THs (RTH) [1,3]. THR isoform selective agonists interfere with the carboxyterminal helix 12. Helix 12 dynamics is responsible for the interaction of THR with corepressors and coactivators. T3 has higher binding affinity than thyroxine (T4) in THR and the T3 bounded isoforms regulate gene expressions under DNA transcription. The unliganded THR represses basal transcription which is known as transcriptional silencing. The abnormal changes in serum TH concentrations are the indicators of hypothyroidism or hyperthyroidism with subacute thyroiditis which are directly or indirectly associated with T3 regulated gene expressions [4].

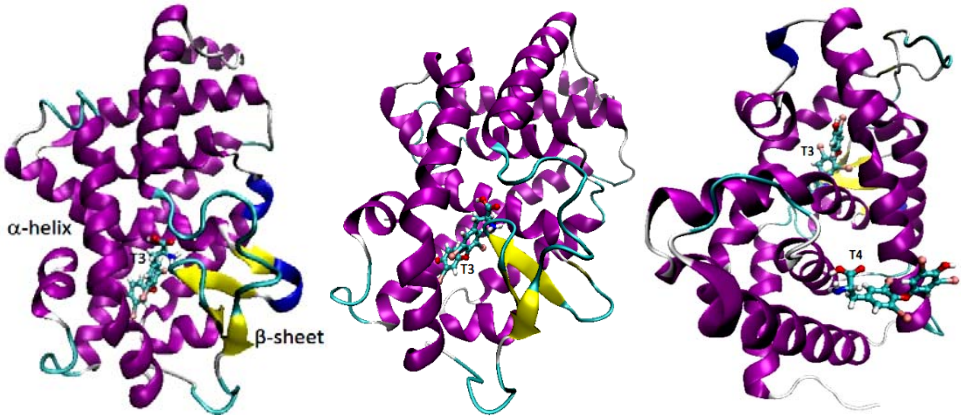


**Figure 1.** T3- or T4-liganded THR isoforms in the cartoon view of globular proteins: (a) THR-β, (b) THR-β1, and (c) THR-α.

Biologically active molecules are responsible for the heat conduction after the sudden increase in temperature by means of chemical or photochemical reactions. Heat energy transfers through the vibrational states and the residues of globular proteins giving rise to anisotropic flow of energy. It is central to understantand the protein function including ligand binding and dissociation [5]. Heat capacity of a protein-hormone system at a particular temperature depends on folding and unfolding states, polar and non-polar groups in solution, hydration states, and protein-ligand interactions [6]. The heat capacity of a native globular protein is close to the value found from the heat capacities of individual amino acid residues in an extended polypeptide chain [7]. Moreover, T3-liganded and unliganded THRs have the different heat capacities. Anharmonicity enhances thermal conductivity of proteins by the energy flow through localized normal modes of vibration [8]. Heat capacity and thermal conductivity being the temperature dependent quantities, thermal diffusivity also depends on temperature. The temperature gradient differs from chemically active cites to LBDs providing microscopic basis for the signal transduction. The energy fluctuation and dissipation or the temperature dependent changes in internal energy during molecular dynamics simulations (MDS) support to calculate heat capacity of the biomolecular system. The mean energy contributing heat capacity of such complex system is calculated from the ensemble averages of individual terms in

potential function describing the system [6]. The temperature relaxation across protein-water interface is the basis of finding thermal diffusivity and then thermal conductivity [9,10]. This process relies on the principles of transient non-equilibrium thermodynamics.

## 2. Methodology

### *2.1. Theory*

Enthalpy or mean energy (E) is expressed in terms of ensemble averages of energy terms ($U_i$) describing a complex molecular system [6], i.e.

$$E = \langle U \rangle = \sum_{i=1}^{N} \langle U_i \rangle = \sum_{i=1}^{N} E_i \tag{1}$$

where i refers to the energy related to bond angle, bond length, dihedral, van der Waal, electrostatic, improper and cross-terms giving rise to Hamiltonian or net potential function (U). Each of these terms contributes heat capacity of the system. The terms $\langle U_i \rangle$ differ in case of any perturbation, or mutation, or liganded and unliganded THR so that the total energy obtained is used to compute Boltzmann weight. The heat capacity, using the method of energy fluctuation in canonical ensemble [6,11], is defined by:

$$C_V = \frac{dE}{dT} = \frac{d\langle U \rangle}{dT} = \frac{\langle \delta U^2 \rangle}{K_B T^2} = \frac{\langle U^2 \rangle - \langle U \rangle^2}{K_B T^2} = mc_V \tag{2}$$

where m is mass and $c_V$ is specific heat capacity of the system, $K_B$ = 0.00198657 kcal $mol^{-1}K^{-1}$ is Boltzmann constant, and T is absolute temperature.

The possible sources of change in heat capacity are protein folding and unfolding including polar and apolar hydration contributions, equilibrium effect, electrostatics, vibrational terms, van der Waal interactions, H-bonding and protein conformational entropy. For the protein in solution, the heat capacity changes due to protein-protein interactions as well as hydration effect. After solvating the globular form of protein in a neutral water-ion solution providing the cellular environment, one can determine the heat capacity of the solvated protein by method of mixture or mole fraction [12,13]. Under thermal equilibrium, $Mc_V = M_P c_V^p + M_W c_V^w$ where the suffix "p" refers to protein-ligands and "w" refers to water-ions. Then, the heat capacity of the protein-hormone system in solution is given by:

$$c_V^p = \frac{Mc_V - M_W c_V^w}{M_P} \tag{3}$$

Knowing the relative masses and the specific heat capacities of mixture and solution, we can determine the specific heat capacity of the protein-hormone system under ideal condition. For this purpose, we perform MDS approach separately for the solvated system or mixture and for the water-ion solution at constant temperature.

The properties of the biological macromolecules explain their functional impact on the living organisms in response to an external perturbation such as thermal gradient. The linear response theory describes the small perturbation relating non-equilibrium transport to equilibrium thermodynamic properties of the system. The complex biomolecular system is solvated under

non-periodic boundary conditions forming a spherical droplet. The local temperature $T(r,t)$ of the system depends on position (r) and time (t) which is governed by the heat diffusion equation:

$$\frac{\partial T(r,t)}{\partial t} = D\nabla^2 T(r,t) \tag{4}$$

where D is thermal diffusivity. For the radius R of the solvated protein-ligand in a globular form, the boundary conditions are: $T(r,0) = T_i$ for $r < R$, and $T(r,t) = T_f$ for $r > R$ where $T_i$ is initial temperature of the system and $T_f$ is final temperature of the surrounding fluid-shell of thickness $\Delta r$. Using these boundary conditions, solution of the Eq 4 [14] in the form of mean temperature of the protein-ligand system is written as:

$$\langle T(t)\rangle = T_f + 6\frac{T_i - T_f}{\pi^2}\sum_{n=1}^{\infty}\frac{1}{n^2}\exp\left[-\left(\frac{n\pi}{R}\right)^2 Dt\right] \tag{5}$$

Knowing the thermal diffusivity (D) by fitting the simulated data with Eq 5, and using density ($\rho$) and specific heat ($c_V$), we can determine thermal conductivity (k) of the protein-hormone system in solution from the relation:

$$k = \rho c_V D \tag{6}$$

### *2.2. Molecular dynamics simulation*

Crystal structures of three THR isoforms consisting of TH-ligands (T3 and/or T4): THRT3-β, THRT3-β1 and THRT3T4-α were obtained from the protein data bank (pdb) codes 3GWS [15], 1XZX [16] and 4LNX [17], respectively. CHARMM-force field topologies and parameters [18–20] were implemented to prepare the simulation packages for solvation, energy minimization, equilibration and production runs by using visual molecular dynamics (VMD) [21] and nanoscale molecular dynamics (NAMD) [22] interfaces. The ligands T3 and T4 were parameterized suitably [20] for the NAMD runs.

The separate THR isoforms: THR-β, THRT3-β, THRT3-β1 and THRT3T4-α were solvated fully in an explicit solvent of neutral water-ions providing the cellular environment. Here, THRT3T4-α was truncated in size by omitting initial residue IDs from 145 to 156 of almost free strand. At first, THR-β as well as THRT3-β was solvated under periodic boundary conditions in TIP3P-water box of cell basis vectors 50.36, 60.92 and 74.78 Å, neutrallized by adding $Na^+$ and $Cl^-$ ions in the concentration of 0.15 mol/L, performed energy minimization up to 3000 conjugate gradient (CG) steps and then separate equilibration runs were performed up to 2 ns at five different constant temperatures 300, 305, 310, 315 and 320 K. The Langevin constant temperature and pressure (1 atm) controls were used with damping coefficient of 1 $ps^{-1}$ and integrator papameter of 2 fs/step by keeping rigid bonds of H-atoms. The force field related switching, cut-off and pair list distances were 10, 12 and 14 Å, repectively with 1–4 scaling 1.0. The mean energy, $\langle U\rangle$ of THR-β and that of THRT3-β at the five different temperatures were noted down from the last 0.5 ns runs. The slope of straight line fit in $\langle U\rangle$ vs. T plot provides the heat capacity ($C_V$) of a mixture of solvating T3-liganded or unliganded THR at the body scale temperature 310 K. The same procedure with identical terms and conditions was implemented to a neutral water-ion box of cell basis vectors 30, 45 and 60 Å to find the heat capacity ($C_V^w$) of the solvent only. It is to be noted that $C_V^w$

found for the solvent (water) by keeping rigid bonds of H-atoms with 2 fs/step is contributed by the non-bond (electrostatic and van der Waal) energies only. Then, from Eq 3, specific heat capacities ($c_V^p$) of THR-β and THRT3-β were obtained and compared.

Each of the THR isoforms was solvated in a water-sphere (TIP3P water model) neutralized with $Na^+$ and $Cl^-$ ions in the concentration of 0.15 mol/L to study their heat conduction properties such as heat capacity ($C_V^p$), thermal diffusivity (D) and thermal conductivity (k). During the solvation under non-periodic boundary conditions, the radii of THRT3-β, THRT3-β1 and THRT3T4-α related water-droplets were 37.48, 36.99 and 31.29 Å, respectively. The force-filed and integrator parameters, and Langevin dynamics for constant temperature control were fixed as mentioned in the periodic boundary conditions. Each of the systems was geometrically optimized up to the sufficient (2000–5000) CG steps and equilibrated up to 20 ns. Conformational stability of the system was monitored by plotting graphs for root mean square deviation (RMSD) and/or radius of gyration (RG) during equilibration as well as production runs. The systems were also subjected to the additional production runs of 2 ns each in NVT ensemble at 310 K to find the heat capacity ($C_V$) by using energy fluctuations (Eq 2). Putting $C_V$ of protein-ligand solvated sphere, $c_V^w$ of water-ion solvent, and the related masses in Eq 3, the specific heat $c_V^p$ of a THR isoform was obtained. The specific heat found from $d\langle U\rangle/dT$ by fitting straight line in the periodic boundary conditions as stated above and the specific heat found from energy fluctuation method in non-periodic boundary conditions were compared taking the cases of THR-β and THRT3-β.

The final coordinates of each equilibrated droplet consisting of a THR isoform were taken after its 20 ns run at 310 K. The inner sphere ($r < R$) was kept at initial temperature, $T_i$ = 310 K and the outer shell ($r > R$) was fixed at the final temperature, $T_f$ = 200 K where R = 33 Å and $\Delta r$ = 4.48 Å for THRT3-β; R = 33 Å and $\Delta r$ = 3.99 Å for THRT3-β; and R = 27 Å and $\Delta r$ = 4.29 Å for THRT3T4-α. Then, NAMD simulations of temperature relaxation were performed without any constraint imposed into the atomic vibrations to monitor the change in system's temperature. The cooling process was done up to 20 ps each. By fitting the temperature data with the theoretical expression in Eq 5, the thermal diffusivity of each isoform was obatined and compared. Finally, the system's thermal conductivity was obtained using Eq 6.

## 3. Results and discussion

The separately performed 20 ns equilibration runs at 310 K of THR-isoforms solvated in water-droplets result mean ± SD of protein's RMSD: 2.13 ± 0.38 Å for THRT3-β, 1.98 ± 0.21 Å for THRT3-β1, and 2.24 ± 0.31 Å for THRT3T4-α; and the related RGs are 18.74 ± 0.07, 18.84 ± 0.11, and 18.41 ± 0.06 Å, respectively. In case of unliganded THR-β, RG is 18.70 ± 0.09 Å and RMSD is 2.61 ± 0.50 Å during its 20 ns long equilibration. Almost constant values of RG with small SD indicate that the protein-hormone systems are conformationally stable during their equilibration runs as plotted as shown in Figure 2a. The small fluctuations seen in RMSD plots (Figure 2b) are due to formation and breaking of H-bonds among the more stable residues, α-helix and β-sheets of the protein systems while searching for their conformational stability during the course of simulations. The additional production runs up to 2 ns in canonical (NVT) ensemble yield more small values of

RMSD: 1.23 ± 0.11, 1.41 ± 0.18 and 1.13 ± 0.11 Å for THRT3-β, THRT3-β1 and THRT3T4-α proteins, respectively.

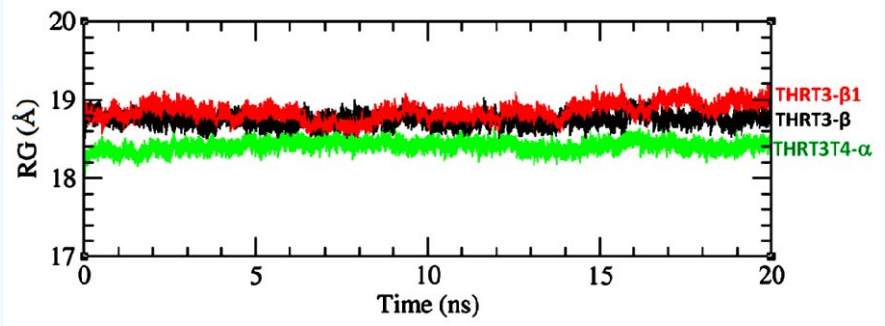


(a)

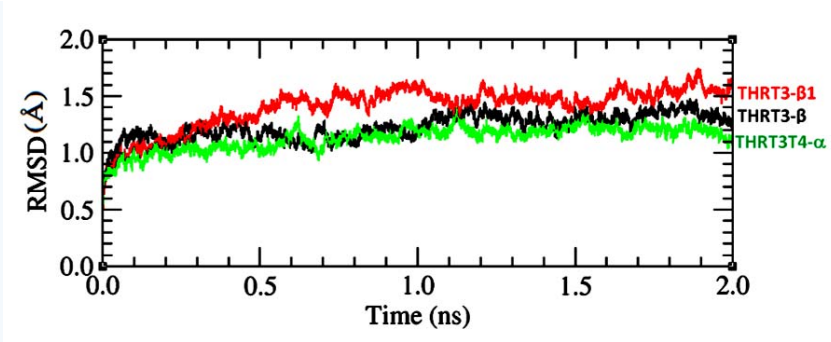


(b)

**Figure 2.** RG and RMSD plots for the protein backbone in case of (a) equilibration run, and (b) NVT production run of different water-droplets solvating the THR-isoform.

Five NVT simulations up to 2 ns each at temperature difference of 5 K about the body scale temperature 310 K result the values of <U> for liganded and unliganded THR-β under the periodic boundary conditions. The slope of linear fit in <U> vs. T plot (Figure 3a) obtains the heat capacity, $C_V$ of the entire THRT3-β solvated water-box which is 84.59 ± 0.74 kcal $mol^{-1}K^{-1}$ at about 310 K. Since the total mass of THRT3-β solvated water-box is 131765 amu, the related specific heat, $c_V$ is 2688.52 ± 23.52 $Jkg^{-1}K^{-1}$. Similarly, $C_V$ of THR-β solvated water-box (mass = 131186 amu) is 85.59 ± 1.12 kcal $mol^{-1}K^{-1}$ and the related $c_V$ is 2732.31 ± 35.75 $Jkg^{-1}K^{-1}$. Upon implementing the same procedure with identical terms and conditions for the simulations of a neutral water-ion box with 2 fs/step and rigid bonds of H-atoms, its heat capacity, $C_V^w$ contributed by electrostatic and van der Waal energy terms is 31.72 ± 0.43 kcal $mol^{-1}K^{-1}$. Since mass of the modelled water-ion box is 45357 amu, the related specific heat, $c_V^w$ = 2928.75 ± 39.70 $Jkg^{-1}K^{-1}$. Figure 3b shows the best linear fit of <U> vs. T for the water-box where the slope of straight line gives $C_V^w$. The mass of THR-β is 27640 amu and that of THRT3-β is 28291 amu. By using Eq 3, the specific heat capacities, $c_V^p$ of THR-β and THRT3-β in water-ion solution are 1996.25 ± 20.95 $Jkg^{-1}K^{-1}$ and 1809.88 ± 35.66 $Jkg^{-1}K^{-1}$, respectively. This difference in heat capacity is due to the presence of ligand (T3) in LBD of THR and the T3-receptor interactions as explained in [23,24]. Hydrophobic, vibrational and conformational contributions to the heat capacity changes are involved in the protein-ligand interactions.

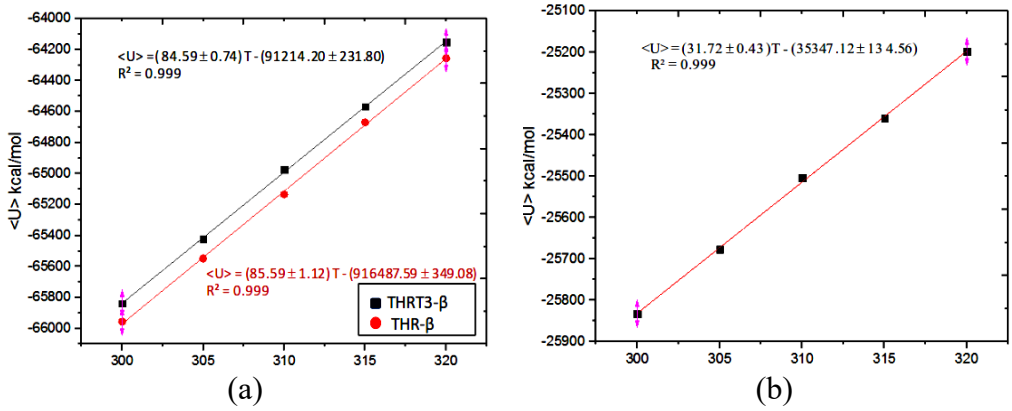


**Figure 3.** Linear best fits for the change in mean energy or net potential function with temperature of (a) THRT3-β and THR-β solvated water-boxes, and (b) neutral water-ion box where the slope of straight line represents heat capacity of the related system.

The heat capacities of the systems are also determined from the mean energy fluctuations in their canonical ensembles (Eq 2). The specific heat capacities of the globular protein-hormone systems found from this technique (see $c_V^p$ of THR-β and THRT3-β in Table 2) are in close agreement with their values found from the method of linear fit for ⟨U⟩ vs. T (Figure 3a). The flutuations in mean energy of THR-β and THRT3-β solvated droplets are shown in Figure 4a where the values of ⟨U⟩ at 310 K are −66286.35 ± 128.43 and −66218.22 ± 128.76 kcal/mol, respectively. Figure 4b demonstrates the fluctutating energy levels of THR-isoform solvated droplets. The obtained values of mean square fluctuations of energy, masses of THR-isoform slovated droplets and the related heat capacities are depicted in Table 1. We use $c_V^w$ = 2928.75 ± 39.70 $Jkg^{-1}K^{-1}$ and $c_V$ from Table 1 to find the specific heats $c_V^p$ of THRs (Table 2) in solution with the help of Eq 3. $c_V^p$ of the protein-hormone system, determined in this study (e.g. 2030.62 ± 105.32 $Jkg^{-1}K^{-1}$ for THRT3-β) at 310 K, lies within the experimental range: 1200 to 2300 $Jkg^{-1}K^{-1}$ for the native state globular proteins at 25 ºC as given by Privalov et al. 1986 [25]. The heat capacity changes of proteins at different temperatures representing folding and unfolding states are explained by Privalov et al. 2007 [26]. The values of $c_V^p$ for THRs, in this technique, are a bit higher than the heat capacities: 6.5 ± 2.1 $kJmol^{-1}K^{-1}$ for myoglobin and 180 ± 35 $kJmol^{-1}K^{-1}$ for $Ca^{2+}$ ATP-ase (ISU4) in water calculated by Lervik et al. 2010 using MDS method [9]. In the previous studies [8,13,27,28], the average heat capaacity of a native globular protein in solution is about 1500 $Jkg^{-1}K^{-1}$ at 300 K. In a computational work of antifreeze protein performed by Pandey et al. 2017 [29], the hydration states of the protein depending on protein-water H-bonds make influence on its partial heat capacity so that $c_V^p$ ranges from 0.494 cal $g^{-1}K^{-1}$ for the dry state protein to 0.606 cal $g^{-1}K^{-1}$ for the fully hydrated protein at about 300 K. Our results of $c_V^p$ for THRs lie in the range of specific heat for the proteins in the hydration limit given by Pandey's study.

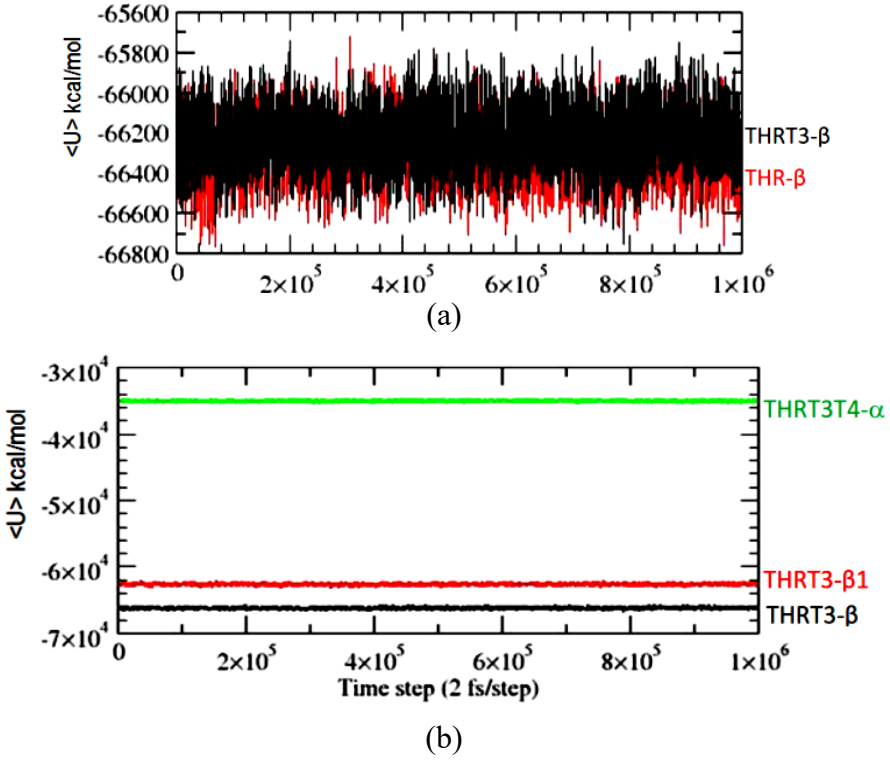


**Figure 4.** Mean energy fluctuations for (a) liganded and unliganded THR-β, and (b) three THR-isoforms during 2 ns long NVT simulations after 20 ns equilibration run for each system.

**Table 1.** Heat capacity of THRs solvated droplets (THR-protein + T3/T4 ligand + water + ions) at T = (310 ± 1) K in the NVT ensemble having average poteintial energy ⟨U⟩ where $K_B$ = 0.00198657 kcal $mol^{-1}K^{-1}$.

| Molecule in water sphere | No. of atoms in mixture | Total mass, M (amu) | $\langle U^2 \rangle$ (k cal $mol^{-1})^2$ | $\langle U \rangle^2$ (k cal $mol^{-1})^2$ | $C_V = \frac{\langle U^2 \rangle - \langle U \rangle^2}{K_B T^2}$ (k cal $mol^{-1}K^{-1}$) | $c_V$ (J $kg^{-1}K^{-1}$) |
|---|---|---|---|---|---|---|
| THR-β | 21157 | 132213 | 4393896241.65 | 4393879748.25 | 86.39 ± 0.28[@] | 2736.42 ± 8.87 |
| THRT3-β | 21192 | 132864 | 4384867565.23 | 4384850985.47 | 86.85 ± 0.28 | 2737.51 ± 8.82 |
| THRT3-β1 | 20266 | 127468 | 3925226341.90 | 3925210205.54 | 84.52 ± 0.27 | 2776.85 ± 8.87 |
| THRT3T4-a | 12249 | 79395.7 | 1225218557.93 | 1225208975.47 | 50.19 ± 0.16 | 2647.36 ± 8.44 |

[@] The error has been calculated from $C_V = C_V(U, T)$, i. e. $\Delta C_V = C_V \sqrt{\left(\frac{\Delta U}{U}\right)^2 + \left(\frac{\Delta T}{T}\right)^2}$ where ΔU and ΔT are standard errors in potential energy and temperature, respectively.

**Table 2.** Specific heat capacity ($c_V^P$), thermal diffusivity (D) corresponding to temperature relaxation between 310 to 200 K and thermal conductivity (k) of THRs in solution where the specific heat contributed by solvent (water + ions) in the droplet is 2928.75 ± 39.70 $Jkg^{-1}K^{-1}$ and density of the protein-hormone system in solution is (950 ± 50) $kgm^{-3}$ at 310 K.

| Molecule | No. of atoms | Mass, $m_p$(amu) | $c_V^P$ ($Jkg^{-1}K^{-1}$)[a] | D ($m^2/s$)[b] | k ($Wm^{-1}K^{-1}$)[c] |
|---|---|---|---|---|---|
| THR-β | 3895 | 27640 | 2008.75 ± 107.77 | (1.56 ± 0.02) × $10^{-7}$ | 0.30 ± 0.023[@@] |
| THRT3-β | 3930 | 28291 | 2030.62 ± 105.32 | (1.57 ± 0.03) × $10^{-7}$ | 0.30 ± 0.023 |
| THRT3-β1 | 4014 | 29069 | 2244.53 ± 95.73 | (1.35 ± 0.05) × $10^{-7}$ | 0.29 ± 0.022 |
| THRT3T4-α | 3986 | 28853 | 2154.44 ± 46.32 | (1.28 ± 0.04) × $10^{-7}$ | 0.26 ± 0.017 |

[@@] The error has been calculated from $k = k(C_V, D, \rho)$, i. e. $\Delta k = k\sqrt{\left(\frac{\Delta C_V}{C_V}\right)^2 + \left(\frac{\Delta D}{D}\right)^2 + \left(\frac{\Delta \rho}{\rho}\right)^2}$ where $\Delta C_V$, $\Delta D$ and $\Delta \rho$ are standard errors in specific heat, thermal diffusivity and density, respectively.

[a] From the calorimetric measurements by Privalov et al. 1986 [25], $c_V^P$ of native globular proteins ranges from 1200 to 2300 $Jkg^{-1}K^{-1}$ at 300 K.

[b] D (water) = 14.6 $Å^2/ps$, D (protein) = 21.1 $Å^2/ps$ for green fluoroscent protein (GFP), 18.7 $Å^2/ps$ for myoglobin [8]; and D (protein) = 4–18 $Å^2/ps$ at the temperature relaxation from 350 to 250 K [9].

[c] k (water) = 0.64 $Wm^{-1}K^{-1}$ & k (protein) = 0.13–0.28 $Wm^{-1}K^{-1}$ at 300 K [8,9].

Thermal diffusivity of THRs ranges from 1.28 × $10^{-7}$ to 1.57 × $10^{-7}$ $m^2/s$ at the temperature relaxation from 310 to 200 K that is calculated from the best fitting of theoretical expression (Eq 5) with the simulated data (Figure 5). This result is near to the thermal diffusivity of water ($D_w$ = 1.46 × $10^{-7}$ $m^2/s$) and proteins ($D_p$ = 2.11 × $10^{-7}$ $m^2/s$ for GFP and 1.87 × $10^{-7}$ $m^2/s$ for myoglobin) reported by Yu et al. 2005 [8]. According to Lervik et al. 2010 [9], $D_p$ ranges from 0.4 × $10^{-7}$ $m^2/s$ to 1.8 × $10^{-7}$ $m^2/s$ for the different proteins at the temperature relaxation from 350 to 250 K. We observed a little bit higher thermal diffusivity for THRT3-β than that for THRT3-β1 and THRT3T4-α while cooling them by using the principle of thermal relaxation through the protein-water boundary. The slightly different heat transfer properties observed in THR isoforms (Figure 5) are associated with their structural evidences for the inter-residue H-bonding, energy transport channels and thermal boundary conductance between protein and water [30]. The H-bonding between protein and water facilitate vibrational energy and thermal transport across the interface.

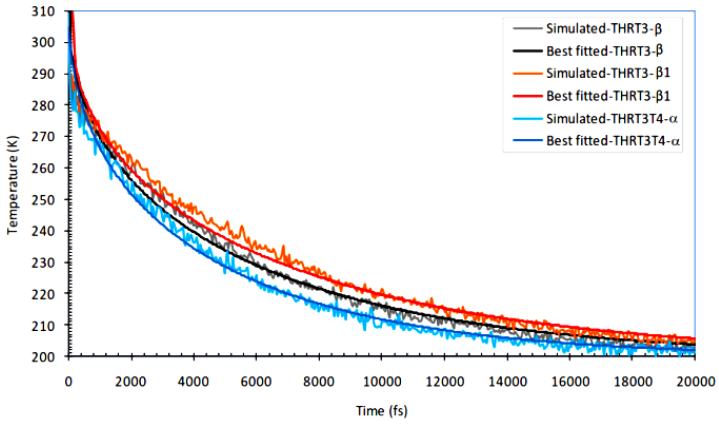


**Figure 5.** Cooling curves for thyroid hormone receptors.

Thermal conductivity of THR proteins, as depicted in Table 2, ranges from 0.26–0.30 $Wm^{-1}K^{-1}$ provided with the standard error of about 0.02 $Wm^{-1}K^{-1}$. This result shows that the protein-hormone systems are bad conductors of heat in comparision to water ($k_w$ = 0.64 $Wm^{-1}K^{-1}$). As reported by Yu et al. 2005 [8], thermal conductivity of both GFP and myoglobin is $k_p$ = 0.27 $Wm^{-1}K^{-1}$. The value of $k_p$ ranges from 0.13–0.23 $Wm^{-1}K^{-1}$ for the different proteins according to Lervik et al. 2010 [9]. The slightly higher value of $k_p$ has been observed for THRT3-β than that for THRT3-β1 and THRT3T4-α. Such change in heat conduction property is related to the effect of protein surface curvature, hydrophilic and hydrophobic patches and H-bonding between protein residues and protein-water interface [9,30]. According to the theory of non-equilibrium thermodynamics, the development of temperature gradient across THRs-water interface and the related thermal conduction are important biophysical phenomena linked with the functions of the protein-hormone systems towards the regulation of body temperature. The result of lower values of thermal conductivity of proteins than that of water is supporting the principle of body temperature regulation.

## 4. Conclusion

We have performed molecular dynamics simulations to find heat transfer coefficients of THRs. Heat capcity has been determined by using formula of mole fraction to the constituents of THR solvated periodic-box as well as nano-droplet of water. Numerical differentiation or slope of the best fitted straight line in mean potential function vs. temperature of the periodic box yields the same heat capacity as obtained from the method of mean energy fluctuations of the nano-droplet in canonical ensemble. The heat capacity of THR isoforms in solution ranges from 2000 to 2200 $Jkg^{-1}K^{-1}$ with the standard error limit of about 100 $Jkg^{-1}K^{-1}$ at 310 K. This result lies within the range of 1200 to 2300 $Jkg^{-1}K^{-1}$ as reported by Privalov et al. 1986 and a bit higher than 1500 $Jkg^{-1}K^{-1}$ as given by Yu et al. 2005 for the native globular proteins at 300 K. Our results for the specific heats of the protein-hormone systems are also in the close agreement with that of antifreeze protein in the hydration limit ranging from 2065 $Jkg^{-1}K^{-1}$ for dry state to 2533 $Jkg^{-1}K^{-1}$ for fully hydrated protein at about 300 K as studied by Pandey et al. 2017. In overt hypothyroid disorder, THRs become free of T3. The heat capaity values of T3-liganded and unliganded THR-β are different in some extent due to the change in degrees of freedom, protein-ligand interactions, H-bonding, and hydrophobic, vibrational and conformational changes in presence and absence of T3-hormone in LBD of the receptor. Thermal properties of THRs are directly associated with gene expressions and regulation of body temperature. Thermal diffusivity of THRs has been found to be ranging from $1.28 \times 10^{-7}$ to $1.57 \times 10^{-7}$ $m^2/s$ near to $1.46 \times 10^{-7}$ $m^2/s$ of water at body scale temperature 310 K. A little bit higher value of thermal diffusion coefficient for THRT3-β than that of THRT3-β1 and THRT3T4-α is associated with the effect of inter-residue and protein-water H-bonding, thermal transport channels and boundary conductance in the protein-water interface. Thermal conductivity of THRs ranges from 0.26–0.30 $Wm^{-1}K^{-1}$ with the higher value for THRT3-β in the standard error limit of about 0.02 $Wm^{-1}K^{-1}$ which is about half the value, 0.64 $Wm^{-1}K^{-1}$ for water at 310 K. Our result for the thermal conductivity is also consistent with 0.27 $Wm^{-1}K^{-1}$ as reported by Yu et al. 2005 for GFP and myoglobin. The slightly different values of the heat transfer coefficients for THR-isoforms are related to H-bonding in protein-water interface, surface curvature, and hydrophobic and hydrophillic patches. In conclusion, specific heat, thermal diffusivity and thermal conductivity of THRs are

consistent with that of other proteins as published in the previous literatures supporting the theory and the methodology implemented for their calculations.

**Acknowledgement**

The authors are thankful to Prof. Dr. Raju Khanal, Central Department of Physics, Tribhuvan University, Kathmandu, Nepal for providing the computing facilities. This work has been partially supported by Nepal Academy of Science and Technology (NAST) through a grant of PhD fellowship to the first author.

**Conflict of interest**

The authors declare that they have no conflict of interest.

**References**

1. Brent GA (2012) Mechanisms of thyroid hormone action. *J Clin Invest* 122: 3035–3043.
2. Souza PCT, Puhl AC, Martínez L, et al. (2014) Identification of a new hormone-binding site on the surface of thyroid hormone receptor. *Mol Endocrinol* 28: 534–545.
3. Bochukova E, Schoenmakers N, Agostini M, et al. (2012) A mutation in the thyroid hormone receptor alpha gene. *New Eng J Med* 366: 243–249.
4. Brent GA (1994) The molecular basis of thyroid hormone action. *Eng J Med* 331: 847–853.
5. Leitner DM (2008) Energy flow in proteins. *Annu Rev Phys Chem* 59: 233–259.
6. Prabhu NV, Sharp KA (2005) Heat capacity in proteins. *Annu Rev Phys Chem* 56: 521–548.
7. Privalov PL, Tiktopulo EI, Venyaminov SY, et al. (1989) Heat capacity and conformation of proteins in the denatured state. *J Mol Biol* 205: 737–750.
8. Yu X, Leitner DM (2005) Heat flow in proteins: Computation of thermal transport coefficients. *J Chem Phys* 122: 054902.
9. Lervik A, Bresme F, Kjelstrup S, et al. (2010) Heat transfer in protein-water interfaces. *Phys Chem Chem Phys* 12: 1610–1617.
10. Helbing J, Devereux M, Nienhaus K, et al. (2011) Temperature dependence of the heat diffusivity of proteins. *J Phys Chem A* 116: 2620–2628.
11. Nosé S (1984) A molecular dynamics method for simulations in the canonical ensemble. *Mol Phys* 52: 255–268.
12. Suurkuusk J (1974) Specific heat measurements on lysozyme, chymotrypsinogen, and ovalbumin in aqueous solution and in solid state. *Acta Chem Scand B* 28: 409–417.
13. Yang PH, Rupley JA (1979) Protein-water interactions. Heat capacity of the lysozyme-water system. *Biochemistry* 18: 2654–2661.
14. Lervik A, Bresme F, Kjelstrup S (2009) Heat transfer in soft nanoscale interfaces: The influence of interface curvature. *Soft Matter* 5: 2407–2414.
15. Nascimento AS, Dia SMG, Nunes FM, et al. (2006) Structural rearrangements in the thyroid hormone receptor hinge domain and their putative role in the receptor function. *J Mol Biol* 360: 586–598.

16. Sandler B, Webb P, Apriletti JW, et al. (2004) Thyroxine-thyroid hormone receptor interactions. *J Biol Chem* 279: 55801–55808.
17. Souza PCT, Puhl AC, Martínez L, et al. (2014) Identification of a new hormone-binding site on the surface of thyroid hormone receptor. *Mol Endocrinol* 28: 534–545.
18. Mackerell AD, Feig M, Brooks CL (2004) Extending the treatment of backbone energetics in protein force fields: Limitations of gas-phase quantum mechanics in reproducing protein conformational distributions in molecular dynamics simulations. *J Comp Chem* 25: 1400–1415.
19. Mackerell JAD, Bashford D, Bellott MLDR, et al. (1998) All-atom empirical potential for molecular modeling and dynamics studies of proteins. *J Phys Chem B* 102: 3586–3616.
20. Zoete V, Cuendet MA, Grosdidier A, et al. (2011) SwissParam: A fast force field generation tool for small organic molecules. *J Comp Chem* 32: 2359–2368.
21. Humphrey W, Dalke A, Schulten K (1996) VMD: Visual molecular dynamics. *J Mol Graph* 14: 33–38.
22. Phillips JC, Braun R, Wang W, et al. (2005) Scalable molecular dynamics with NAMD. *J Comp Chem* 26: 1781–1802.
23. Eftink MR, Anusiem AC, Biltonen RL (1983) Enthalpy-entropy compensation and heat capacity changes for protein-ligand interactions: General thermodynamic models and data for the binding of nucleotides to ribonuclease A. *Biochemistry* 22: 3884–3896.
24. Sturtevant JM (1977) Heat capacity and entropy changes in processes involving proteins. *Proc Natl Acad Sci* 74: 2236–2240.
25. Privalov PL, Potekhin SA (1986) Scanning microcalorimetry in studying temperature-induced changes in proteins. *Method enzymol* 131: 4–51.
26. Privalov PL, Dragan AI (2007) Microcalorimetry of biological macromolecules. *Biophys Chem* 126: 16–24.
27. Gomez J, Hilser VJ, Xie D, et al. (1995) The heat capacity of proteins. *Proteins: Struct, Funct, Bioinf* 22: 404–412.
28. Cooper A (2000) Heat capacity of hydrogen-bonded networks: An alternative view of protein folding thermodynamics. *Biophys Chem* 85: 25–39.
29. Pandey HD, Leitner DM (2017) Thermodynamics of hydration water around an antifreeze protein: A molecular simulation study. *J Phys Chem B* 121: 9498–9507.
30. Xu Y, Leitner DM (2014) Vibrational energy flow through the green fluorescent protein-water interface: Communication maps and thermal boundary conductance. *J Phys Chem B* 118: 7818–7826.


AIMS Press

© 2018 the Author(s), licensee AIMS Press. This is an open access article distributed under the terms of the Creative Commons Attribution License (http://creativecommons.org/licenses/by/4.0)

Scientific Research Publishing

Journal of Biosciences and Medicines, 2018, 6, 59-73
http://www.scirp.org/journal/jbm
ISSN Online: 2327-509X
ISSN Print: 2327-5081

# Age- and Gender-Specific Changes in Thyroid Size and Thyroid Function Test Values of Euthyroid Subjects

**Tika Ram Lamichhane[1], Sandeep Prashad Pant[1], Binod Lamichhane[1], Chhabindra Gautam[1], Sharma Paudel[2], Binod Kumar Yadav[3], Hari Prasad Lamichhane[1*]**

[1]Central Department of Physics, Tribhuvan University, Kathmandu, Nepal
[2]Department of Radiology & Imaging, Tribhuvan University Teaching Hospital, Kathmandu, Nepal
[3]Department of Biochemistry, Tribhuvan University Teaching Hospital, Kathmandu, Nepal
Email: *hlamichhane1@gmail.com

**How to cite this paper:** Lamichhane, T.R., Pant, S.P., Lamichhane, B., Gautam, C., Paudel, S., Yadav, B.K. and Lamichhane, H.P. (2018) Age- and Gender-Specific Changes in Thyroid Size and Thyroid Function Test Values of Euthyroid Subjects. *Journal of Biosciences and Medicines*, **6**, 59-73.
https://doi.org/10.4236/jbm.2018.611007

**Received:** May 18, 2018
**Accepted:** November 16, 2018
**Published:** November 19, 2018

## Abstract

**Background:** The thyroid status is evaluated by two clinical diagnostic tests which are thyroid ultrasonography and thyroid function tests. The objective of this research is to critically analyze the age and gender based variations of thyroid volume and thyroid hormone levels in the hospital based euthyroid subjects. **Methodology:** A total of 221 euthyroid subjects aged 1 - 86 years were selected to observe the normal thyroid size by ultrasonography at Department of Radiology and the thyroid function test values (FT3, FT4 and TSH) of 2413 euthyroid subjects aged (<1)-93 years were observed at Department of Biochemistry, Tribhuvan University Teaching Hospital, Kathmandu, Nepal during January 2017 to February 2018. The observed data were analyzed graphically and statistically to check the cross-correlations among the variables. **Results:** The best fitted equations with significant correlation coefficients and $p < 0.05$ provide the empirical relations between any two of the observed variables: age, thyroid lobe volumes, FT3, FT4 and TSH. The mean ± SD ($p < 0.0001$) of thyroid volume, FT3, FT4 and TSH are 4.74 ± 2.30 mL, 5.46 ± 0.82 pmol/L, 14.09 ± 2.71 pmol/L and 2.30 ± 0.98 mIU/L, respectively. **Conclusion:** The thyroid size first increases and then decreases whereas the thyroxin level first decreases and then increases with aging. Left lobe volume is almost same for both genders and right lobe volume is higher in males. The thyroid size in menarche and menopause periods of females is larger than that of males. Such age- and gender-specific changes recommend the new reference ranges for the normal thyroid functions.

## Keywords

Euthyroid Subject, Thyroid Function Test, Thyroid Hormone Levels, Thyroid

Ultrasonography, Empirical Relation

## 1. Introduction

Thyroid hormones (TH) play the important role in the development and the maintenance of homeostasis through the interactions with autonomic nervous system and the regulations of cardiovascular and metabolic functions [1] [2]. The disorders seen in thyroid hormone regulations during embryonal and early postnatal stages can persist into adulthood also. Thyroid stimulating hormone (TSH) is an important marker to diagnose thyroid status clinically. Many studies related to the age and gender based variations of serum free thyroid hormones (TH: FT3 and FT4) and TSH have uncertainties [3] [4] [5]. As reported in [3] [5], TSH distributes in higher concentration with aging regardless the status of thyroid antibodies and the increased TSH makes impact on lipid profile influenced by age in both genders. There is log-linear relationship among FT3, FT4 and TSH based on age- and gender-specific responses [6].

The routine assessment of thyroid status basically relies on ultrasonographic (USG) examinations and thyroid function tests (TFT) determining the serum concentrations of FT3, FT4 and TSH. More precise and accurate parameters are to be prescribed in defining a patient's thyroid status. There is a regional influence of iodine supply on establishing the reference ranges for the normal thyroid functioning [7]. Even a mild alteration in thyroid functioning causes psychiatric problem, weight gain or loss, atrial fibrillation and osteoporosis [8]. So, the thyroid clinical diagnosis seems to be historically sensitive. The biologically active life stages of females make differences in studying the working mechanism of their endocrine system. The thyroid function test report as well as thyroid size normally changes in menarche, pregnancy and menopause periods. More critically saying that the differential genetic mechanisms are potentially associated with the thyroid function regulation in both genders. In euthyroid subjects, the TFT values lie within a narrow range suggesting a unique hypothalamus-pituitary-thyroid (HPT) axis working under the controlled way by negative feedback mechanism of thyroid cycle for each individual.

Iodine deficiency is still present in mild levels in Nepal leading to the prevalence of subclinical hypothyroidism in all age groups of both genders. The nutritional iodine intake makes changes on thyroid hormone levels in the blood stream, then on TSH production and even on thyroid size. The neonatal thyroid is sensitive to maternal iodine intake and its impact can persist lifelong. Age, gender, body mass index, living status, thinking and feeding habits, genetics, environmental factors, and non-thyroid illness and associated medications influence normal thyroid status [9] [10]. A number of earlier studies [11] [12] [13] [14] [15] have analyzed factors that affect thyroid size and they have also reported the reference intervals for the normal thyroid volume with different un-

certainties.

There are seasonal and diurnal as well as nocturnal variations of TH-levels even in normal thyroid conditions. The serum free T3 decreases in winter season due to the accelerating disposal of thyroid hormones in cold described as the polar T3 syndrome [16]. Without any change observed in thyroid status, about 20% variation in TSH level is found [17]. The reference levels of TSH, FT3 and FT4 are slightly varying for the different constrained groups of healthy people as reported in [4] [18] [19] [20]. In a hospital based study performed at central Nepal, out of 5230 subjects ranging from early infant to elderly age, 71% of them have euthyroidism with serum FT3 = 2.3 ± 0.6 pg/mL, FT4 = 11.5 ± 2.0 pg/mL and TSH = 2.3 ± 1.1 mIU/L [20]. In another hospital based study performed in hilly region of Nepal, 76.7% of 3136 subjects have clinically diagnosed euthyroidism [21]. In the studies of age-based variations of serum FT4 in normal thyroid subjects, its concentration trends to decrease slightly with aging having the smaller values for males than for females in younger age below 60 years [4] [22] [23] [24]. As the functioning of thyroid gland is influenced by secretion and regulation of TSH, T3 and T4 hormones, our study is designed to analyze the correlation between thyroid gland volume and TFT values of euthyroid subjects along with age and gender based variations.

## 2. Materials and Methods

The thyroid USG of hospital based euthyroid subjects was performed at the Department of Radiology and the TFT values were observed at the Department of Biochemistry, Tribhuvan University Teaching Hospital (TUTH), Kathmandu, Nepal during January 2017 to February 2018. This study was carried out by the informed consent under the guidelines of and taking authority from the Institutional Review Board (IRB), TUTH.

A total of 90 males and 131 females aged 1 - 86 years were selected as euthyroid subjects after the USG observations. The USG machine, SAMSUNG UGEO H60 with 7.5 MHz linear transducer was used in brightness mode (B-mode) to produce good quality image by adjusting actual frequency of ultrasound, emission time, sonation angle, size and curvature of the transducer and by minimizing effects of reverberation, enhancement, edge and mirror artifacts [25] [26] [27]. The included subjects were examined in the supine position with the neck hyperextended and transverse as well as longitudinal sections of thyroid lobes were scanned to measure the appropriate volumes and to confirm the normal status of the thyroid gland. The subjects having abnormal thyroid with nodules, vascularity, thyroiditis, hyper- and hypoechogenicity, and heterogeneous exotextures were excluded in this study. The thyroid volume was obtained by using ellipsoid formula (V= length × width × thickness × 0.52) for each lobe [12] [13] [14]. Multiple USG measurements were done in case of imaging problems due to the body composition differences such as short neck, and kyphosis. Age, sex, family history of thyroid problems, demographic locations, thinking, sleeping

and feeding habits, and USG results: antero posterior length, craniocaudal length and width or transverse and mediolateral length, echogenicity, and disease related findings of both thyroid lobes of all individuals were recorded in the pre-designed data collection sheet for further analysis.

The TFT values of 2413 clinically euthyroid subjects including 1748 females and 665 males of early infant age (<1 years) to elderly age (93 years) were observed to analyze the normal levels of serum free T3, T4 and TSH varying with age and sex. About 2 - 3 mL blood sample was taken from antecubital vein in a plain vial. The sample was allowed to clot and then it was centrifuged at 4000 rpm for 10 minutes to separate serum. The measurements of FT3, FT4 and TSH were done using the technique of enhanced chemiluminescence immunoassay (ECI) [28] [29] with Vitros 3600 machine. The normal reference ranges of TFT values used at the laboratory were 4.26 - 8.10 pmol/L for FT3, 10.20 - 28.20 pmol/L for FT4 and 0.46 - 4.68 mIU/L for TSH.

The statistical as well as graphical analysis was performed among the age and gender based variables such as thyroid lobe volumes, FT3, FT4 and TSH using the softwares: Origin-2017 and MS Excel-2007. The standard deviations and/or standard errors were calculated in each of the mean values. The possible linear and second order polynomials were fitted providing the related equations with standard errors in their coefficients. The degrees of correlation among the variables were evaluated with Pearson's correlation test and the results with $p < 0.05$ were accepted as statistically significant.

## 3. Results and Discussion

The results from observed data and analysis are classified into three categories: ultrasonographic (USG) results, thyroid function test (TFT) results and USG & TFT cross-sectional analysis of the hospital based euthyroid subjects to explain the possible correlations among the variables such as age, thyroid lobe volumes, FT3, FT4 and TSH of males and females.

### 3.1. Thyroid Ultrasonographic Results

From the USG reports of euthyroid subjects having mean age 32 ± 17.18 years ranging 1 to 86 years, the mean ± SD of left lobe volume (LLV), right lobe volume (RLV) and thyroid gland volume (TGV) are 2.12 ± 1.07 mL, 2.61 ± 1.40 mL and 4.74 ± 2.30 mL, respectively with $p < 0.0001$. Here, RLV has been found to be greater than LLV. The results with the range of normal thyroid size are listed in **Table 1**. The graph (**Figure 1(a)**) for y(TGV) vs. x(age) of the people satisfies the trendline of second order polynomial with $R^2 = 0.197$ whose equation is

$$y = (-0.002 \pm 0.0004)x^2 + (0.19 \pm 0.03)x + (1.45 \pm 0.47) \quad (1)$$

where the included errors indicate the standard errors in the related coefficients.

The volume of normal thyroid gland is greater for adults than for early pubertal

**Table 1.** Normal thyroid size ($p < 0.0001$) of the euthyroid subjects.

| Variables | Age (yr) | LLV (mL) | RLV (mL) | TGV (mL) |
|---|---|---|---|---|
| **Mean** | 32.02 | 2.12 | 2.61 | 4.74 |
| **SE** | 1.16 | 0.07 | 0.09 | 0.15 |
| **SD** | 17.18 | 1.07 | 1.40 | 2.30 |
| **Min.** | 1.50 | 0.16 | 0.24 | 0.40 |
| **Max.** | 86.00 | 7.01 | 7.76 | 13.87 |

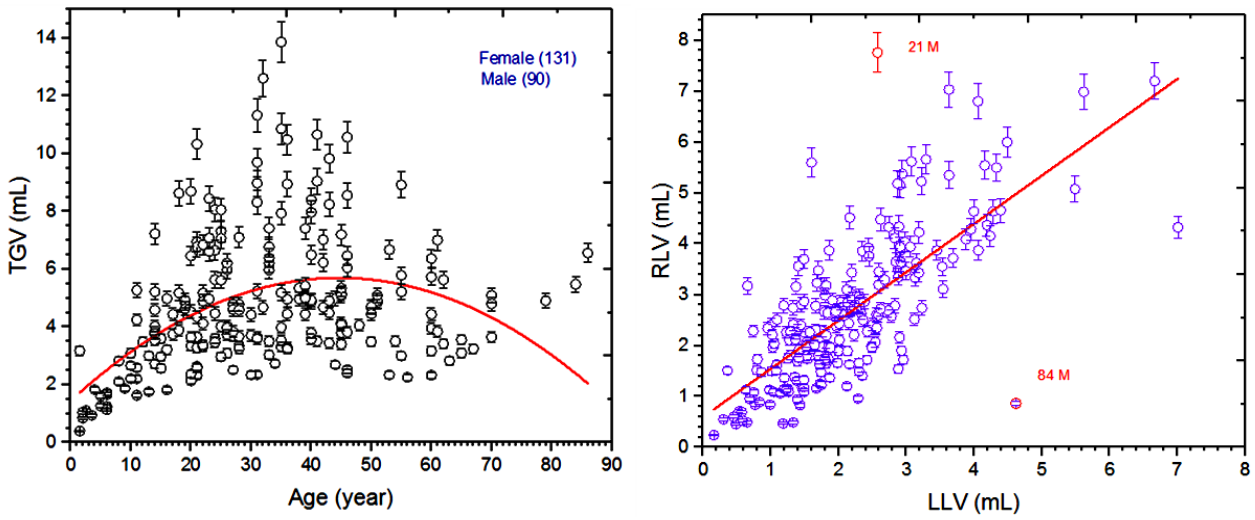


(a) (b)

**Figure 1.** (a) Thyroid size with aging, and (b) positive correlation between right lobe and left lobe volumes. The error-bars indicate 5% of the measured value.

and elderly which is in agreement with the results in [13] [14] [30]. However, the mean thyroid volume excluding isthmus in our study is found to be smaller for both genders than that reported by [13] [14] [30]. Seker *et al.* (2010) reported the mean thyroid volume as 13.00 ± 6.27 mL for the age range of 15 - 78 years [30]. Our result for the normal thyroid size is still smaller than 6.63 ± 2.50 mL as studied by Kayastha *et al.* (2010) for the age range of 1-83 years [10].

There is a linear correlation between LLV and RLV as demonstrated in **Figure 1(b)**. The equation of linear fit with Pearson's $r = 0.727$ and $p < 0.001$ for y(LLV) vs. x(RLV) is

$$y = (0.95 \pm 0.06)x + (0.60 \pm 0.14) \quad (2)$$

This means that RLV can be estimated by knowing LLV.

Taking average values ($p < 0.05$) for both genders from **Table 2**, the thyroid size is maximum, *i.e.* 6.09 ± 2.78 mL in the age group of 31 - 40 years. Its value is the least, *i.e.* 1.73 ± 0.17 mL in the childhood range of 1 - 10 years. This variation of thyroid size is due to the various reasons including the change in body mass index and body surface area. If we analyze the gender based variations of thyroid volume, it is maximum, *i.e.* 7.84 ± 3.18 mL for males in the age group of 31 - 40

years and 5.62 ± 2.49 mL for females in the age group of 41 - 50 years as depicted in **Table 2** and compared by the column plots in **Figure 2(a)**. Here, the thyroid volume is greater for females than for males in the age groups of 11 - 20 and 41 - 50 years and otherwise, it is greater for males. It is to be noted that the age groups of 11 - 20 and 41 - 50 years for females include the periods of menarche and menopause respectively. The thyroid of healthy Nepalese people has smaller size in both genders than that reported in [30] [31]. Seker *et al.* (2010) reported the mean thyroid volume as 15.87 ± 7.18 mL for males and 10.94 ± 4.53 mL for females [30]. In the study of 500 healthy adults performed by Oberhofer *et al.* (1989), the mean TGV of males is 14.94 mL and that of females is 12.09 mL [31]. The main cause behind such variation of thyroid size is the demographic status of subjects under study.

In this study, the mean ± SD ($p < 0.0001$) of LLV and RLV are 2.12 ± 0.98 mL and 2.54 ± 1.29 mL, respectively for females aged 33.46 ± 15.10 years. Similarly, for males of age 29.92 ± 19.72 years, LLV is 2.13 ± 1.20 mL and RLV is 2.73 ± 1.55 mL. The gender based minimum and maximum range of the thyroid lobe volumes with the standard errors are listed in **Table 3**. The variations of LLV

**Table 2.** Normal thyroid size ($p < 0.05$) averaged over different age groups.

| Age (yr) | Female | | | Male | | |
|---|---|---|---|---|---|---|
| | TGV (mL) | SE | N | TGV (mL) | SE | N |
| **01 - 10** | 1.53 | 0.22 | 8 | 1.86 | 0.25 | 12 |
| **11 - 20** | 4.27 | 0.43 | 17 | 3.88 | 0.35 | 21 |
| **21 - 30** | 4.41 | 0.23 | 32 | 5.54 | 0.52 | 20 |
| **31 - 40** | 5.31 | 0.40 | 31 | 7.84 | 0.85 | 14 |
| **41 - 50** | 5.62 | 0.48 | 27 | 4.74 | 0.19 | 7 |
| **51 - 60** | 4.40 | 0.73 | 9 | 4.91 | 0.41 | 9 |
| **61 - 90** | 4.09 | 0.42 | 7 | 4.93 | 0.56 | 7 |

**Table 3.** Normal ranges of thyroid lobe volumes ($p < 0.0001$) in males and females.

| Gender | Values | Age (yr) | LLV (mL) | RLV (mL) | TGV (mL) |
|---|---|---|---|---|---|
| **Female** | Mean | 33.46 | 2.12 | 2.54 | 4.66 |
| | SE | 1.32 | 0.09 | 0.11 | 0.19 |
| | SD | 15.10 | 0.98 | 1.29 | 2.12 |
| | Min. | 1.50 | 0.16 | 0.24 | 0.40 |
| | Max. | 79.00 | 5.62 | 7.03 | 12.61 |
| **Male** | Mean | 29.92 | 2.13 | 2.73 | 4.85 |
| | SE | 2.08 | 0.13 | 0.16 | 0.27 |
| | SD | 19.72 | 1.20 | 1.55 | 2.56 |
| | Min. | 1.50 | 0.30 | 0.49 | 0.85 |
| | Max. | 86.00 | 7.01 | 7.76 | 13.87 |

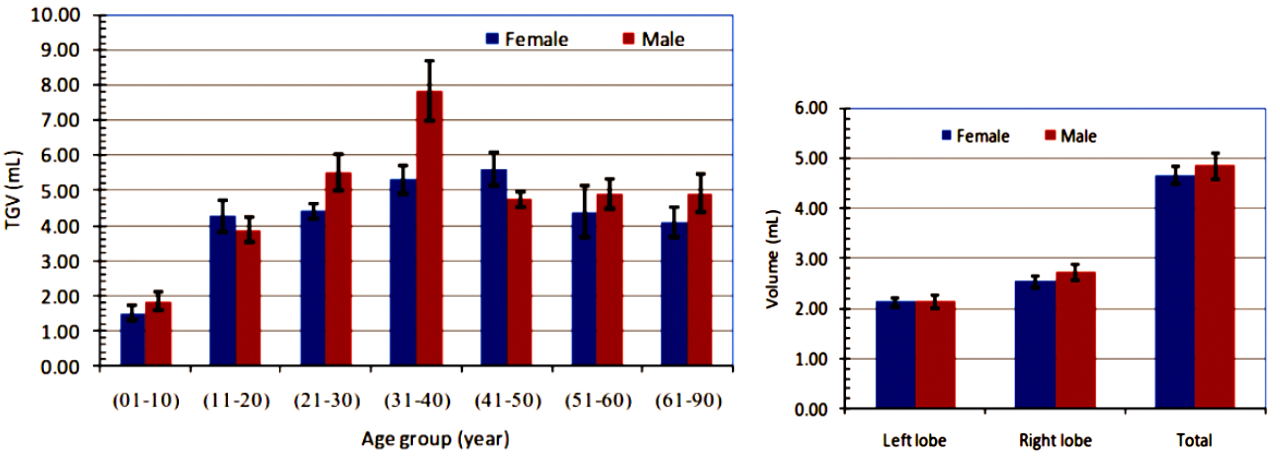


**Figure 2.** (a) Normal thyroid size related to the gender based age groups including standard error bars, and (b) gender-specific changes in the normal thyroid size with the standard error bars.

and RLV are shown by the column plots in **Figure 2(b)**. Here, LLV is almost same for both genders whereas RLV is higher for males than for females. In general, RLV is greater than LLV. The right handed subjects have significantly larger volume of right thyroid lobe as explained by Ying *et al.* (2009) [32]. Lewinisky *et al.* (1982) and Gerendai *et al.* (2001) suggest that there is unilateral differentiation of hypothalamus to enlarge the right lobe of thyroid gland [33] [34].

### 3.2. Thyroid Function Test Results

From the TFT reports of 1737 female and 634 male euthyroid subjects aged 1 - 93 years, the mean values with the standard deviations ($p < 0.0001$) of serum TSH, FT4 and FT3 are observed to be 2.30 ± 0.98 mIU/L, 14.09 ± 2.71 pmol/L and 5.46 ± 0.82 pmol/L respectively. The observed ranges of normal TFT values are listed in **Table 4**. These results are not much deviated from the TFT values of euthyroid subjects reported in Mahato *et al.* (2015) [20]. However, the mean value of FT4 in this study is less than that in Rohil *et al.* (2010) [35]. To analyze the correlations of FT3 with FT4 and that of FT3 or FT4 with TSH, the linear fits of the corresponding data are performed as shown in **Figure 3**. Here, the linear equation of the best fit between $y_1$ (FT3) and $x_1$ (FT4) with Pearson's r = 0.095, p-value < 0.001 and the standard errors in the slope and intercept (**Figure 3(a)**) is

$$y_1 = (0.03 \pm 0.006)x_1 + (5.05 \pm 0.088) \quad (3)$$

Also, the linear fit between $y_2$ (FT3) and $x_2$ (TSH) shown in **Figure 3(b)** obtains the equation of a straight line (3) with the standard errors in slope and intercept, Pearson's r = −0.061 and p-value < 0.001.

$$y_2 = (-0.05 \pm 0.017)x_2 + (5.58 \pm 0.04) \quad (4)$$

Similarly, the equation of linear fit between $y_3$ (FT4) and $x_3$ (TSH) as in **Figure 3(b)** with Pearson's r = −0.113 and p-value = 0.002 is

**Table 4.** TFT values ($p < 0.0001$) of the clinically euthyroid subjects.

| Variables | TSH (mIU/L) | FT4 (pmol/L) | FT3 (pmol/L) |
|---|---|---|---|
| **Mean** | 2.30 | 14.09 | 5.46 |
| **SE** | 0.02 | 0.06 | 0.02 |
| **SD** | 0.98 | 2.71 | 0.82 |
| **Min.** | 0.46 | 10.20 | 4.26 |
| **Max.** | 4.68 | 28.20 | 8.10 |

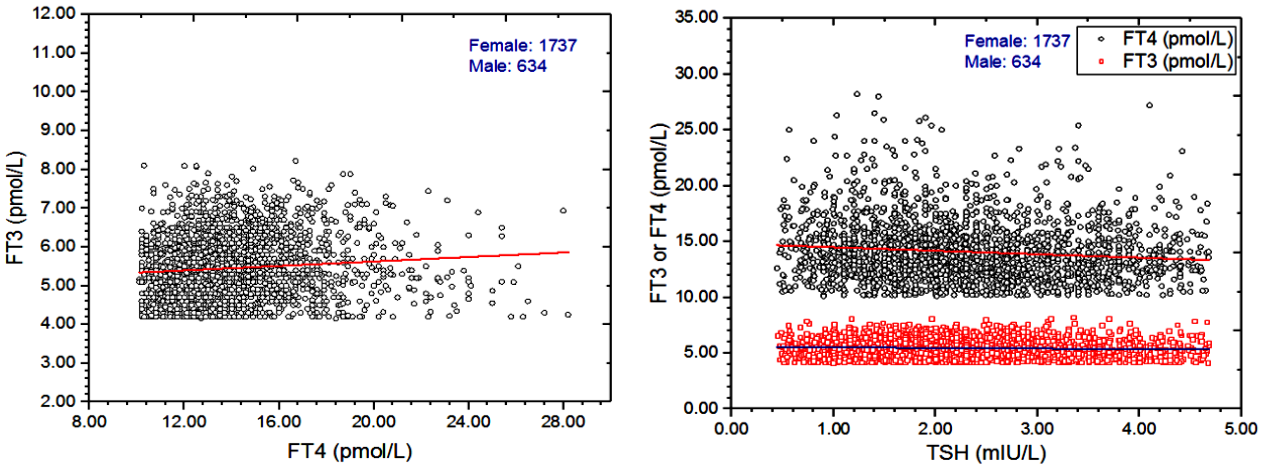


(a) (b)

**Figure 3.** Linear correlations between (a) FT3 & FT4 and (b) FT3 or FT4 & TSH of the euthyroid subjects.

$$y_3 = (-0.31 \pm 0.056)x_3 + (14.81 \pm 0.14) \quad (5)$$

There is a positive correlation between FT3 & FT4 whereas negative correlations between FT3 or FT4 & TSH. This signifies that T3 and T4 are feeded back to hypothalamus and pituitary through the blood stream and under the controlled mechanism on HPT-axis, T3 and T4 are produced by thyroid gland. Finally, the thyroid cycle completes under with the regulation of thyroid hormones.

In the infant age (<1 years), TSH, FT3 and FT4 all are higher than in the adults. The serum free TH levels are observed to be decreased and then increased slowly in advancing from child to adult and then to elderly age for both genders (**Figure 4**). However, TSH is the highest, *i.e.* 2.57 ± 0.89 pmol/L in the early childhood < 1 years and it is the lowest, *i.e.* 2.05 ± 0.93 pmol/L ($p < 0.0001$) in the elderly of 71 - 100 years. If we analyze the results depicted in **Table 5** & **Table 6**, we see the almost negative correlations between FT3 or FT4 and TSH along each age group of male as well as female adults. This is the fact behind negative feedback mechanism of thyroid hormones in the thyroid cycle. In many researches [22] [23] [24], serum FT4 is observed to be low in the middle age subjects. Fontes *et al.* (2013) reported that TSH increases and conversely, FT4 decreases with aging [22]. In a study performed by Chaurasia *et al.* (2011) at

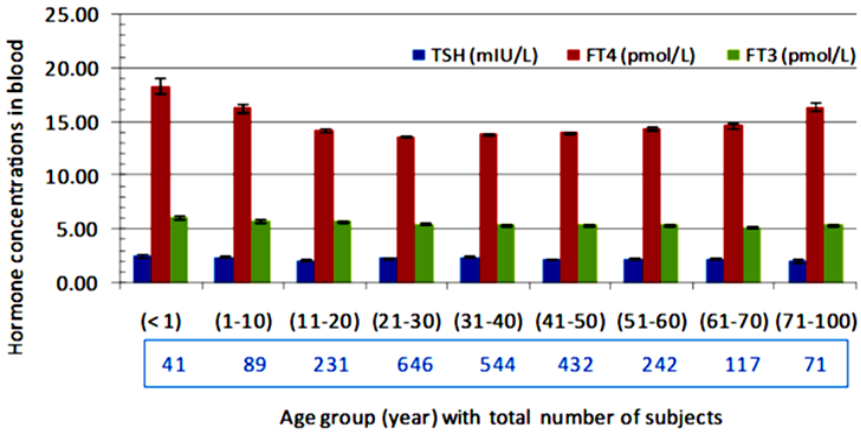


**Figure 4.** Age-specific changes in the normal TFT values with the standard error bars.

**Table 5.** TFT values averaged in the different age groups of 1748 female euthyroid subjects.

| | Age (yr) | (<1) | (1 - 10) | (11 - 20) | (21 - 30) | (31 - 40) | (41 - 50) | (51 - 60) | (61 - 70) | (71 - 80) | (81 - 100) |
|---|---|---|---|---|---|---|---|---|---|---|---|
| **TSH (mIU/L)** | Mean | 2.58 | 2.30 | 2.11 | 2.34 | 2.50 | 2.29 | 2.35 | 2.31 | 2.12 | 2.55 |
| | SD | 0.91 | 0.89 | 1.00 | 0.94 | 0.92 | 0.95 | 1.07 | 1.21 | 0.88 | 1.32 |
| **FT4 (pmol/L)** | Mean | 19.87 | 16.73 | 13.99 | 13.49 | 13.76 | 13.98 | 14.50 | 14.58 | 16.75 | 17.90 |
| | SD | 5.63 | 2.82 | 2.74 | 2.13 | 2.49 | 2.42 | 2.65 | 2.49 | 3.84 | 4.15 |
| **FT3 (pmol/L)** | Mean | 5.59 | 5.65* | 5.62 | 5.46 | 5.32 | 5.33 | 5.40 | 5.04 | 5.19 | 5.64 |
| | SD | 1.13 | 0.95 | 0.80 | 0.81 | 0.80 | 0.76 | 0.81 | 0.68 | 0.83 | 0.94 |
| | **N** | 11 | 39 | 162 | 511 | 408 | 332 | 175 | 72 | 31 | 7 |

*The ANOVA-single factor $p < 0.0001$ for all of the TFT values averaged over the age groups except for FT3 = 5.67 ± 0.95 ($p = 0.57$) in the age group 1 - 10 years.

**Table 6.** TFT values averaged in the different age groups of 665 male euthyroid subjects.

| | Age (yr) | (<1) | (1 - 10) | (11 - 20) | (21 - 30) | (31 - 40) | (41 - 50) | (51 - 60) | (61 - 70) | (71 - 80) | (81 - 100) |
|---|---|---|---|---|---|---|---|---|---|---|---|
| **TSH (mIU/L)** | Mean | 2.56 | 2.56 | 2.11 | 2.22 | 2.28 | 2.03 | 2.12 | 2.15 | 1.88 | 1.88 |
| | SD | 0.88 | 1.17 | 0.91 | 0.97 | 0.91 | 0.90 | 1.05 | 1.30 | 0.92 | 0.74 |
| **FT4 (pmol/L)** | Mean | 17.78 | 15.91 | 14.81 | 13.90 | 14.02 | 14.10 | 14.19 | 14.69 | 15.14 | 17.46 |
| | SD | 4.03 | 3.84 | 3.47 | 2.58 | 2.88 | 2.70 | 3.12 | 3.86 | 2.93 | 3.71 |
| **FT3 (pmol/L)** | Mean | 6.20 | 5.88* | 5.96 | 5.69 | 5.54 | 5.64 | 5.45 | 5.41 | 5.36 | 6.07 |
| | SD | 0.94 | 1.01 | 0.87 | 0.79 | 0.80 | 0.82 | 0.84 | 0.77 | 0.77 | 0.92 |
| | **N** | 30 | 50 | 69 | 135 | 136 | 100 | 67 | 45 | 26 | 7 |

*The ANOVA-single factor $p < 0.0001$ for all of the TFT values averaged over the age groups except for FT3 = 5.88 ± 1.01 ($p = 0.86$) in the age group 1 - 10 years.

Gujarat, India, T4 levels are found to be lower in 20 - 40 years than other age groups [23]. Lipson *et al.* 1979 interprets that TSH has significant positive correlation and T3 has weak negative correlation with aging of the euthyroid adults [24]. The variation of TH levels with aging is associated with brain development, autonomous tissues, nutritional status, gender based biological activities and en-

vironmental factors.

The age and gender based variations of TFT reports are depicted in **Table 5** & **Table 6** where the concentrations of the serum free TH remain almost same from 11 to 60 years in both male and female euthyroid subjects. If we draw the column plots of age dependent TH levels separately for the both genders, they follow almost same pattern as in the given **Figure 4**. The pattern of change in TSH is more distinct which is 2.34 ± 1.1 mIU/L for males and 1.88 ± 0.81 mIU/L for females in the age > 71 years than in other age groups. In the infant age group < 1 years, TSH as well as T3/T4 are higher in both genders. According to Franklyn *et al.* (1985), the age based changes in serum free TH are not much evident but FT3 is lower in females than in males aged 16 - 29 years [36]. In the study of Sujuky *et al.* (2012), FT3 or FT4 has negative correlation with aging of males, but no correlation in females, and TSH increases with aging in both genders [6].

### 3.3. USG and TFT Cross-Sectional Analysis

In a cross-sectional study of USG and TFT values of 34 euthyroid adults (18 - 50 years), the mean ± SD ($p < 0.0001$) of age, thyroid volume, FT3, FT4 and TSH are 33.56 ± 11.13 years, 5.05 ± 2.06 mL, 5.62 ± 0.80 pmol/L, 14.89 ± 3.38 pmol/L and 2.31 ± 0.89 mIU/L, respectively. The cross-correlations among TSH, FT3 and FT4 have been demonstrated in **Figure 5(a)**. Here, FT4 is exceptionally high near to the upper boundary of the given reference level without fall in TSH of 16$^{th}$ subject which may be related to the undiagnosed non-thyroid illness. Otherwise, the serum free thyroxin (FT4) lies within the small range. In many subjects, the values of TSH lying below its average line are associated with the values of FT3 and/or FT4 lying above their average lines and vice versa. This is due to the negative feedback mechanism of TH to hypothalamus and pituitary to

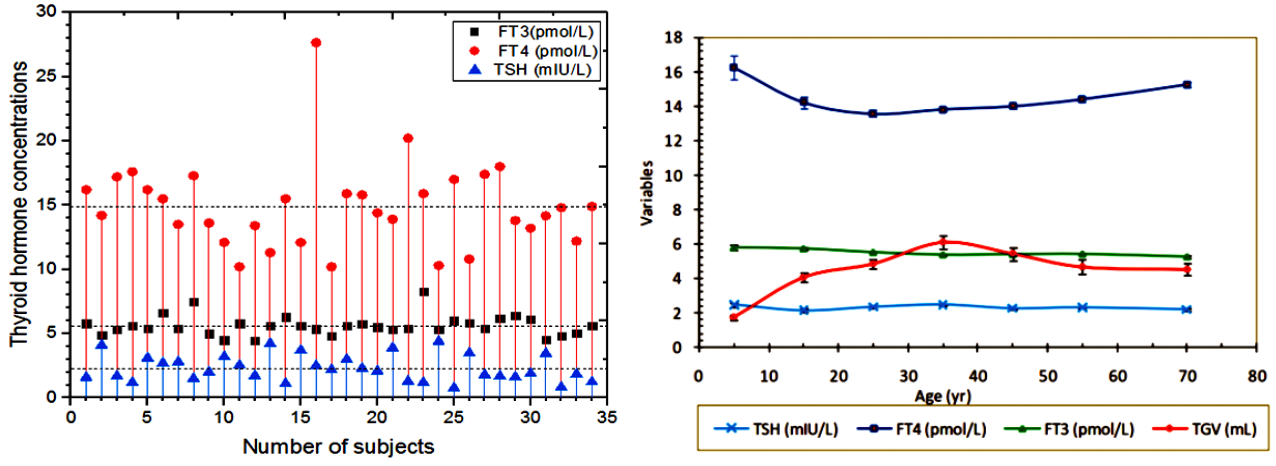


(a) (b)

**Figure 5.** (a) Fluctuations in TFT values in 34 adults having normal thyroid where the horizontal dotted lines represent the observed mean values, and (b) healthy thyroid status with aging where the markers indicate the mean values in the age groups of 10 years interval.

trigger the production of thyrotropin (TSH) by means of which they are produced in a controlled way from the thyroid gland.

The thyroid size and the TFT values varying with different age groups of euthyroid subjects are plotted in **Figure 5(b)**. The results in this study show that FT3 and TSH remain almost constant, but FT4 decreases and then increases with aging. Conversely, the normal thyroid size increases and then decreases with aging.

Age, gender, thyroid size, FT3, FT4 and TSH are included as covariates. Lack of health awareness in rural areas, urbanization with increased environmental pollutants and reduced physical activity, socio-economic conditions, nutritional status, biologically activated life stages, mental and physical stress, and genetics play the crucial role in the thyroid malfunction and the development of metabolic syndrome. The alterations in thyroid functions and prevalence of thyroid diseases are higher in women than in men due to the change in lipid profile, hyperinsulinemia, android obesity, and hypertension [37]. The aging results the increased thyroid dysfunction and prevalence of metabolic syndrome. Along with the adverse changes in TFT values by estrogenic protective defects, women have higher inclination towards thyroid dysfunction than men. Moreover, the gender based changes in thyroid size can also be observed distinctly in menarche and menopause periods.

## 4. Conclusions

In this study, the thyroid gland of the euthyroid subjects has mean ± SD ($p < 0.001$) of LLV and RLV as 2.12 ± 1.07 mL, 2.61 ± 1.40 mL, respectively. RLV with higher value has significant positive linear correlation with LLV ($r = 0.727$, $p < 0.001$). TGV increases and then decreases with aging having larger value for adults than that for children and elderly. LLV of both genders is almost same, but RLV and TGV of males are larger than that of females. In the age groups including periods of menarche (11 - 20 years) and menopause (41 - 50 years) of females, the size of their thyroid gland is larger than that of males. TGV is maximum in the age group of 31 - 40 years for males and it is maximum in the age group of 41 - 50 years for females.

The TFT values of the hospital based euthyroid subjects have mean ± SD ($p < 0.0001$) of FT3, FT4 and TSH as 5.46 ± 0.82 pmol/L, 14.09 ± 2.71 pmol/L and 2.30 ± 0.98 mIU/L, respectively. FT3 has a weak positive linear correlation ($r = 0.095$, $p < 0.001$) with FT4. FT4 has a small degree of negative linear correlation ($r = -0.113$, $p = 0.002$) with TSH. The TFT values are higher for the early infant age group (< 1 years). FT3 and TSH are not significantly changed, but FT4 decreases from children to adults and then increases slightly to elderly in the similar way for the both genders.

The thyroid size increases and then decreases, but conversely, FT4 decreases and then increases with aging by means of increased thyroid dysfunction and prevalence of metabolic syndrome in the elderly. In this normal thyroid analysis,

FT3 and FT4 have negative correlations with TSH supporting the principle of negative feedback mechanism in the thyroid cycle.

## Ethical Consent and Approval

This research work has been performed under the ethical guidelines provided by and taking authority from Institutional Review Board (IRB), Institute of Medicine (IOM), Tribhuvan University Teaching Hospital (TUTH), Maharajgunj, Kathmandu, Nepal.

## Acknowledgements

We are thankful to the head and members of Department of Radiology, Department of Biochemistry and Institutional Review Board-TU Teaching Hospital for their technical supports in this research work.

## Authors' Contributions

All authors were involved in the research and they read and approved the final manuscript.

## Funding

This work was partially supported by Nepal Academy of Science and Technology (NAST) through a grant of PhD fellowship to the first author.

## Conflicts of Interest

The authors declare that they have no conflict of interest.

## References

[1] Warner, A. and Mittag, J. (2012) Thyroid Hormone and the Central Control of Homeostasis. *Journal of Molecular Endocrinology*, **49**, R29-R35. https://doi.org/10.1530/JME-12-0068

[2] Führer, D., Brix, K. and Biebermann, H. (2015) Understanding the Healthy Thyroid State in 2015. *European Thyroid Journal*, **4**, 1-8. https://doi.org/10.1159/000431318

[3] Vadiveloo, T., Donnan, P.T., Murphy, M.J. and Leese, G.P. (2013) Age- and Gender-Specific TSH Reference Intervals in People with No Obvious Thyroid Disease in Tayside, Scotland: The Thyroid Epidemiology, Audit, and Research Study (TEARS). *The Journal of Clinical Endocrinology & Metabolism*, **98**, 1147-1153. https://doi.org/10.1210/jc.2012-3191

[4] Kratzsch, J., Fiedler, G.M., Leichtle, A., Brügel, M., Buchbinder, S., Otto, L., Sabri, O., Matthes, G. and Thiery, J. (2005) New Reference Intervals for Thyrotropin and Thyroid Hormones Based on National Academy of Clinical Biochemistry criteria and Regular Ultrasonography of the Thyroid. *Clinical Chemistry*, **51**, 1480-1486. https://doi.org/10.1373/clinchem.2004.047399

[5] Bremner, A.P., Feddema, P., Leedman, P.J., Brown, S.J., Beilby, J.P., Lim, E.M., Wilson, S.G., O'leary, P.C. and Walsh, J.P. (2012) Age-Related Changes in Thyroid Function: A Longitudinal Study of a Community-Based Cohort. *The Journal of Clinical Endocrinology*, **97**, 1554-1562. https://doi.org/10.1210/jc.2011-3020

[6] Suzuki, S., Nishio, S.I., Takeda, T. and Komatsu, M. (2012) Gender-Specific Regulation of Response to Thyroid Hormone in Aging. *Thyroid Research*, **5**, 1-8. https://doi.org/10.1186/1756-6614-5-1

[7] Völzke, H., Alte, D., Kohlmann, T., Lüdemann, J., Nauck, M., John, U. and Meng, W. (2005) Reference Intervals of Serum Thyroid Function Tests in a Previously Iodine-Deficient Area. *Thyroid*, **15**, 279-285. https://doi.org/10.1089/thy.2005.15.279

[8] Porcu, E., Medici, M., Pistis, G., Volpato, C.B., Wilson, S.G., Cappola, A.R., Bos, S.D., Deelen, J., den Heijer, M., Freathy, R.M. and Lahti, J. (2013) A Meta-Analysis of Thyroid-Related Traits Reveals Novel Loci and Gender-Specific Differences in the Regulation of Thyroid Function. *PLoS Genetics*, **9**, e1003266. https://doi.org/10.1371/journal.pgen.1003266

[9] Hansen, P.S., Brix, T.H., Bennedbæk, F.N., Bonnema, S.J., Kyvik, K.O. and Hegedüs, L. (2004) Genetic and Environmental Causes of Individual Differences in Thyroid Size: A Study of Healthy Danish Twins. *The Journal of Clinical Endocrinology & Metabolism*, **89**, 2071-2077. https://doi.org/10.1210/jc.2003-031999

[10] Kayastha, P., Paudel, S., Shrestha, D.M., Ghimire, R.J. and Pradhan, S. (2010) Study of Thyroid Volume by Ultrasonography in Clinically Euthyroid Patients. *Journal of Institute of Medicine*, **32**, 36-43.

[11] Turcios, S., Lence-Anta, J.J., Santana, J.L., Pereda, C.M., Velasco, M., Chappe, M., Infante, I., Bustillo, M., García, A., Clero, E. and Maillard, S. (2015) Thyroid Volume and Its Relation to Anthropometric Measures in a Healthy Cuban Population. *European Thyroid Journal*, **4**, 55-61. https://doi.org/10.1159/000371346

[12] Ivanac, G., Rožman, B., Škreb, F., Brkljačić, B. and Pavić, L. (2004) Ultrasonographic Measurement of the Thyroid Volume. *Collegium Antropologicum*, **28**, 287-291. https://hrcak.srce.hr/4907

[13] Chanoine, J.P., Toppet, V., Lagasse, R., Spehl, M. and Delange, F. (1991) Determination of Thyroid Volume by Ultrasound from the Neonatal Period to Late Adolescence. *European Journal of Pediatrics*, **150**, 395-399. https://doi.org/10.1007/BF02093716

[14] Hegedus, L., Perrild, H., Poulsen, L.R., Andersen, J.R., Holm, B., Schnohr, P., Jensen, G. and Hansen, J.M. (1983) The Determination of Thyroid Volume by Ultrasound and Its Relationship to Body Weight, Age, and Sex in Normal Subjects. *The Journal of Clinical Endocrinology & Metabolism*, **56**, 260-263. https://doi.org/10.1210/jcem-56-2-260

[15] Berghout, A., Wiersinga, W.M., Smits, N.J. and Touber, J.L. (1987) Determinants of Thyroid Volume as Measured by Ultrasonography in Healthy Adults in a Non-Iodine Deficient Area. *Clinical Endocrinology*, **26**, 273-280. https://doi.org/10.1111/j.1365-2265.1987.tb00784.x

[16] Leppäluoto, J., Sikkilä, K. and Hassi, J. (1998) Seasonal Variation of Serum TSH and Thyroid Hormones in Males Living in Subarctic Environmental Conditions. *International Journal of Circumpolar Health*, **57**, 383-385.

[17] Raj, K.C.S. (2014) Thyroid Function Tests and Its Interpretation. *Journal of Pathology of Nepal*, **4**, 584-590. https://doi.org/10.3126/jpn.v4i7.10318

[18] Biondi, B. (2013) The Normal TSH Reference Range: What Has Changed in the Last Decade? *The Journal of Clinical Endocrinology & Metabolism*, **98**, 3584-3587. https://doi.org/10.1210/jc.2013-2760

[19] Shivaraj, G., Prakash, B.D., Sonal, V., Shruthi, K., Vinayak, H. and Avinash, M. (2009) Thyroid Function Tests: A Review. *European Review for Medical and Phar-*

*macological Sciences*, **13**, 341-349.

[20] Mahato, R.V., Jha, B., Singh, K.P., Yadav, B.K., Shah, S.K. and Lamsal, M. (2015) Status of Thyroid Disorders in Central Nepal: A Tertiary Care Hospital Based Study. International. *Journal of Applied Science and Biotechnology*, **3**, 119-122. https://doi.org/10.3126/ijasbt.v3i1.12218

[21] Dangol, R.K., Lanjekar, P. and Pulipati, C. (2017) Thyroid Function Abnormalities among Hospital Patients of Hilly Nepal. *Journal of Lumbini Medical College*, **5**, 29-33. https://doi.org/10.22502/jlmc.v5i1.118

[22] Fontes, R., Coeli, C.R., Aguiar, F. and Vaisman, M. (2013) Reference Interval of Thyroid Stimulating Hormone and Free Thyroxine in a Reference Population over 60 Years Old and in Very Old Subjects (over 80 Years): Comparison to Young Subjects. *Thyroid Research*, **6**, 13. https://doi.org/10.1186/1756-6614-6-13

[23] Chaurasia, P., Modi, B., Mangukiya, S., Jadav, P. and Shah, R. (2011) Variation in Thyroid Hormones Level among People of Different Age, Gender and Seasons, Piparia, Gujarat. *National Journal of Medical Research*, **1**, 57-59.

[24] Lipson, A., Nickoloff, E.L., Hsu, T.H., Kasecamp, W.R., Drew, H.M., Shakir, R. and Wagner, J.H. (1979) A Study of Age-Dependent Changes in Thyroid Function Tests in Adults. *Journal of Nuclear Medicine: Official Publication, Society of Nuclear Medicine*, **20**, 1124-1130.

[25] Chaudhary, V. and Shahina, B. (2013) Thyroid Ultrasound. *Indian Journal of Endocrinology and Metabolism*, **17**, 219. https://doi.org/10.4103/2230-8210.109667

[26] Hendee, W.R. and Ritenour, E.R. (2011) Medical Imaging Physics. 4th Edition, John Wiley & Sons, US.

[27] Abu-Zidan, F.M., Hefny, A.F. and Corr, P. (2011) Clinical Ultrasound Physics. *Journal of Emergencies, Trauma and Shock*, **4**, 501.

[28] Fereja, T.H., Hymete, A. and Gunasekaran, T. (2013) A Recent Review on Chemiluminescence Reaction, Principle and Application on Pharmaceutical Analysis. *ISRN Spectroscopy*, **2013**, Article ID: 230858.

[29] Weeks, I., Sturgess, M.L. and Woodhead, J.S. (1986) Chemiluminescence Immunoassay: An Overview. *Clinical Science*, **70**, 403-408. https://doi.org/10.1042/cs0700403

[30] Şeker, S. and Taş, İ. (2010) Determination of Tthyroid Volume and Its Relation with Isthmus Thickness. *European Journal of General Medicine*, **7**, 125-129. https://doi.org/10.29333/ejgm/82838

[31] Oberhofer, R., Ober, A., Oberkofler, F. and Amor, H. (1989) Thyroid Gland Volumes of Healthy Adults in an Area with Endemic Goiter. *Acta Medica Austriaca*, **16**, 38-41.

[32] Ying, M. and Yung, D. (2009) Asymmetry of Thyroid Lobe Volume in Normal Chinese Subjects: Association with Handedness and Position of Esophagus. *The Anatomical Record*, **292**, 169-174. https://doi.org/10.1002/ar.20803

[33] Lewiński, A., Gerendai, I., Pawlikowski, M. and Halász, B. (1982) Unilateral Posterior Deafferentation of Hypothalamus and Mitotic Activity of Thyroid Follicular Cells under Normal Conditions and after Hemithyroidectomy. *Endocrinologia Experimentalis*, **16**, 75-80.

[34] Gerendai, I. and Halász, B. (2001) Asymmetry of the Neuroendocrine System. *Physiology*, **16**, 92-95. https://doi.org/10.1152/physiologyonline.2001.16.2.92

[35] Rohil, V., Mishra, A.K., Shrewastwa, M.K., Mehta, K.D., Lamsal, M., Baral, N. and Majhi, S. (2010) Subclinical Hypothyroidism in Eastern Nepal: A Hospital Based

Study. *Kathmandu University Medical Journal*, **8**, 231-237.
https://doi.org/10.3126/kumj.v8i2.3565

[36] Franklyn, J.A., Ramsden, D.B. and Sheppard, M.C. (1985) The Influence of Age and Sex on Tests of Thyroid Function. *Annals of Clinical Biochemistry*, **22**, 502-505.
https://doi.org/10.1177/000456328502200506

[37] Meng, Z., Liu, M., Zhang, Q., Liu, L., Song, K., Tan, J., Jia, Q., Zhang, G., Wang, R., He, Y. and Ren, X. (2015) Gender and Age Impacts on the Association between Thyroid Function and Metabolic Syndrome in Chinese. *Medicine*, **94**, 1-9.

## Abbreviations

USG: Ultrasonography
TFT: Thyroid Function Test
LLV: Left Lobe Volume
RLV: Right Lobe Volume
TGV: Thyroid Gland Volume
TH: Thyroid Hormones
FT3: Free Triiodothyronine
FT4: Free Thyroxine
TSH: Thyroid Stimulating Hormone

# *Certificate of Appreciation*

This certificate is awarded to

## TIKA RAM LAMICHHANE

**For attendance**

**at the**

**14th Asia-Pacific Physics Conference 2019 (APPC14)**

**organised by**

**The Association of Asia Pacific Physical Societies (AAPPS)**
**and**
**Institut Fizik Malaysia**

♦ 17-21 November 2019 ♦
Borneo Convention Centre Kuching
Sarawak, Malaysia

Prof. Dr. Kurunathan Ratnavelu
Chairman, Local Organizing Committee
Malaysia

# *Certificate of Appreciation*

This certificate is awarded to

## TIKA RAM LAMICHHANE

**for the oral presentation with the title**

**"Thiocyanate-induced Conformational Changes on Thyroid Hormone Receptor-Beta by Model Ligand-T2SCN Interactions"**
**at the**

**14th Asia-Pacific Physics Conference 2019 (APPC14)**

**organised by**
**The Association of Asia Pacific Physical Societies (AAPPS)**
**and**
**Institut Fizik Malaysia**

♦ 17-21 November 2019 ♦
Borneo Convention Centre Kuching
Sarawak, Malaysia

Prof. Dr. Kurunathan Ratnavelu
Chairman, Local Organizing Committee
Malaysia

# International Conference on Nanosciences and High Energy Physics (ICNHEP-2019)

February 4-6, 2019

Central Department of Physics

Tribhuvan University, Kirtipur, Nepal

# Certificate

This is to Certify that Dr./Mr./Ms ..... Tikaram Lamichhane ..... has participated in "ICNHEP-2019" and presented a research paper entitled "... Biophysical analysis of Thyroid function test reports." .....

The ICNHEP-2019 Review committee appreciates the work agrees for

Best Poster Award in M.Sc./Ph.D Category.

Prof. Dr. Ram Pd. Khatiwada
Dean, IoST, TU, Kirtipur

Dr. Gopi Chandra Kaphle
Convener, ICNHEP-2019

Prof. Dr. Binil Aryal
Head CDP, TU, Kirtipur

# International Conference on Nanosciences and High Energy Physics (ICNHEP-2019)

February 4-6, 2019

Central Department of Physics

Tribhuvan University, Kirtipur, Nepal

# Certificate

This is to Certify that Dr./Mr./Ms Tika Ram Lamichhane has participated in "ICNHEP-2019" and presented a invited talk/ research paper.

The title of the talk / paper is "Echo dephasing and heat capacity from constrained and unconstrained dynamics of Triiodothyronine nuclear receptor protein"

Prof. Dr. Ram Pd. Khatiwada
Dean, IoST, TU, Kirtipur

Dr. Gopi Chandra Kaphle
Convener, ICNHEP-2019

Prof. Dr. Binil Aryal
Head CDP, TU, Kirtipur

# INTERNATIONAL CONFERENCE ON
# EXPLORATIONS IN PHYSICS (ICEP-2018)

29-31 May, 2018, Kathmandu, Nepal

**Tika Ram Lamichhane**

Central Department of Physics, Tribhuvan University, Kathmandu, Nepal

Contributed a poster presentation entitled

**Biophysical Analysis of Thyroid Function Test Reports of Euthyroid Subjects**

during the conference

| Chief Guest | Campus Chief | SOC Chair |
|---|---|---|
| Prof. Dr. Jiba Raj Pokharel | Rajesh Mahaju | Assoc. Prof. Dr. Leela Pradhan Joshi |
| Vice Chancellor, NAST | Amrit Campus | Amrit Campus |

Engineering Information Institute

# The 4th Conference on Advances in Biochemistry and Molecular Biology

## Certificate

**December 3 2018**

Dear Tika Ram Lamichhane
PhD Scholar, Tribhuvan University, Nepal.

Thank you very much for your support to **The 4th Conference on Advances in Biochemistry and Molecular Biology (CABMB 2018)** which has been held from December 1-3, 2018 in Sanya, China.

This is to confirm that you have attended the conference and made an oral presentation. your paper:
ID: CABMB2018_10000
Title: Age- and Gender-Specific Changes in Thyroid Size and Thyroid Function Test Values of Euthyroid Subjects

We believe that your presentation made great significance to the conference.

This conference is organized by the Engineering Information Institute and co-sponsored by the Scientific Research Publishing. CABMB 2018 is a valuable and important platform for inspiring international and interdisciplinary exchange at the forefront of Advances in Biochemistry and Molecular Biology. The Conference brings together academicians, researchers, biomedical engineers/technologists, and practitioners from all over the world.

Thanks again for your great supports in Sanya, China!

Best Regards,
CABMB Organizing Committee
Email: bio_mar@engii.org
Tel: +86 15172479625
QQ: 3025797047

International conference on

# Nano-Materials and Computational Physics

## 27-28 December 2017

Central Department of Physics
Tribhuvan University, Kirtipur, Nepal

## Participation Certificate

Tika Ram Lamichhane

Central Department of Physics, T.U., Kirtipur

participated the conference during 27-28 December 2017 and contributed oral/poster presentation entitled

Non-equilibrium Thermodynamic Properties of Thyroid Hormone Receptor-beta.

| | | |
|---|---|---|
| **Prof. Dr. Ram Pd Khatiwada** | **Dr. Gopi Chandra Kaphle** | **Prof. Dr. Binil Aryal** |
| Dean | Secretary | Head |
| IoST, Tribhuvan University, Kirtipur | Organizing Committee | CDP, TU, Kirtipur |

Lecture Series on

# Research Methodology

*6 November – 22 December 2017*

Central Department of Physics
Tribhuvan University, Kirtipur, Nepal

## Participation Certificate

Tika Ram Lamichhane

Central Department of physics T. U.

participated in **21 hours lecture series** on **Research Methodology** delivered by **Prof. Dr. Subodh R. Shenoy**, TIFR, India during 6 November to 22 December 2017.

Subodh R. Shenoy

***Prof. Dr. Subodh R. Shenoy***
Guest Speaker
Tata Institute of Fundamental Research, India

Binil Aryal

***Prof. Dr. Binil Aryal***
Head
CDP, TU, Kirtipur